

Intracorporeal anchoring and guiding system with permanent magnet force modulation

THÈSE N° 5698 (2013)

PRÉSENTÉE LE 8 MAI 2013

À LA FACULTÉ DES SCIENCES ET TECHNIQUES DE L'INGÉNIEUR
LABORATOIRE DE SYSTÈMES ROBOTIQUES 1
PROGRAMME DOCTORAL EN SYSTÈMES DE PRODUCTION ET ROBOTIQUE

ÉCOLE POLYTECHNIQUE FÉDÉRALE DE LAUSANNE

POUR L'OBTENTION DU GRADE DE DOCTEUR ÈS SCIENCES

PAR

Lionel FLACTION

acceptée sur proposition du jury:

Prof. J. Paik, présidente du jury
Prof. H. Bleuler, directeur de thèse
Dr P. Osypka, rapporteur
Prof. Ph. Renaud, rapporteur
Dr V. Verin, rapporteur



ÉCOLE POLYTECHNIQUE
FÉDÉRALE DE LAUSANNE

Suisse
2013

The magnetic force is animate, or imitates a soul;
in many respects it surpasses the human soul while
it is united to an organic body.

— William Gilbert
“father of the magnetic philosophy”,
in *De Magnete*, 1600.

*To my wife and my daughters
Astrid, Emma and Nina*

Acknowledgements

This research project on intracorporeal magnetic guidance originated from an interventional cardiologist Dr. Vitali Verin, whose intention is to simplify and make more efficient the treatment of atrial fibrillation. Beyond the technical achievements of this research project, the close collaboration with him allowed me to develop solid relations with experts from the medical, technical and business world. Moreover, I learned a lot about the importance of the business aspects in the development of medical technologies. This thesis reflects the many discussions I have shared with the people I had the chance to meet and work with during my research. I would like to express my sincere gratitude to the following people:

I am grateful to my advisor Prof. Hannes Bleuler for offering me the opportunity to work at the Laboratoire de Systèmes Robotiques (LSRO) at EPFL. I feel fortunate for the complete freedom he gave me in carrying out this research project. He has always been supporting during all these years.

I am deeply indebted to Dr. Vitali Verin, the inventor of the Maestro-AF concept. He is a visionary and an endless source of creativity. I learned a lot from him. I have been always amazed by his passion and optimism in thinking on tomorrow's medical devices. He passed on a bit of this passion to me.

I would like also to thank deeply my friend and colleague Bandar Hakim. I have never regretted my choice of "hiring" him to share with me this adventure. Beyond our friendship, he is a great listener and devoted person. He has been always very supportive through his wise suggestions. ¹جزاك الله خيرا

My gratitude also goes to the jury members for their evaluation of this work and comments for the final version of this document: Prof. Jamie Paik for her pleasant and efficient moderation of the private defence; Prof. Philippe Renaud for his fresh and pertinent look on the subject; and Prof. Peter Osypka for his comments from such a technically qualified and business-experienced person.

I would like to thank also Jan Sandtner for his very valuable inputs during the project. His knowledge and experience in magnetism are impressive. I am also grateful for his careful proofreading of my thesis.

The Maestro-team is not complete without Andrew Watson. I have witnessed so much growth and confidence building in him during our different collaborations along the years as a student-assistant. He has been an invaluable "finisher" on many tasks.

Furthermore, I thank my former students, Zied Ben Tanfous, François Curdy, Rodérik Berthelin, Cedric Schwab, Maxime Etori and Kari Arnston, for their excellent ideas, contributions and work.

I would like to acknowledge the help and support of Prof. Jason Carey in the Mechanical

¹May God reward you with goodness: "Jazak Allah Kheran"

Engineering Department at the University of Alberta. He gave me much more than a copy of his thesis on the prediction of mechanical properties of catheters. He has been a precious adviser. I am very grateful to him for his generosity, guidance and support. Sooner or later we will meet each other in person.

I am also grateful to our microengineering workshop, especially Alfred Thomas, Claude Cheseaux, Alexandre Stettler and Nicolas Favre-Victoire for their interest in the project and their positive attitude to take up new manufacturing challenges. In addition, I would like to thank the very professional team of Dr. Beat Walpoth at the Hôpitaux Universitaires de Genève (HUG) with whom we could conduct our *in vivo* experimentation. Furthermore, I am very grateful to the people of Osypka AG for their “product-like” prototypes of catheters and their personal engagement in the project.

Many thanks go also to all my “long-term” and “visiting” colleagues and friends at the lab. They are all part of this unique multicultural LSRO experience! It was a great pleasure being with them. I cannot forget to mention Ulrich Spaelter, who introduced me to this research project at the very beginning. Thank you so much. At my arrival at LSRO, I had the chance to participate on the development of a simulator for colonoscopy procedures with two close colleagues and friends Evren Samur and Pascal Maillard. My best thanks to our secretary Evelyn Rovero for her kind help during all this time.

I would like also to thank Ricardo Pérez Suárez for his dedicated and meticulous proofreading of this thesis and his excellent remarks and suggestions.

I would like to express my gratitude to my parents. They made the right choices to keep me on track at school. Finishing my education with a PhD is my way to thank them.

Especially, I owe my deepest gratitude to my dear wife Astrid for her love and unconditional support during this work. I am aware that living with an engineer might be a bit hard from time to time, being preoccupied and thinking for solutions to problems outside of the regular office hours... She has always been patient and capable of finding the right words to cheer me up at every normal bottoms of the PhD cycle. She has also given me two wonderful daughters during my stay at the lab. They are my three most precious gifts and my everyday source of joy. I dedicate this thesis to them.

I would like to thank the Commission for Technology and Innovation CTI for their financial support in the framework of the Maestro-AF project, 10289.1PFLS-LS.

Lausanne, March 27, 2013

Lionel Flaction

Contents

Acknowledgements	vii
Abstract (English/Français)	xiii
Nomenclature	xvii
1 Introduction	1
1.1 Motivation	1
1.2 Background and Prior Investigation	2
1.3 Objectives and Approach	2
1.4 Thesis Outline	3
2 Magnetic Anchoring and Guidance Principle: a State of the Art	5
2.1 Origins	5
2.2 Magnetic Manipulation in Medical Instrumentation	5
2.2.1 Ophthalmologic Applications	5
2.2.2 Cardiovascular Applications	7
2.2.3 Gastrointestinal Applications	13
2.2.4 Laparoscopic Applications	16
2.2.5 Neurosurgical Applications	18
2.3 Magnetic Force Modulation Principle	19
2.3.1 Electromagnets	20
2.3.2 Permanent Magnets	21
2.4 Magnetic Anchoring and Guidance System	21
2.4.1 Magnetic Anchoring Systems	22
2.4.2 Magnetic Guiding Systems	22
2.5 Intracorporeal Magnetic Anchoring and Guiding Systems	23
2.5.1 Prior Investigation	23
2.6 Summary	24
3 Magnetic Force Modulation at Small Scale	27
3.1 Magnetic Modulation Principles	28
3.1.1 Motivation	28
3.1.2 Implementation	28
3.1.3 Methodology	29
3.2 Separation Distance Modulation	30
3.2.1 Displacement of Permanent Magnets	30

Contents

3.3	Magnetic Field Modulation	34
3.3.1	Electromagnets	34
3.3.2	Rotation of Permanent Magnets	37
3.3.3	Shielding	44
3.4	Actuation Principle	50
3.4.1	Mechanical	50
3.4.2	Electromechanical	51
3.4.3	Hydro-pneumatic	51
3.5	Conclusion and Comparison	53
3.5.1	Magnetic Comparison	53
3.5.2	Design Implementation	54
3.5.3	Conclusion	54
4	Magnetic Force Modulator	57
4.1	Mechanical Design	57
4.1.1	Modulator Design	57
4.1.2	Actuation	58
4.1.3	Implementation	60
4.2	Mechanical Analysis	63
4.2.1	Theoretical Modulator Actuation Force	63
4.2.2	Experimental Modulator Actuation Force	67
4.2.3	Comparison of Theoretical and Experimental Actuation Force	68
4.2.4	Effect of the Modulation Range on the Actuation Force	70
4.3	Magnetic Analysis	71
4.3.1	Magnetic Coupling Force	71
4.3.2	Magnetic Forces and Torques	71
4.4	Expected Performances of a Catheteric Modulator	74
4.5	Fabrication	76
4.6	Summary	77
5	Guidance Analysis	79
5.1	Guidance Modes	79
5.1.1	Passive Mode	79
5.1.2	Active Mode	79
5.2	Characterization Setup	85
5.3	Guidance Modes Comparison	87
5.3.1	Method	87
5.3.2	Results	88
5.3.3	Implementation Modes	96
5.4	Conclusion	96
6	Magnetic Guidance on Cardiac Tissue	97
6.1	Experiments	97
6.2	Results	98
6.2.1	Guidance in Vibrating Mode	102
6.2.2	Working Conditions	102
6.2.3	Force Modulation Advantages	103
6.3	Conclusion	104

7 Friction in Intracorporeal Guidance	105
7.0.1 Mechanical Friction Phenomenon	105
7.1 Methodology	106
7.1.1 Experimental Setup	107
7.1.2 Cylinder Material	107
7.1.3 Tissue and Blood Preparation	109
7.1.4 Factors Selection for a Screening on Friction	109
7.1.5 Designs of Experiments	109
7.1.6 Experiments	110
7.2 Results	112
7.2.1 Factors Affecting Friction	112
7.3 Discussion	114
7.4 Conclusion	120
8 Applications for Intracorporeal Guiding Systems	123
8.1 Atrial Fibrillation	124
8.2 Wolff-Parkinson-White Syndrome	128
8.3 Ventricular Tachycardia	130
9 Synthesis and Conclusion	131
A Appendices	135
A.1 Factorial Design Matrices	135
A.2 List of Factors Aliases	136
Bibliography	139
List of Figures	147
List of Tables	151
Curriculum Vitae	153

Abstract

Magnetic manipulation of objects within the body is a growing field of research since the second half of the last century. Therapeutic and diagnostic capabilities offered by such technology are extended with the clinical need to make procedures less invasive and traumatic for the patients. Ophthalmologists were among the first to explore magnetic manipulation for removing iron fragments from the interior of the eye. Subsequently, the intubation devices were developed for extracting foreign objects from the body. The first case of magnetic guidance is an intravascular catheter magnetically guided by large external magnets in the 1950s. Half a century later, magnetic actuation of medical devices has led to many developments growing in complexity, such as wireless endoscopic capsule for exploring the gastrointestinal tract; intraocular microrobots of sub-millimetric size performing delicate tasks; internal magnetic laparoscopic instruments magnetically coupled through the abdominal wall without the need of additional incisions; or enormous systems for remote magnetic steering of catheters in cardiovascular or neurological procedures.

Technically, magnetic guidance requires variable, reshapable or steerable magnetic fields and therefore is generally associated with large magnetic arrangements of coils or permanent magnets surrounding the patient; while magnetic anchoring is achievable by external permanent magnets of adequate size placed or dragged manually on the surface of the body.

In this thesis work, we propose a novel type of magnetic guidance. Instead of having the guiding part external to the body, we propose to perform the guidance locally, on-site, by having the guiding part within the body in close vicinity of the element to be guided. Although the separation distance between the guiding and guided member is decreased, the required magnetic field to be generated is still significant with regards to the size of the system. Moreover, the magnetic attractions force should be adjusted in order to provide a robust guidance over variable and dynamic anatomical conditions. Electromagnets are an ideal solution by their ability to control the strength, polarity and shape of the generated magnetic field. However, obtaining a substantial magnetic field strength becomes challenging in the millimetric scale. Rare-earth magnets produce strong magnetic fields and become interesting when size is limited. But, they produce a constant field and the resulting attractive forces are strongly depending on the distance, which can be a safety issue.

To overcome these hurdles, we present a proof-of-concept of intracorporeal force modulation with steerable permanent magnets. We demonstrate through several examples that the magnetic forces applied to the guided element can be modulated by combining permanent magnets together or with other ferromagnetic materials.

A first prototype of force modulator is produced, characterized and tested *in vitro*. We analyze the behavior of this “magnetotractive” system of guidance through two operating

Contents

modes, namely passive and active guidance modes. While the passive guidance mode uses static magnetic fields, the active guidance mode allows the variation of the magnetic field during the guidance. Operating at static magnetic field implies that the coupling force within the system depends on the tissue thickness and irregularities. As the coupling force decreases approximately as the square of the distance, levels of coupling force could rapidly change during the guidance. Therefore, having the capability of adjusting the coupling force provides flexibility of the method. We demonstrate that active control can be achieved by a combination of several movable permanent magnets. This provides smoother guidance and superior robustness in comparison with the passive mode. On the guided element, we empirically identify the parameters representing the most significant effect on friction during the guidance. These findings could be very helpful in the design of magnetic guidance systems.

Finally, we show that magnetic attractive forces applied on the guided element could be adjusted with permanent magnet arrangements. This solution not only offers larger amplitude of force with regards to its size, but the range of modulation is significant in comparison with electromagnets. In addition, we demonstrate *in vitro* that intracorporeal magnetic guidance with steerable permanent magnets is feasible over variable and irregular tissue thickness. Therefore, this novel type of guidance has the potential to facilitate for example the treatment of cardiac arrhythmias.

Keywords: magnetic guidance, permanent magnet, variable force, friction, catheter, atrial fibrillation.

Résumé

La manipulation d'objets magnétiques à l'intérieur du corps est un champ de recherche qui n'a cessé d'être exploité ces cinquante dernières années. Les possibilités thérapeutiques et de diagnostics offertes par cette technique se sont étendues, poussées par la nécessité de rendre les interventions moins invasives et traumatiques pour le patient.

Les ophtalmologues ont été les premiers à explorer cette technique dans le but de retirer des fragments de fer de l'intérieur de l'œil. Ensuite sont apparus des dispositifs d'intubation pour l'extraction de corps étrangers ayant été avalés. Le premier cas de guidage magnétique a été recensé dans les années 1950 et consistait en un cathéter intravasculaire guidé magnétiquement par un gros aimant externe. Un demi siècle plus tard, l'actionnement magnétique de dispositifs médicaux a permis de nombreux développements de plus en plus complexes tels que des capsules endoscopiques pour l'exploration de l'appareil gastro-intestinal, des microrobots intraoculaires de quelques dixièmes de millimètres réalisant des tâches délicates, des instruments magnétiques de laparoscopie couplés magnétiquement à travers la paroi de l'abdomen réduisant ainsi le nombre d'incisions, ou encore de gigantesques systèmes contrôlés à distance pour faciliter la navigation de cathéters lors d'opérations cardiovasculaires ou neurologiques.

D'un point de vue technique, le guidage magnétique requière des champs magnétiques d'intensité et de forme variables pouvant être orientés. Ceux-ci sont généralement réalisés par d'importants arrangements de bobines ou d'aimants permanents qui entourent le patient alors qu'un ancrage magnétique peut être réalisé au moyen d'aimants permanents positionnés ou déplacés manuellement sur la surface de la peau.

Ce travail de thèse propose un nouveau type de guidage magnétique. Au lieu d'avoir l'élément guidant à l'extérieur du corps, nous proposons de réaliser le guidage localement, *in situ*, en amenant la partie guidante à l'intérieur du corps à proximité de l'élément à guider. Malgré une réduction de la distance séparant l'élément guidant de l'élément guidé, les champs magnétiques à fournir restent conséquents en rapport avec la taille du système. De plus, les attractions magnétiques doivent pouvoir être ajustables afin de rendre le guidage robuste et ce dans des conditions anatomiques variables et dynamiques. Les électroaimants apparaissent donc comme une solution idéale grâce aux possibilités qu'ils offrent de contrôler l'intensité, la polarité et la forme du champ magnétique. Cependant, obtenir suffisamment de force magnétique devient difficile à l'échelle millimétrique. Les aimants en terres rares produisent de puissants champs magnétiques et deviennent intéressants à utiliser lorsque la taille est limitée. Néanmoins, ils produisent un champ constant qui rend les forces d'attraction dépendantes de la distance ce qui peut être dangereux d'un point de vue médical.

Pour surmonter ces difficultés, nous présentons l'étude de faisabilité d'un modulateur de forces magnétiques intracorporel à partir d'aimants permanents orientables. Nous démon-

trons à travers différents exemples que les forces magnétiques appliquées sur l'élément guidé peuvent être modulées en combinant divers aimants permanents ou à l'aide de matériaux ferromagnétiques.

Un premier prototype de modulateur de forces est réalisé, caractérisé et testé en conditions *in vitro*. Nous analysons le comportement du système de guidage "magnétotractif" à travers deux modes de commandes, à savoir en mode de guidage passif ou actif. Alors que le mode passif s'effectue avec des champs magnétiques statiques, le mode actif permet la variation du champ magnétique durant le guidage. L'utilisation de champs magnétiques statiques implique que la force de couplage du système dépend de l'épaisseur du tissu et de ses irrégularités. Comme la force de couplage décroît approximativement au carré de la distance, les niveaux de couplage peuvent radicalement changer d'intensité durant le guidage. En conséquence, pouvoir ajuster cette force rend cette méthode plus flexible. Nous démontrons dans ce travail qu'un contrôle actif du champ magnétique peut être réalisé par une combinaison de plusieurs aimants permanents orientables. Cela apporte un guidage en douceur et davantage de robustesse en comparaison avec le mode passif. En ce qui concerne l'élément guidé, nous avons identifié de manière empirique les paramètres représentant une source de frottement importante durant le guidage. Ces constatations peuvent être fort utiles dans le design de ces systèmes.

Au terme de notre travail, nous avons démontré que les forces magnétiques peuvent être ajustées à l'aide d'arrangements d'aimants permanents. Cette solution n'offre pas seulement une grande intensité de forces tenant compte de leur taille, mais aussi une plage de modulation importante en comparaison avec les électroaimants. Par ailleurs, nous avons montré, en condition *in vitro*, que le guidage magnétique intracorporel à l'aide d'aimants permanents orientables est réalisable sur des tissus anatomiques irréguliers et variables en épaisseur. Cette nouvelle forme de guidage magnétique a donc le potentiel de faciliter par exemple des opérations médicales comme le traitement d'arythmies cardiaques.

Mots-clés : guidage magnétique, aimant permanent, force variable, frottement, cathéter, fibrillation auriculaire.

Nomenclature

Symbols

a_0	Constant effect
a_i	Main half effects
a_{ij}	Two-way order interaction effect
A	Cross-sectional area of the wire
B	Magnetic field
d	Magnet diameter or separation distance
d_0	Constant separation distance
D	Diameter of the off-center tube or slotted tube
e	Difference between the process variable and the desired setpoint
E	Modulus of elasticity
F_0	Desired coupling force
F	Magnetic coupling force or magnetic force
F_a	Actuation force
$F_{a,m1}$	Actuation force for model I
$F_{a,m2}$	Actuation force for model II
F_c	Radial coupling force
F_d	Axial dragging force
F_s	Friction force between the pin and the slot
F_x	Magnetic force along x axis
F_y	Magnetic force along y axis
F_z	Magnetic force along z axis
G	Shear modulus
I	Electrical current
J	Polar moment of inertia
K_i	Integral gain
K_p	Proportional gain
l	Length of the coil wire
L	Rod length or cable length
l_{mag}	Magnet length
l_{mod}	Modulator length
m	Magnetic moment
$M_{y,A}$	Moment along y at point A
$M_{z,A}$	Moment along z at point A
N	Reaction force
P	Resistive heating or mechanical load

Contents

r	Rod radius
T	Twisting moment
T_x	Magnetic torque along x axis
u_{out}	Controller output
x_i	Factor i
x_{ij}	Interaction between two factors i and j
Y	Friction force

Greek Letters

α	Angular deformation
β	Shift angle due axial misalignment of the magnets
δ	Material elongation
Δ_r	Off-center distance of a tube
Δ_x	Axial misalignment
Δ_y	Lateral misalignment
Δ_z	Separation distance variation
μ_1	Friction coefficient between the pin sliding on the slot
μ_r	Relative magnetic permeability
φ	Angle of the helical slot
ρ	Static resistivity
σ	Axial stress
τ	Magnetic torque
τ_α	Angular stress
θ	Steerable magnets angle
$\theta_{m,0}$	A priori modulation angle

Acronyms

ANOVA	ANalysis Of VAriance
AC	Alternating Current
AC	Ablation Catheter
AF	Atrial Fibrillation
AV	Atrioventricular node
CGCI	Catheter Guidance Control and Imaging
CNC	Computer Numerical Control
DC	Direct Current
DOE	Design Of Experiment
DOF	Degree(s) of Freedom
EC	Escorting Catheter
EPFL	École Polytechnique Fédérale de Lausanne
ETHZ	Eidgenössische Technische Hochschule Zürich
FD	Factorial Design
FDA	Food and Drug Administration

FEM	Finite Element Modelling
FFB	Force Feedback
FFD	Fractional Factorial Design or Feed Forward
GI	Gastrointestinal Tract
LESS	Laparoendoscopic Single Site Surgery
LP	Low-Pass filter
MAC	Magnetic Air Capsule
MAGS	Magnetic Anchoring and Guidance Systems
MAESTRO-AF	Magnetic Ablation ESCorting for Treatment Of Atrial Fibrillation
MAS	Magnetic Anchoring Systems
MGCE	Magnetically Guided Capsule Endoscopy
MGOe	megaGauss Oersteds
MGS	Magnetic Guiding Systems
MRI	Magnetic resonance imaging
MSS	Magnetic Stereotactic System
NdFeB	Neodymium Iron Boron magnet
NOTES	Natural Orifice Translumenal Endoscopic Surgery
OFAT	One Factor At a Time
PCA	Percutaneous Catheter Ablation
PID	Proportional–Integral–Derivative controller
PI	Proportional–Integral controller
PM	Permanent Magnet
PMMA	Poly(methyl methacrylate), Plexiglas
POD	Para-Operational Device
RF	Radio-Frequency
SA	Sinoatrial node
SPCE	Self-Propelling Capsule Endoscope
VT	Ventricular Tachycardia
WPW	Wolff–Parkinson–White syndrome

1 Introduction

1.1 Motivation

Humans have always been fascinated by the invisible magnetic interactions produced by magnets on other ferromagnetic material. The earliest use of these forces in “medicine” is most likely to be found in the writings of an Hindu surgeon, Sucruta, in 600 BC, where he describes how to extract an iron arrow tip by using a natural magnetic stone [Andrä and Nowak, 2007]. This know-how remained as a curiosity until the scientific and technological progress of 19th and 20th centuries could benefit of the magnetic phenomenon.

Magnetic manipulation of objects within the body is a growing field of research since the second half of the last century. Therapeutic and diagnostic capabilities offered by such technology are growing with the clinical need to make procedures less invasive and traumatic for the patient. In the middle of the 19th century, ophthalmologists were among the first to explore magnetic manipulation for removing iron fragments from the interior of the eye. Then, the intubation devices for extracting foreign objects from the body were introduced. The first case of magnetic guidance is an intravascular catheter magnetically guided by a large external magnet in the 1950s [Tillander, 1951]. Half a century later, magnetic actuation of medical devices has led to many developments growing in complexity such as a wireless capsule endoscope exploring the gastrointestinal tract; intraocular microrobots of sub-millimetric size performing delicate tasks; internal magnetic laparoscopic instruments magnetically coupled through the abdominal wall without the need of additional incisions; or enormous systems for remote magnetic steering of catheters in cardiovascular or neurological procedures. These systems can be described as a Magnetic Anchoring and Guidance Systems (MAGS).

Technically, magnetic guidance requires variable, reshapable or steerable magnetic fields which are generally associated with large and complex arrangements of coils or permanent magnets surrounding the patients. Such magnetic systems require elaborate control algorithms and are operated remotely from a control room. Robotized and remote procedures are the current trend in medicine.

The term guidance is extensive. It includes magnetic navigation in hollow space, steering of catheter as well as dragging of endoscopic capsules in the intestines. Magnetic navigation requires complex and precise control of the magnetic field direction and gradients. Electromagnets or superconductive coils are the most suitable for navigation. Magnetic propulsion of a guided element can be achieved by orienting, rotating or alternating magnetic fields. Changing the field direction is generally sufficient for steering and aligning the tip of a catheter with the magnetic field lines. Permanent magnets represent a good alternative

1. Introduction

for this purpose, but electromagnets are more commonly used in practice. Magnetottractive forces to pull or drag a guided part within the body can be achieved with an external hand-held electromagnet or a permanent magnet controlled manually or remotely above the surface of the body. The common point of these guiding systems is their ability to provide a “contactless” magnetic effect on the internal guided part deep inside the body.

Temporary magnetic anchoring functions are insured by external permanent magnets of adequate size placed or dragged manually by the physician on the surface of the body. As the external guiding part is designed for manual handling, the magnetic effects on the guided part is limited to few centimeters.

In this dissertation, we propose a novel type of magnetic guidance. Instead of having large and complex guiding systems surrounding the patient or having smaller magnetic elements on the surface of the body, an alternative solution could be to perform the guidance locally, on-site, by having the guiding part also inserted in the body. To the best of our knowledge, intracorporeal magnetic guidance has not been explored for medical applications. The intracorporeal guiding part should be small enough to be inserted in a minimally invasive way. On-site guidance is particularly applicable in the cardiovascular system due to numerous vessels around the cardiac muscle.

1.2 Background and Prior Investigation

The aim of this thesis is to evaluate the technical feasibility of an intracorporeal magnetic guiding system. We believe that on-site guidance is particularly applicable for cardiovascular applications such as the treatment of cardiac arrhythmias due to the presence of numerous vessels around the cardiac muscle. Cardiac arrhythmias can be treated by radiofrequency catheter ablation, which consist of inactivating abnormal electrical pathways in the heart. Such procedures are extremely challenging due to the manipulation of the catheter in a very dynamic environment as well as the limited systems for internal visualisation. In this context, a research project introduced by Dr. Vitali Verin was conducted in our Robotic Systems Laboratory (LSRO) at EPFL. This project called Maestro-AF proposes to use an intracorporeal magnetic guiding system to facilitate positioning and guidance of catheters for the treatment of cardiac arrhythmias.

Preliminary work has been conducted and is briefly reported in section 2.5.1. Reasons for focusing our research on magnetic guidance with force modulation are also given.

1.3 Objectives and Approach

The ultimate goal of this thesis is to evaluate the technical feasibility of such magnetic guidance, more precisely intracorporeal guidance with force modulation by means of steerable permanent magnets. Intracorporeal guidance is strewn with technical obstacles and physiological challenges. Although the separation distance between the guiding and guided member is decreased, the required magnetic field to be generated is significant at this scale. Moreover, the magnetic attractions should be adjusted in order to provide a robust guidance over variable anatomical conditions. In addition, magnetottractive guidance can be associated with large frictional interactions with tissue if the attraction forces are uncontrolled.

Electromagnets are an ideal solution for modulating the magnetic field. However, obtaining substantial magnetic field strength becomes challenging at small scale. Resistive

heating is an additional drawback. Rare-earth permanent magnets such as Neodymium Iron Boron (NdFeB) magnets produce strong magnetic fields and become interesting when size is limited. However, the magnetic fields are constant and the resulting attractive forces are dependent on the distance separating the MAGS, which can be a safety issue.

In this work, we provide different solutions for modulating the magnetic attraction forces applied to the guided part. We focus our analysis on solutions using ferromagnetic materials and permanent magnet arrangements of a size compatible (≤ 10 mm in diameter) with minimally invasive devices. Moreover, we study the actuation principles for controlling the magnetic field of the guiding part. As a result of these investigation, we designed and fabricated a force modulator with two steerable permanent magnets actuated by a mechanical transmission.

With this modulator, we analyze *in vitro* the behavior of the guidance system through two operating modes, namely passive and active guidance modes. While the passive guidance mode uses a static magnetic field, the active guidance mode allows the variation of the magnetic field during the guidance. Operating at static magnetic field implies that the coupling force within the system depends on the tissue thickness and irregularities. As the coupling force varies approximatively with the square of the distance, the level of coupling force could rapidly change during the guidance. Therefore, having the capability of adjusting the coupling force provides flexibility to the method. We show in this work the limitation of magnetic guidance when performed with static magnetic fields, namely with single permanent magnets. We demonstrate *in vitro* that active control provides smoother guidance and superior robustness in comparison with the passive mode.

Regarding the guided element, we empirically investigate and identify the parameters representing a significant source of friction during the guidance. We give some guidelines to minimize friction interactions between a cylindrical guided tip sliding over a soft anatomical tissue.

In conclusion, our objective is to demonstrate that magnetic attractive forces can be adjusted with permanent magnets arrangements. Not only this solution offers a larger amplitude of force relative to its size, but the range of modulation is considerably larger in comparison with electromagnets. In addition, we demonstrate *in vitro* that intracorporeal active magnetic guidance with steerable permanent magnets is feasible and compatible with anatomical conditions. Therefore, we believe that this novel type of guidance can extend the field of MAGS applications and has the potential to facilitate catheterization procedures such as the treatment of atrial fibrillation.

1.4 Thesis Outline

This thesis work is presented in 9 chapters as follows. Chapter 2 introduces the concept of magnetic anchoring and guidance in the medical field and provides a review of the technical developments based on this principle.

In chapter 3, different solutions for modulating the magnetic attractions between the guiding and guided part are exposed. The effort is made on designing magnetic force modulator of a size compatible with minimally-invasive devices. At this scale, electromagnets are limited while permanent magnets become particularly suitable for magnetic guidance. Concepts of modulators providing magnetic fields modulation are detailed and compared. Chapter 4 details the implementation of a magnetic force modulator using two steerable permanent magnets in a catheter tip.

1. Introduction

Passive and active modes of guidance are studied and compared in chapter 5. This chapter, describes the sequences occurring during the magnetic guidance and gives the required conditions for achieving an intracorporeal magnetic guidance. Guidance executed with static or variable magnetic field are also compared. Chapter 6 demonstrates through *in vitro* experiments, how modulating the coupling force between the MAGS members increases the robustness of the magnetic guidance.

Chapter 7 focuses on the frictional interactions occurring during the magnetic dragging of the guided part. Twelve parameters that could potentially affect friction have been selected. These parameters are of physical, geometrical, physiological and temporal nature. A statistical analysis determines the most significant parameters playing a role in the friction phenomenon on soft anatomical tissue. Some guidelines to minimize frictional interactions are also given.

Examples of applications for intracorporeal magnetic guiding systems are given in chapter 8. The complex ramifications of the cardiovascular system is particularly suitable for on-site guidance, which can facilitate catheter ablation procedures.

Finally, the contributions and conclusions of this work are summarized in chapter 9.

2 Magnetic Anchoring and Guidance

Principle: a State of the Art

This chapter introduces the concept of magnetic anchoring and guidance in the medical field and provides a review of technical development based on this principle.

2.1 Origins

The first reported relation between man and magnet was made by the Greek Thales of Miletus (ca. 624-547 BC). For him, as the soul somehow produces motion, he believed that, as a magnet could also produce motion by moving iron, it must also possess a soul. Miraculous healing properties of magnetic materials were most likely accepted throughout history based on this kind of beliefs [Andrä and Nowak, 2007].

According to Andrä, the earliest use of attracting forces of natural magnets in medicine was found in the writings of a Hindu surgeon, Susruta (600 BC), who described in his book how to extract an iron arrow tip by using a natural magnetic stone. According to the same source, these findings were probably not explored until 1290 when Gilbertus Anglicus reported the use of magnets to remove iron obstructed in the flesh.

Similar descriptions more or less credible of magnetic extractions of iron have been reported during centuries, leading to other types of extraction such as the removal of iron particles embedded in the eye.

2.2 Magnetic Manipulation in Medical Instrumentation

2.2.1 Ophthalmologic Applications

Ophthalmologists were among the first to explore magnetic manipulation as the eye nature is able to provide in most cases a direct visualisation of foreign bodies to be removed. The physician could carefully control and follow the removal of the object during the manipulation. Many examples can be found in the literature. The German Dr. Nicolaus Meyer performed with a permanent magnet, the first removal of iron fragments from the interior of the eye, in 1842. In 1879, his compatriot Dr. Julius Hirschberg became the first ophthalmologist doing this task with a hand-held electromagnet, figure 2.1, [Rohrbach, 2002]. Hand-held magnets, by their size, have the advantage to be easily manipulated around the surface of the eye in order to attract the object to the appropriate exit point.

Further developments were carried out by the Swiss ophthalmologist Dr. Otto Haab in collaboration with the Swiss Federal Institute of Technology (ETHZ) in 1892. Dr. Haab managed to remove foreign body at greater distance from the eye by using the “giant

2. Magnetic Anchoring and Guidance Principle: a State of the Art

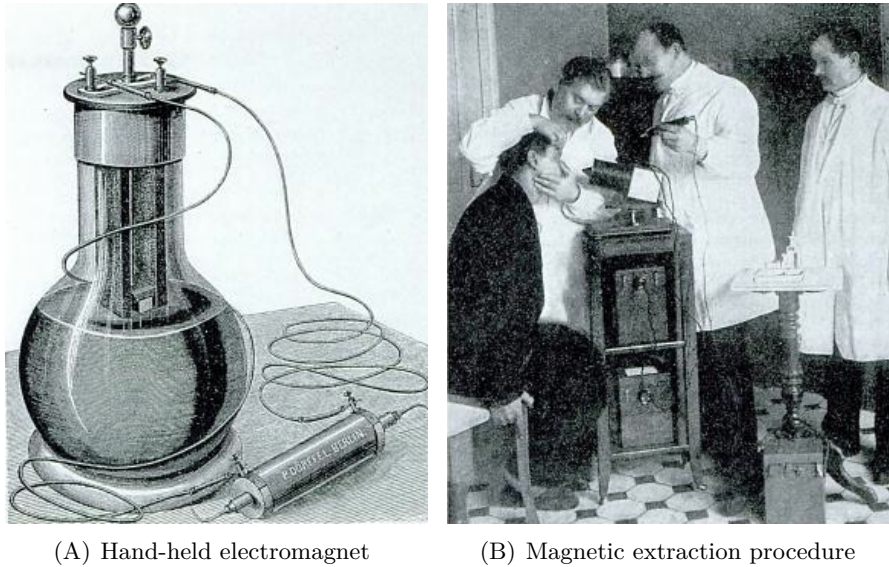


Figure 2.1: First case of magnetic extraction of intraocular foreign bodies with the help of an electromagnet developed by Hirshberg in 1885.

magnet”, an electromagnet of 130 kg designed at ETHZ, figure 2.2, [Andrä and Nowak, 2007]. Hirschberg and Haab engaged a scientific battle through articles as their view of the

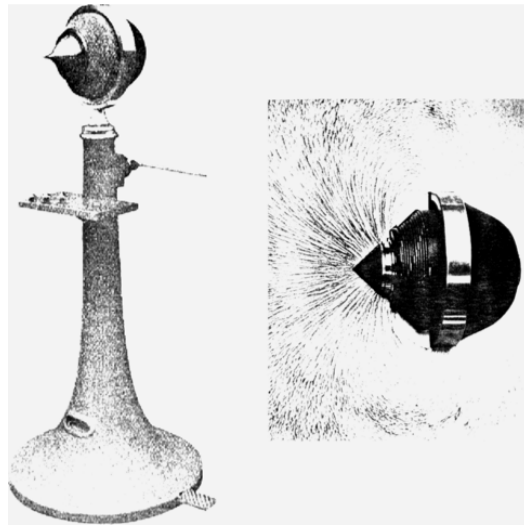


Figure 2.2: A “giant magnet” developed at ETHZ and used by Haab to remove intraocular foreign bodies in 1892.

procedure differed with respect to the type of magnet to be used and the way to remove the foreign bodies. Finally, it has been demonstrated in 1970 that both techniques represented the same risk [Springer, 1970]. Today, these methods are slowly disappearing pushed by the progress in modern eye surgery.

More recently, the group of Bradley Nelson at ETHZ developed an electromagnetic system for 5-DoF wireless micromanipulation, the OctoMag [Kummer et al., 2010], figure 2.3. The system achieves precise manipulation of an untethered microrobot under closed-

2.2 Magnetic Manipulation in Medical Instrumentation

loop control with visual tracking, but it can also be controlled manually on operator visual feedback. Magnetic manipulation is typically achieved with uniform-gradient field generated by orthogonal electromagnetic arrangements. The control of the Octomag is particularly unique due to its utilization of complex nonuniform magnetic fields. Although the OctoMag is originally designed to control intraocular microrobots to perform delicate procedures such as retinal-vein cannulation or drug delivery, it has a potential for other medical applications. In 2010, Aeon Scientific AG, a spin-off from that laboratory, was founded with the goal of developing the next generation medical equipment based on this electromagnetic manipulation technology. Their new type of catheter steering system will be dedicated first to support cardiac arrhythmias procedures.

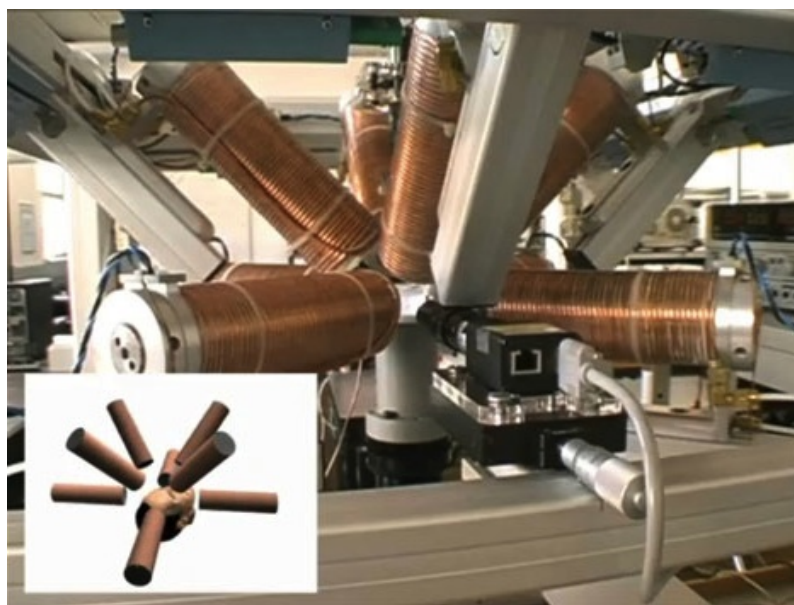


Figure 2.3: Octomag, an electromagnetic system for 5-DoF wireless micromanipulation.

2.2.2 Cardiovascular Applications

The vascular system is a complex and tortuous system to be explored with minimally invasive techniques. It offers an amazing access to various locations inside the body and at the same time is a driving force for technical progress such as miniaturization and imaging systems.

The first step in intravascular magnetic guidance was accomplished by the Swedish Hans Tillander in the early 1950s [Tillander, 1951]. He used large external magnets of 1.1 kW and 350 kg to manually steer a transvascular catheter with articulated tip into the main branches from the aorta. His goal was to align the flexible tip along the magnetic field lines and by repositioning the field, it could produce the expected bend and direction, figure 2.4. Visual difficulties of the tip with the existing X-ray machine, stopped his research for several years. The magnetic exploration of the heart was born. However, his method of magnetic guidance was used to steer a catheter already introduced and driven by hand. Through collaborations, several technical innovations and improvements were achieved on the imaging system as well as on the weight of the magnet and type of

2. Magnetic Anchoring and Guidance Principle: a State of the Art

ferromagnetic material used for the catheter tip. Tillander managed finally to prove the validity of his methodology on numerous animals [Tillander, 1970].

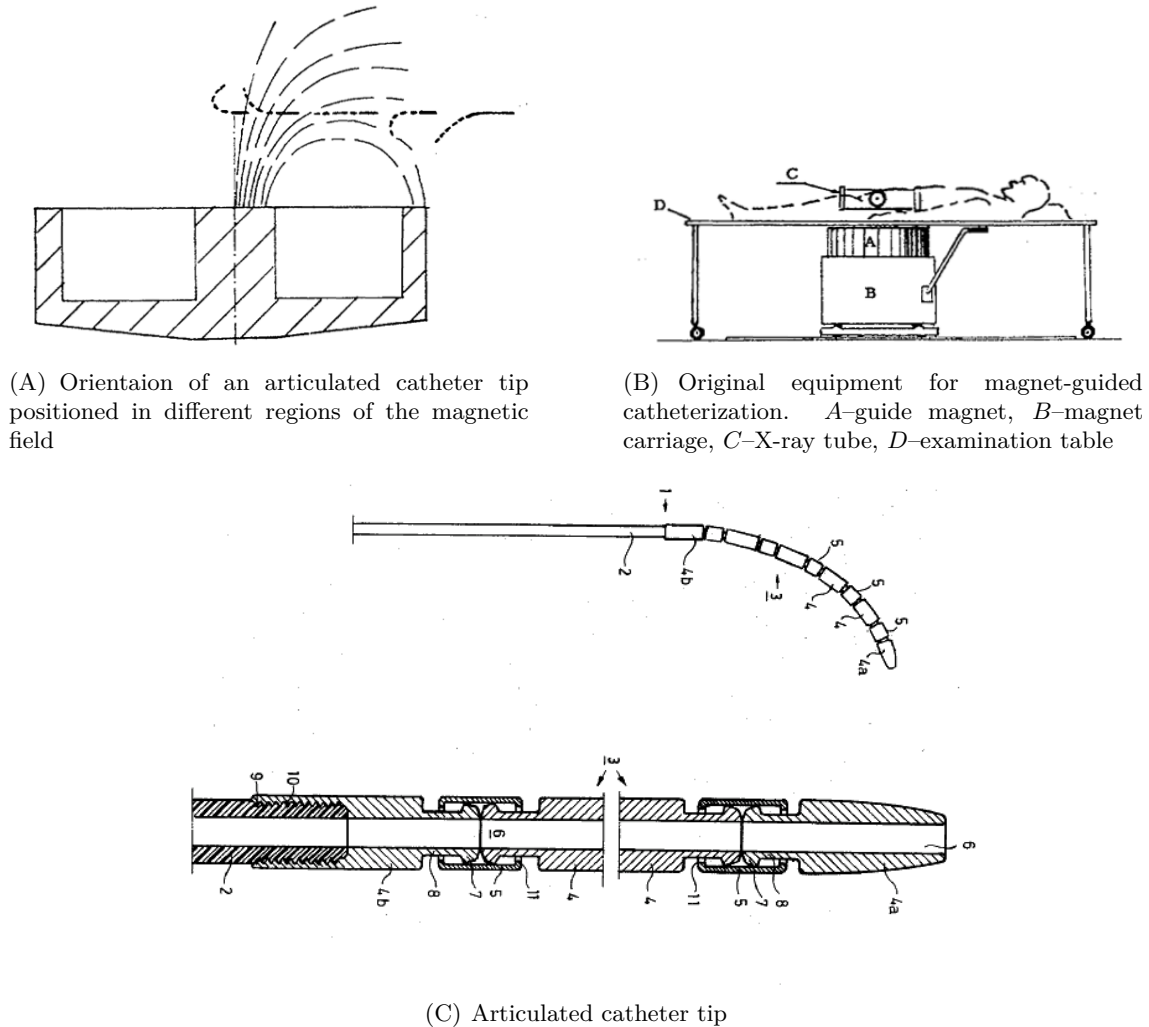
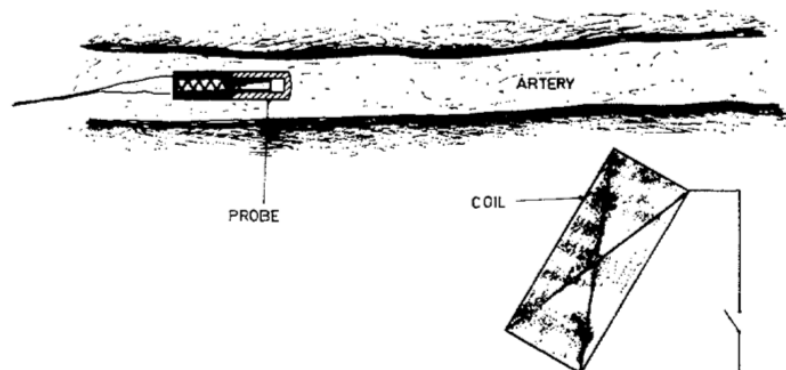


Figure 2.4: Intravascular magnetic guidance developed by Tillander in the early 1950s.

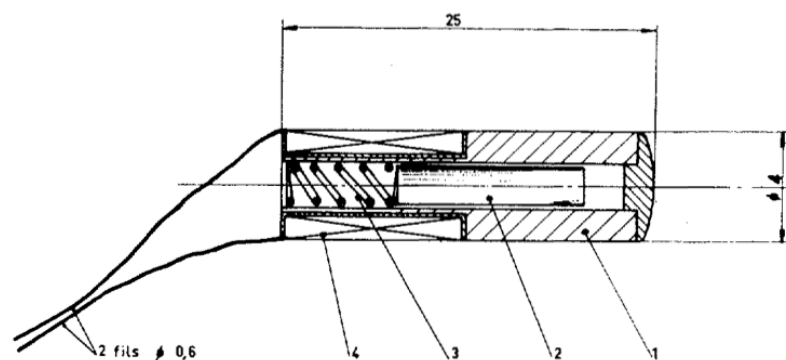
In 1969, Sobiepanek understood that true magnetic propulsion of a small magnetic probe was requiring enormous and powerful equipment to obtain sufficient magnetic field. The main source of resistance to a magnetic displacement of the probes comes from the friction with the vessels and from the blood flow. To overcome these obstacles, Sobiepanek designed a “percussion-type” electromagnetic probe to help in clearing thrombic obstructions of coronary arteries. The probe was composed of a spring loaded plunger made of ferromagnetic material, figure 2.5. The probe is driven by an external pulsating magnetic field produced outside the body by one or several coils. The probe is displaced with the following actions: In the starting position, the plunger is at the rear of the tip (left-hand side of figure 2.5(B)) and the current in the external coil and return coil are zero. At a given instant, an external field pulsation produces a magnetic force on the plunger, which projects the plunger forward until producing an impact on the opposite extremity of the probe. The shock produces a force pulse on the probe which displaces the probe. At this moment, the return coil goes in action while the external field has disappeared. This type

2.2 Magnetic Manipulation in Medical Instrumentation

of locomotion offers a displacement with a reduced average friction with the vessel wall and a more controlled guidance.



(A) Schematic control of a percussion-type probe by a single coil

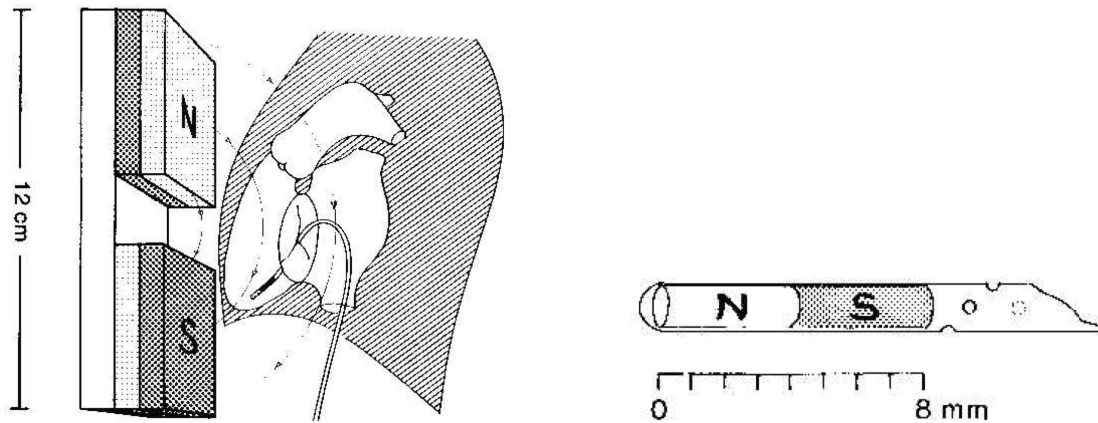


(B) Electromagnetic probe. 1-body of probe, 2-plunger, 3-return spring, 4-return coil

Figure 2.5: Percussion-type electromagnetic probe of Sobiepanek in 1969.

Hand-magnets were also used to facilitate the navigation of magnetic catheters. Ram and Meyer managed to displace magnetically a small catheter tip on a neonate in order to collect blood samples for oximetry and to perform angiography for diagnosis of congenital defects [Ram and Meyer, 1991], figure 2.6. By the low thickness of neonatal thorax, the catheter could be displaced 4 cm below the magnet poles of the hand magnet. The magnetic interactions could be intensified by either increasing the distance between the poles of the external flat horseshoe magnet or the size of the catheter tip. Another example of magnetic guidance with a hand-magnet is proposed by Modny and Bambara in 1957 [Modny, 1958]. They developed a method for stripping varicose veins in which a magnetically attractable plumb traverses a varicose vein by magnetic attraction exerted upon it from outside the body. The traditional method consisted of using a wire that was advanced manually inside the vein and associated with multiple incisions along the veins at each time the wire was facing difficulties to advance forwards. With their system, Modny and Bambara achieved to advance magnetically their “plumb line” all the way to its final destination reducing the number of incisions to only an entrance and an exit point, figure 2.7. According to Gillies, one of the largest research programs to date in magnetic catheterization was the development of a magnetically guided “para-operational

2. Magnetic Anchoring and Guidance Principle: a State of the Art



(A) Lateral view of the right heart. The catheter tip is aligned and displaced by moving around the chest the magnetic field lines produced by Neodym magnets

(B) Catheter tip equipped with a Samarium Cobalt magnet of 1.2 mm in diameter

Figure 2.6: Ram and Meyer reports the first clinical case of heart catheterization in a neonate with complex congenital heart disease, using a strong external permanent magnet to control the magnetic tip of a catheter in the body.

device” (POD) [Gillies et al., 1994]. Magnetic propulsion and steering of a POD catheter was introduced for the first time in 1963 by the group of Frei at the Weizmann Institute of Science of Israel [Frei, 1967]. The navigation of the vascular system and the exploration of the bronchial tree was the focus of this research. The propulsion was achieved by an external AC-magnetic field which induced in the tip of the catheter a “fish-like” swimming action. Several kind of POD systems were developed depending on the endovascular applications. The basic POD catheter was a short piece of silicone tubing of 7 cm long and 1.3 mm in diameter in which a platinum-cobalt magnet of 4 mm long and 1 mm in diameter was attached at one extremity of the tube, figure 2.8. In addition, different types of fins were attached to it in order to facilitate the locomotion. The other extremity of the tube was attached to a long stiffer polyurethane tube. The catheter was initially advanced by hand in the vessels and when magnetic guidance was required a large external electromagnet was used to steer and propel the tip of the catheter. A DC-field was combined with an AC-field for this purpose. The DC-field was used to align the POD and its gradient for exerting a force on the permanent magnets, while the AC-field made the tip vibrate.

In 1975, Savitz and his colleagues replaced the standard room-temperature coil by a superconducting coil that could carry a current of 17.5 A. The coils could be displaced and oriented by hydraulic actuators, which provided precision on the strength and direction of the force applied to the POD tip [Gillies et al., 1994]. Although, several studies have demonstrated the technical feasibility of the PODs, the concept failed to reach clinical acceptance [Andrä and Nowak, 2007].

In the early 2000s, the American company Stereotaxis Inc. developed further a stereotactic system originally elaborated for neurosurgery by McNeil and his colleagues few years earlier. [McNeil et al., 1995b, McNeil et al., 1995a] (see section 2.2.5). The definition of stereotaxis is the guidance of an object through space with reference to an externally fixed and highly accurate frame or reference [Gillies et al., 1994]. A Magnetic Guidance

2.2 Magnetic Manipulation in Medical Instrumentation

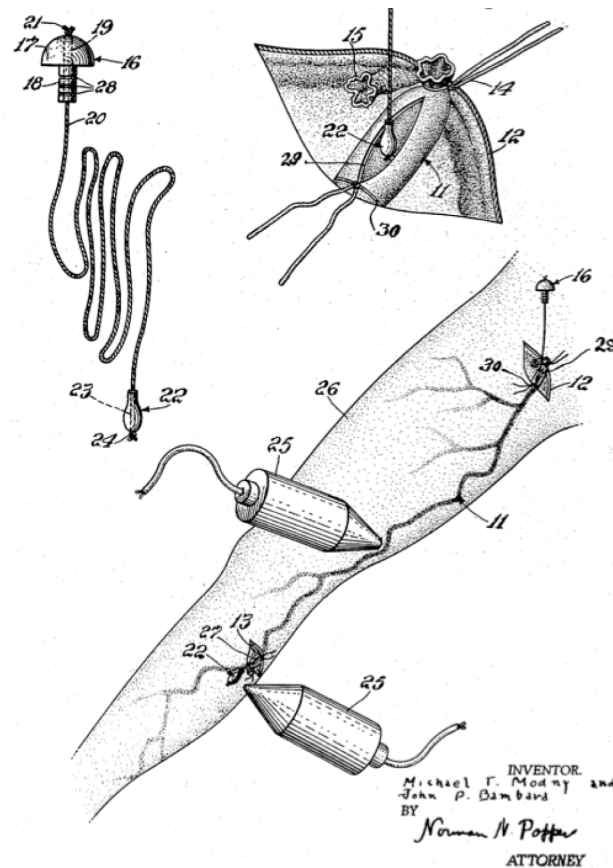


Figure 2.7: Method developed by Modny and Bambara for stripping varicose veins by using a “plumb line” magnetically guided with an external hand-held magnet, 1957. Labels: 16–stripper, 20–nylon line, 22–ferromagnetic plumb, 25–hand-held magnet.

System (MGS) was used to control the movements and positions of an ablation catheter within the heart, figure 2.9. The first generation was the Telstar system composed of three superconducting electromagnets (0.15 T) cooled by liquid helium, figure 2.9(A). The magnetic ablation catheter was deflected by the magnetic field. The magnitude of the force exerted on the catheter tip is maximal when the tip is perpendicular to the magnetic field and goes down to zero when the catheter tip is aligned with the field lines. Navigation to a precise target required two or three manipulations of the magnetic field, where each manipulation was established within 20 seconds. In parallel, the catheter was manually advanced or retracted to facilitate the access to the desired target. Navigation accuracy was estimated to be below 1 mm [Faddis et al., 2002, Faddis et al., 2003]. Although this system was technically capable, it did not allow remote catheter ablation.

The second generation is the Niobe system, which now allows for the first time complete remote catheter navigation. The company replaced the superconducting coils by two huge steerable NdFeB magnets placed in a housing and controlled by a joystick. [Patterson et al., 2006], figure 2.9(B). These magnets provide a steerable uniform magnetic field (0.08 T) within a spherical navigation volume of 20 cm in diameter. The Niobe system received FDA approval in 2003. Today, the fourth generation of this system is available (Niobe-ES). A computer-controlled catheter advancer system (Cardiodrive) and a graphic workstation (Navigant) are complementing the steerable permanent magnets. The system

2. Magnetic Anchoring and Guidance Principle: a State of the Art

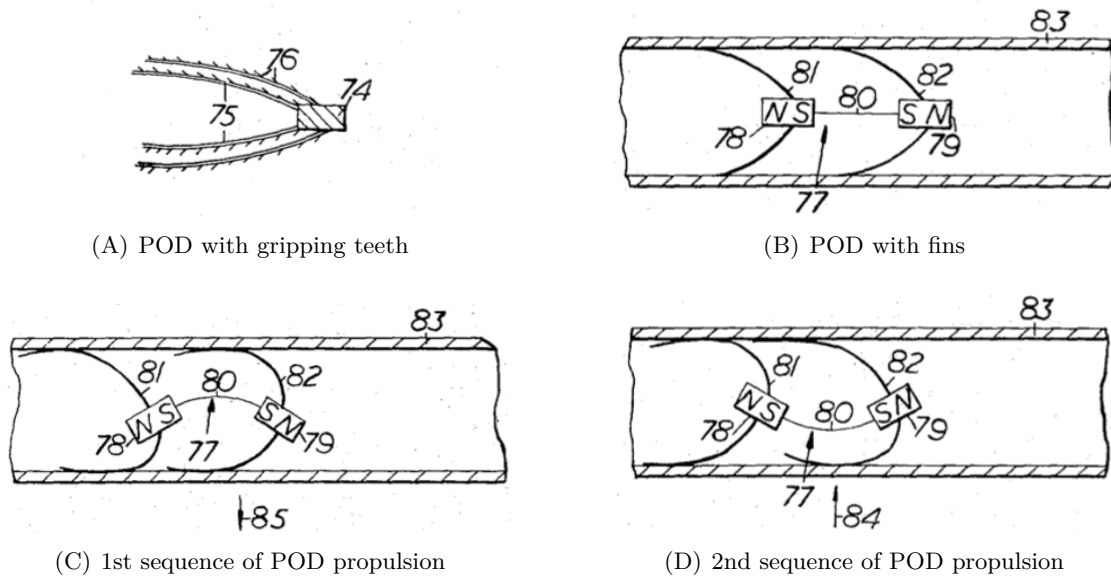


Figure 2.8: Magnetic propulsion of a POD catheter tip attached to a stiffer polymer tube (not represented). A DC-field was combined with an AC-field. The DC-field was used to align the POD and its gradient for exerting a force on the permanent magnet(s), while the AC-field (labels -84, -85) made the tip vibrating and moving (C) and (D).

is controlled by a click of the mouse and allows remote control of an ablation catheter from a control room. According to the company, over 164 units have been installed worldwide [Stereotaxis, 2012].



(A) Telstar magnetic navigation system



(B) Niobe magnetic navigation system

Figure 2.9: Magnetic navigation systems from Stererotaxis, Inc..

An alternative to the Stereotaxis system is proposed by Magnetecs Corp., figure 2.10. A real-time, high-speed, closed-loop, magnetic system (Catheter Guidance Control and Imaging) comprising eight cooled-electromagnets creates unique dynamically shaped magnetic fields around the subject's torso [Gang et al., 2011]. The real-time reshaping of these magnetic fields and the ability to vary the intensity of the torque and force fields differentiate the CGCI from the existing magnetic Niobe system. Magnetecs received the

CE-Mark in late 2011.



Figure 2.10: The CGCI magnetic system from Magnetec Corp..

2.2.3 Gastrointestinal Applications

Removal of foreign bodies in the stomach by the use of magnetic catheter appears in the literature in the 1940s. “Magnetotraction” procedure was successful and many cases have been reported [Equen et al., 1957, Gillies et al., 1994]. Several devices are commercially available since the 1990s.

In the same idea, magnetic intubating devices were magnetically guided through the gastrointestinal (GI) tract with an external field. The magnetic field was produced either by a hand-held permanent magnet [Devine and Devine, 1953] or an electromagnet [McCarthy, 1962, Towbin et al., 1990].

In the early 2000s, Iddan and his colleagues at Given Imaging Ltd. successfully tested on humans the first wireless capsule endoscopy for the exploration of the GI tract without the discomfort of the traditional endoscope [Iddan et al., 2000]. The capsule is swallowed by the patient and while moving by peristaltic waves, it transmits images wirelessly. As the progression of the capsule is not controlled, there is probability of missing a sign of disease. Capsule endoscopy is a promising technique but limited by the lack of a controlled capsule locomotion.

The laboratory of Ishiyama at Tohoku University developed a capsule endoscope magnetically actuated with an external rotational magnetic field, figure 2.11. A spiral shape capsule containing a diametrically magnetized permanent magnet could be rotated and propelled up to 5 mm/s in a phantom silicon tube by applying a rotational external field. Animal trials are under investigations [Chiba et al., 2005].

Morita *et al.* tested *in vivo* a self-propelling capsule endoscope (SPCE) by using an external oscillating field [Morita et al., 2010]. A commercially available capsule endoscope (Pillcam SB, Given Imaging Ltd.) was linked with a spring to a fin comprising a magnet, figure 2.12(A). By orientating an external AC-field, the SPCE could be displaced remotely on different sites of animal stomach while transmitting images.

Magnetic propulsion of capsule endoscopy is also under investigation by Kósa *et al.*, figure 2.12(B). They developed a miniature swimming mechanism that uses the magnetic fields of Magnetic Resonance Imaging (MRI) system for both propulsion and wireless energy delivery [Kósa et al., 2008, Kósa et al., 2012]. The propulsion is ensured by one to

2. Magnetic Anchoring and Guidance Principle: a State of the Art

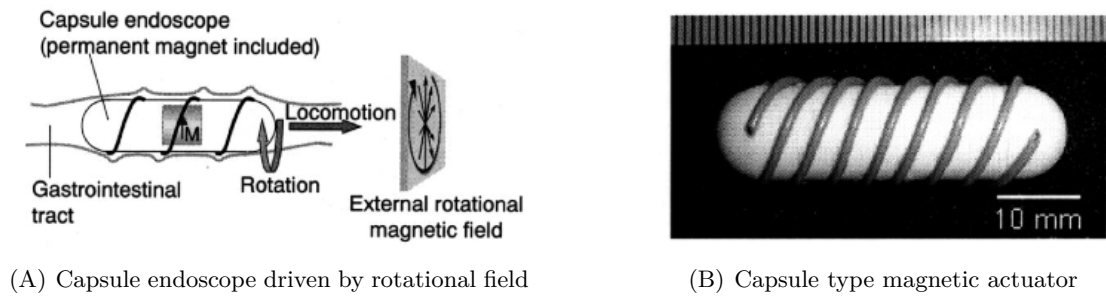


Figure 2.11: Magnetic propulsion of capsule endoscopy developed at Tohoku University, 2003.

several coils, mounted in a row on a swimming tail. When current is alternating in these coils, interaction with static magnetic field of the MRI will generate a waving movement in the tail. In addition, MRI's radio frequency field is used to power the electronics that generates alternating current in the coils.

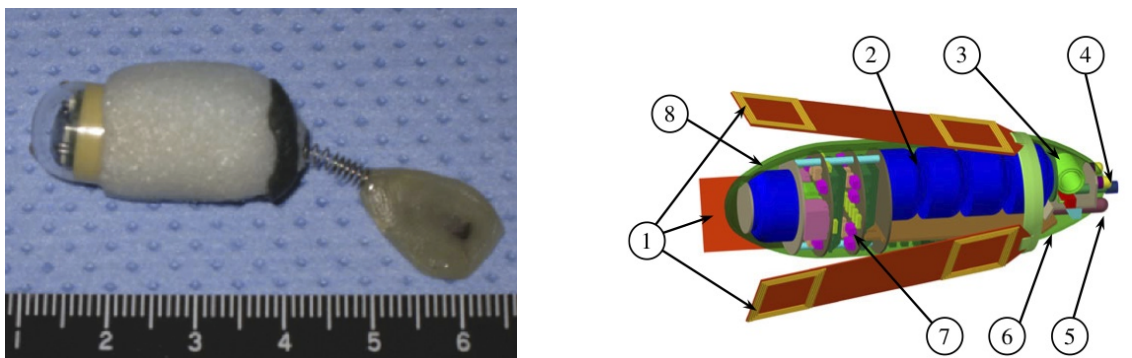
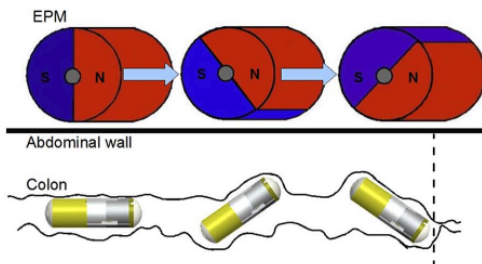


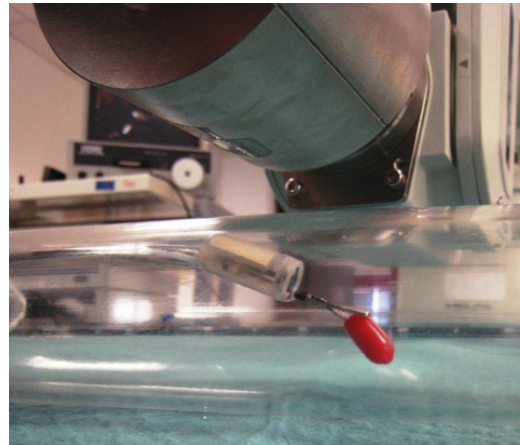
Figure 2.12: Magnetic propulsion for capsule endoscopy. (A) Morita *et al.*, (B) Kósa *et al.*.

A large external permanent magnet was preferred by the group of Paolo Dario at the Scuola Superiore Sant'Anna to guide magnetically different versions of capsule endoscopy, figure 2.13. This method is particularly applicable to explore intestines. A large diametrically magnetized NdFeB magnet of 60 mm in diameter and 70 mm in length was displaced and oriented either manually or robotically [Simi *et al.*, 2010, Valdastrì *et al.*, 2010, Valdastrì *et al.*, 2011]. Comparison between robotic versus manual magnetic steering is proposed by the same authors [Ciuti *et al.*, 2009]. These developments were mainly achieved in the framework of the European VECTOR project. The aim of this project is to develop intelligent endoscopic capsules using innovations in micro and nanotechnology for advanced diagnostics and therapy in the human digestive tract.

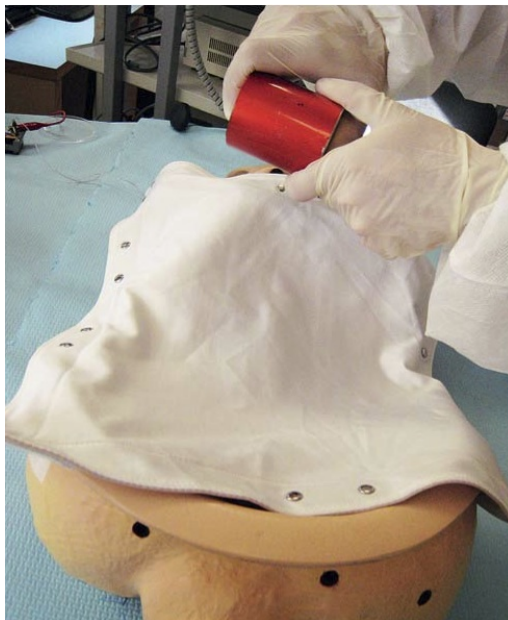
Magnetic steering with the help of a large steerable magnetic field was also studied for exploring the stomach. Carpi and Pappone demonstrated the possibility of achieving



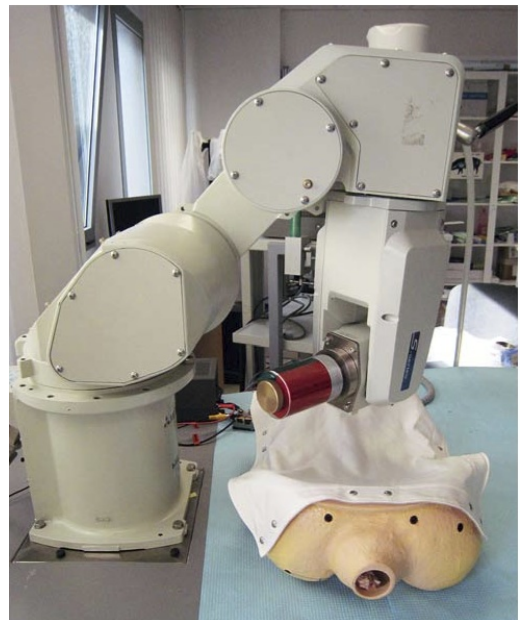
(A) Capsule endoscope pulled and tilted with an external magnet



(B) Magnetic Air Capsule (MAC) guided with an external magnet mounted on a robotic manipulator



(C) Manual control of the magnetic guidance



(D) Robotic control of the magnetic guidance

Figure 2.13: Capsule endoscopy with a large external magnet controlled manually or robotically, Scuola Superiore Sant'Anna.

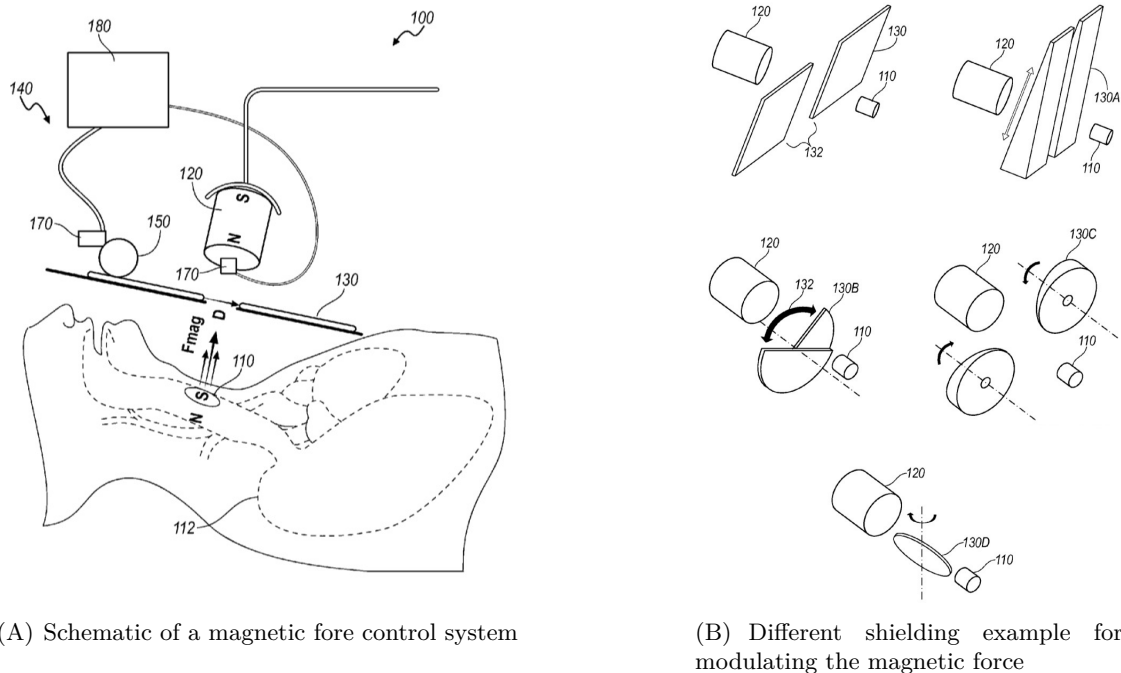
controlled magnetic manoeuvre in the stomach with a commercially available system currently used for cardiac catheterization (Niobe, Stereotaxis Inc.) [Carpi and Pappone, 2009].

Keller *et al.* reported a method of Magnetically Guided Capsule Endoscopy (MGCE) with an Olympus system currently under development [Keller *et al.*, 2012]. The system comprises six pairs of coils that are able to control the Olympus capsule in 5-DoF. A human clinical study has recently been achieved with this system.

Brewer *et al.* described a system for closed-loop force control of a permanent magnet using shielding materials [Brewer *et al.*, 2008]. The idea consists of inserting a highly-

2. Magnetic Anchoring and Guidance Principle: a State of the Art

permeable magnetic shielding material between the magnets, figure 2.14. The magnetic shielding reroutes the field lines between the magnets through the shielding itself, thereby reducing the magnetic flux that one magnet exerts on the other. The ideal shielding setup is to use a material that has high permeability to attract the field lines as well as a high saturation to reroute a large amount of magnetic flux. However, materials fulfilling both requirements are rare.



(A) Schematic of a magnetic force control system

(B) Different shielding examples for modulating the magnetic force

Figure 2.14: Method for guiding a medical instrument with magnetic force control, Brewer *et al.*. Labels: 110,120–magnet, 130A–D–magnetic shield.

2.2.4 Laparoscopic Applications

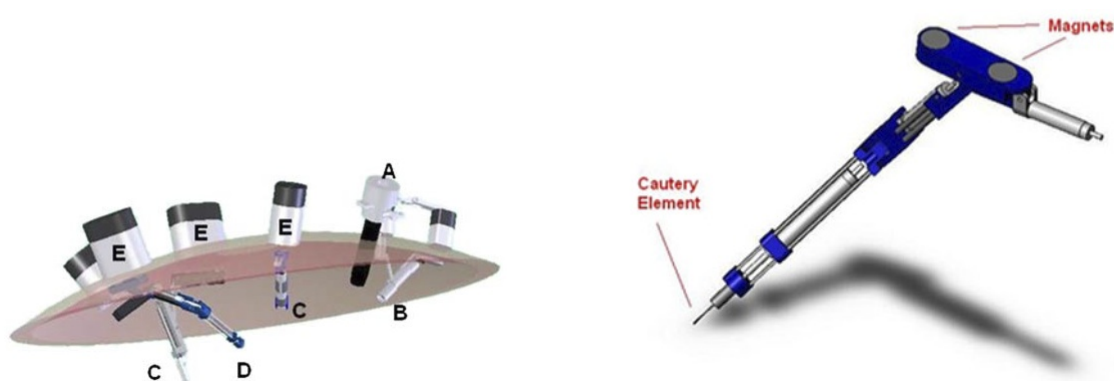
Advantages of laparoscopic surgery in comparison with open surgery are well recognized and are today the new standard for many procedures. Triangulation of the instruments is one of the main criteria in conventional laparoscopy. Several incisions are required to position correctly the instruments in order to facilitate the traction and anatomic dissection. Moreover, triangulation minimizes internal and external “sword fighting” of laparoscopic instruments. The main limitations in conventional laparoscopy are the fulcrum effect (inverted movement) of the instruments and the fixed working envelope around each incision. Although, current robotic systems can overcome some of these drawbacks, three to four incisions of 1 to 2 cm long are still required.

A new enthusiasm in the medical community is perceptible to reduce the invasiveness of laparoscopic surgery. In this context, Laparoendoscopic Single Site Surgery (LESS), also called “belly-button” surgery has been introduced. Moreover, Natural Orifice Transluminal Endoscopic Surgery (NOTES) intends to push back the frontier by using natural orifices (mouth, vagina or rectum) instead of external abdominal incisions. However, the new techniques are associated with a loss of triangulation and working envelope as well as the collision of instruments.

2.2 Magnetic Manipulation in Medical Instrumentation

To overcome these limitations, development of deployable intracorporeal instrumentation have been initiated. One approach consists of using internal magnetic instruments which can be coupled with an external hand-held magnet through the abdominal wall. Instruments are inserted through a unique incision, deployed in the abdomen and magnetically anchored or guided with an external magnet at an appropriate location.

Since 2002, Cadeddu and colleagues at University of Texas Southwestern Medical Center are developing Magnetic Anchoring and Guidance System (MAGS) for deployable instrumentations, figure 2.15. MAGS retractors, MAGS camera and MAGS cautery dissectors have been developed [Park et al., 2007, Raman et al., 2009, Best et al., 2010, Best and Cadeddu, 2010]. Several successful *in vivo* cases have also been reported [Cadeddu et al., 2009, Arain et al., 2011].



(A) Schematic representation of a MAGS platform. A–trocar, B–MAGS camera, C–retractors, D–robotic cauterizer and E–external magnets

(B) MAGS cautery dissector



(C) MAGS camera with two LED lights



(D) MAGS camera control with an external magnet. Camera wire exits through an abdominal single port

Figure 2.15: Magnetic Anchoring and Guidance System (MAGS) for deployable instrumentations, Cadeddu *et al.*

In the framework of the IMANLAP project, Dominguez *et al.* developed a novel way of using magnetic anchoring for retraction using magnetic forceps and grasper, therefore providing enough triangulation without additional incisions [Dominguez et al., 2009, Padilla et al., 2011, Martinez-Ferro, 2012]. This new technique gives the possibility of retraction

2. Magnetic Anchoring and Guidance Principle: a State of the Art

and triangulation from different angles as conventional multiple ports laparoscopy.

Kume *et al.* reported the successful use of a magnetic anchor for retraction during a proctectomy on pig [Kume et al., 2008]. Removal of the rectum is often required in case of rectal cancer.

Fakhry *et al.* showed that the use of the magnetic wireless camera coupled through the abdominal wall with an external handle is feasible and can provide a wider field of view than classical endoscope [Fakhry et al., 2008].

The group of Oleynikov at the University of Nebraska developed a dexterous, miniature robot with 6-DoF for NOTES surgery, that is anchored to the abdominal wall using an external magnetic handle [Lehman et al., 2008]. This attachment method enables the surgeon to reposition easily the robot in different regions of the abdomen.

2.2.5 Neurosurgical Applications

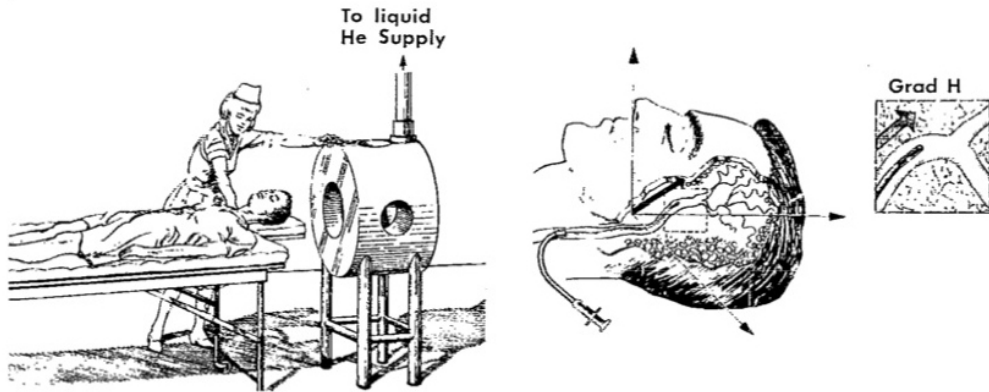
Research on magnetic catheterization was also introduced in the neurological field. Catheters were magnetically guided in the blood vessels of the brain in order to induce thrombosis of aneurysms or deliver drugs directly to the tumors. We can cite the POD catheter also developed for the brain by Hilal and Driller in the late 1960s [Driller et al., 1969]. The catheter was equipped at its tip with an Alnico permanent magnet of 0.7 mm in diameter and 3.0 mm long and was guided manually by an external hand-held Alnico magnet or electromagnet. This catheter could be advanced into the middle cerebral artery in human clinical trials.

Combining AC and DC fields, Molcho *et al.* used the POD catheter to deliver chemotherapeutic drugs in malignant brain tumors [Molcho et al., 1970]. Other versions of the POD were also used to occlude arteriovenous malformation with a detachable magnetic tip or to treat inoperable aneurysms [Hilal et al., 1974].

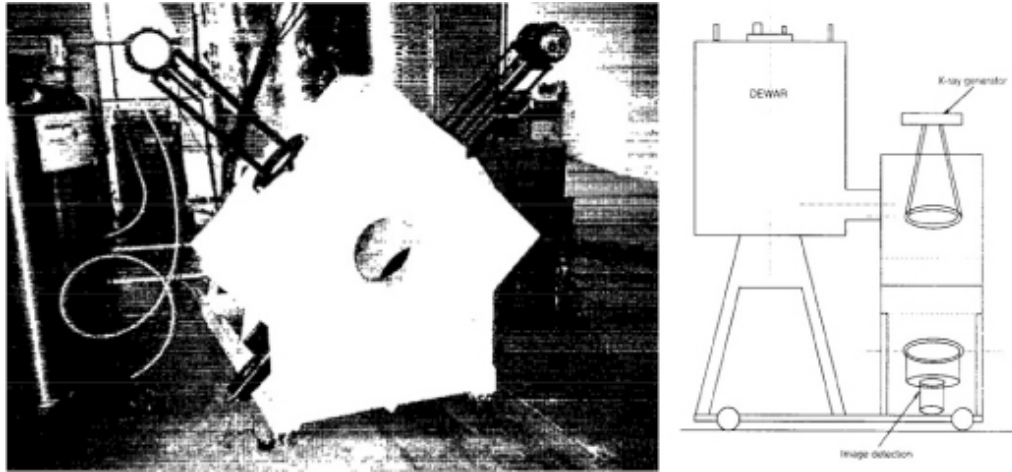
Magnetic guidance was also used in neurosurgical stereotaxis, a minimally-invasive technique introduced in the middle of last century. The technique consists of guiding a surgical probe through the brain, which is referenced to a fixed well-defined external frame. We can cite Montgomery *et al.* who developed the first Magnetic Stereotactic System (MSS) using superconducting coils for neurological use, especially for steering of magnetic catheters into cerebral vessels [Montgomery et al., 1969]. The system could exert an arbitrarily directed force of 200 times that of gravity on a tip anywhere within the head. It was composed of three pairs of orthogonal coils integrated into a cylindrical cryostat. The catheter could be steered in every direction by superposing the fields and gradients of each individual coil, figure 2.16(A). The fifth generation of the MSS system, a “six coils helmet” was improved by McNeil *et al.* [McNeil et al., 1995a, McNeil et al., 1995b], figure 2.16(B). These developments finally led to the commercialization of a MSS system by Stereotaxis Inc..

More recently, Krings *et al.* evaluated *in vitro* the Niobe system (Stereotaxis Inc.) to control the deflection of a microguidewire of 35 μm in diameter during the navigation along tortuous paths of the brain [Krings et al., 2006]. The microguidewire is equipped with a 2 mm long permanent magnet at the tip. The advantage compared to standard guidewire, is that it can be reshaped during the navigation without having to remove the guidewire from the body.

2.3 Magnetic Force Modulation Principle



(A) Illustrative conception of a Magnetic Stereotactic System for manoeuvring a catheter in the cerebrovascular system, Montgomery *et al.*, 1969



(B) The fabricated Magnetic Stereotaxis System coil and cryogenic arrangement, McNeil *et al.*, 1995. Mass of the entire helmet/coil system is around 1'300 kg

Figure 2.16: Magnetic Stereotaxis Systems.

2.3 Magnetic Force Modulation Principle

As seen in the previous section, examples of magnetic anchoring or magnetic guidance are various and applied in many medical fields. Anchoring systems represent the most elementary form of magnetic manipulation. A single external permanent magnet could be sufficient to attract, anchor or guide an object within the body. Guiding systems require more sophisticated magnetic designs and control algorithm. Magnetic fields and gradients are used to produce forces and torques on a magnetic element located inside the body. A static magnetic field generates a torque on a magnetic element while a magnetic gradient induces a translational motion, figure 2.17. By controlling these fields and gradients, the guided part can be moved in different locations of the body. If we consider a magnetic element placed in a magnetic field \mathbf{B} , a magnetic moment \mathbf{m} will be produced on the element either by a permanent magnetization or induction. For both cases, the magnetic force on the element is given by:

$$\mathbf{F} = \nabla(\mathbf{m} \cdot \mathbf{B}) \quad (2.1)$$

2. Magnetic Anchoring and Guidance Principle: a State of the Art

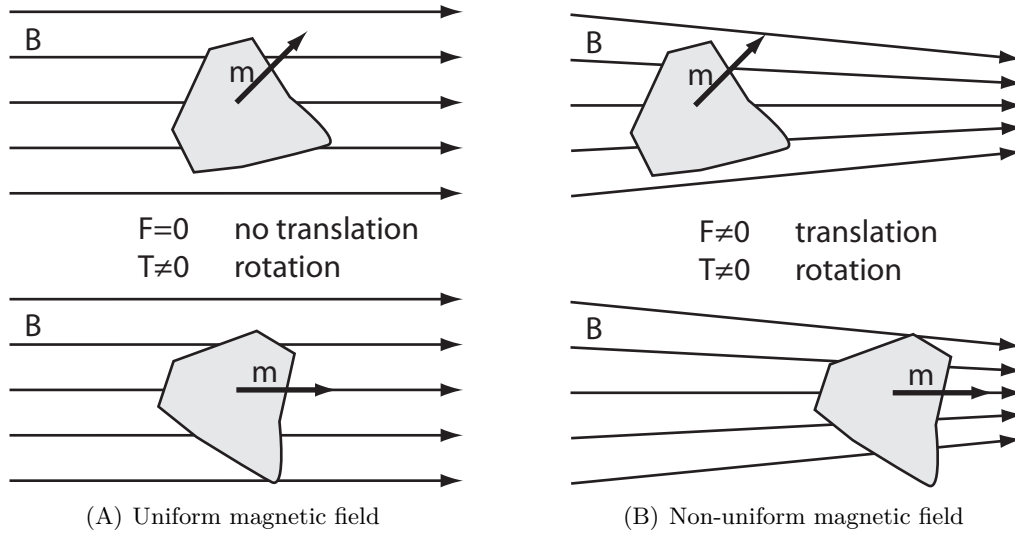


Figure 2.17: Forces and torques applied to a element of magnetic moment m under a external magnetic field. The magnetic field generates a torque T on the magnetic field while the magnetic gradient generates a force F which induces a translational motion in the direction of the field gradient.

In case of a permanent magnetization, a torque \mathbf{T} will tend to align the magnetic element parallel to the external magnetic field:

$$\mathbf{T} = \mathbf{m} \times \mathbf{B} \quad (2.2)$$

In case of an induced magnetic moment, the element will be automatically aligned along \mathbf{B} .

In summary, the modulation techniques for controlling and adjusting the magnetic interactions on the guided element are either achieved by means of electromagnets or permanent magnets.

2.3.1 Electromagnets

Electromagnets are an ideal solution for magnetic guidance due to the ability to control the strength, polarity and shape of the magnetic field. In addition, electromagnets produce AC or DC driving sources. As seen previously, an AC field can be, for example, the source of a magnetic propulsion used in POD catheter devices. A DC magnetic field produced by current flowing in a coil offers a simple way of modulating magnetic attraction with the guided part. When strong magnetic fields are required in a limited volume, supraconducting coils might be used as they accept much higher current densities. Generally, liquid-cooled coils are limited to a current density around 1'000 A turns/cm² as opposed to superconducting coils which can accept easily 30 times larger current densities. However, superconducting coils are not able to provide dynamic magnetic fields, as eddy current heating induced in the material surrounding the coils may create significant sources of heat. Electromagnets are also chosen for their safety. The magnetic field can be controlled without requiring any moving parts. Moreover, no fields are present when the coils are not powered.

2.3.2 Permanent Magnets

Permanent magnets are an alternative to electromagnets in magnetic guidance systems. They produce a constant field once they have been magnetized. The material composing the permanent magnet has a significant impact on the intensity of the magnetic field. Moreover, the material defines how the magnetic flux is affected by the temperature and how easily the magnet can be demagnetized when placed in an opposite magnetic field.

Permanent magnets can be classified in four main categories, from the weakest to the strongest, based on their composition:

- Ceramic or Ferrite
- Alnico: Aluminium-Nickel-Cobalt
- Rear-earth Magnets: Samarium-Cobalt (SmCo)
- Rear-earth Magnets: Neodymium-Iron-Boron (NdFeB)

General characteristics of the four types of permanent magnets are summarized in table 2.1.

Table 2.1: Characteristics of the types of permanent magnets.

Type	Advantages	Disadvantages
Ferrite	Very cheap, high operational temp. (280°)	Lowest magnetic energy (4.0 MGOe)
Alnico	Highest operational temp. (540°)	Demagnetizable by high magnetic field
SmCo	Powerful (32 MGOe), high op. temp. (300°)	Fragile
NdFeB	Highest magnetic energy (52 MGOe)	Fragile, limited operational temp. (80°)

MGOe: megaGauss Oersted

Permanent magnets have the advantage to be simple to use and are often chosen for magnetic anchoring functions. Using permanent magnets for guidance can become challenging due to their difficulty to provide a variable force on the guided element. The force acting on the guided part can be modulated by increasing the distance with the guided part or by changing the orientation of the external magnets. Therefore, modulating the magnetic force with reasonable bandwidth by moving these external magnets would be very difficult due to their large size and inertia. Permanent magnets are influenced by highly-permeable ferromagnetic material in their vicinity. Shielding material attracts the field lines and therefore can reduce the magnetic attraction that one magnet exerts on the other. However, this method may be limited by the saturation of the material, namely its ability to conduct magnetic flux.

2.4 Magnetic Anchoring and Guidance System

Acronyms defining the concept of magnetic guidance or anchoring are abundant in the literature. In order to facilitate the comprehension, we propose to use the acronym MAGS in this dissertation. MAGS stands for Magnetic Anchoring and Guidance Systems. Although this acronym was introduced by Cadeddu *et al.* to describe the deployable magnetic laparoscopic instruments, the term is broad enough to cover any type of magnetic devices providing an anchoring and/or a guiding function.

2. Magnetic Anchoring and Guidance Principle: a State of the Art

In this sense, MAGS could be defined as a system consisting of two magnetic elements separated by a piece of tissue (the abdomen for example), where one internal element could be temporarily anchored or guided with the help of a second element that is generally external but can also be internal, as illustrated in figure 2.18.

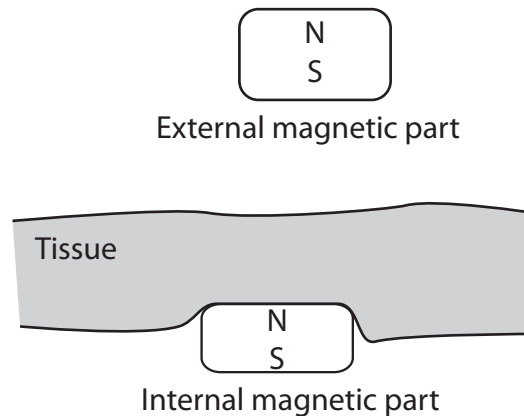


Figure 2.18: MAGS: Magnetic Anchoring and Guidance System.

MAGS could be classified into the following categories based on their functions and principles:

- Magnetic Anchoring Systems
- Magnetic Guiding Systems:
 - Magnetic Navigation
 - Magnetic Propulsion
 - Magnetic Steering
 - Magnetic Traction

2.4.1 Magnetic Anchoring Systems

Magnetic anchoring devices are generally simple. The anchoring function is provided either by an external hand-held electromagnet or a permanent magnet placed on the surface of the body. The coupling force is controlled generally by choosing the right combination of magnets depending on the separation distance, namely the abdomen wall thickness.

2.4.2 Magnetic Guiding Systems

Systems providing magnetic guidance are usually complex and large and are surrounding the patient. The term guidance is of extensive use as it includes the magnetic navigation of elements in hollow space, the steering of catheters as well as dragging of endoscopic capsules in the intestines. Magnetic navigation requires a complex and precise control of the magnetic field directions and gradients. Electromagnets are the most suitable solution for navigation. Magnetic propulsion of the guided part is achieved by orienting or rotating the magnetic fields. Varying the field direction is generally sufficient for steering and aligning the tip catheter with the magnetic field lines. Permanent magnets represent a good alternative for this purpose but electromagnets are more commonly used in practice. Magnetottractive forces to pull or drag a guided part within the body can be achieved with

an external hand-held electromagnet or a permanent magnet manoeuvred manually or remotely above the surface of the body. The “contactless” magnetic effect on the internal guided part is the common point of these external guiding systems.

2.5 Intracorporeal Magnetic Anchoring and Guiding Systems

The aim of this thesis is to evaluate the technical feasibility of an intracorporeal magnetic guiding system. As an alternative solution to large and complex guiding systems surrounding the patient or to manual external magnet with limited magnetic effect, we propose a system able to perform the guidance locally, on-site, by having the guiding part also inserted inside the body.

We believe that on-site guidance is particularly applicable for cardiovascular applications such as the treatment of cardiac arrhythmias due to the presence of numerous vessels around the cardiac muscle. Radiofrequency catheter ablation has become a commonly used and well established procedure to provide a therapeutic option for many patients [Scaglione et al., 2011]. Radiofrequency catheter ablation consists of inactivating abnormal electrical pathways in the heart. These procedures are extremely challenging due to difficult manipulation of the catheter in a very dynamic environment as well as the limited systems for internal visualisation. We believe that an intracorporeal magnetic guiding system could facilitate the positioning and guidance of catheters on the beating cardiac tissue. More details of potential applications are given in chapter 8.

2.5.1 Prior Investigation

The achievement of intracorporeal magnetic guidance is strewn with technical obstacles. The first question we investigated concerns the magnetic force required to insure a coupling of the Magnetic Anchoring and Guidance System (MAGS) at a millimetric scale. Although the separation distance within the MAGS is reduced to one or two centimeters, the required magnetic field is significant. Therefore what are the methods to generate sufficient magnetic field within the body?

Electromagnets are an ideal solution for modulating the magnetic field. However, obtaining substantial magnetic field strength becomes challenging at small scale. Resistive heating by electromagnets is an additional drawback.

Rare-earth magnets such as NdFeB magnets produce strong magnetic fields and become interesting when size is limited. Permanent magnets have the advantage of not requiring any control electronics to produce a magnetic field. However, the magnetic field is constant and the resulting magnetic interactions with the guided part are dependent of the separation distance as well as the orientation of the MAGS members.

Magnetic forces achievable with air-coil electromagnets and permanent magnets were investigated with Finite Element Modelling (FEM). Due to the use of curved magnetic elements and side by side configuration, an analytical approach to calculate the magnetic force becomes very complex. The ideal direction of the magnetization of the magnets was also studied, as well as different types of magnetic configuration.

Considering a separation distance of several millimeters, numerical analysis shows that a pair of permanent magnets provides higher attraction forces over electromagnets or a pair of permanent magnet – soft iron material. Moreover, diametrical magnetization in

2. Magnetic Anchoring and Guidance Principle: a State of the Art

comparison with axial magnetization of the magnets provides not only higher magnetic attractions, but are also less subject to repulsion when slightly misaligned. Misalignments of the MAGS occur naturally during magnetottractive guidance as the dragging force, responsible of guidance, appears only when the magnets are misaligned. It may be understood that axial magnetization of the magnets is easily subject to magnetic repulsion during guidance. The magnetic poles are located at the extremities of an axially magnetized permanent magnet. When two magnets are aligned, the field lines exit, by convention, the north pole of one magnet and enter the south pole of the opposite magnet. When a large axial misalignment occurs during the guidance, for example, due to anatomical variation, extremities of the magnets do not face attractive poles but rather tend to face repulsive poles. Therefore, this may lead to the decoupling of the catheters.

Based on these findings, prototypes of catheters were produced and tested *in vitro* as well as *in vivo* on porcine models. Magnetic guidance of magnetic catheters equipped with simple permanent magnets of the right size was easily achievable *in vitro* on constant tissue thickness of few millimeters. However, reproducing similar guidance on a beating heart was limited to short distance of guidance and frequently associated with stick and slip phenomenon. These limitations are most likely attributed to inadequate coupling forces resulting from anatomical variations and experimental conditions. On one hand, the magnetic catheters should be powerful enough to be automatically attracted and coupled when brought in close vicinity. On the other hand, once they are coupled and sandwiching the tissue, their magnetic attraction as well as the resulting friction with tissue may be too strong to allow a proper guidance.

At that stage of experimentation, we concluded that intracorporeal guidance of catheters equipped with simple permanent magnets is limited to constant tissue thickness and therefore hardly achievable on tissue varying in thickness or in frictional properties.

Consequently, the working hypothesis for this dissertation is based on the fact that the magnetic fields within the MAGS should be adjustable in order to provide a constant guiding force independent of tissue irregularities and thickness variation.

To overcome these hurdles, we present in the following chapters different solutions of modulating the magnetic attractions between two magnetic elements in close vicinity. Furthermore, we focus our analysis on intracorporeal guidance with force modulation by means of steerable permanent magnets.

2.6 Summary

As seen in this chapter, examples of magnetic anchoring and magnetic guidance are numerous and applied in many fields of medicine.

Magnetic anchoring devices are generally simple. An external hand-held electromagnet or a permanent magnet placed on the surface of the body is sufficient to provide a temporarily anchoring function. The coupling force is controlled generally by choosing the right combination of magnets depending the abdomen wall thickness.

Systems providing magnetic guidance are usually more complex and large and are surrounding the patient. The “contactless” magnetic effect on the internal guided part is the common point of these external guiding systems. Magnetic navigation requires advanced and precise control of the magnetic field directions and gradients. Electromagnets are the most suitable solution for navigation. Magnetic propulsion of the guided part can be achieved by orienting or rotating magnetic fields. Magnetic steering of catheters is

achieved with permanent magnets or electromagnets. Magnetottractive guidance of guided part within the body can be achieved with an external hand-held electromagnet or a permanent magnet manoeuvred manually or remotely above the surface of the body.

As an alternative solution to large and complex guiding systems, we propose a system able to perform the guidance locally, on-site, by having the guiding part also inserted inside the body. We believe that on-site guidance could particularly facilitate the positioning and guidance of ablation catheters in the treatment of cardiac arrhythmias due to numerous presence of vessels around the cardiac muscle.

3 Magnetic Force Modulation at Small Scale

Magnetic Anchoring and Guidance Systems (MAGS) require variable, reshapable or steerable magnetic fields which are generally associated with large and complex arrangements of coils or permanent magnets surrounding the patients. Such magnetic systems require elaborated control algorithms and are operated remotely from a control room. We can cite, for example, the Niobe-Stereotaxis system for cardiac arrhythmias management by ablation catheter [Faddis et al., 2002] or an industrial robot controlling a large external permanent magnet to guide an endoscopic capsule in the digestive tract [Ciuti et al., 2009]. More details and examples can be found in chapter 2. The common point of these guiding systems is their ability to provide a “contactless” magnetic effect on the internal guided part deep inside the body.

To the best of our knowledge, no existing devices offer active intracorporeal magnetic guidance where both components are inserted inside the body. As previously mentioned, this thesis is closely connected with the development of a novel magnetic master-slave system, consisting of a catheter system to treat cardiac arrhythmias [Verin and Sandtner, 2008], [Verin and Flaction, 2011]. The catheters are equipped with permanent magnets (PM) and are sandwiching the cardiac tissue. The catheter inside the heart can be displaced with the help of a second catheter in close vicinity to the heart. The control of the magnetic force and dragging of the catheter ablation tip, over the cardiac tissue, are key points for the success of this application.

The aim of this chapter is to present different methods of modulating magnetic attractions between two magnetic means of a size compatible with minimally-invasive devices, such as for example ablation catheters. Electromagnets are an ideal solution because of the ability to control the strength, polarity and shape of the magnetic field. However, obtaining substantial magnetic field strength becomes challenging at small scale. Rare earth magnets produce strong magnetic fields and become interesting when size is limited. However, they produce a constant field. Combining permanent magnets together or with other ferromagnetic material can modify the magnetic field generated with such arrangements. Different concepts of modulators varying the magnetic field, namely the attraction force in the MAGS are detailed and compared in this section.

3.1 Magnetic Modulation Principles

3.1.1 Motivation

MAGS propose a magnetic anchoring and/or a guidance of a guided object. The current state of the art shows the absence of modulation principles in the “anchoring” group of MAGS and the use of large modulation principle for the “guidance” group of devices. The modulation of the magnetic field, respectively the magnetic attraction between the two magnetic members, has several advantages:

- **Improved navigation:** Controlling the magnetic field direction, intensity or both help in the guidance of a magnetic member inside the body. However, the existing modulation systems act mainly on orienting the direction of the magnetic field rather than on its amplitude [Faddis et al., 2002, Ciuti et al., 2009].
- **Adequate coupling force:** An excessive force may lead to tissue damage [Best and Cadeddu, 2010]. On the other hand, a weak force could lead to disconnection of the MAGS.

In the case of intracorporeal MAGS, where both magnetic parts are inserted inside the body, the modulation of the magnetic coupling force may provide the following benefits:

- **Optimal coupling and dragging force:** Modulating the magnetic field has the advantage of providing the right level of attraction forces between the magnetic members. Anatomical variations of the tissue during the guidance result in a change of the coupling strength between the magnetic parts. A reduction of tissue thickness could lead to high frictional interactions between the device and the tissue. On the other hand, an increase of thickness could lead to insufficient dragging force. In both cases, a passive guidance is limited to fixed anatomical conditions.
- **Coupling of the MAGS:** A strong magnetic field is required to easily couple the two magnetic elements inside the body, but once sandwiching the tissue, their magnetic attraction may be reduced to allow the dragging of the guided element.
- **Safe navigation:** When the MAGS is introduced into the body, the risk of having both magnetic members in very close vicinity is not negligible. If both magnetic components are composed or partially composed of permanent magnets, a high attraction force could lead to the perforation of the tissue or to a hazardous situation for disconnecting the two members. Therefore, being able to reduce the attraction force by modulating the magnetic field represents a considerable safety measure.

3.1.2 Implementation

Magnetic fields are produced by electric currents, which can be macroscopic currents in wires, or microscopic currents associated with electrons in atomic orbits. Electromagnets are an ideal solution because of the ability to control the strength, polarity and shape of the magnetic field. However, the efficiency of electromagnets is reduced at small scale when the size is limited. Obtaining a substantial magnetic field strength is difficult due to excessive heat generated by Joules effect and the limited available volume to produce sufficient magnetomotive force (ampere-turn).

Permanent magnets provide a constant field, which can be influenced by the presence of ferromagnetic materials or by mechanically changing the orientation of the magnet.

3.1 Magnetic Modulation Principles

Differences between electromagnets and permanent magnets are summarized in table 3.1.

Table 3.1: Comparison between electromagnets and permanent magnets.

Electromagnet	Permanent magnet
Varying strength	Fixed strength
Variable field	Permanent field
Complex geometry	Simple geometry
Requires energy	No energy needed
Stronger at big scale	Stronger at small scale
Produce heat	Sensitive to heat
Expensive, few hundreds of CHF	Cheap, few CHF
Electronically controllable	Mechanically controllable

Developing an intracorporeal MAGS, where both magnetic members are inserted into the body, requires a maximum magnetic field strength in a minimum volume. Permanent magnets, such as rare earth magnets, are better candidates than electromagnets in this context. However, one may wonder how the magnetic attraction in the MAGS, composed of permanent magnets, can be varied? The following section presents solutions to modulate the magnetic field between two members of a MAGS using ferromagnetic materials. These solutions can be divided in two categories:

- Separation distance modulation
- Magnetic field modulation

3.1.3 Methodology

Force modulation concepts are described and compared under the same design specifications. These specifications take into consideration the manufacturing feasibility of such designs. The treatment of cardiac arrhythmias by magnetic coupled catheters is the chosen application to illustrate and compare the proposed modulators.

As shown in section 2.5.1, diametrically magnetized magnets offer better guidance than axially magnetized magnets. Therefore, a parallel coupling of the MAGS members is mainly considered for the design of the modulators. The maximum diameter for the active catheter, namely the guiding member, is 5 mm and for the passive catheter, namely the guided member, is 3.5 mm. The active catheter should contain at least two temperature sensors on its surface as well as an inner lumen. Temperature sensors, such as thermocouples, are used to monitor with precision, the tissue temperature during the radio-frequency ablation of the tissue. The inner lumen is used to pass a guidewire in order to facilitate the introduction of the active catheter in different vessels of the heart. Therefore, the available volume for the magnetic force modulator, in the tip of the active magnetic member, is most likely to be (depending on the design) a cylinder of 4 mm in

3. Magnetic Force Modulation at Small Scale

diameter and 10 mm in length (4x10 mm). This volume should comprise the magnetic material and mechanical components for the actuation of the modulator. The passive magnetic tip comprises a single cylindrical permanent magnet of 3x10 mm. The distance separating the two magnetic means varies in the millimetric range, typically from 2 to 10 mm. For the analysis, the separation distance is set to 5 mm between the outer surfaces of the magnetic means, which corresponds to a reasonable separation distance for guidance in the cardiac vessels.

Permanent magnets are made of Neodymium-Iron-Boron alloys (NdFeB). The magnets are diametrically magnetized with a magnetization of 1'115 kA/m or with a magnetic energy density of 52 MGOe (414 kJ/m³). Electrical steel, permalloy or mu-metal can be used as ferromagnetic material for the electromagnet core and shield modulator. The relative permeability of these materials is $\mu_r=4'000$, 50'000 and 100'000 respectively.

Knowledge of the magnetic interactions occurring in MAGS during guidance is essential in the development of magnetic force modulator. Analytical calculation of the magnetic forces and torques are limited to basic geometries of magnets and well defined external magnetic field [Tunay, 2004, Abbott et al., 2007, Vokoun et al., 2009]. Due to the curved surfaces of the magnetic parts as well as the complex shaped of the magnetic gradients, analytical calculation of the magnetic forces is too complex and unrealistic. A Finite Element Method (FEM) software — Comsol Multiphysics 4.2, was used for the magnetic analysis of each modulator. All the designs were simulated in 2- and 3-dimensions using the Magnetic Fields interface from AC/DC module, stationary solver and tetrahedral meshing elements.

Normalization

The attraction forces in the MAGS, presented in the figures of this chapter, are normalized to a reference fixed permanent magnet occupying the available volume of the force modulator (4x10 mm). The reference considers a parallel coupling of the magnetic members and provides an upper limit for the maximum possible coupling strength between the magnetic tips at this size. In addition, this relative comparison gives an indication of the decrease in the maximum coupling strength by having a modulator, in comparison with no modulation. In others terms, it quantifies the decrease in the coupling force of the MAGS due to the implementation of a modulation function.

3.2 Separation Distance Modulation

The magnetic field falls off inversely with the distance from its poles. Following this physical law, forces between the MAGS components can be modulated by varying the distance between the magnets. Adjusting the coupling force this way is dependent on the MAGS design and operating conditions.

The following concepts of modulators consist of displacing a permanent magnet inside a MAGS member tip.

3.2.1 Displacement of Permanent Magnets

The displacement of a permanent magnet inside a MAGS member tip can be achieved either axially, namely along the axis of the member, or radially, namely perpendicular to the axis of the member.

3.2.1.1 Axial Displacement

Concept

Figure 3.1 illustrates how the magnetic field strength can be modulated by varying the separation distance between two cylindrical permanent magnets composing the MAGS. A movable cylindrical permanent magnet, axially magnetized, is displaced inside the tip of the lower member. Magnet shapes and magnetization direction are here to illustrate the concept. The displacement can be achieved by various methods, as explained in section 3.4. A displacement along the axis direction of the MAGS member implies a perpendicular magnetic coupling of the members, namely a T-shaped configuration. This configuration may require more space to be achieved, which is not always possible and depends on the specific application.

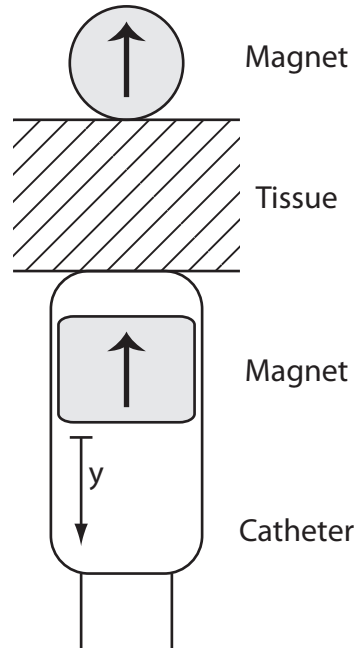


Figure 3.1: Coupling force modulation by varying the separation distance between the permanent magnets. A cylindrical magnet axially magnetised is displaced along the y -axis. This configuration requires perpendicular coupling of the MAGS members, that it to say magnetic catheters sandwich the tissue in T-shaped configuration.

The range of displacement y of the movable magnet is given by:

$$y \in [0, l_{mod} - l_{mag}], \quad l_{mag} < l_{mod} \quad (3.1)$$

where

l_{mag} : Magnet length

l_{mod} : Modulator length

3. Magnetic Force Modulation at Small Scale

Magnetic Analysis

Figure 3.2 shows the coupling force acting in the MAGS versus the magnet axial displacement. The horizontal line represents the maximum coupling force, in the perpendicular configuration of the MAGS, when the magnet occupies the whole space (4x10 mm) of the modulator. Coupling the MAGS perpendicular instead of parallel orientation induces a decrease of 22% for the coupling force according to the results. The decrease in the maximum coupling strength for the three magnet lengths is : 55% (2.5 mm), 36% (5.0 mm) and 27% (7.5 mm).

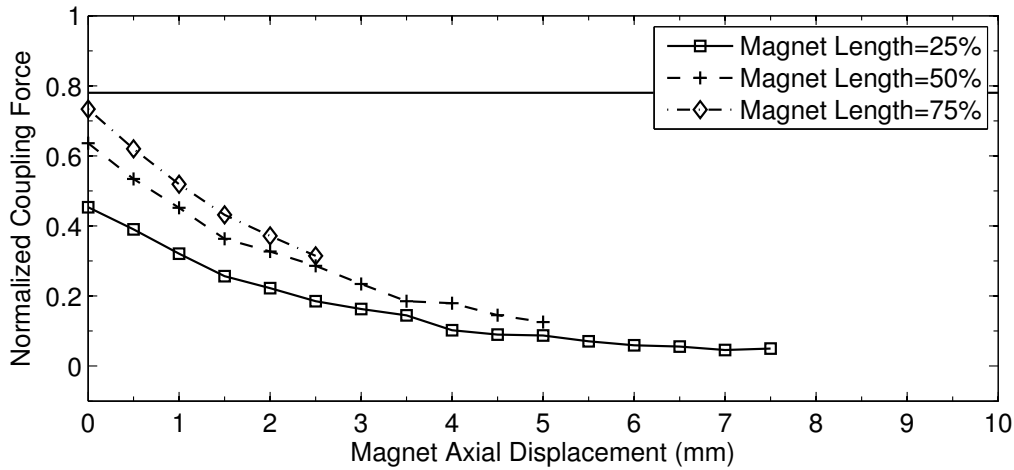


Figure 3.2: 3-dimensional FEM results of the coupling force as a function of the axial displacement of the magnet and its length. The displacement range is related to the magnet length. The horizontal line represents the maximum coupling force, in the perpendicular configuration of the MAGS, when the magnet occupies the whole space (4x10 mm) of the modulator. Legends: Magnet Length= 25% means magnet length=2.5 mm, displacement=[0,7.5] mm.

3.2.1.2 Radial Displacement

Concept

Figure 3.3 shows how the magnetic field strength can be varied by changing the separation distance of the permanent magnets composing the MAGS. Modulator a) uses a steerable off-center non magnetic tube to adjust the separation distance and therefore the attraction forces between the magnets. As the magnets are diametrically magnetized, the lower magnet will most likely stay aligned with the upper magnet during its displacement, if the magnetic torque acting on the magnet is larger than the friction with the inner surface of the tube.

The position of the magnet within the modulator (x, y) as a function of the rotation angle θ may be written as follows:

$$\begin{pmatrix} x \\ y \end{pmatrix} = \Delta r \begin{pmatrix} \sin \theta \\ \cos \theta \end{pmatrix} = \frac{(D - d)}{2} \begin{pmatrix} \sin \theta \\ \cos \theta \end{pmatrix}, \quad d < D \quad (3.2)$$

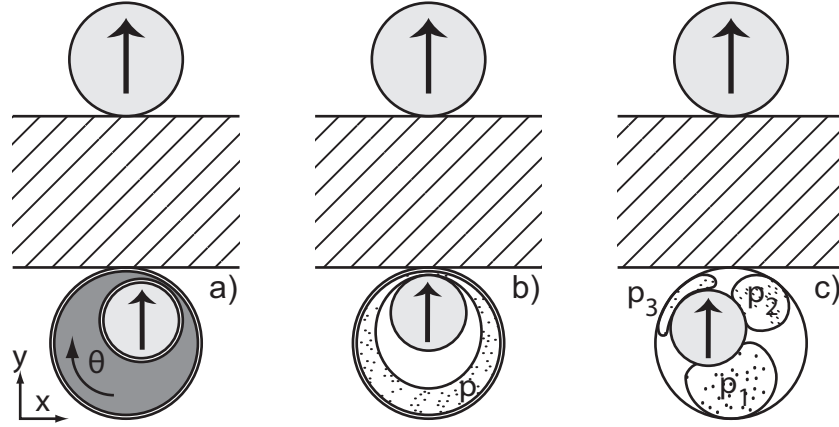


Figure 3.3: Coupling force modulation by varying the separation distance between the permanent magnets. The magnetic members of the MAGS are coupled in parallel. a) Steerable off-center tube. b) Inflatable tubular balloon around the magnet. c) Three inflatable balloons.

where

D : Diameter of the off-center tube

Δr : Position of the off-center hole in the tube

d : Diameter of the magnet

The maximum displacement range Δd corresponds to $(D - d)$. Intuitively, one may think that a trade-off exists between the modulation range and the maximum amplitude of the coupling force, as the displacement range is related to the magnet diameter. In fact, the magnet diameter defines mainly the maximum coupling strength and not the range of modulation as shown in figure 3.4. One potential drawback of this design is the lateral force generated during the steering of the tube. The same configuration is also possible with two axially magnetized magnets. However, the coupling force is slightly inferior. Other shapes such as hemicylindrical or oval are possible for the movable magnet. However, such magnets should be axially magnetized to avoid any unwanted rotation of the magnetic field during the displacement.

Modulator b) employs a tubular balloon around the magnet. The magnet is centred inside the tip by controlling the pressure applied into the balloon. Applying a pressure higher than the pressure exerted by the magnet on the balloon causes a centring of the magnet. The range of displacement y of the magnet is:

$$y \in \left[0, \frac{(D - d)}{2} \right], \quad d < D \quad (3.3)$$

The range of displacement is half the range of configuration a). A potential drawback of modulator b) concerns the precise positioning of the magnet. The position of the magnet in the balloon resulting from the equilibrium of pressure is affected by the variation of tissue thickness or irregularities. This limitation can be overcome by using a liquid instead of a gas inside the balloon.

Modulator c) is a variation of modulator b). Replacing the tubular balloon by three (or two) expendable balloons increases (double) the range of displacement as the movable

3. Magnetic Force Modulation at Small Scale

magnet could be displaced inside the inner diameter of the tip. However, the complexity of the control increases since different values of pressure and/or volumes have to be handled.

The proposed designs of figure 3.3 have the advantage to offer a parallel coupling of the MAGS regardless of the orientation of the tips. This is achieved by considering that diametrically magnetized permanent magnets may be free to rotate inside the tips to provide always the maximum possible attraction force for a given distance.

Magnetic Analysis

Figure 3.4 shows the coupling force acting between the two magnetic means of the MAGS for the concept using an off center tube to displace the magnet radially, figure 3.3 a). The modulation range of the coupling force is similar for the different configurations and represents only 20% of the maximum normalized force. This design offers a very limited range of modulation. It is interesting to notice that decreasing the diameter of the magnets in order to increase the range of displacement has negligible effect on the modulation range. Modulation range and coupling force can be deduced from these results in order to be applied to the designs using one or more balloons, figure 3.1 b) and c). The lateral force generated during the steering of the tube can be considered as negligible in comparison to the coupling force and therefore has minimum influence on the guidance behaviour.

3.3 Magnetic Field Modulation

As seen in section 3.2, the magnetic attraction between two permanent magnets can be achieved by varying the separation distance between the magnets of the MAGS. Another approach consists of changing the magnetic field of a permanent magnet by either adding an external field (electromagnet) or combining several movable permanent magnets or using ferromagnetic materials to contain the field locally (shielding).

3.3.1 Electromagnets

Concept

Figure 3.5 shows an electromagnet composed of a ferromagnetic core surrounded by a coil. A diametrically magnetized permanent magnet could also be used for the core. The coil is oriented in such a way to produce a diametrical magnetic field. The upper magnetic part is a permanent magnet diametrically magnetized. Therefore, an attraction with the ferromagnetic core of the electromagnet is present even in the absence of electrical current. The magnetic field produced by the current flowing in the coil either increases or decreases the attraction force in the MAGS. One important drawback of the electromagnet is the heat generated by Joule effect that may be calculated according to:

$$P = RI^2 = \frac{\rho l}{A} I^2 \quad (3.4)$$

where

ρ : Static resistivity

l : Length of the wire

I : Current in the coil

A : Cross-sectional area of the wire

3.3 Magnetic Field Modulation

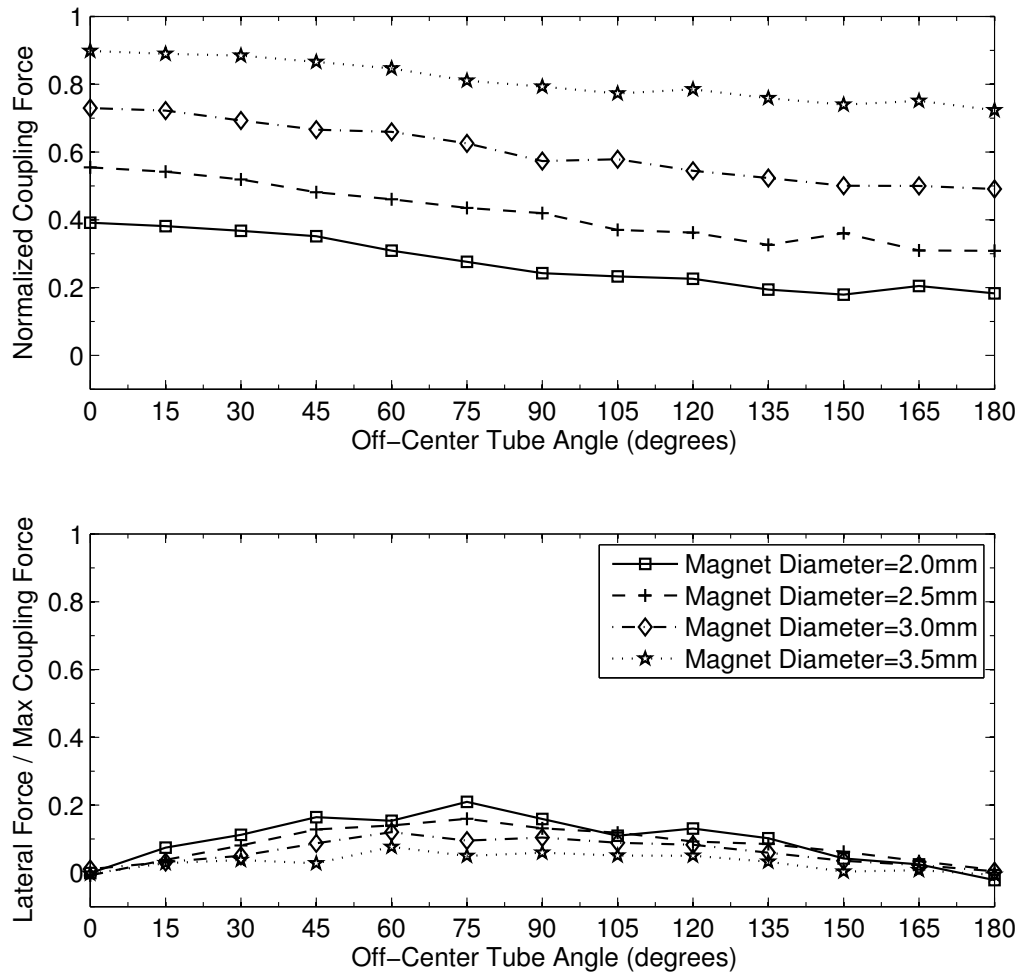


Figure 3.4: 3-dimensional FEM results of the coupling force in function of the radial displacement of the magnet and of its diameter. The displacement range is related to the magnet diameter. The magnet diameter defines mainly the maximum coupling strength and not the range of modulation. The modulation range of the coupling force is similar for the different configurations and corresponds to only 20% of the maximum normalized force.

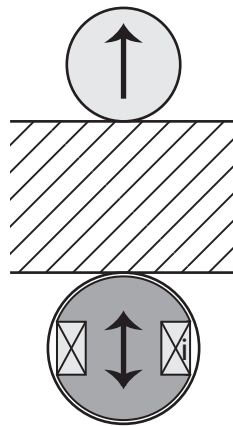


Figure 3.5: Electromagnet: Combination of a ferromagnetic core surrounded by a coil where a flow of electric current produces a magnetic field along the axis of the coil.

3. Magnetic Force Modulation at Small Scale

Another limitation of this concept is in the coupling orientation. Only two orientations are possible: a) the coil axis is aligned with the passive permanent magnet and b) the passive magnet is free to rotate inside the tip of the guided member. The modulator orientation should be kept constant during the guidance.

Magnetic Analysis

Figure 3.6 shows the coupling force between the two magnetic members of the MAGS for the case of an electromagnet composed either of an iron core or a permanent magnet core. The decrease of the maximum achievable coupling force with an electromagnet of this size and at 200 ampere-turns is 8% lower for the permanent magnet core and 77% lower for the iron core. Moreover the modulation range is very limited: 8% for the permanent magnet core and 26% for the iron core. A magnetomotive force of 200 ampere-turns is achievable with a current of 1 A flowing in a copper coil made of $1 \times 2 \text{ mm}^2$ cross-section made with a wire of 0.1 mm in diameter. One ampere is the maximum allowed current for a wire of this dimension. Applying equation 3.4 for the proposed configuration gives a generated heat of $\sim 10 \text{ W}$.

At small scale, the range of force modulation permitted by the iron core electromagnet is too small to be considered as a working alternative. Replacing the ferromagnetic core by a permanent magnet will not improve the magnetic performances. It will only increase the coupling strength, not the modulation range. However, the coil could be used in a state to generate attractive or repulsive magnetic pulses depending on the core. These pulses may reduce the frictional interactions with the tissue and may improve the guidance due to a possible vibrating effect on the guided part. However, achieving an efficient vibrational state on the guided part is hindered by the damping properties of soft tissue. Moreover, the guidance with such a modulator stays limited to a rather constant tissue thickness as the coil cannot achieve an important continuous force due to resistive heating and current capacity of the coil.

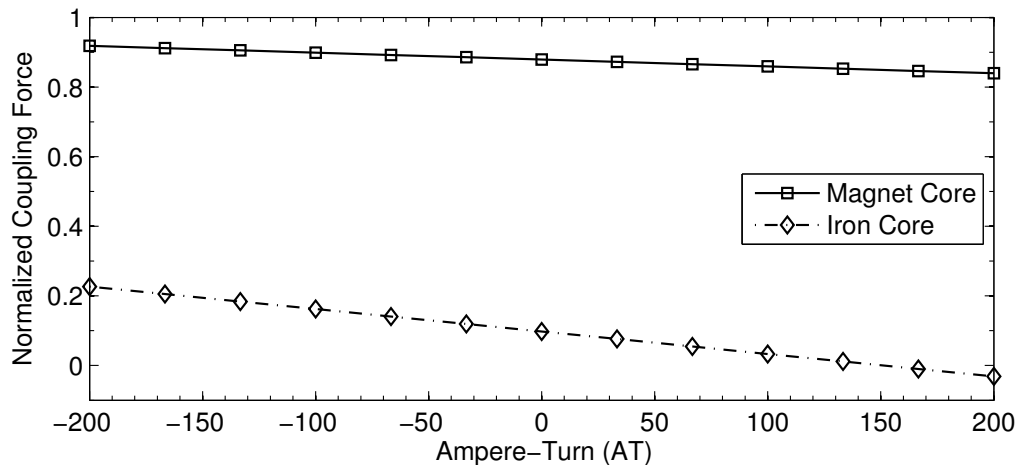


Figure 3.6: 3-dimensional FEM results of the coupling force as a function of the magnetomotive force (ampere-turn). The force is normalized to a reference fixed permanent magnet occupying the available volume of the modulator.

3.3.2 Rotation of Permanent Magnets

An original approach of modulating the magnetic attraction in the MAGS is to utilize additional movable magnets in order to vary the overall magnetic field of the modulator. The use of several permanent magnets to generate and modulate the perceived magnetic force has the benefit to provide strong magnetic field at small scale compared to other solutions, such as the implementation of electromagnets. However, as permanent magnets provide constant fields, the attractive or repulsive forces between the magnetic parts of the modulator generates high mechanical constraints which should be addressed in the design of the modulator.

The proposed designs are divided in two categories referring to the disposition of the magnets:

- Parallel magnets arrangement
- Coaxial magnets arrangement

3.3.2.1 Parallel Magnets Arrangement

Concept

Figure 3.7 shows how the magnetic field is modulated using two parallel magnets diametrically magnetized. The direction of the field is changed by steering the magnets simultaneously in opposite direction, figure 3.7 a).

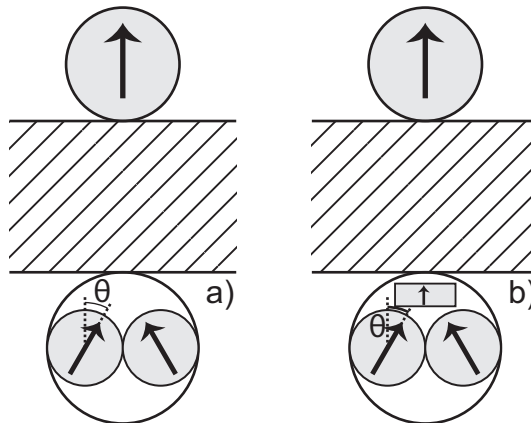


Figure 3.7: Arrangement of parallel permanent magnets to modulate the magnetic field. The coupling force is adjusted by steering the cylindrical magnets simultaneously in opposite direction. a) Two steerable diametrically magnetized permanent magnets. b) Two steerable diametrically magnetized magnets plus one static vertically magnetized magnet, which boosts the maximum coupling strength of the MAGS.

Due to the symmetrical rotation of the magnets, the field is modulated along the vertical axis without creating undesired lateral forces between the MAGS members. However, significant space is lost. The addition of a third magnet increases the maximum attraction force in the MAGS, without impeding the possibility of generating a repulsive magnetic field. A potential limitation of these modulators is in the coupling orientation. As far as the passive magnet is free to rotate inside the tip of the guided member, the coupling of the magnetic elements is possible for two tips orientations for the concept a), and limited to a unique orientation for the concept b). The orientation of the modulator should be kept constant to insure a robust guidance.

3. Magnetic Force Modulation at Small Scale

Magnetic Analysis

The basic principle for these two modulators is to steer two identical permanent magnets (2x10 mm) simultaneously in opposite directions to modulate the attraction force between the magnetic parts. To increase the attraction force, a static permanent magnet (0.8x2x10 mm) is placed along the modulation axis.

Figure 3.8 and figure 3.9 illustrate how the magnetic field flows and changes between the two magnetic members at different steering angle θ of the magnets. The arrows show the direction of the field flowing from north pole to south pole. Arrows are normalized for visualization purpose.

According to the results obtained from FEM and shown in figure 3.10 shows the coupling force acting between the two magnetic means of the MAGS. The decrease in the maximum coupling force by having such a magnetic modulator is 48% and 23% for the modulator with two and three magnets, respectively.

3.3 Magnetic Field Modulation

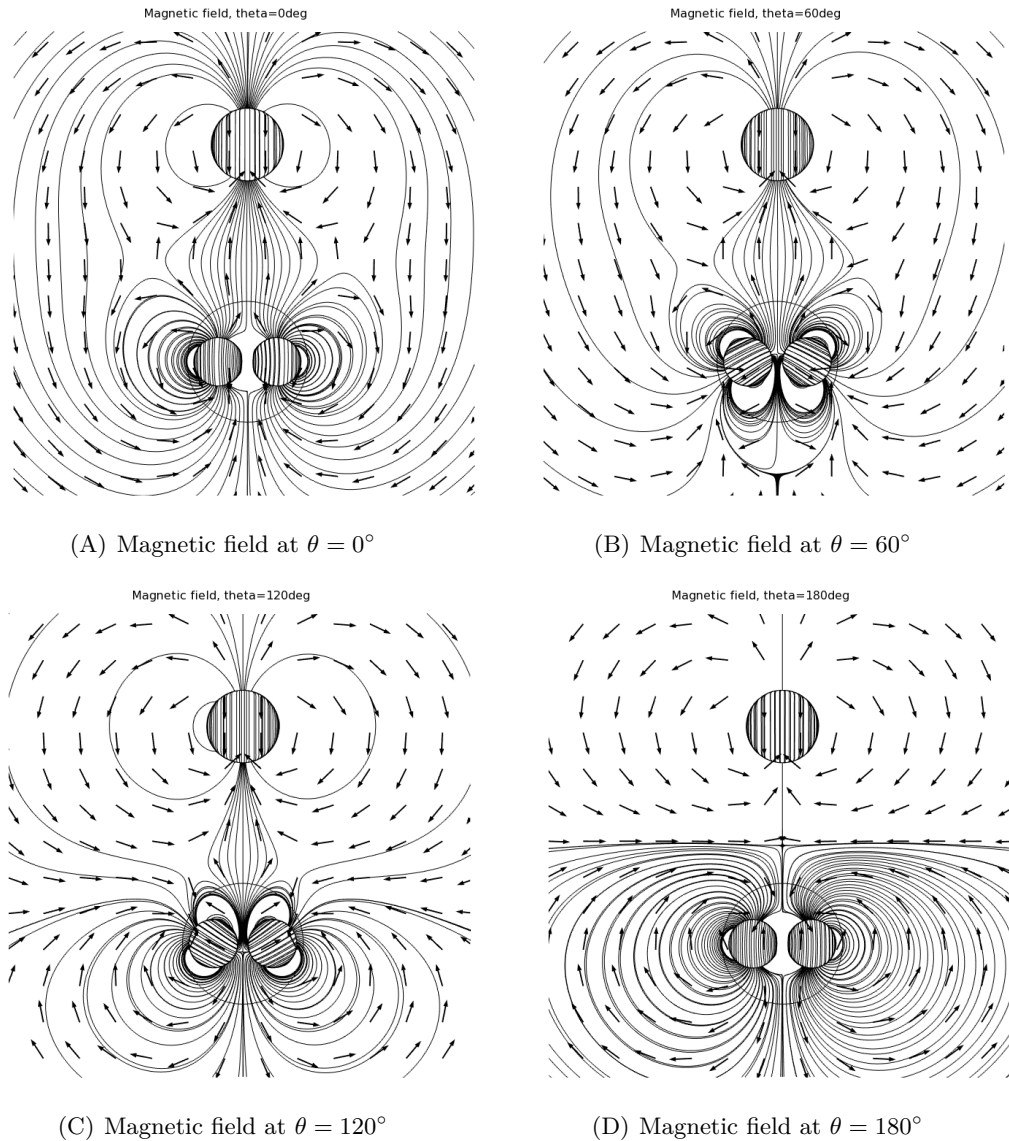


Figure 3.8: The magnetic field is represented for different steering angles θ of the magnet. The upper magnetic part is represented by a single magnet magnetized diametrically and the lower magnetic element (modulator) is composed of two steerable magnets also magnetized diametrically. (A) The field density, namely the attraction force is maximum at $\theta = 0^\circ$. (B) The symmetric rotation of the magnets decrease the attraction force, here at $\theta = 60^\circ$. (C) At $\theta = 120^\circ$, the force between the two magnetic members is close to zero. (D) At $\theta = 180^\circ$, the force has become repulsive and the configuration is unstable. If the upper magnet is free to rotate, it will be flipped by 180° to a stable and attractive configuration.

3. Magnetic Force Modulation at Small Scale

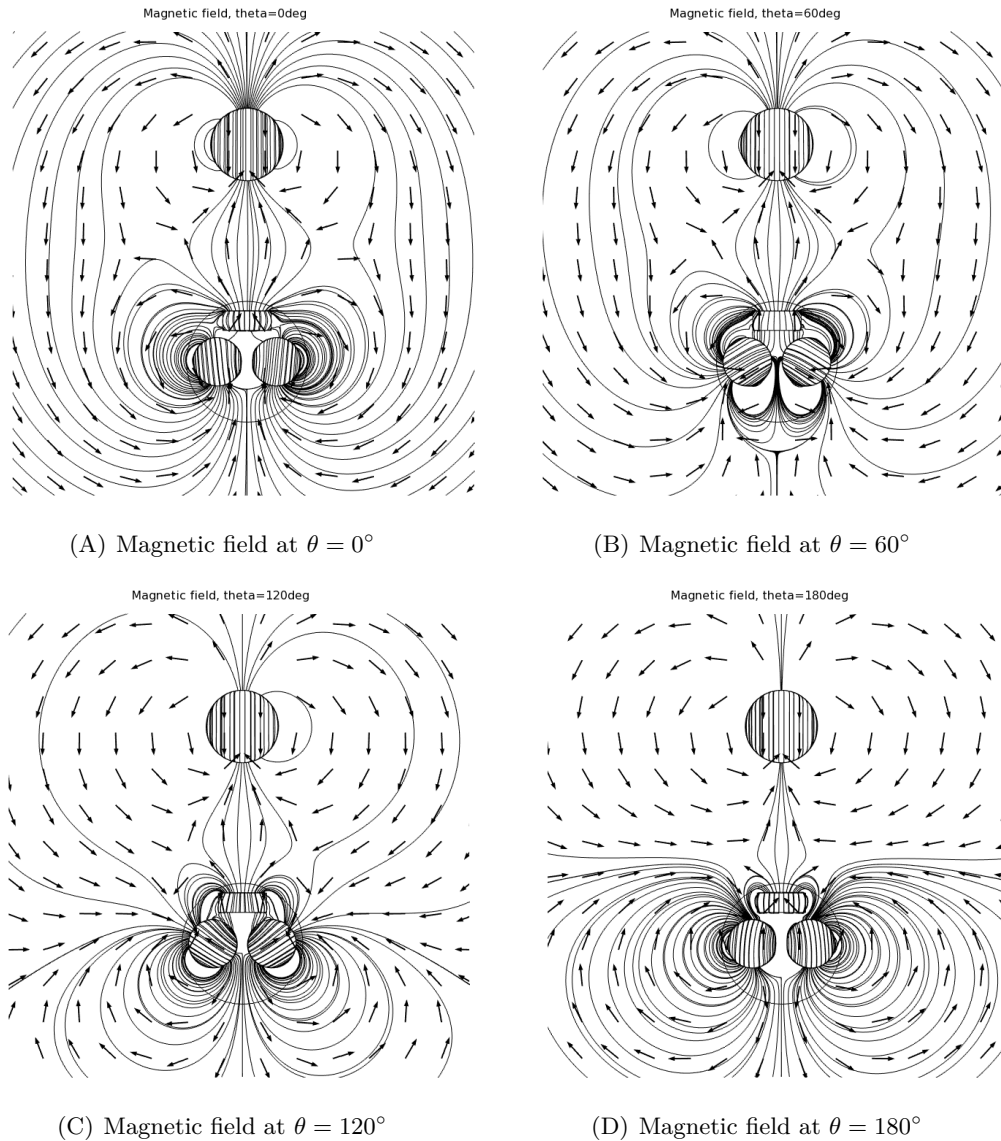


Figure 3.9: The magnetic field is represented for different steering angles θ of the magnet. The upper magnetic element is represented by a single magnet magnetized diametrically and the lower magnetic part is composed of two steerable magnets also magnetized diametrically and fixed rectangular magnet. This fixed magnet creates sufficient field to keep the magnetic means always attracted. (A) The attraction force is maximum at $\theta = 0^\circ$. (B–C) The symmetric rotation of the magnets decreases the attraction forces. (D) At $\theta = 180^\circ$, the attraction force is close to zero, but has not become repulsive.

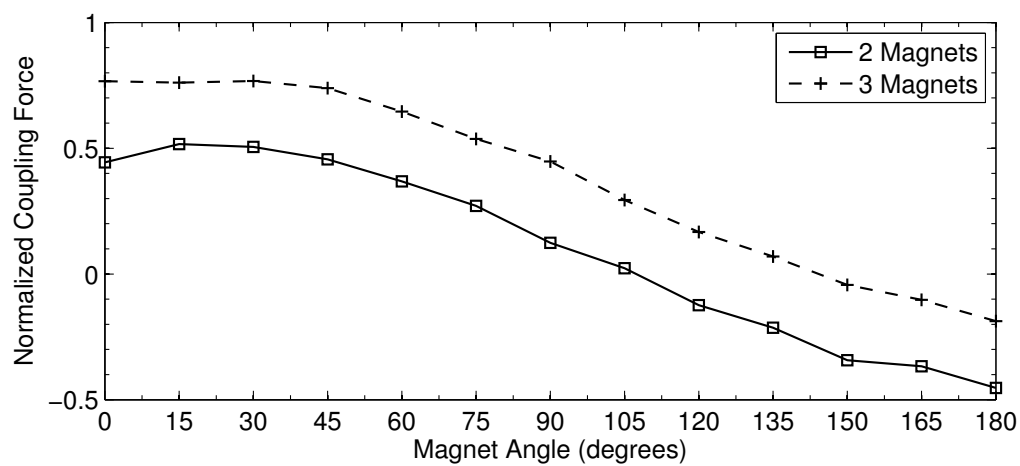


Figure 3.10: 3-dimensional FEM results of the coupling force in function of magnets angle for the two concepts using steerable parallel magnets. Legends: 2 Magnets and 3 Magnets corresponds to concept a) and b) respectively of figure 3.7.

3. Magnetic Force Modulation at Small Scale

3.3.2.2 Coaxial Magnets Arrangement

Concept

Figure 3.11 shows an arrangement of three magnets used to modulate the magnetic field. The three magnets are diametrically magnetized. The two magnets on the extremities are linked together and fixed to the tip, while the magnet in the middle can be steered. Steering of this intermediate magnet creates an opposite flux lines in the magnetic field and therefore modifies the coupling strength of the MAGS. However, it implies lateral forces in the MAGS, which could potentially represent a drawback. Another limitation of this concept is the coupling orientation. The magnetic member can be coupled in two orientations, as far as the passive magnet is free to rotate inside the tip of the guided member.

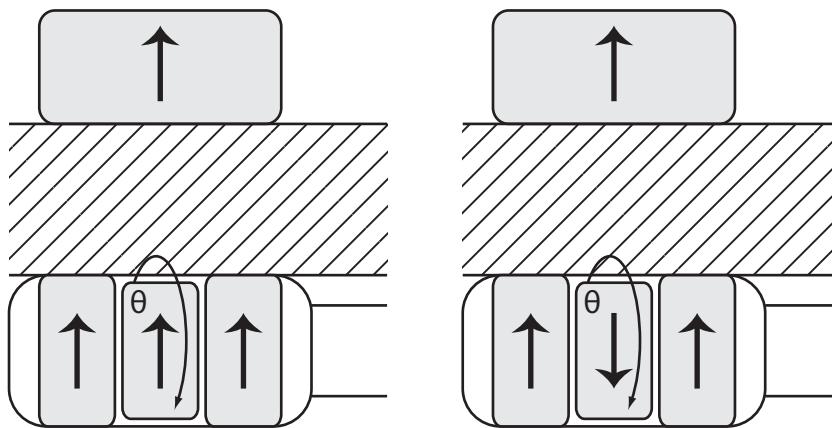


Figure 3.11: Arrangement of three coaxial diametrically magnetized permanent magnets to modulate the magnetic field. The two magnets on the extremity are aligned and connected together. By steering the intermediate magnet, the overall magnetic field is modified. Maximum attraction configuration (left). Minimum attraction force (right).

Magnetic Analysis

Figure 3.12 illustrates how the magnetic field flows and is modulated between the two magnetic means at several steering angles θ of the intermediate magnet. The arrows show the direction of the magnetic field, flowing from north pole to south pole, and are normalized for visualization purposes.

Figure 3.13 shows the coupling force acting between the two magnetic means of the MAGS. The maximum achievable coupling force is decreased by 30% with this modulator, which is rather encouraging. The larger the volume dedicated to the steerable magnet, the wider the range of modulation. However, the wider the range of modulation, the stronger the lateral forces generated, which can be quite significant in comparison with the coupling force. At least one half of the overall volume should be dedicated to the steerable magnet in order to bring the coupling strength close to zero.

One of the major drawbacks for this configuration concerns the guidance behavior. As a reminder, the guided part of the MAGS always follows with a small offset compared to the guiding member during the guidance. This offset position combined with the lateral force generated by the rotation of the middle magnet of the modulator create a misalignment between the tips. The resulting yaw angle (angular movement around the vertical axis of

3.3 Magnetic Field Modulation

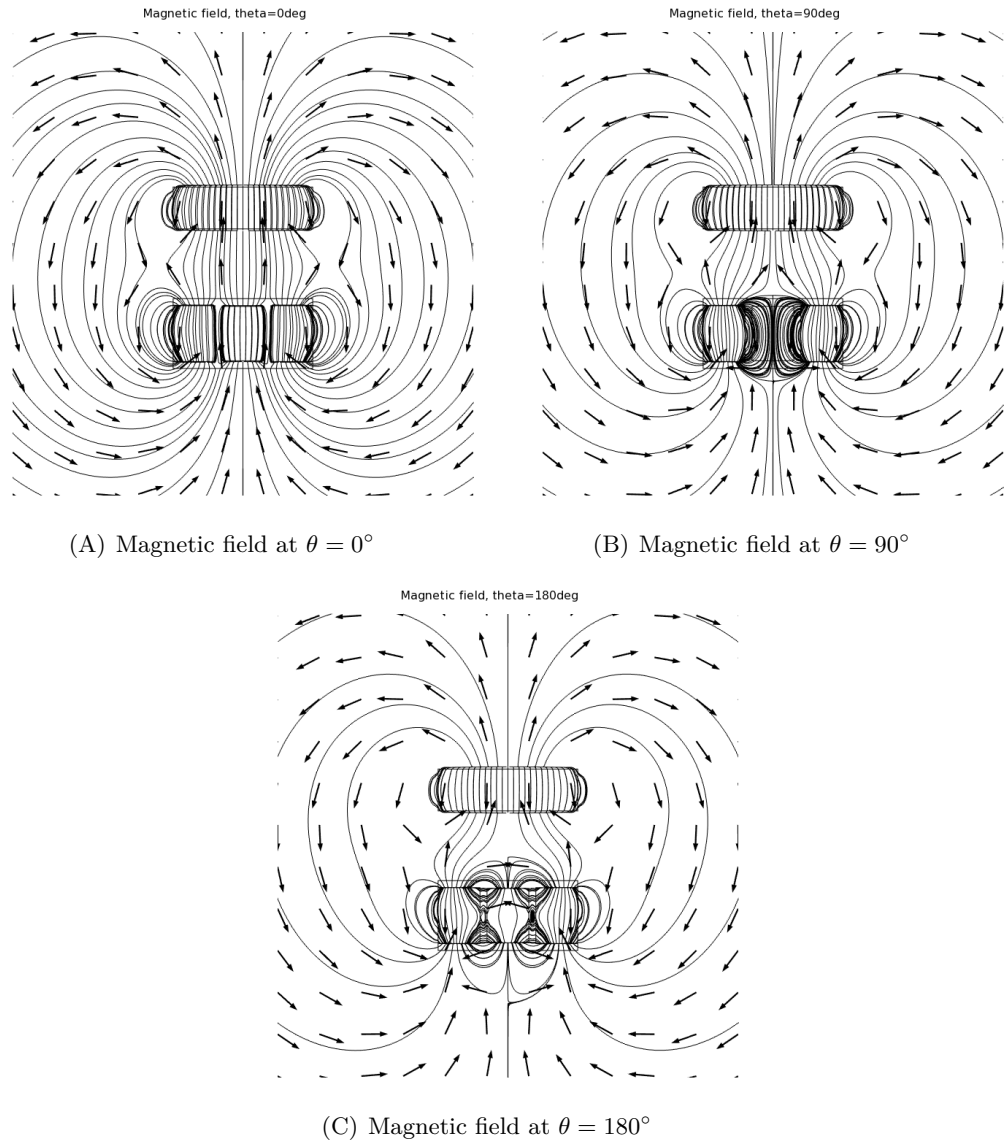


Figure 3.12: The upper magnet is a single cylindrical element magnetized diametrically and the lower part (modulator) is composed of one steerable cylindrical magnet and two fixed cylindrical magnets at the extremities, all magnetized diametrically. The magnetic field is represented for different steering angles θ of the middle magnet. (A) The attraction force is maximum for $\theta = 0^\circ$. (B) The density of field lines decreases with the rotation of the middle magnet, here for $\theta = 90^\circ$. (C) At $\theta = 180^\circ$, the attraction force is minimum.

guided part) reduces the coupling strength. Moreover, the frictional interaction between the surface and the guided member tends to increase the angle of misalignment, which might lead to the disconnection of the MAGS. This especially true on soft surface or on hard surface with high friction coefficient.

3. Magnetic Force Modulation at Small Scale

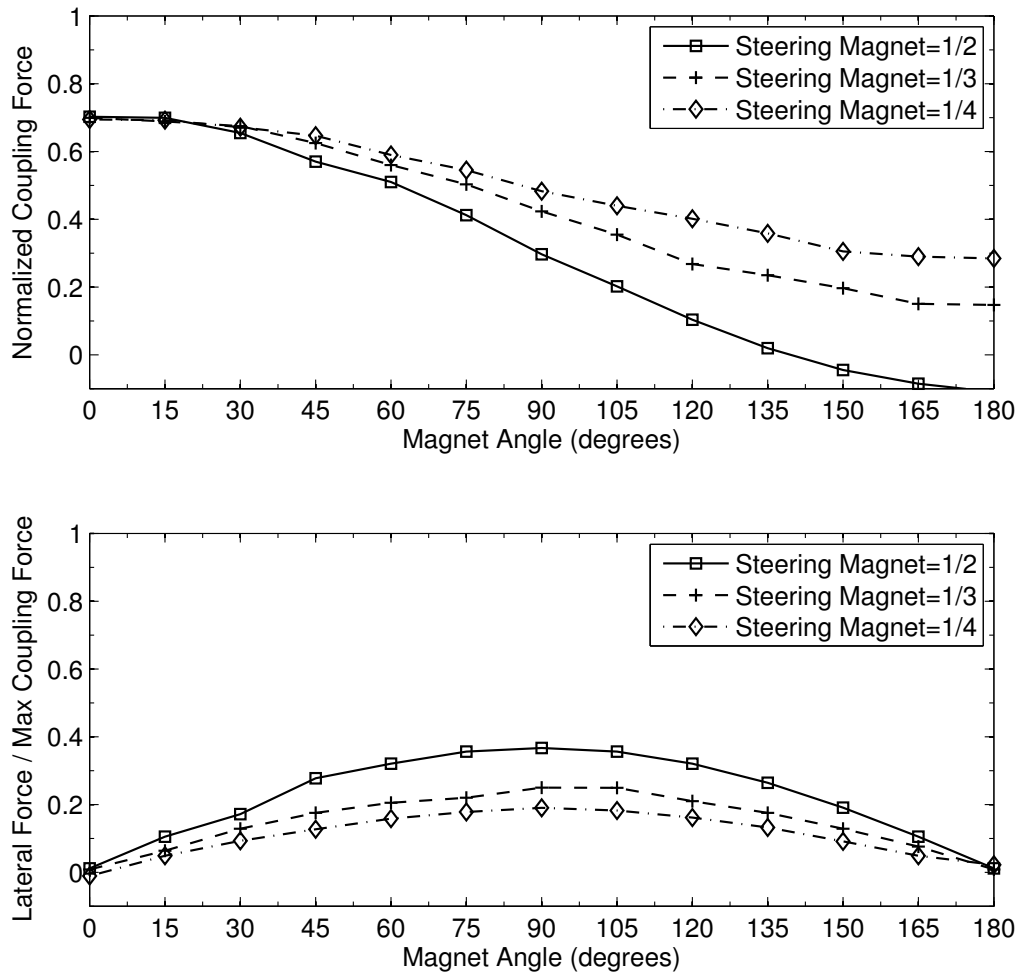


Figure 3.13: 3-dimensional FEM results of the coupling force in function of the steering magnet angle for the modulator composed of three coaxial magnets. The lateral force generated by the rotation of the middle magnet is normalized with respect to the coupling force at zero angle. Legends: Steering magnet=1/2, 1/3 and 1/4 means that the steerable magnet volume represents half, one third, one fourth of the modulator volume.

3.3.3 Shielding

Concept

Another approach to modulate the attraction force in the MAGS, consists of shielding the magnetic field around the permanent magnet of the modulator. Ferromagnetic materials of high permeability ($\mu_r=4'000$) is placed between the poles of the magnet to contain locally the magnetic field, which therefore reduces the magnetic field perceived by the second member of the MAGS.

Figure 3.14 illustrates a pair of steerable tubular sections containing the magnetic field locally around the permanent magnet. This concept may have the advantage to offer a parallel coupling of the MAGS independent of the orientation of the tips.

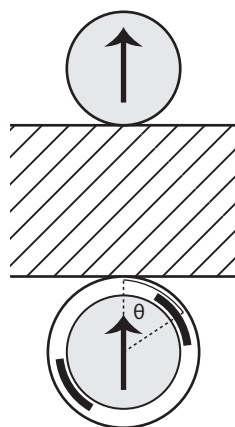


Figure 3.14: A pair of tubular ferromagnetic sections is used to shield and modulate the magnetic attraction between the permanent magnets. The coupling force is maximum at $\theta = 0^\circ$ and minimum at $\theta = 90^\circ$. The size (angle) of the shield sections dictates not only the modulation range but also the amplitude of the coupling force. The asymmetry of the design results in the creation of a lateral force and an axial torque on the permanent magnets.

Magnetic Analysis

Figure 3.15 illustrates how the magnetic field flows and is varying between the two magnetic means at several steering angles θ of the ferromagnetic shield. The arrows show the direction of the field, flowing from a north pole to a south pole, and are normalized for visualization purpose. One can understand the asymmetry of the field created by the steering of the shield.

Figure 3.16 shows the coupling and lateral forces acting in the MAGS. There is a trade-off between the coupling force and the modulation range. The range of modulation increases with the angle of the shield sections. On the other hand, the maximum coupling strength decreases with the angle of the shield sections. The coupling force is decreasing from 35% to 51% with this modulator depending on the opening of the shield sections. Lateral force generated by the asymmetry of the magnetic field is rather significant in comparison with the coupling force.

According to FEM results shown in figure 3.16, a wide angle, such as $\theta = 140^\circ$, for the shield sections is preferred in order to maximize the range of modulation, without reducing too severely the maximum coupling strength in the MAGS.

Changing the shield thickness of the sections seems to have very little influence on the coupling force as represented on figure 3.17. A possible optimization of this modulator would be to minimize the thickness of the shield in order to maximize the volume for the permanent magnet. However, the smaller the air gap between the shield and the magnets, the bigger the attraction forces between these two components. The actuation torque to rotate the shield can become significant, even at this scale.

Another parameter to study is the effect of the relative permeability of the shield on the modulation range. Shield made of electrical steel ($\mu_r=4'000$), permalloy ($\mu_r=50'000$) and mu-metal ($\mu_r=100'000$) have been chosen for the simulation. The results show that electrical steel is already sufficient to affect the magnetic field as shown in figure 3.18. Materials with higher permeability do not improve the performances for the studied configuration.

3. Magnetic Force Modulation at Small Scale

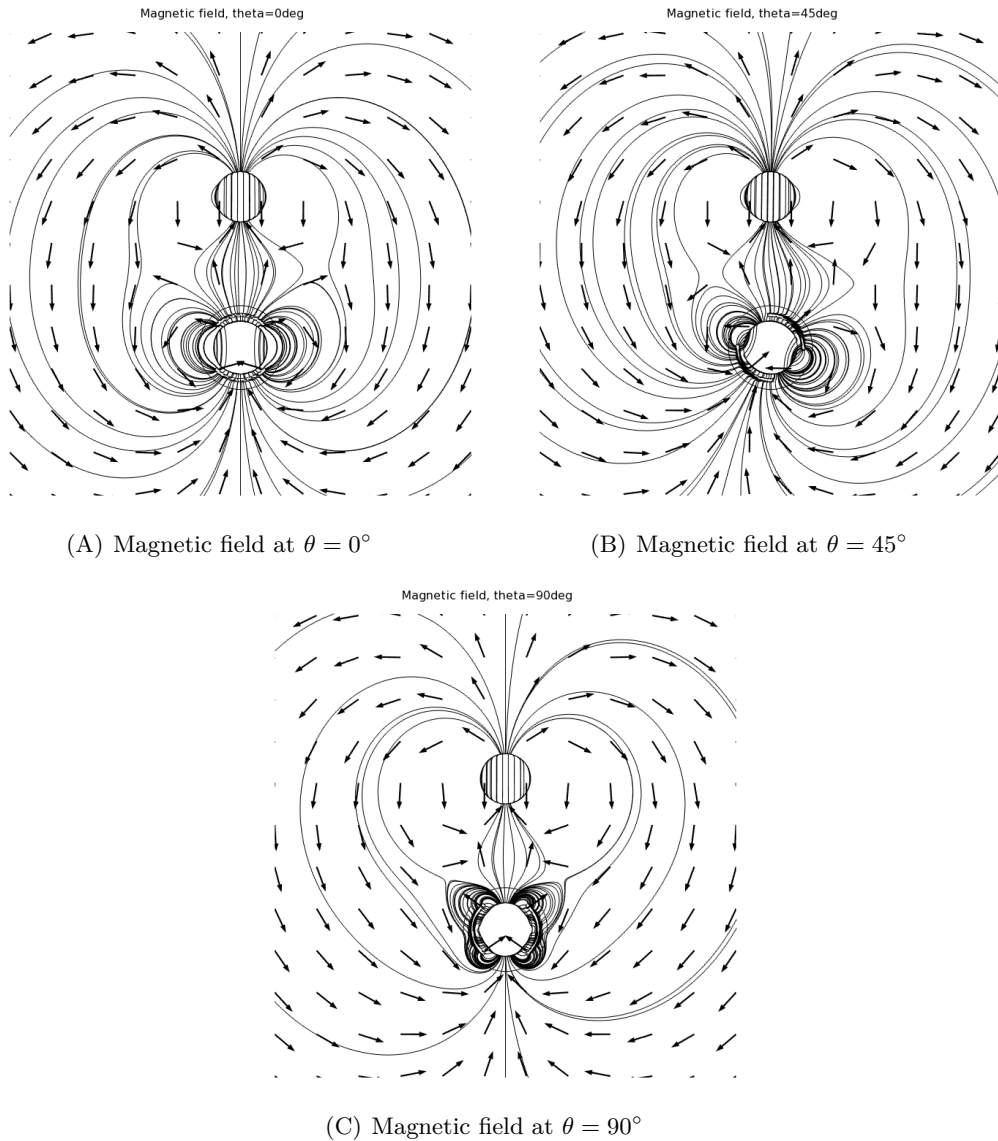


Figure 3.15: The upper magnetic element is represented by a single cylindrical magnet magnetized diametrically and the lower magnetic part (modulator) is composed of a pair of steerable ferromagnetic tubular sections, which can be steered around the diametrically magnetized permanent magnet. The magnetic field is represented for different steering angles θ of the shield. (A) The attraction force between the upper and lower part is maximum for $\theta = 0^\circ$. (B) The attraction force decreases with the rotation of the shield, here for $\theta = 45^\circ$. The field becomes asymmetric and produces lateral force on the MAGS. (C) At $\theta = 90^\circ$, the attraction force is minimum.

3.3 Magnetic Field Modulation

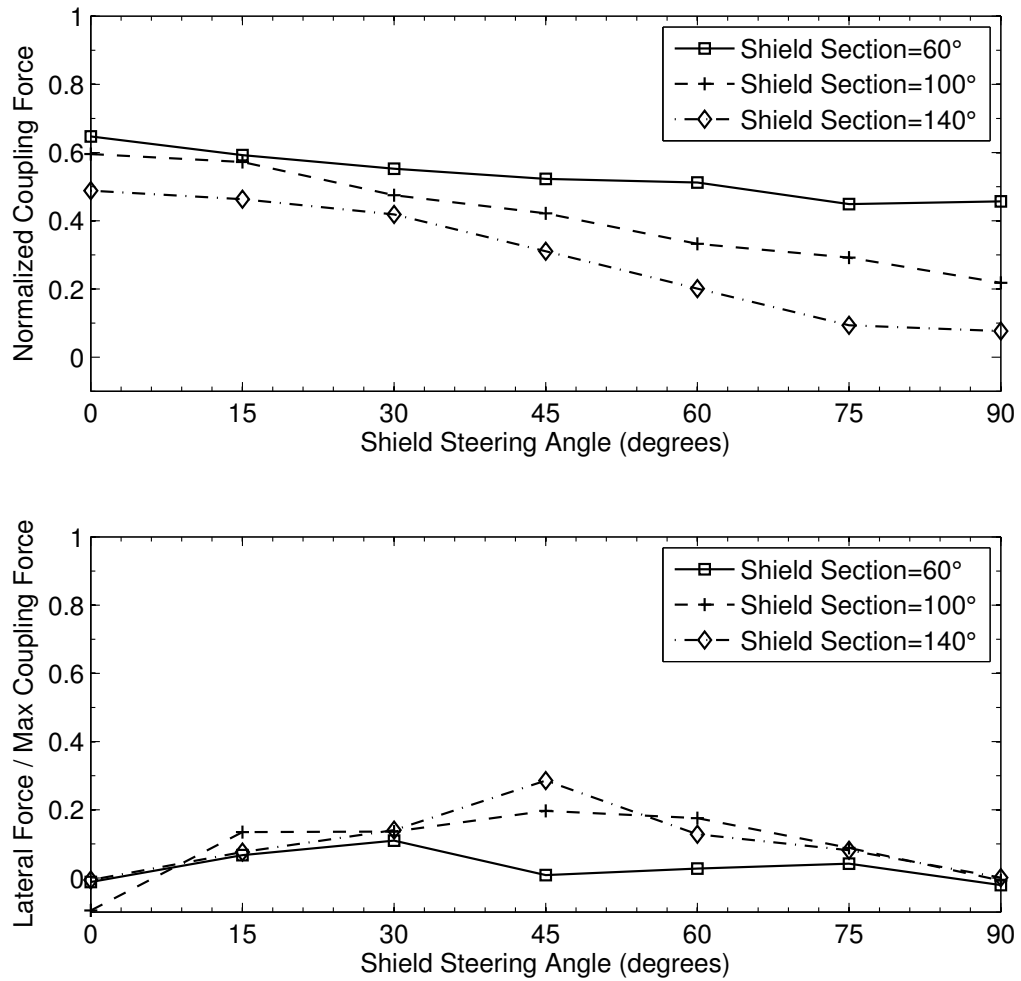


Figure 3.16: 3-dimensional FEM results of the coupling and lateral force as a function of steerable shield angle. Different shield section angles are compared for constant thicknesses of 0.3 mm and 10 mm long. The lateral force generated by the rotation of the ferromagnetic shield is normalized with respect to the coupling force at zero angle. The range of modulation increases with the angle of the shield sections. On the other hand, the maximum coupling strength decreases with the angle shield sections.

3. Magnetic Force Modulation at Small Scale

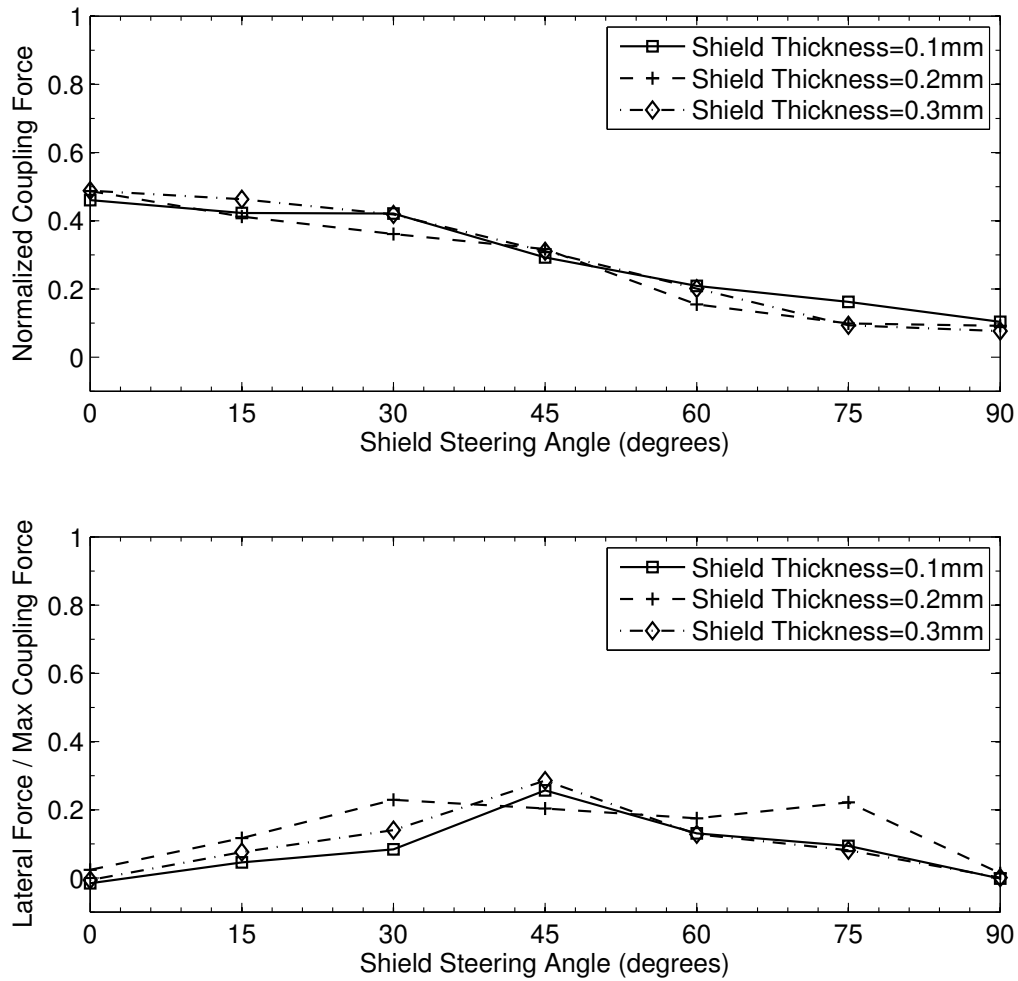


Figure 3.17: 3-dimensional FEM results of the coupling and lateral force as a function of steerable shield angle. Different shield thickness at a section angle of 140° are compared. The lateral force induced by the rotation of the ferromagnetic shield is normalized with respect to the coupling force at zero angle. In the analyzed range, increasing the thickness of the shield seems to have negligible effect on the modulation range or the coupling force.

3.3 Magnetic Field Modulation

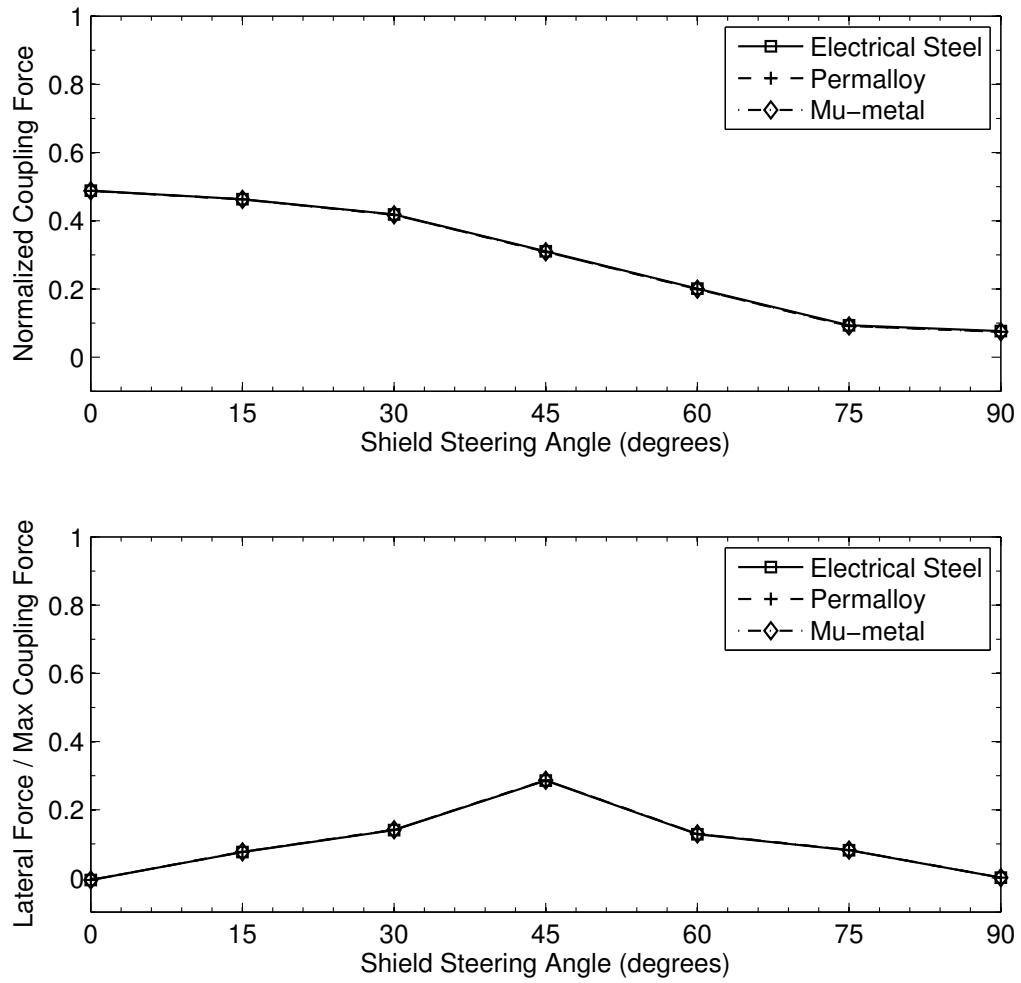


Figure 3.18: 3-dimensional FEM results of the coupling and lateral force in function of steerable shield angle. Different relative permeability at a section angle of 140° are considered. In the analyzed range, increasing the relative permeability of the shield seems to have no benefit on the modulation range or the coupling force.

3.4 Actuation Principle

The actuation of the proposed magnetic force modulators could be of different nature such as mechanical, electromechanical or hydro-pneumatic. However, actuation principle in the field of medical devices are generally oriented towards simple, robust, sterilizable, easily certified and affordable mechanisms.

3.4.1 Mechanical

Mechanical actuation is generally preferred in the context of medical devices. Actuating a small mechanism located at the distal part of a device inserted into the body is challenging. Minimally-invasive devices represent a good source of examples describing the implementation of mechanical actuations. Figure 3.19 shows examples of mechanical actuations using cables or rods. The actuation of the mechanism is ensured by displacing axially a cable or rod from the proximal part, namely the handle. Cables or rods have good mechanical properties when used in traction/compression respectively. By using basic mechanical equations, we can demonstrate that cables are not suitable to transmit torques but rather axial forces.

The stress σ and the elongation δ induced by a load on a circular rod is given by:

$$\sigma = \frac{P}{A} \quad (3.5)$$

$$\delta = \frac{PL}{AE} \quad (3.6)$$

where

P : Load

L : Length of the rod

A : Cross-section of the rod

E : Modulus of elasticity or Young's modulus of the material.

On the other hand, using cables or rods in torsion is not suitable due to their high angular deformation range. The stress τ_α and the deformation α induced by a twisting moment on a circular rod is given by:

$$\tau_\alpha = \frac{Tr}{J} \quad (3.7)$$

$$\alpha = \frac{TL}{GJ} \quad (3.8)$$

where

T : Twisting moment

r : Radius of the rod

L : Length of the rod

G : Shear modulus of the material

J : Polar moment of inertia

To illustrate this range of deformation, cable actuation of the modulators of figure 3.1 and figure 3.11 can be considered. The traction force required to pull the magnet axially by means of a stainless steel cable ($E=200$ GPa) is ~ 0.4 N, without considering the friction of the cable with its sheath. Applying a traction force of 0.4 N on a cable of 0.3 mm in diameter and 1 m in length will result in an elongation of only ~ 0.03 mm.

On the other hand, a torsion moment of 1 Nmm to steer the middle magnet of the second modulator applied on the same cable will result in a twist angle of: $2'830^\circ$!

Equation 3.8 is not valid for such deformation, but is however sufficient to demonstrate that the rotational movement of modulator components should be achieved through a conversion from a longitudinal displacement of the cable. Details of a possible conversion has been used in the implemented magnetic fore modulator and are presented in section 4.1.

3.4.2 Electromechanical

Modulating a magnetic field by means of a coil has the advantage to offer an easy control of the strength and polarity of the field. However, a substantial magnetic fields are only achievable with high currents, which results in significant generation of heat. Cooling down the modulator is therefore necessary, which complicates the system. The cooling effect can be produced by an internal and continuous flow of liquid in the modulator.

3.4.3 Hydro-pneumatic

Compressed gas or liquid may be utilized to transmit power for shifting components of the modulator. Given modulators of section 3.2.1.2 may be actuated by means of this type of energy. However, such an actuation will complicate the design and development of the device.

3.5 Conclusion and Comparison

3.5.1 Magnetic Comparison

Various modulators have been proposed and analyzed. Figure 3.20 compared the magnetic performances of these modulators. The coupling force is normalized to a given fixed permanent magnet (reference) occupying the available volume defined for the modulator. According to the FEM results, the design with two parallel steerable magnets boosted with a fixed magnet gives the widest range of modulation with a minimum loss of coupling force. In comparison, electromagnets give the worst performance at this scale in terms of continuous coupling force modulation.

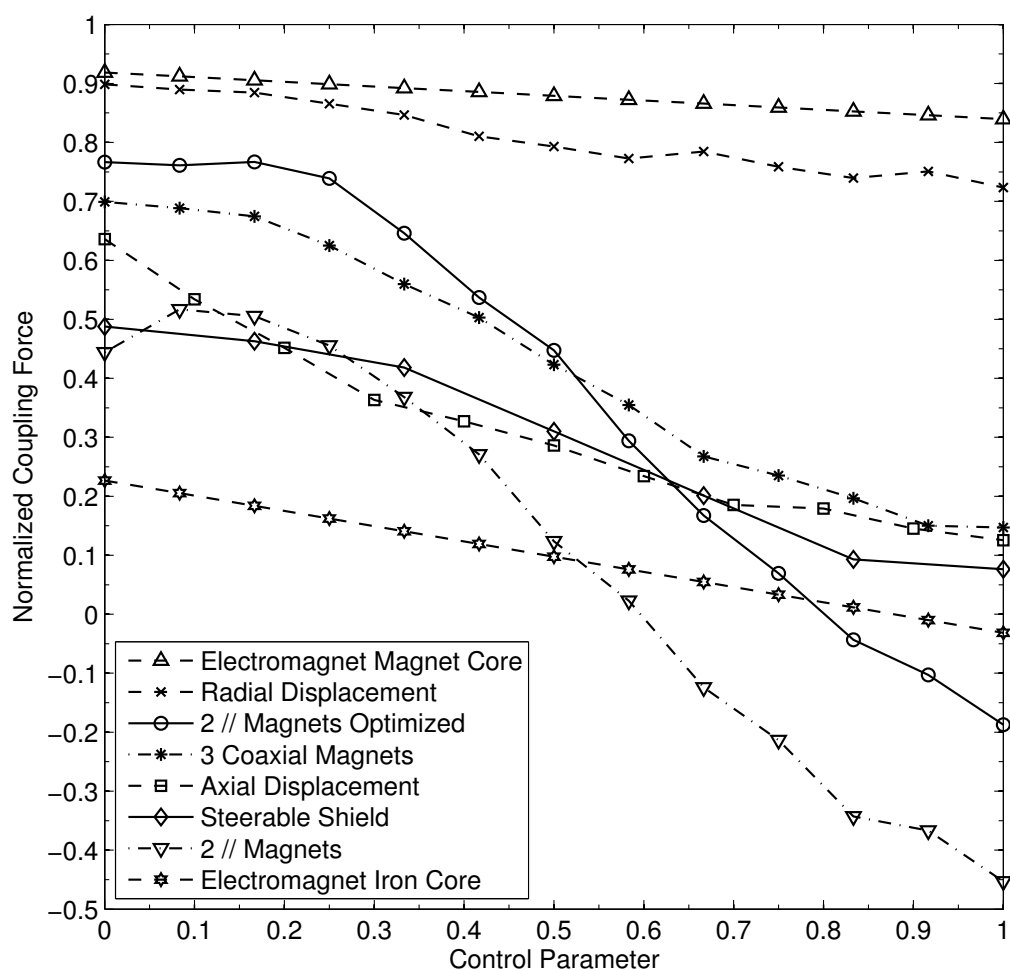


Figure 3.20: Modulation comparison of the modulators relative to a given fixed permanent magnet (reference) occupying the available volume defined for the modulator. The x -axis represents a control parameter, namely a displacement, a steering angle or current depending on the modulator. Clearly, the design with 2 parallel steerable magnets optimized with a fixed magnet offers the widest range of modulation with a minimum loss of coupling force. Modulation by mean of an electromagnet is by far the worst scenario in terms of continuous coupling force modulation. Modulators based on permanent magnets offer the best perspective at small scale.

3. Magnetic Force Modulation at Small Scale

3.5.2 Design Implementation

Shifting or Steering Ferromagnetic Components

Modulation achieved by displacing a permanent magnet inside the tip of magnetic means may require different actuations depending on the direction of the displacement. An axial displacement, in the context of a perpendicular coupling of the magnetic parts, can be easily achieved by mechanical actuation. A thin cable attached to the movable magnet can perform this task. Moreover, a cable actuation requires very limited space.

In the case of a radial displacement of the modulating magnet, hydro-pneumatic actuation of balloon(s) represents a possible solution. Channel(s) containing gas or liquid and attached to a regulation system need to be implemented. If the radial displacement is achieved by steering an off-center tube, a mechanical actuation might be considered. Consequently, a mechanism must provide the conversion of the rotation movement to a longitudinal displacement. The same mechanism can be considered to steer a permanent magnet or a ferromagnetic shield. An example of this actuation is detailed in section 4.1. Internal forces and torques within the magnetic components of the modulator can be significant. Low friction and hard material, such as ruby or bronze might be considered to increase the life time of the modulator.

Electromagnet

Modulation by controlling a current in a coil is a well known solution. As seen in this chapter, producing a sufficient magnetic field cannot be achieved without generating significant heat. The increase of temperature in the MAGS should be limited by a cooling system. The cooling system can be realized with an internal and continuous flow of liquid. Two channels might be considered in the design. Direct contact between the liquid and the coil should be avoided.

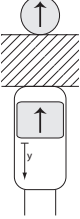
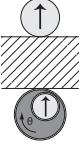
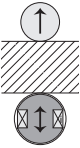
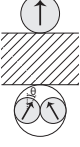

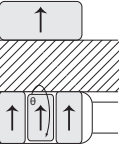
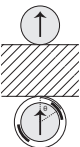
3.5.3 Conclusion

Modulating the attraction force between two intracorporeal MAGS elements has been presented and several concepts of modulators have been proposed, analyzed and compared. FEM modelling of the magnetic interactions was essential for comparing the different designs of modulators as well as for understanding how the MAGS may behave during the guidance. Attraction forces in the MAGS are generally achieved by means of an electromagnet. However, when the MAGS becomes small enough to be inserted into the body, electrical current is not sufficient to produce adequate modulation of the magnetic field. Modulators composed of movable permanent magnets become an alternative, especially the modulator composed of two parallel steerable magnets and one fixed magnet. This design offers a wide modulation range and a good coupling strength. This design has been patented [Verin and Sandtner, 2008] and its implementation is discussed in chapter 4.

Table 3.2 gives an overview of the proposed force modulators in terms of magnetic performances, guidance behavior and implementation.

3.5 Conclusion and Comparison

Table 3.2: Overview of the force modulators. The modulation range is normalized to a reference fixed permanent magnet occupying the available volume of the force modulator.

	Modulation Range	Advantages	Disadvantages	Implementation
	[13% , 64%]	-Symmetric field -Actuation	-Perpendicular coupling -Large tip size	Low complexity
	[72% , 90%]	-High coupling force -Coupling in every orientations	Lateral force	Difficult
	[-3% , 22%]	-Symmetric field -Control -Magnetic pulses	-Heat -Cooling required -2 coupling orientations	Standard
	[-45% , 45%]	-Symmetric field -Inverse polarity	-2 coupling orientations	Difficult
	[-19% , 77%]	-Symmetric field -Highest modulation range	-High internal forces -1 coupling orientation	Difficult
	[15% , 70%]	Modulation range	-Poor guidance -2 coupling orientations	-Complex -Tubular magnets
	[8% , 49%]	-Coupling in every orientations	Lateral force	Complex

4 Magnetic Force Modulator

This chapter details the implementation of a magnetic force modulator using steerable permanent magnets in a catheter tip. The Maestro-AF project (see section 8.1) was considered to illustrate the beneficial use of such a modulator. The first section is dedicated to the mechanical design of the modulator and its mechanical actuation. A modulator has been realized and its magnetic and mechanical performances are characterized. The measured magnetic attractions forces are compared with a FEM model and the actuation force is compared with two analytical models. Finally and before concluding this chapter, some reflections are done on the manufacturing process of the modulator.

4.1 Mechanical Design

Results presented in chapter 3 demonstrated that modulating the coupling force within the MAGS by means of steerable permanent magnets gives the best results in terms of modulation range and maximum coupling force. This section details the mechanical design of a force modulator, composed of two parallel steerable magnets reinforced with a fixed magnet, implemented in catheter tip, figure 4.1.

4.1.1 Modulator Design

The ideal modulator should provide the wider range of modulation in a minimum volume in order to provide a robust intracorporeal magnetic guidance in variable anatomical conditions. The coupling strength between magnetic members of a MAGS is adjustable by means of two steerable magnets, which are cylindrical and diametrically magnetized, as shown in figure 4.1. A fixed magnet is used to boost the coupling strength in the MAGS without impeding its modulation ability.

Based on this idea, a magnetic force modulator has been integrated in a catheter tip, as illustrated in figure 4.2. The modulator is composed of three permanent magnets made of Neodymium-Iron-Boron (NdFeB) alloy. The two steerable magnets are magnetized diametrically and are mounted on thin harden-bronze tubes. These non-magnetic tubes contain an helical slot used for their rotation. The extremity of the tubes are terminated by small taps designed to reduce the diameter of the rotating part in contact with a ruby bushing in order to minimize the resistance to the rotation of the magnets. As the exerted force on the bushing is relatively high, ruby has been chosen for its hardness, durability and relatively low friction coefficient; $\mu=0.1-0.2$ for steel-ruby contact. To increase the coupling strength of the MAGS, a third magnet with a vertical magnetization is placed in the axis of modulation.

4. Magnetic Force Modulator

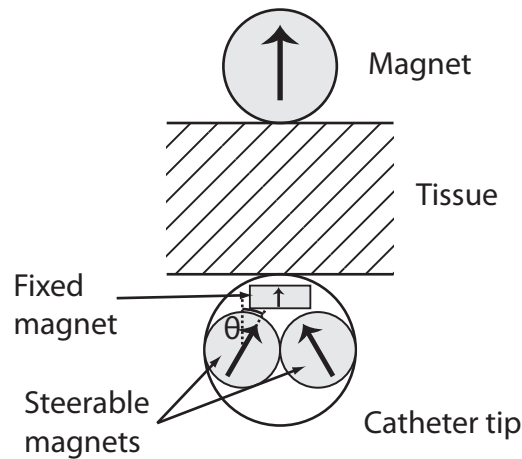


Figure 4.1: Concept of magnetic force modulator based on two steerable permanent magnets.

The actuation of the steerable magnets is cable driven. As seen in chapter 3, cables used in traction/compression have very good mechanical properties to actuate such a mechanism. However, they cannot transmit torsion. Therefore, a mechanism converts the axial displacement of the cable into a rotational movement of the magnets. This conversion of movement is inspired from the well-known “lipstick tube” mechanism.

Two additional features have been added: a guide wire lumen and temperature sensors. The guide wire lumen is used to facilitate the insertion of the device inside the cardiovascular system. A thin wire, called guide-wire is inserted first into the right anatomic location. Then, the device can be inserted “over the wire” like any other standard device for catheterization. The temperature sensors are used to monitor the tissue temperature during the treatment. Two type T temperature sensors are disposed on the perimeter of the tip surface. The surface of the tip is divided in four zones in order to measure locally the temperature of the tissue.

The proximity of the MAGS members sandwiching the tissue can be used for other applications and diagnostic purposes. Therefore, depending on the application, the temperature sensors can be replaced by other types of sensors such as optical or chemical. Intracorporeal MAGS not only provides local guidance of a guided object, but has the enormous advantage to be used for collecting or monitoring tissue information during a diagnostic or a treatment procedure.

4.1.2 Actuation

The mechanical actuation of the steerable magnets of the modulator is based on the “lipstick” tube. The lipstick mechanism converts a rotational movement of its base into a longitudinal displacement of its content. It was invented under this form by the American James Bruce Mason Jr. in 1923 [Angeloglou, 1970]. Following his invention, more than hundred patents of lipstick designs were issued in the following few years. The patent drawings of the first swivel-up lipstick tube and its first improvement are illustrated in figure 4.3, [Mason, 1923, Kendall, 1924].

Following this idea, the mechanical actuation of the steerable magnets of the modulator is achieved with an “inverted lipstick” movement: a longitudinal displacement of the cable

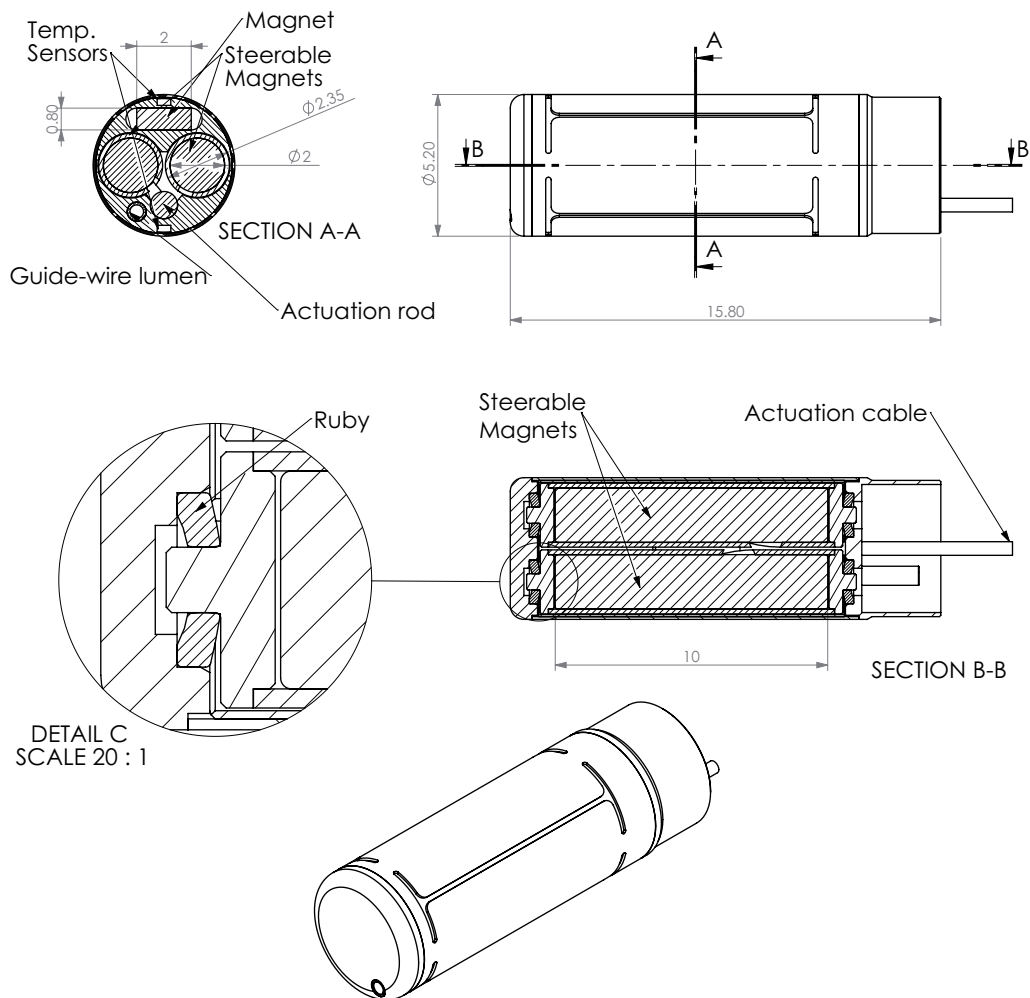
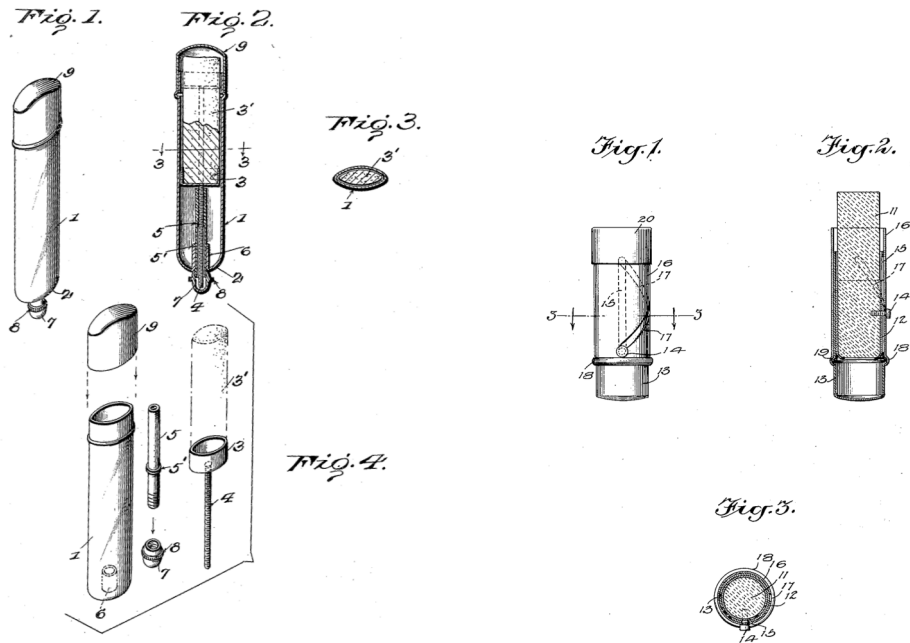


Figure 4.2: View of the magnetic force modulator integrated into the tip of an ablation catheter of 5 mm in diameter.

induces a rotation of the magnets. The rotation is made by two pins sliding on helical slots, as illustrated in figure 4.4. Due to size limitations, the pins are not in the same plane, but shifted to maximize their fixation in the actuation rod. The helical slots are also shifted and mirrored so as to make the synchronous rotation of the magnets in opposite direction possible.

4. Magnetic Force Modulator



(A) The first swivel-up tube for lipstick, Mason, 1923.

(B) Compact design of the lipstick tube, Kendall, 1924

Figure 4.3: Patent drawings of lipstick tube mechanisms: a rotational movement of its base induces a longitudinal displacement of its content.

4.1.3 Implementation

The first step of the implementation consisted of realizing a first prototype scaled up 2:1. A scaled-up version has the advantage to simplify the manufacturing as well as its characterization. The aim is to validate *in vitro* the concept of force modulation before its implementation at real scale in a catheter tip. The manufacturing of the prototype is illustrated in figure 4.5.

4.1 Mechanical Design

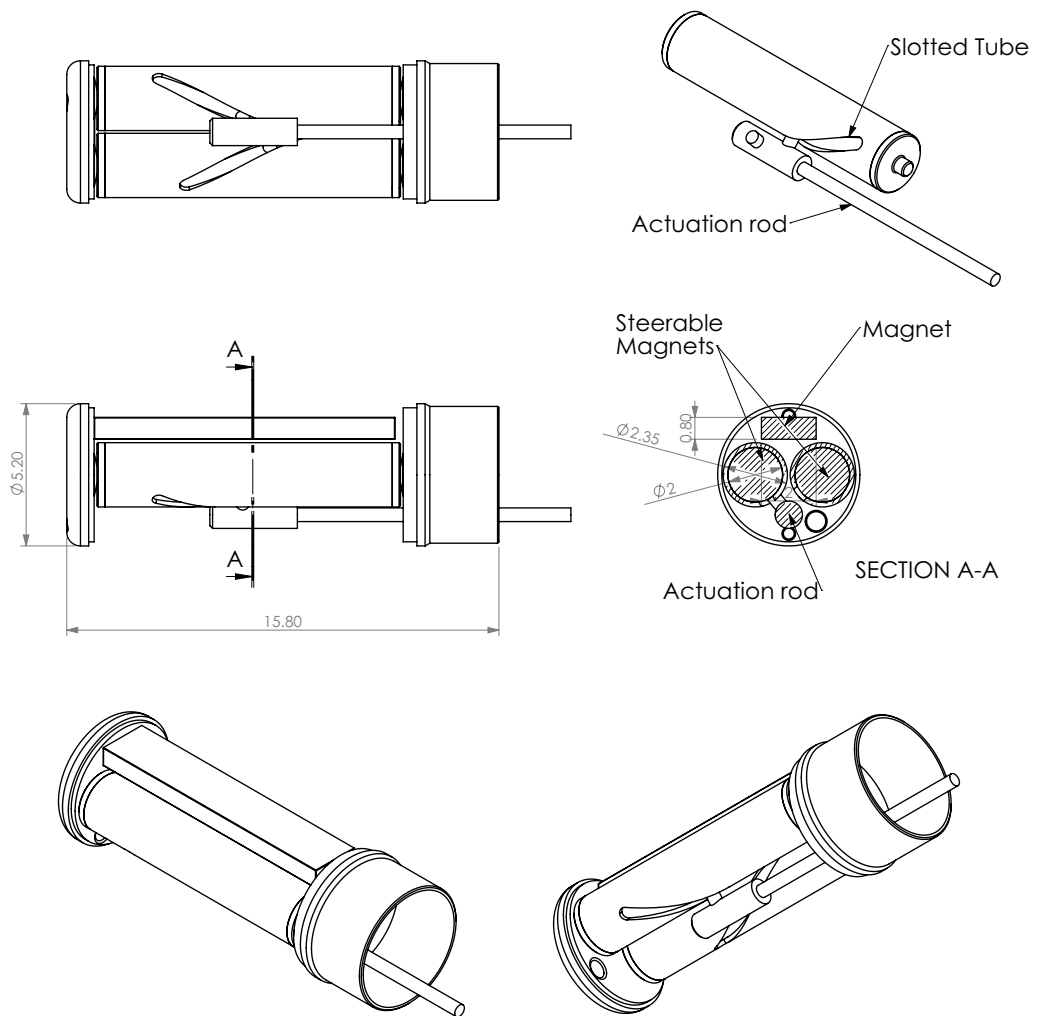


Figure 4.4: Selective views of the actuation mechanism used to steer the magnets of the magnetic force modulator integrated in a catheter tip. An actuation rod, ended by two pins in contact with helical slots, is shifted axially resulting in a rotation of the magnets.

4. Magnetic Force Modulator

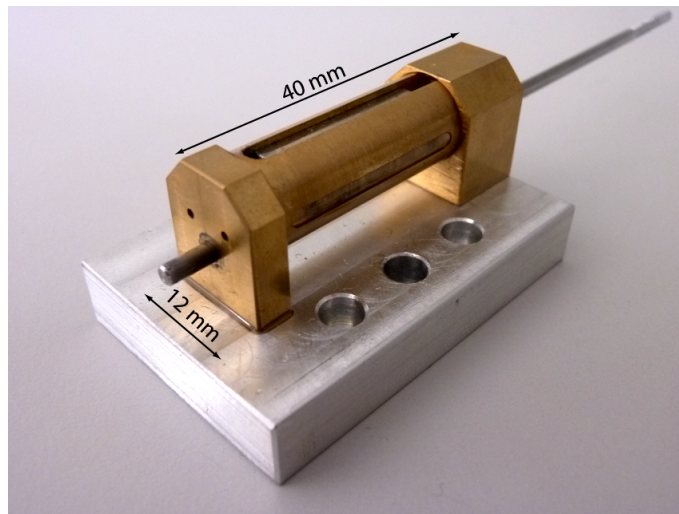


Figure 4.5: View of the scaled-up magnetic force modulator for *in vitro* validation. The modulator is integrated in a cylinder of 10 mm in diameter which contains two cylindrical magnets (NdFeB-N52, 4x20 mm) and one square magnet (NdFeB-N52, 1.5x4x20 mm).

4.2 Mechanical Analysis

The mechanical analysis is focused on the most challenging part of the design, which is the actuation force required to steer the permanent magnets. The major goal of this analysis is to set and solve the equations of force and torques in order to quantify the actuation force.

Despite the fact that the modulator offers a wide range of force modulation, the rotation of the steerable magnets has been limited from 0° to 135° in order to reduce the actuation force by having a wider helix angle of about 75° .

4.2.1 Theoretical Modulator Actuation Force

Two theoretical models are proposed to describe the actuation force of the modulator: A simplified first model (Model I) takes into account the pin slot interactions. A second model (Model II) further considers the interactions in the ruby bushings. Both models neglect friction at the ruby pivot as well as the interactions of the actuation rod with the brass bushing situated in the extremities of the modulator.

Based on the free-body diagrams of figure 4.6, the actuation force F_a required to actuate the modulator, namely steering the permanent magnets can be calculated for the two models.

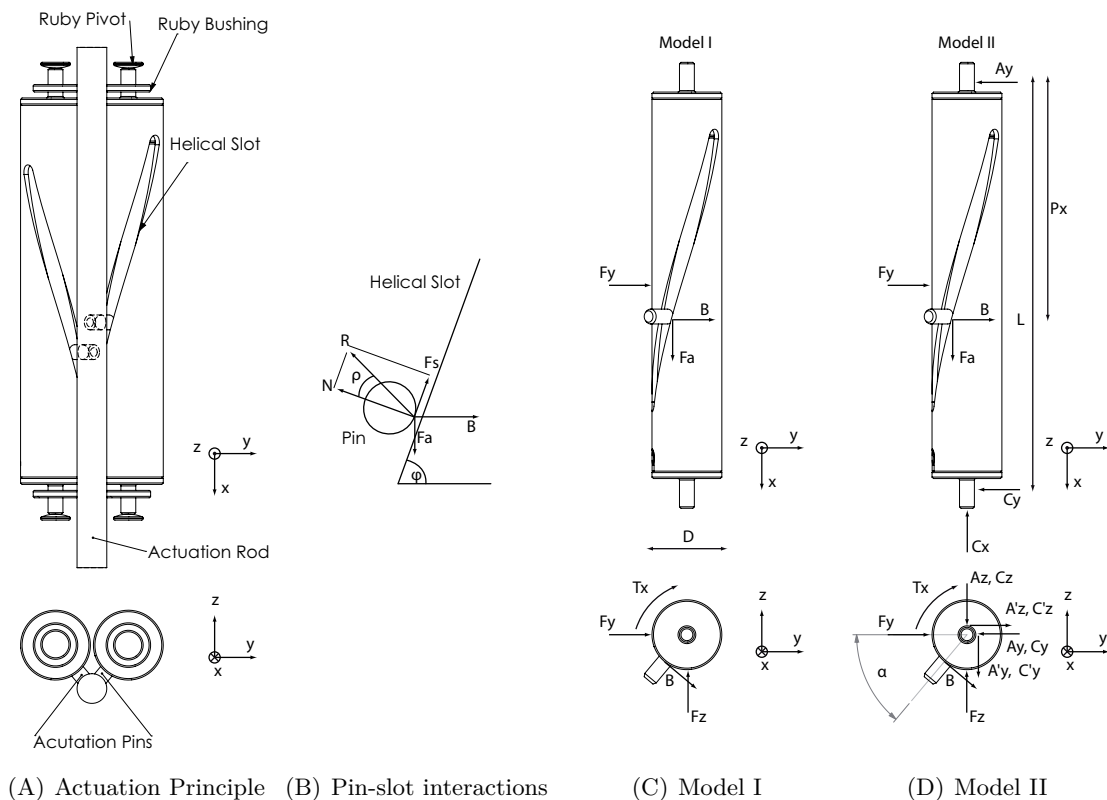


Figure 4.6: Free-body diagrams of modulator subsystems used in the different systems of equations and to calculate the resulting actuations forces.

4. Magnetic Force Modulator

Complex magnetic interactions occur in the modulator between the steerable magnets and the third square magnet. These interactions not only depends on the steerable magnets orientations but also on the proximity with the guided MAGS element. Due to this magnetic complexity, the magnetic torque $T_x(\theta)$ and forces $F_y(\theta)$ and $F_z(\theta)$ of the steerable permanent magnet are obtained, as a function of the modulator angle θ , by FEM calculation, figure 4.7. To simplify the notations, $T_x(\theta)$, $F_y(\theta)$ and $F_z(\theta)$ are noted T_x , F_y and F_z . One can notice how significant are these interactions. Moreover, the magnetic torque changes sign (direction) during the rotation of the steerable magnets. The torque is null at $\theta=50^\circ$, which correspond to the theoretical point of equilibrium θ_0 of the modulator.

Consequently, as the magnetic torque changes direction during a pull-push actuation cycle, four actuation cases are considered:

1. Pulling phase, pin sliding with the help of the magnetic torque
2. Pulling phase, pin sliding against the magnetic torque
3. Pushing phase, pin sliding with the help of the magnetic torque
4. Pushing phase, pin sliding against the magnetic torque

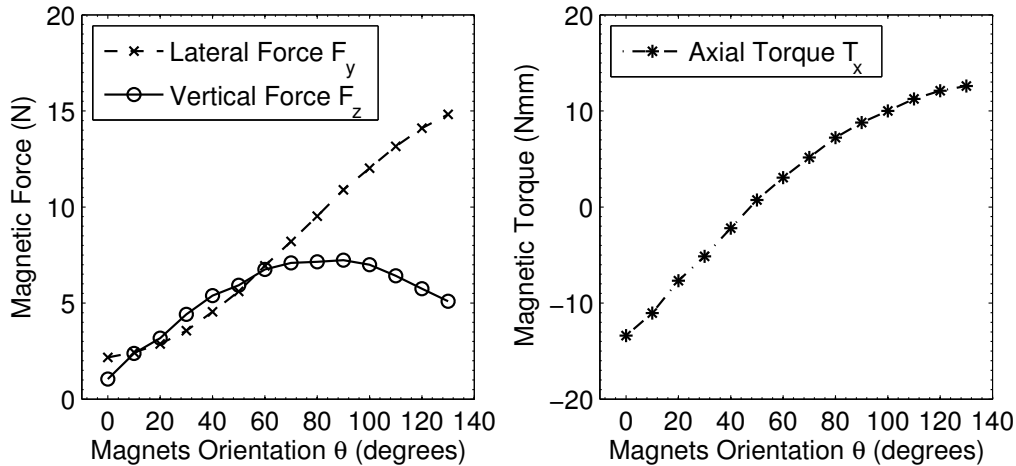


Figure 4.7: 3D-FEM results of the lateral and vertical magnetic forces as well as the magnetic torque acting on the steerable magnets. The steerable permanent magnets are repulsed laterally and attracted by the third square magnet. The magnetic torque change sign at $\theta=50^\circ$, which is also the theoretical point of equilibrium of the modulator, indicated as θ_0 .

Model I

A first approach consists of neglecting the friction on the bushings. Only the friction between the sliding pin and the slot is considered. The set of equations for the body

diagram of figures 4.6(B) and 4.6(C) are given by:

$$\left\{ \begin{array}{l} x: F_a - N\cos(\varphi) - F_s\sin(\varphi) = 0 \\ y: B - N\sin(\varphi) + F_s\cos(\varphi) = 0 \\ M_x: T_x - B\frac{D}{2} = 0 \\ \tan(\rho) = \frac{F_s}{N} = \mu_1 \end{array} \right.$$

where

N : Reaction force

F_s : Friction force between the pin and the slot

μ_1 : Friction coefficient between the pin sliding on the slot

T_x : Magnetic torque acting on one steerable permanent magnet

F_y, F_z : Magnetic forces acting on one steerable permanent magnet

D : Outer diameter of the slotted tube

φ : Angle of the helical slot

The unknown variables are F_a , B , F_s and N . The set of equations describing Model I can be solved as follows:

$$\begin{aligned} B &= N(\sin(\varphi) - \mu_1\cos(\varphi)) \\ F_a &= N(\cos(\varphi) + \mu_1\sin(\varphi)) \\ N &= \frac{F_a}{\cos(\varphi) + \mu_1\sin(\varphi)} \\ B &= \frac{F_a(\sin(\varphi) - \mu_1\cos(\varphi))}{\cos(\varphi) + \mu_1\sin(\varphi)}, / \cos(\varphi) \\ B &= \frac{F_a(\tan(\varphi) - \mu_1)}{1 + \mu_1\tan(\varphi)} = \frac{F_a(\tan(\varphi) - \tan(\rho))}{1 + \tan(\rho)\tan(\varphi)} = F_a\tan(\varphi - \rho) \end{aligned} \quad (4.1)$$

As a result of some algebraic manipulation, the actuation force to actuate both magnets $F_{a,m1}$ can be expressed:

$$F_{a,m1} = 2F_a = \frac{2B}{\tan(\varphi - \rho)} = \frac{2T_x}{\frac{D}{2}\tan(\varphi - \rho)} \quad (4.2)$$

Applying equation 4.2 to the four actuation cases, a full pulling-pushing cycle is given by:

$$F_{a,m1} = \begin{cases} 2\frac{T_x}{\frac{D}{2}\tan(\varphi + \rho)}, \text{ pulling phase, } \theta \in [0, \theta_0] \\ 2\frac{T_x}{\frac{D}{2}\tan(\varphi - \rho)}, \text{ pulling phase, } \theta \in [\theta_0, \theta_{max}] \\ 2\frac{T_x}{\frac{D}{2}\tan(\varphi + \rho)}, \text{ pushing phase, } \theta \in [\theta_{max}, \theta_0] \\ 2\frac{T_x}{\frac{D}{2}\tan(\varphi - \rho)}, \text{ pushing phase, } \theta \in [\theta_0, 0] \end{cases} \quad (4.3)$$

4. Magnetic Force Modulator

where θ_0 is the angle at which the magnetic torque on the steerable magnet is null. Equation 4.3 with its validity regions is plotted in figure 4.8. One can notice that the actuation force cycle has a “bow tie” shape due to the change of magnetic torque at $\theta=50^\circ$. The hysteresis increases with the friction coefficient between the slider and the slot. The standard friction coefficient for harden steel (pin) and bronze (slot) is ~ 0.35 . As the force exerted on the thin slot is significant, the choice of materials is important, figure 4.9. The use of lubricant as well as a good choice material is necessary to reduce the actuation force and extend the service life of the modulator.

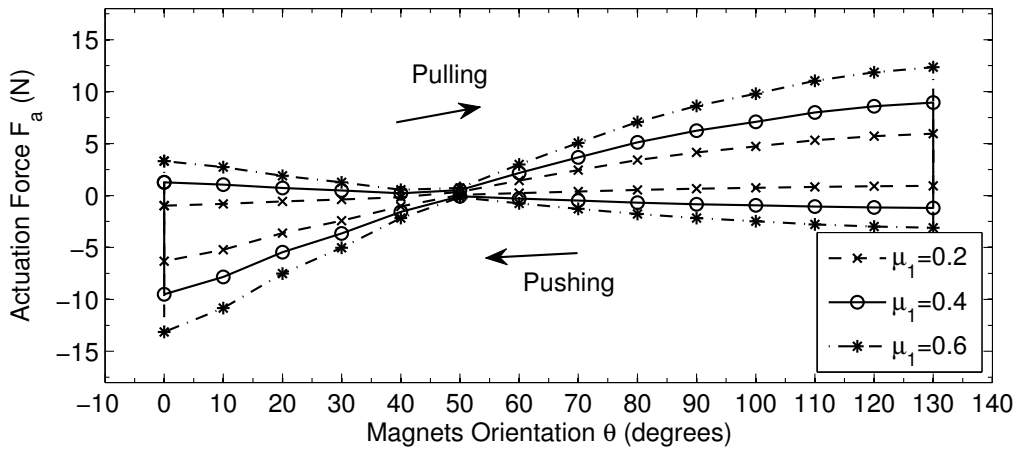


Figure 4.8: Theoretical actuation force for pull-push cycle based on model I, where only the friction interactions located at the pin-slot interface. The actuation force cycle has a “bow tie” shape due to the change of magnetic torque at $\theta=50^\circ$, which is the theoretical equilibrium point θ_0 . The curves do not exactly pass trough zero as they are made from discrete values. The friction coefficient value between the pin (hard steel) and the helical slot (bronze) increases the hysteresis. A standard friction coefficient for steel on bronze is $\mu_1=0.35$, which gives a maximal actuation force around 7 N.

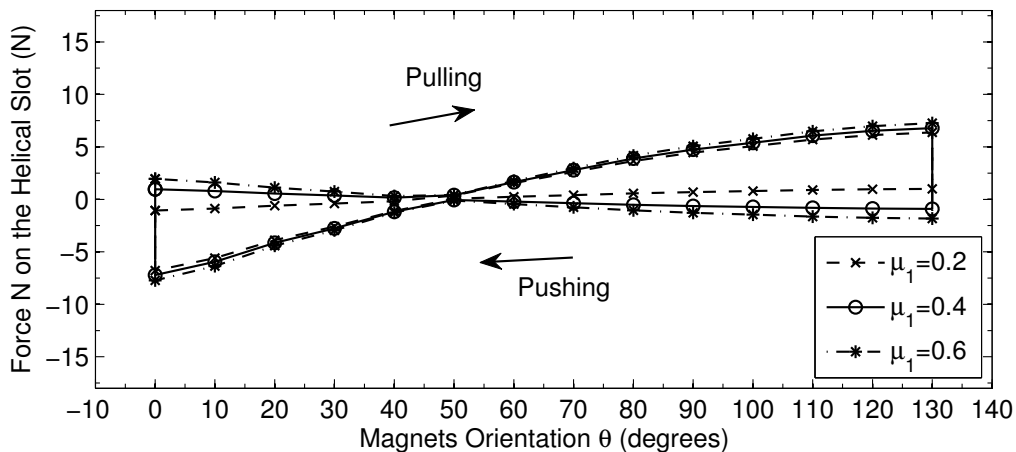


Figure 4.9: Theoretical normal force acting on the helical slot using model I. As the slot is thin (0.35 mm), the resulting pressure is rather significant.

4. Magnetic Force Modulator

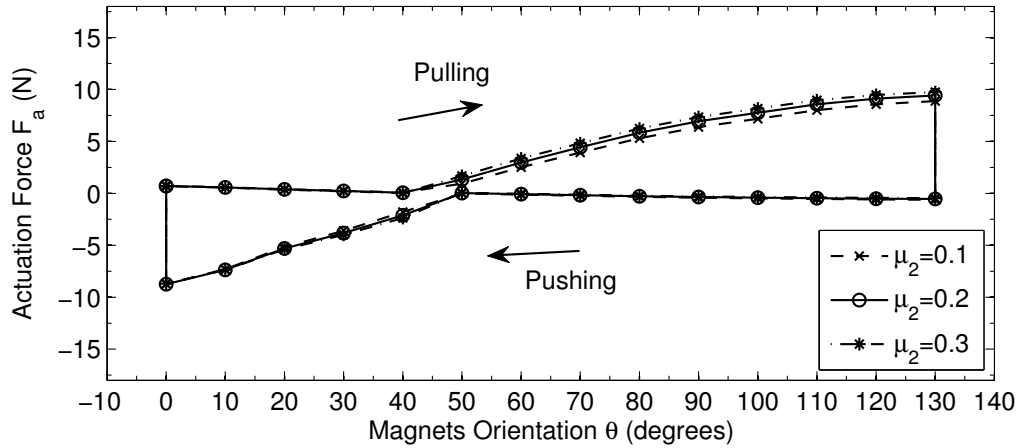


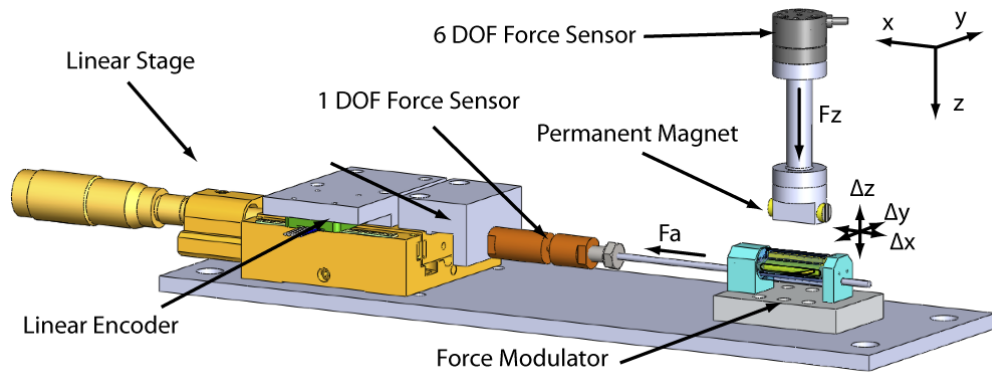
Figure 4.10: Theoretical actuation force for pull-push cycle based on model II where friction exerted on the ruby bushing is further considered. The frictional contributions on the ruby bushings is affecting the width of the “knot” of the “bow tie” shaped hysteresis. Two equilibrium points are possible depending on the phase of the actuation cycle. One may notice that the contribution from the friction on the ruby bushings μ_2 is much smaller than the contribution from the pin-slot interface.

be observed that the second magnetic element of the MAGS influence the pulling force especially at small separation distance. The pulling cycle requires more actuation force than the pushing phase. The hysteresis is due to the friction in the system, namely the friction at the pin-slot interface and the friction in the bushings. During the pulling phase, the magnetic torques are opposed to the rotation of the magnets. In the pushing phase, these magnetic torques act in the same direction as the pushing force, and therefore reduce the required force to actuate the modulator. As the modulator is sensitive to lubrication and particles generated from friction, the measurements are shown for a single push-pull cycle at each configuration.

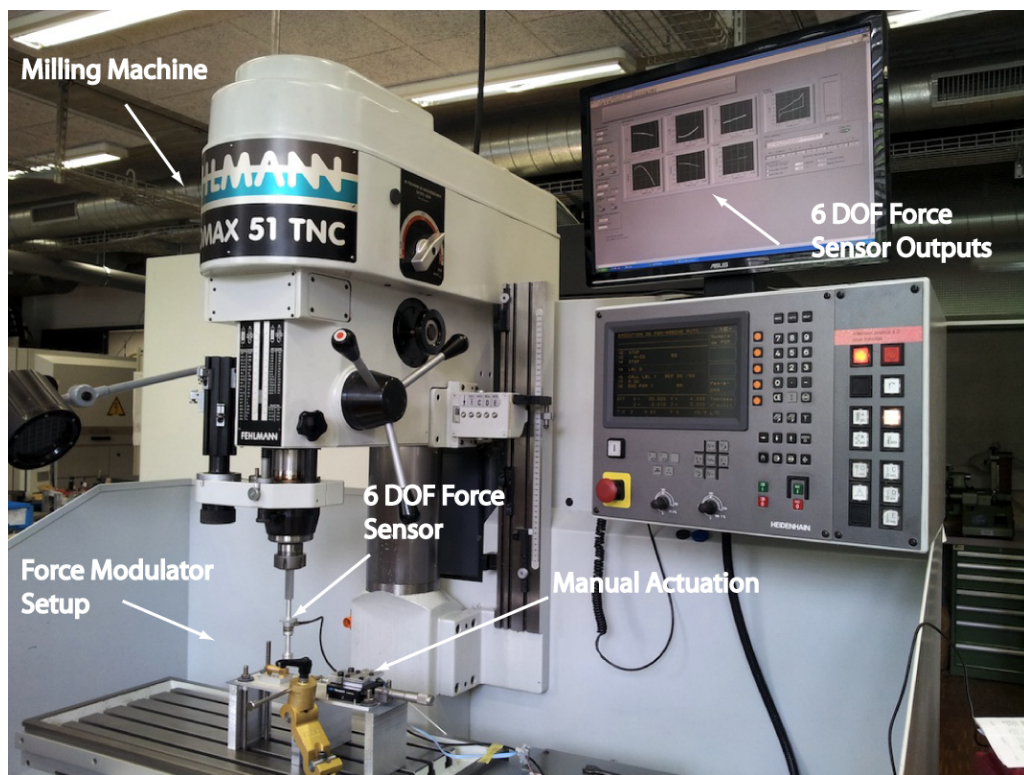
4.2.3 Comparison of Theoretical and Experimental Actuation Force

Theoretical models and experimental measurements of the actuation forces are compared in figure 4.13. The “bow tie” shape of the theoretical actuation force is not present on the experimental data. This may be explained by a very small angular misalignment of the two steerable magnets. An angular misalignment of the magnets generates undesirable lateral forces within the MAGS, as shown in the next section in figure 4.17. The zero magnetic torque of the modulator is not identical for both magnets. In other terms, the zero magnetic torque of the modulator has disappeared: when one magnet reaches its zero magnetic torque, the second magnet is still under a magnetic torque. As the actuation force is the force required to rotate both magnets, the prototype is always subject to a magnetic torque during its actuation.

Another difference between the modelling results and the measurements is visible at the extremities of the hysteresis loop. The measured actuation force is higher than the theoretical value most likely due to an increase of friction in these regions. High magnetic torques might have eroded the slots surface resulting in a increase of friction.



(A) Actuated and sensorized modulator



(B) Measurement setup mounted on a milling machine

Figure 4.11: Measurement of the actuation force F_a required to rotate the steerable magnets as well as the magnet forces and torques within the MAGS. (A) The pull-push force is obtained with a 1-DOF force sensor. The actuation rod is linked to a linear stage equipped with a linear encoder, which provides the actuation force in function of the magnet orientation. The passive magnet is mounted on a 6-DOF force sensor to measure the magnetic interactions within the MAGS. (B) A milling machine is used to position with precision the passive magnet at different separation distances Δ_z from the modulator surface and at several lateral offset positions Δ_x and Δ_y .

4. Magnetic Force Modulator

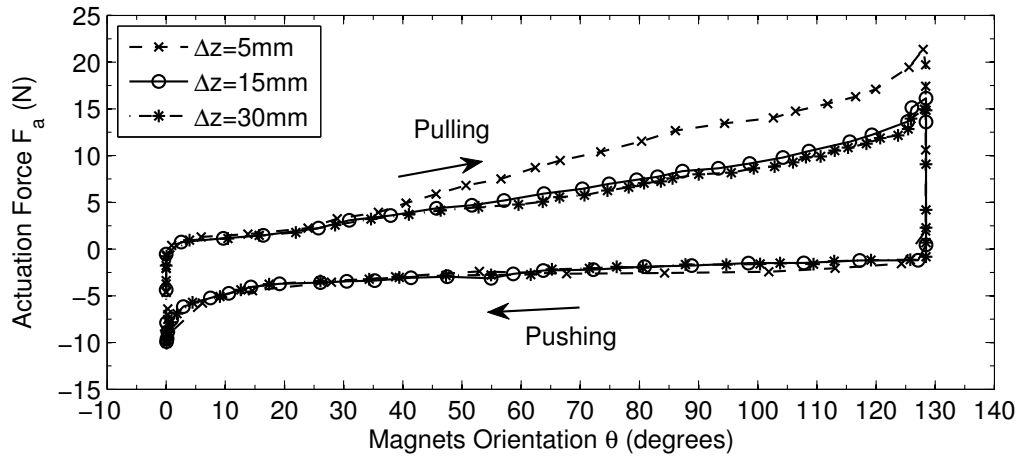


Figure 4.12: Measurement of the force required to actuate the *in vitro* modulator in a full pull-push cycle. A separation distance of $\Delta z=30$ mm represents the typical force profile to actuate the modulator under no external magnetic interactions.

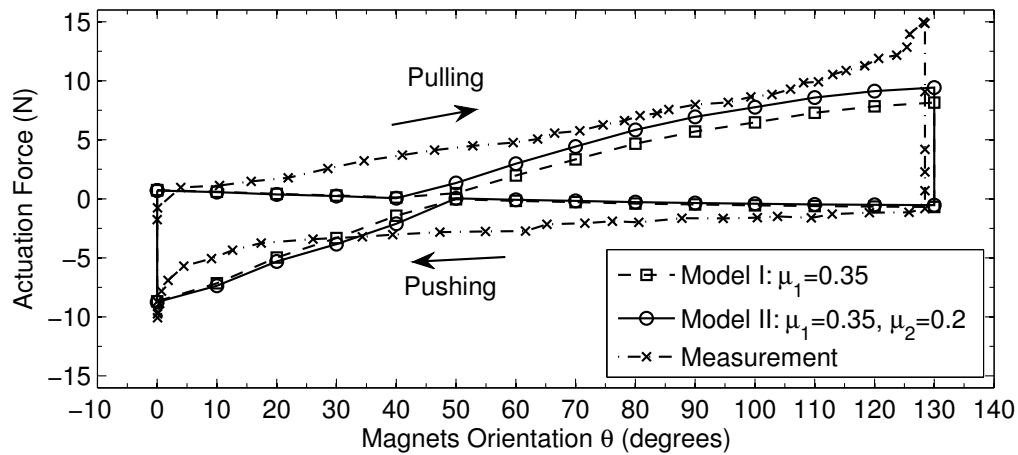


Figure 4.13: Theoretical calculation and experimental measurements of the actuation force. μ_1 is the friction coefficient at the pin-slot interface and μ_2 for the ruby bushing contribution.

4.2.4 Effect of the Modulation Range on the Actuation Force

Although the rotation of the steerable magnets of the modulator has been intentionally limited to 135° in order to reduce the actuation force, the effect of the rotation range on the actuation force is represented in figure 4.14. A wider modulation range, namely a wider rotation range of the magnets, implies a smaller angle for the helical slot resulting in an increase of the actuation force. However, this increase is balanced by the decrease of the axial magnetic torque T_x of the magnets appearing at the end of the pulling phase.

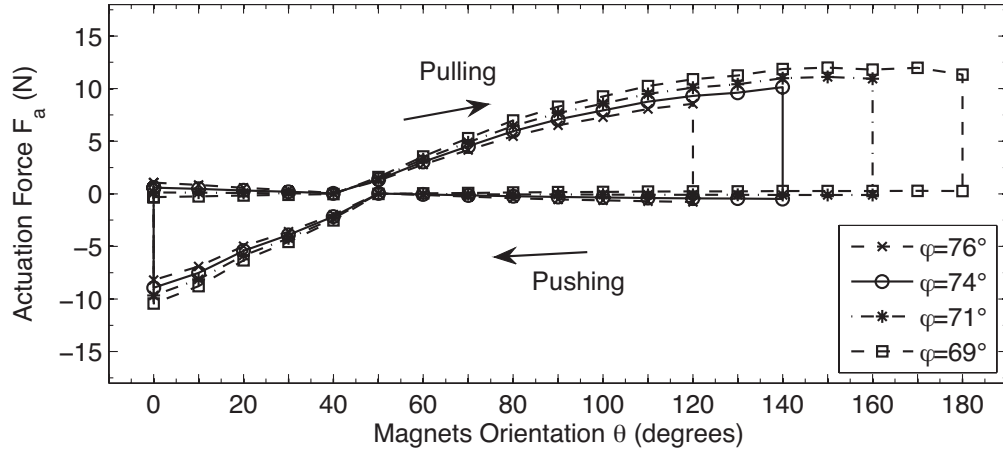


Figure 4.14: Theoretical calculation of the actuation force as a function of the modulation range based on Model II. φ is the angle of the helical slot, which converts an axial displacement of the actuation rod into a rotation of the magnets.

4.3 Magnetic Analysis

This section focuses on the magnetic coupling force between the MAGS members. Theoretical FEM calculation are compared with measured data. A variation in the spatial configuration of the MAGS members affects strongly their magnetic interactions as illustrated in this section. The magnetic measurements were achieved with the same experimental setup as for the actuation force measurement.

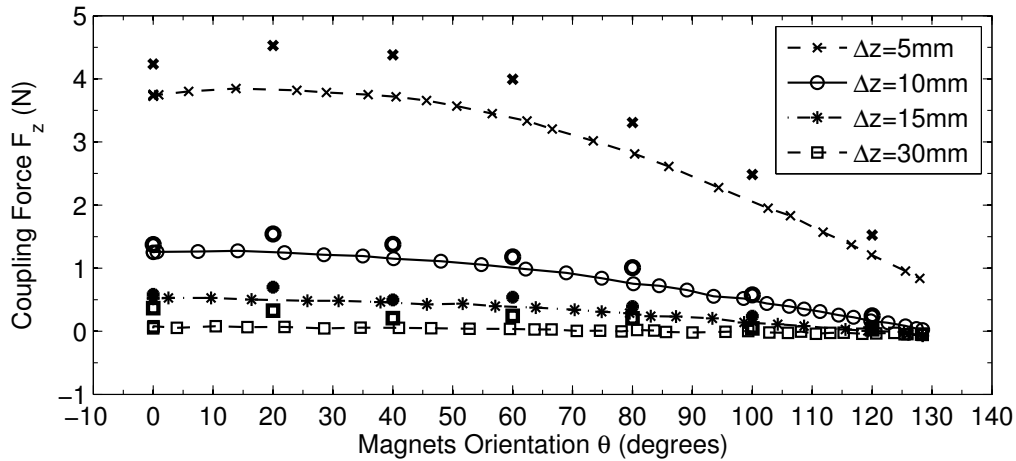
4.3.1 Magnetic Coupling Force

Figure 4.15 shows the experimental coupling force within the MAGS at different separation distances. FEM values of the coupling force are also represented with bold markers. The coupling force can be modulated by steering in opposite direction the two parallel magnet. The maximum coupling force is reached at $\theta=20^\circ$, which corresponds to the situation where the field lines of the steerable permanent magnets are slightly oriented in the direction of the static square magnet. Moreover, one may notice how the coupling force decreases exponentially with the separation distance. Differences between the the FEM calculation and the experimental measurements are mainly explained by the difference in magnetization of the magnet. After investigation, it turns out that the manufactured magnets used in the prototype have a magnetization strength between 5 to 10% lower than the requested specifications which explains the differences.

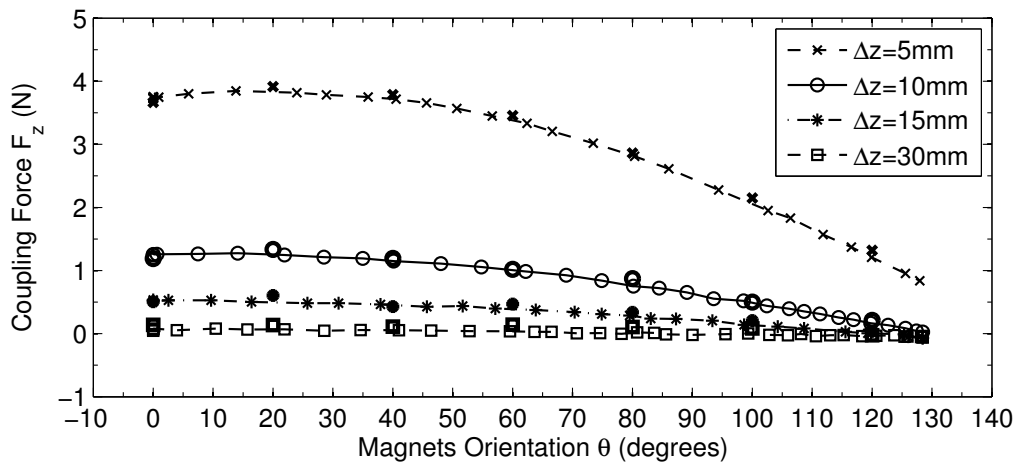
4.3.2 Magnetic Forces and Torques

As seen in the previous subsection, the coupling force can be adjusted by steering the permanent magnets of the modulator. The coupling force is not only related to the separation distance within the MAGS but is also sensitive to any axial or lateral misalignments. For example, an axial misalignment of the two magnetic elements is noticed during the guidance. In fact, the axial dragging force generated by the voluntary axial misalignment is responsible of the magnetic following.

4. Magnetic Force Modulator



(A) Theoretical FEM and experimental coupling force



(B) Adjusted theoretical FEM and experimental coupling force

Figure 4.15: Theoretical FEM and experimental coupling force at different separation distances Δ_z . The bold markers represent the theoretical values and the lines are the experimental data: (A) The experimental coupling force is lower than the theoretical calculation, however they follow the same trend. (B) After investigation, it turns out that the manufactured magnets used in the prototype have a magnetization strength between 5 to 10% lower than the requested specifications. With an adjustment of 7% lower for the magnetization of the PM, the theoretical calculation match the measurements.

Figure 4.16 shows the coupling force and the dragging force as well as the pitch torque as a function of an axial dragging shift of the MAGS members. The pitch torque is the torque occurring to an angular movement (inclination) around the lateral axis of the guided part. One could remark that the coupling force is decreasing in a quasi-linear manner. The coupling force is reduced by 50% at a displacement of half the length of the PM. An offset superior to the length L of the magnet will result in a disconnection of the MAGS as two repulsive poles are coming closer. The magnetic torque generated by the axial dragging shift leads to a tilt of the MAGS members. In other terms, the following passive magnets will tend to slightly nosedive as opposed to the modulator which will tend to tilt back.

The magnetic torque is, in fact, not favourable for the magnetic guidance on deformable surfaces, as it balances the pressure density at the front of the guided magnet, which may increase the friction with the surface as it creates a lip in the tissue at the front of the guided magnet. Therefore, the dragging offset during guidance should be kept as small as possible by either modulating the coupling force or reducing the friction with the tissue by means of medical coatings such as hydrophilic coatings. More details on this phenomenon are given in chapter 7.

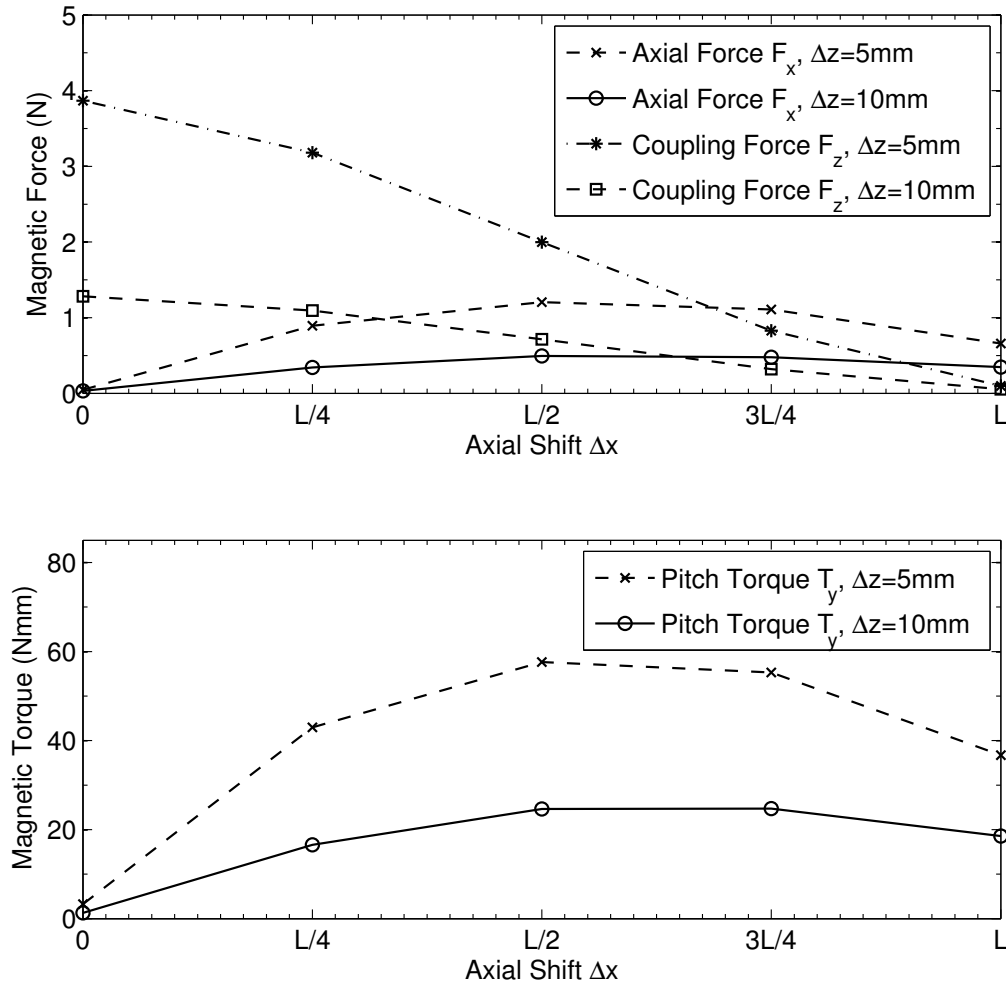


Figure 4.16: Experimental measurements of the magnetic forces and torque as a function of an dragging shift of the passive magnet for two separation distances Δ_z . One could remark that the coupling force is decreasing in a quasi-linear manner. The coupling force is reduced by 50% at a displacement of half the length of the PM. An offset superior to the length L of the magnet will result in a disconnection of the MAGS as two repulsive poles are coming closer.

Figure 4.17 shows the effect of a lateral shift coupled with an axial displacement on the magnetic forces and torques for a separation distance of $\Delta_z=5\text{ mm}$. One could deduce that the dragging and coupling forces are lower if the passive magnet is laterally shifted. Concerning the torques, the roll torque, generated by the lateral shift, is of much bigger magnitude compared to the pitch torque. The roll torque is the torque occurring to an

4. Magnetic Force Modulator

angular movement around the longitudinal axis of guided part. In reality, the passive magnet will rotate along its longitudinal (axial) axis to realign its magnetic field with the modulator. It is important to keep in mind that a lateral shift has a dual effect: The magnetic fields are misaligned and the separation distance is increased even if Δ_z is kept constant. $\Delta_d^2 = \Delta_y^2 + \Delta_z^2$.

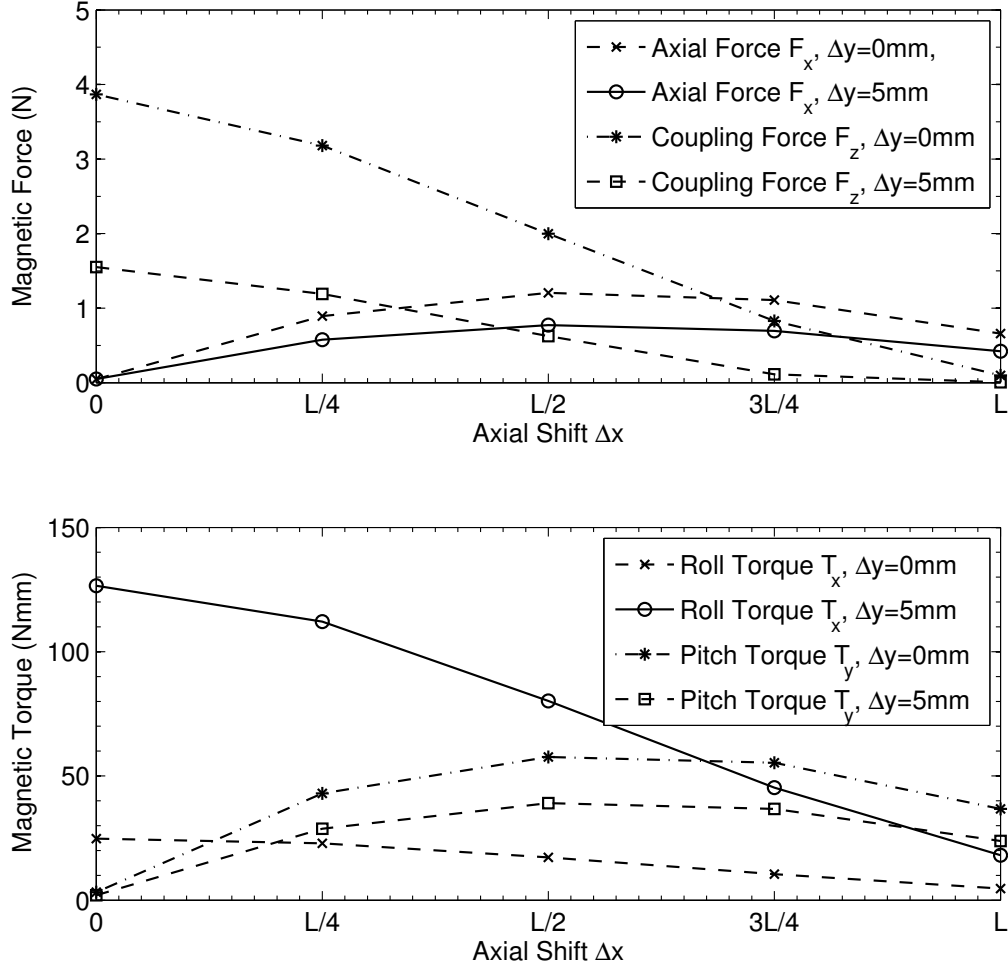


Figure 4.17: Experimental measurements of the magnetic forces and torques within the MAGS as a function of an dragging shift Δ_x as well as a lateral misalignment Δ_y of the passive magnet. L corresponds to the length of the magnet and the separation distance Δ_z has been set to 5 mm.

4.4 Expected Performances of a Catheteric Modulator

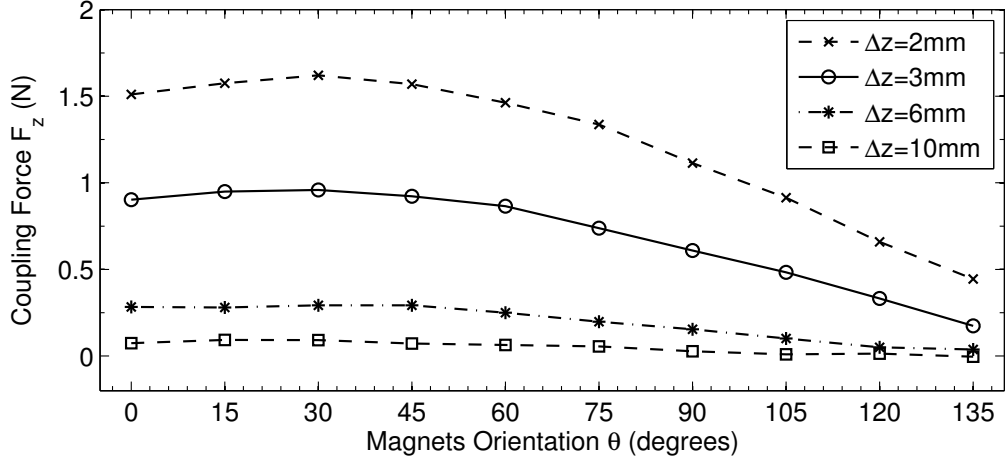
The manufacturing of the *in vitro* prototype, its actuation principle and characterization confirm the technical feasibility of permanent magnets based modulators for adjusting the coupling force in an intracorporeal MAGS.

The next step will be to scale down the modulator to match the dimensional specifications imposed by most cardiovascular applications such as the treatment of atrial fibrillation. Therefore, the dimensions of the *in vitro* prototype have been divided by half

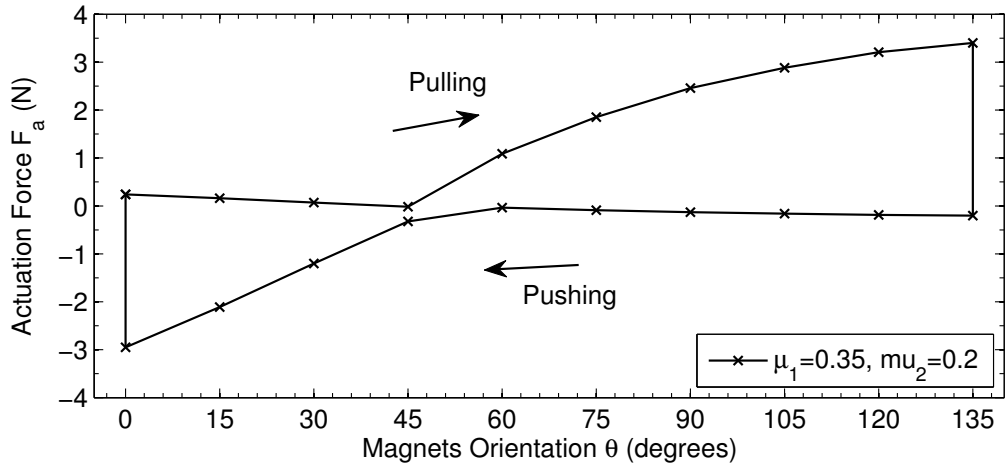
4.4 Expected Performances of a Catheteric Modulator

to a diameter of 5 mm for the active catheter and a diameter of 3.5 mm for the passive catheter.

Preceding the manufacturing, a 3D-FEM modelling of the expected mechanical and magnetic performances of this miniature MAGS has been executed, as shown in figure 4.18(A).



(A) Coupling Force F_z



(B) Actuation Force F_a

Figure 4.18: Expected magnetic and mechanical performances of a catheteric modulator: (A) 3-dimensional FEM results of the coupling force amplitude and modulation range for a catheter MAGS placed at various separation distances Δ_z . (B) Full actuation cycle of the catheter MAGS based on the theoretical model II, equation 4.5.

The fabrication of this force modulator integrated in an actual catheter will be realized in the very near future. This manufacturing and assembly are rather complex and require the expertise of a company active in the catheter field. This step is necessary to validate *in vivo* the technical feasibility of the intracorporeal magnetic guidance in the treatment of cardiac arrhythmias. However, the current *in vitro* prototype is sufficient and more suitable to understand the limitations of magnetic guidance with single magnets and to

4. Magnetic Force Modulator

demonstrate the benefits magnetic guidance with force modulation could provide.

4.5 Fabrication

The *in vitro* prototype of 10 mm in diameter has been produced at EPFL in the micro-engineering workshop. All the metallic parts of the modulator are made of non-magnetic materials except for the sliding pins that steer the permanent magnets which are in hardened steel. Hardened bronze has been chosen for the slotted-tubes that contains the magnets, for its relatively low friction coefficient compared to non magnetic stainless-steel. As the interaction forces between thin slotted-tube and the sliding pins are significant, hardened bronze offers a good compromise in terms of friction and stiffness over other non-magnetic materials such as brass, aluminium, stainless-steel or titanium. The other parts of the modulator are made of brass, except for the actuation rod which is made of stainless steel 316L and the bushings which are made of ruby. The ruby bushings and hemispherical pivots have been purchased from Crelier Fils SA, specialized in the watch industry. To match our specifications, the permanent magnets are custom-made in China through a Germano-Swiss company Supermagnete GmbH. The magnets have been ordered with a magnetization of 1'115 kA/m or with a magnetic energy density of 52 MGOe (414 kJ/m³).

Manufacturing Process

Computer Numerical Control (CNC) and conventional machining was used to realize the metallic parts of the modulator. Tight tolerances are needed in some parts to insure the functionality of the mechanism. Initially, the helical slot has been realized by laser cutting. However, the resulting surface quality of the slot was too rough and a second approach with CNC machining was considered. The result was a slot with much better quality of surface.

Assembly

Even though, the metallic parts of the modulator were realized with the correct tolerances, the assembly of the *in vitro* prototype was not straight forward as the magnets were already magnetized by the supplier.

The first difficulty was to fix the steerable magnet to the slotted tubes at the correct angular orientation. The direction of magnetization was detected manually by means of other ferromagnetic elements that align the magnet in a known position. Then the magnet was attached with an instant adhesive to one of the tube's cap in the right angular orientation. The cap contains an angular reference, which is used to position the slotted tube and the magnet in the right corresponding orientation. This task is delicate and may represent a source of error, which could led to undesired asymmetry in the magnetic field of the modulator.

Once the steerable magnets were correctly mounted on the slotted tubes, the second challenge was to assemble the magnetic elements in the modulator. Their small size and their strong magnetic interactions were the main reasons.

To improve the assembly of the modulator, it will be preferred to magnetize the magnets after the complete assembly of the modulator. However, this scenario requires some special equipment able to create high degree of magnetization in the magnets.

4.6 Summary

The implementation of a magnetic force modulator for minimally-invasive applications has been presented discussed. The mechanical actuation based on the “lipstick” mechanism has been chosen to steer the permanent magnets as it represents the most reasonable approach. A first *in vitro* prototype of 10 mm has been manufactured and characterized. The actuation force required to actuate the modulator has been compared through theoretical models and experimental data. The mechanical and magnetic results confirm the feasibility of using steerable permanent magnets for adjusting the magnetic force within a MAGS of millimetric dimension.

The next step is to fabricate a second prototype of 5 mm in diameter that could be tested in an animal beating heart. This magnetic modulator will be implemented in a catheter tip and dedicated to the treatment of cardiac arrhythmias in accordance with the Maestro-AF project. Expected magnetic performances of this second version have been shown and results are encouraging. Its complete realization is planned in the next few months. It will require the expertise of a company in the field of catheterization. Meanwhile, *in vitro* tests have been performed with the 10 mm prototype and the benefits of modulating the coupling force during the guidance are discussed in chapter 6.

5 Guidance Analysis

The goal of this chapter is the analysis of the magnetic guidance behavior for a MAGS composed of the *in vitro* force modulator and a passive magnet. The force modulator comprises two parallel steerable magnets reinforced with a fixed magnet. Two guidance modes are proposed: a passive mode and an active mode. A custom made characterization setup was used to describe and compare the guidance modes.

5.1 Guidance Modes

Two modes are proposed to guide magnetically the passive element of the MAGS. The first mode is passive and consists of setting the magnetic modulator at a static magnetic field during the guidance. This mode may represent the case of a MAGS where both members are equipped with a single permanent magnet. Active mode consists in adjusting automatically or manually the coupling force in the MAGS during the guidance. To accomplish this task, a force sensor is implemented to provide force feedback information on the coupling force. The latter is used to modulate the magnetic field in order to keep the coupling force of the MAGS constant while guided over variable conditions. Two force feedbacks (FFB) loops are tested. They provides information either on the coupling force or both coupling and dragging force.

5.1.1 Passive Mode

To simulate a MAGS where both parts contain a single permanent magnet, the passive mode consists of setting the modulator's angle θ at a fixed orientation during the guidance. Obtaining the right coupling force in the MAGS by choosing the correct dimensions of the permanent magnets requires user experience and anatomical information such as the separation distance (tissue thickness and variations), type of tissue (soft, hard), etc...

5.1.2 Active Mode

The active mode proposes a manual or an automatic adjustment of the magnetic field in order to provide a constant coupling force for a given range of tissue thickness and MAGS positioning. As seen in chapter 4, the coupling force is very sensitive to any variations in the separation distance but also to any misalignments of the MAGS. Implementing a system that keeps the force constant during the guidance will certainly offer more robustness and safety over the passive mode. To realize this, a feedback in force is needed

5. Guidance Analysis

as well as a controller and an actuator to drive the modulator. The controller will be described in this section and the hardware components will be detailed in section 5.2.

As a matter of fact, another approach without an integrated force sensor could consist of adjusting manually the coupling force during the guidance under visual feedback by means of live fluoroscopic images.¹ The operator varies the coupling strength as a function of the tissue thickness or orientation angles of the MAGS. One can imagine the implementation of an adjusting ruler based on tissue thickness. The operator simply adjusts the coupling force by selecting the corresponding separation distance of the MAGS.

Architecture

The proposed controller architecture comprises three elements: a proportional-integral (PI) controller completed with a feed-forward (FFD) controller, and a force feedback (FFB) loop. Three variants of FFD controller and two variants of FFB loop are suggested and illustrated in figure 5.1.

PI Controller

A proportional–integral–derivative controller (PID controller) is a generic control loop feedback mechanism widely used in industrial control systems. A PID controller calculates an “error” value as the difference between a measured process variable and a desired setpoint. The controller attempts to minimize the error by adjusting the process control inputs. A PI controller is a proportional gain in parallel with an integrator. The proportional gain provides fast error response. The integrator drives the system to a zero steady-state error. Although the derivative term reduces the magnitude of the overshoot produced by the integral component, it is not needed in this case as it slows the response of the controller output.

Defining $u_{out}(t)$ as the controller output, the PI algorithm is described by:

$$u_{out} = K_p e(t) + K_i \int_0^t e(\tau) d\tau \quad (5.1)$$

where

K_p : Proportional gain, a tuning parameter

K_i : Integral gain, a tuning parameter

e : Difference between the process variable and the desired setpoint

A high proportional gain K_p results in a large change in the output for a given change in the error e . If the proportional gain is too high, the system can become unstable. On the other hand, a small gain results in a small output response to a large input error, and a less responsive or less sensitive controller. If the proportional gain is too low, the control action may be too small when responding to system disturbances. A pure proportional controller generally operates with a steady-state error, which can be corrected by adding an integral term.

The integral term is the sum of the errors over time. It gives the accumulated offset that should have been corrected previously. The accumulated error is then multiplied by

¹Fluoroscopy is an imaging technique that uses X-rays to obtain real-time moving images of the internal structures.

the integral gain K_i and added to the controller output. In others terms, the integral term accelerates the movement of the process towards the setpoint (desired value) and eliminates the residual steady-state error that occurs with a pure proportional controller. However, since the integral term responds to accumulated errors from the past, it can cause the present value to overshoot the setpoint value. Therefore, the PI controller parameters should be chosen carefully.

Force Feedback Modes

The potential sources of magnetic feedback are multiple, namely three forces and three torques. However, the magnetic forces are easier to interpret than the torques to understand the guidance behavior. Figure 5.2 represents the attraction forces during the guidance. For simplification, the center of the forces is placed on the centre of mass of the magnets. In reality, the gradient of force is asymmetric when the magnets are misaligned. The magnetic forces are defined as F_d for the dragging force acting in the axial direction of the magnets along the x axis and F_c the coupling force in the radial direction is in the yz plane as the magnetization direction of the magnets may slightly rotate along their axis during the guidance. A 3-DoF sensor is required to measure these attraction forces as the coupling force is the resultant force of the forces in y and z directions. F is the coupling force within the MAGS. It corresponds to the resultant force between F_d and F_c and β is the angle of the force with the yz plane. When, the MAGS parts are aligned, the dragging force F_d and the angle β are null as their the magnetization field direction is in the same plane. Therefore, the force feedback could be achieved either with the coupling force F_c or with the resultant force F .

$$\begin{cases} \text{case 1 : } & F = F_c \\ \text{case 2 : } & F = \sqrt{F_d^2 + F_c^2} \end{cases}$$

These two sources of feedback have been tested and are compared in section 5.3.

Feed-Forward Control Modes

While PI control is a controller which does not require any model of the process, better performance can be obtained by incorporating a model of the process in the control architecture by adding a feed-forward controller. An improvement can be achieved by incorporating a feed-forward with knowledge of the system, and using the PI controller only to control the error.

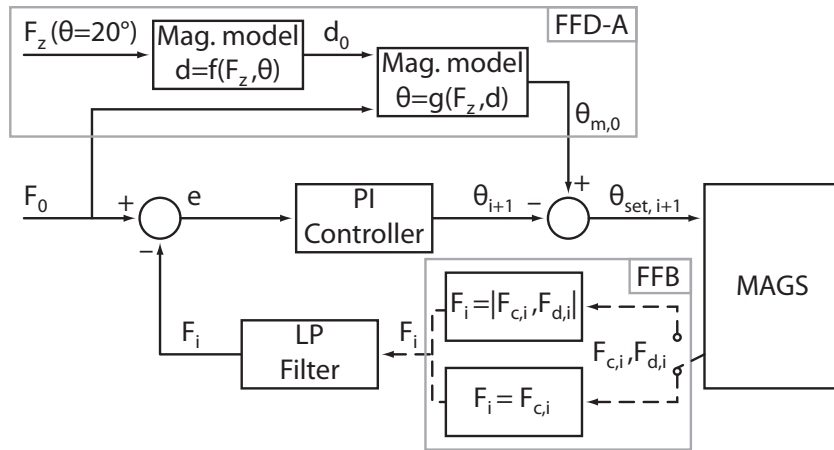
The understanding of the system to control is provided by magnetic models that can predict the modulator's angle as a function of the coupling force and the separation distance as shown in figure 5.3. As the coupling force F_z depends on the angle of the modulator θ and the separation distance d , estimation of the separation distance is required to provide the a priori knowledge of the modulator angle. From the FEM results of figure 5.3, two polynomial functions f and g can be obtained using a surface-fitting tool.

$$\begin{aligned} d &= f(F_z, \theta) = p_0 + p_1x + p_2y + p_3x^2 + p_4xy + p_5y^2 + p_6x^3 + p_7x^2y + p_8xy^2 + p_9y^3 \\ \theta &= g(F_z, d) = p'_0 + p'_1x + p'_2y + p'_3x^2 + p'_4xy + p'_5y^2 + p'_6x^3 + p'_7x^2y + p'_8xy^2 + p'_9y^3 \end{aligned}$$

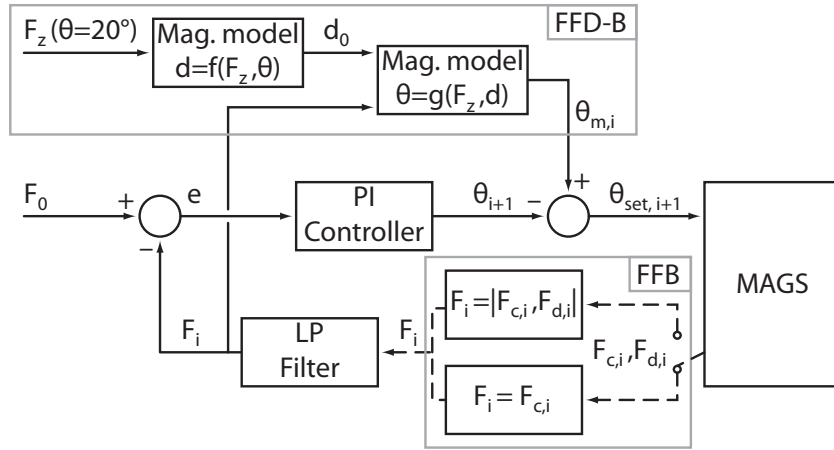
From these polynomial functions describing the magnetic interactions within the MAGS, three feed-forward versions are proposed as shown in figure 5.1. The method proceeds as follows for each control version:

5. Guidance Analysis

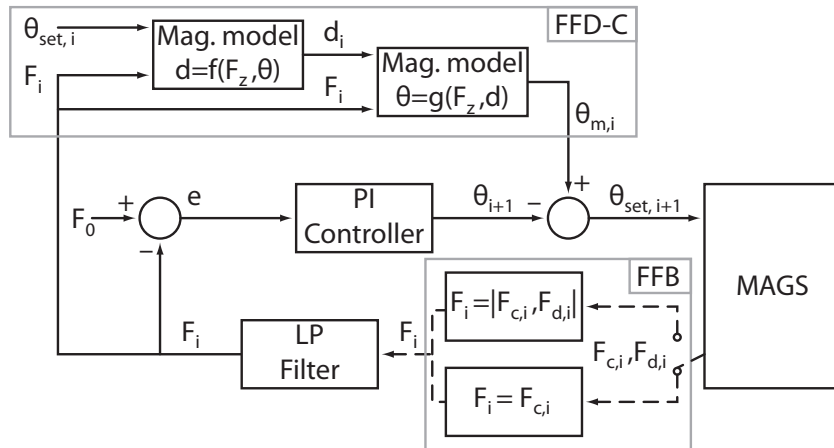
- The FFD-A version is using a constant a priori modulation angle, which is determined at the beginning of the guidance. As the coupling force is maximum for an angle of $\theta=20^\circ$, the separation distance d_0 is obtained by measuring the coupling force at this angle of the modulator. Knowing the separation distance d_0 , the a priori modulation angle $\theta_{m,0}$ is calculated for a desired coupling force F_0 .
- The FFD-B version is also using a constant separation distance during the guidance but the a priori modulation angle is recalculated with each new measurement of the coupling force.
- The FFD-C version is using the current modulator angle and force measurement to estimate the separation distance at each iteration. Then, the a priori modulation angle is calculated with a new separation distance and force measurement at each iteration.



(A) Variant A



(B) Variant B



(C) Variant C

Figure 5.1: Control architectures composed of a PI controller, a force feedback (FFB) loop and three different feed-forward (FFD) parts. The FFD are based on magnetic models linking the magnetic force, the separation distance and the modulator angle. (A) The FFD-A uses a constant FFD contribution. (B) The FFD angle $\theta_{m,i}$ is determined with a current force measurement F_i at a fixed separation distance d_0 . (C) The FFD angle is based on current estimations of the coupling force and the separation distance.

5. Guidance Analysis

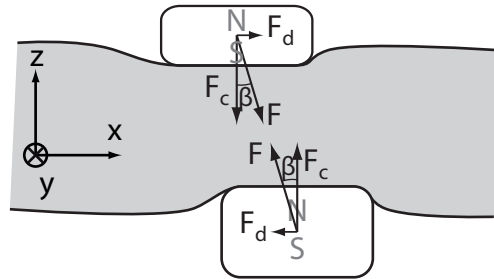


Figure 5.2: Magnetic forces within the MAGS during the guidance. F_d is the dragging force, F_c the coupling force acting in the yz plane. F is the resulting force between F_d and F_c and β the angle of the force with the yz plane. For simplification reasons, the center of the forces is placed on the centre of mass of the magnets. In reality, the gradient becomes asymmetric when the magnets are misaligned.

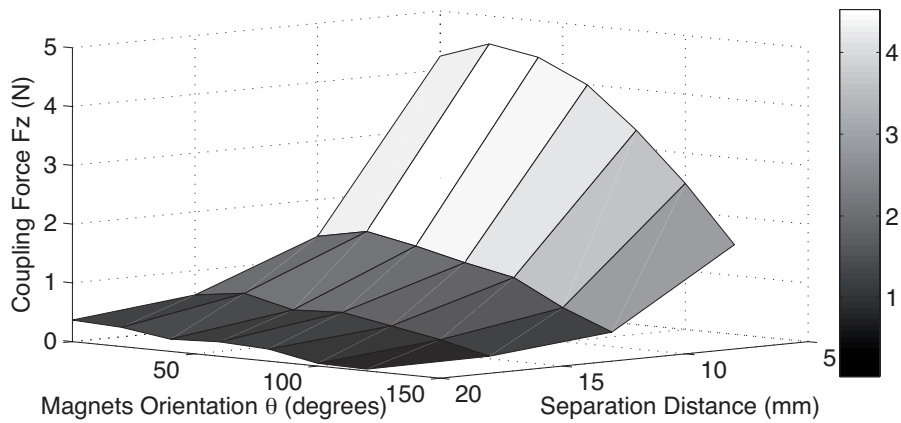


Figure 5.3: FEM results representing the coupling force within the MAGS as a function of the modulator angle and the separation distance.

5.2 Characterization Setup

A custom made setup was designed to demonstrate *in vitro* the benefit of an active control mode in the guidance behavior. Prior to *in vitro* experimentation, an understanding of the control modes and their implications on the magnetic guidance is mandatory. In this sense, the MAGS has been tested on different surfaces as well as with different parameters for the controller. Figure 5.4 represents the schematic of the *in vitro* setup.

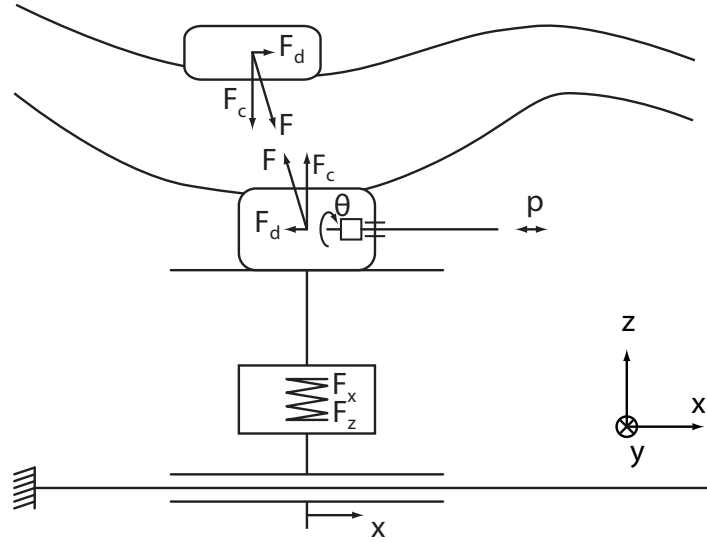


Figure 5.4: Schematic representation of the setup for characterizing the magnetic guidance under different control modes as well as various sliding conditions.

To facilitate the implementation of a force feedback, an external force sensor was preferred. The modulator is actuated by a linear motor, which are mounted on a force sensor. The force sensor measures the coupling force within the MAGS. This information is used by the controller to actuate the modulator. These elements are attached to a linear rail driven by a motor, which allows the displacement of the modulator in the x direction. On the top of the modulator a piece of tissue is attached to the same referential as the base of the setup. The second part of the MAGS is placed on the opposite side of the tissue to ensure the magnetic coupling with the modulator. When the modulator is displaced, an offset (dragging offset) with the passive magnets is produced until the right force conditions are met to have the magnetic guidance.

Based on the setup schematic, a realization has been made as represented in figure 5.5. To actuate the modulator, a linear DC-Servomotors LM2070-040-01 from Faulhaber was purchased. This type of motor offers high dynamics and excellent force to volume ratio. A 6-DoF force sensor, FT09208 Nano17 SI-50-0.50, from ATI Industrial Automation was used to measure the forces within the MAGS. To minimize the undesired magnetic effect coming from surrounding ferromagnetic material in the vicinity of the MAGS, the force sensor has been placed far enough. A counter-weight is introduced on the modulator base in order to balance the torque exerted on the sensor by the weight of the linear motor. A Maxon DC-Motor RE25 equipped with a tachometer DCT22 and a gear box GP26 are coupled to an IGUS linear rail in order to displace the modulator in a speed control operating mode. The controller was implemented with Labview programming from National Instruments combined with an acquisition card, USB-6343, from the same company.

5. Guidance Analysis

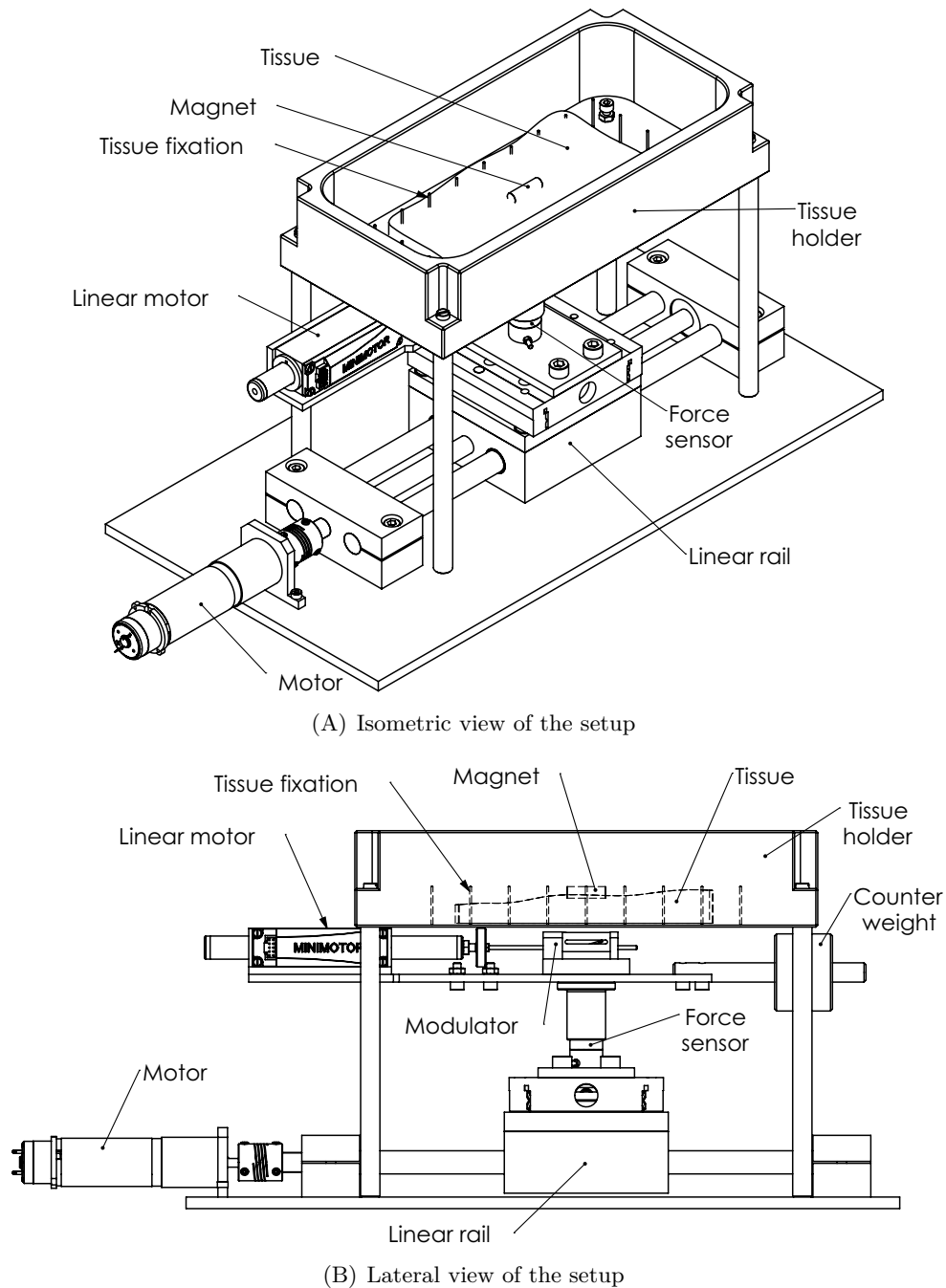


Figure 5.5: Views of the custom made setup for analyzing the magnetic guidance behavior of the *in vitro* modulator. The modulator is actuated by a linear motor, which are mounted on a force sensor. The force sensor measures the coupling force within the MAGS, which is used by the controller to actuate the modulator. These elements are attached to linear rail driven by a motor, which allows the displacement of the modulator in the active control mode. Over the modulator, a tissue holder element comprises a piece of anatomical tissue on which a passive magnet is placed to ensure the magnetic coupling with the modulator. When the modulator is displaced, an offset with the passive magnets is produced until the right force conditions are met to have a proper magnetic guidance.

5.3 Guidance Modes Comparison

Passive and active magnetic guidance have been tested and are compared in this section.

5.3.1 Method

Well-defined sliding conditions are required to compare the passive and active guidance modes. Samples of three flat materials of different hardness was considered. Initialisation at different coupling forces was also tested to see any potential effect on the guidance. The output parameters to analyze the guidance behavior are the measurements of the magnetic forces and their relations as well as visual observation that may occur, such as stick and slip phenomenon. The stick slip phenomenon is a spontaneous jerking motion that can take place when two elements are sliding over each other. Stick-slip is caused by the surfaces alternating between sticking to each other and sliding over each other, with a corresponding change in the friction force. Typically, the static friction coefficient is larger than the kinetic friction coefficient. When an applied force is sufficient to overcome the static friction, the shift of the friction to the kinetic friction can cause a sudden jump in the velocity of the movement. Observing the stick-slip phenomenon may provide useful information on the robustness of the guidance. The larger is the dragging offset of the passive magnets in the static phase, the bigger is the chance that the MAGS may disconnect. Similarly, calculating the shift angle, namely the angle between the resultant force and the vertical axis, is another indicator to represent the displacement offset of the MAGS during the guidance. The ratio of the dragging force over the coupling force may suggest how much dragging force contribution is required to initiate the guidance. In other terms, it may inform on the ease of displacing the passive magnet magnetically as this ratio is also representing the friction coefficient $\mu = F_d/F_c$.

The control parameters and their physical impact on the guidance are listed below:

Control parameter:

- Guidance Modes: passive and active
- Material: foam, rubber or PMMA
- Coupling force setpoint: 0.3 N, 0.5 N or 0.7 N
- Force Feedback: coupling force F_c or resultant force F
- Feed-forwards: FFD-A, -B or -C
- Flat or tilted surface

Measured output parameters:

- Stick slip frequency and length
- Dragging and coupling forces
- Resultant force F and its shift angle β
- Ratio dragging force over coupling force: F_d/F_c

After an initialization phase to set the MAGS coupling force at the right value, the displacement of the modulator stage is ramped-up to ensure a smooth starting phase until reaching a constant speed of (~ 3.5 mm/sec) for the modulator over a distance of 100 mm. Each condition has been repeated three times.

5. Guidance Analysis

5.3.2 Results

Various experimental combinations have been tested. The more relevant results are described in this section. Foam material has been chosen for its softness to describe the guidance behavior.

Guidance Behavior

Figure 5.6 shows the typical magnetic interactions occurring during the displacement of the MAGS. The passive magnet is first placed on foam material and after initialisation, the MAGS are coupled with a force of 0.5 N. Then, the modulator is displaced at constant speed in a passive control mode, namely with no adjustment of the magnetic field during the guidance.

The data shows the presence of two phases: a temporary static phase followed by a dynamic sliding phase. The static phase appears when the modulator starts moving until the dragging force is sufficient to overcome the static friction, causing a sudden jump in the movement. It is interesting to notice that the dragging force rises very quickly and reaches its maximum amplitude before any displacement of the passive magnet occurs. The displacement is produced when the friction force becomes lower due to decrease of the coupling force caused by the dragging offset with the modulator. As soon as the static friction is inferior to the dragging force, the passive magnet is displaced. Even though, natural misalignment of the MAGS is beneficial to decrease friction force, a large dragging offset with the modulator increases the risk of decoupling of the MAGS members as the dragging force may start to decrease before any displacement of the passive magnet occurs.

In the sliding phase, the magnet quickly accelerates to catch up with the modulator until reaching a steady state. This acceleration combined with the inertia of the magnets creates an increase of the coupling force followed by a small decrease to finally reach the steady state.

The shift angle β is another parameter to represent the magnetic guidance behavior. The magnetic guidance in a passive mode on a soft material such as foam shows how large the shift angle before any sliding of the passive magnet could be. The sudden decrease of angle occurs at a dragging offset of 17 mm. As the length of the magnets is 20 mm, the change of phase appears at a dragging offset of 85% of the length of the magnets. One can also easily notice the similarity of curve profiles between the shift angle β given by $\tan^{-1}(F_d/F_c)$ and the friction coefficient μ given F_d/F_c . Even though, the goal of this chapter is not to extract parameter values, but rather to find trends in the data, the friction coefficients of a nickel plated magnet on soft foam can be extracted from the figure: ~ 1 for the static coefficient and ~ 0.75 for the kinetic coefficient.

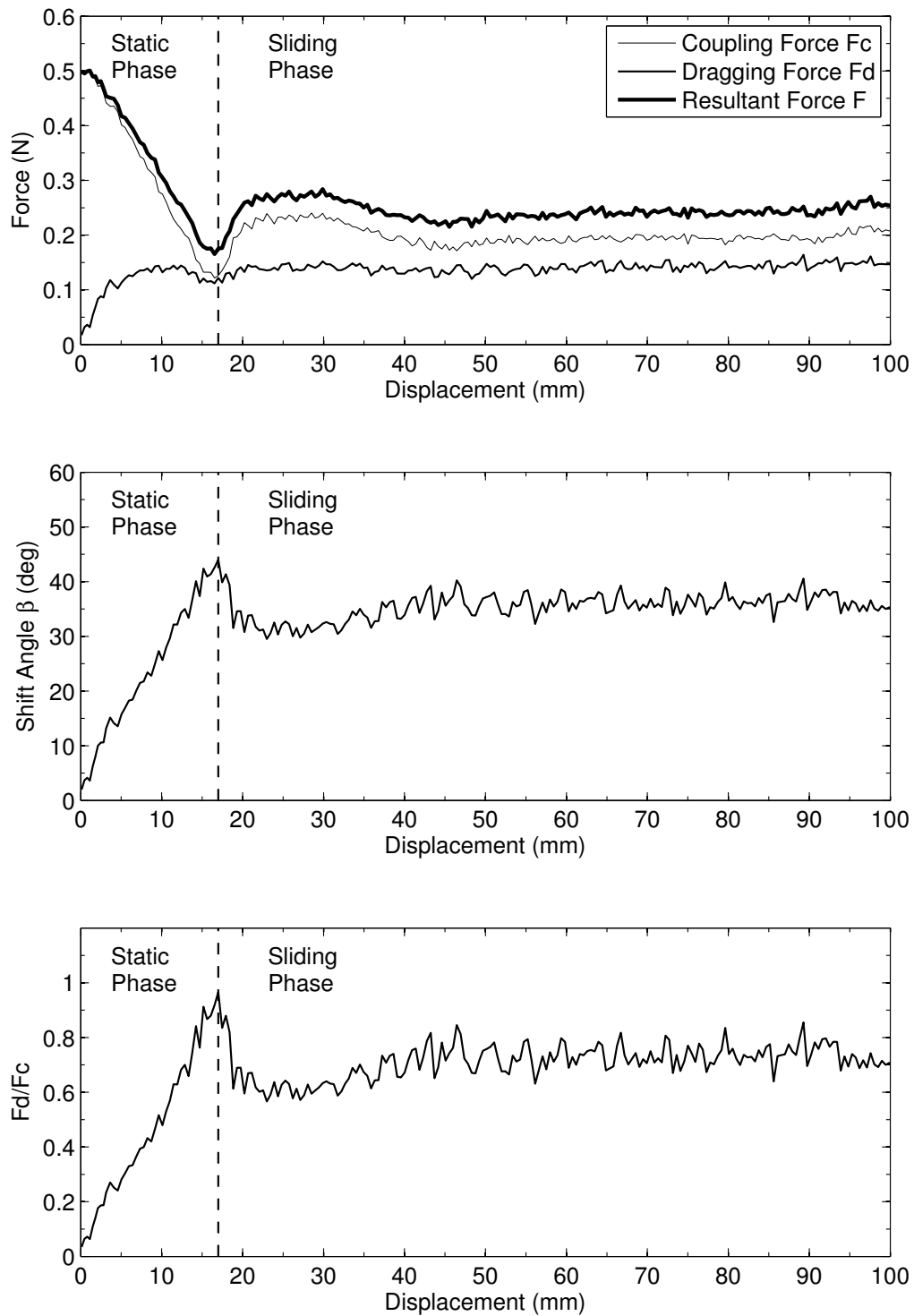


Figure 5.6: Measurements of the magnetic interactions occurring during the displacement of the MAGS on a foam material. The MAGS is initially coupled with a force of 0.5 N, then the modulator is displaced at constant speed in a passive control mode. Two phases are noticeable: a static phase followed by a dynamic sliding phase. The static phase appears when the modulator starts moving until the dragging force is sufficient to overcome the static friction, causing a sudden jump in the movement. Then, the magnet followed the modulator with constant shift angle β or kinetic friction coefficient F_d/F_c .

5. Guidance Analysis

Effect of Material

Three different hardness of material have been chosen to investigate any potential effect of the guidance behavior. Figure 5.7 shows the measurements performed on foam, rubber and PMMA. The conditions of experiments were identical for the different materials. The MAGS were initially coupled at 0.5 N at the same separation distance. Passive mode has been preferred for conducting this investigation due to its static magnetic conditions.

One can notice that the shift angle varies with the hardness of the material or its friction coefficient with the passive magnet. In other terms, the passive magnet follows the modulator with a dragging offset which is related with the friction coefficient of the material. The change of phase from static to dynamic occurs faster for the rubber than the foam as rubber is harder than foam. The change of phase seems to be not visible for the hard PMMA material. In fact, a continuous series of stick and slips occurs on this hard material as shown with the variation of dragging force. The passive magnet changes from a static to a sliding phase during the displacement, which is due to the very low kinetic friction coefficient of this material and the low guiding speed. The passive magnet is able to catch up its dragging offset with the modulator up to an alignment with it associated with a temporary static phase.

Effect of Guidance Modes

Passive and active guidance modes are compared and illustrated for the foam material in figure 5.8. Two types of force feedback are tested for the active mode. $FFD(F_c)$ uses only the coupling force and $FFD(F_d, F_c)$ takes the coupling and dragging force into account. *No FFD* represents the passive mode. When $FFD(F_c)$ is selected, the controller drives the modulator in order to minimize the error between the coupling force and the desired force, 0.5 N in this case. If $FFD(F_d, F_c)$ is selected, the resultant force F between the dragging and coupling force becomes the process value of the controller.

In active guidance mode, the modulator adjusts the magnetic field in order to keep the coupling force constant during the guidance. This compensation initiates the magnetic guidance of the passive magnet earlier in comparison with the passive mode, which decreases significantly the risk of disconnection of the MAGS. Moreover the transition between the static and sliding phases is smoother. In the sliding phase, it is interesting to notice that the steady state for the shift angle is identical for the passive and active modes. In fact, the active mode shows their superiority on irregular surfaces as they can compensate the induced variations of forces while keeping its dragging offset (or shift angle) with the modulator to its minimum.

Regarding the friction coefficient, with no surprise the kinetic friction coefficient is identical for both modes. However, the measured static friction coefficient is larger for the passive mode. This can be explained by the way the change of phase is occurring in the active control mode. Prior to sliding, the passive magnets starts its movement by first deforming the foam material (without sliding) until finally sliding over it. This deformation is possible by the fact that the active mode required more coupling force and therefore more dragging force than in the passive mode.

No guidance difference have been noticed between the two active modes on the tested material. However, the forces involved during the guidance are larger for the $FFD(F_c)$ mode. This last mode has also the advantage to require a force sensor with one less DoF.

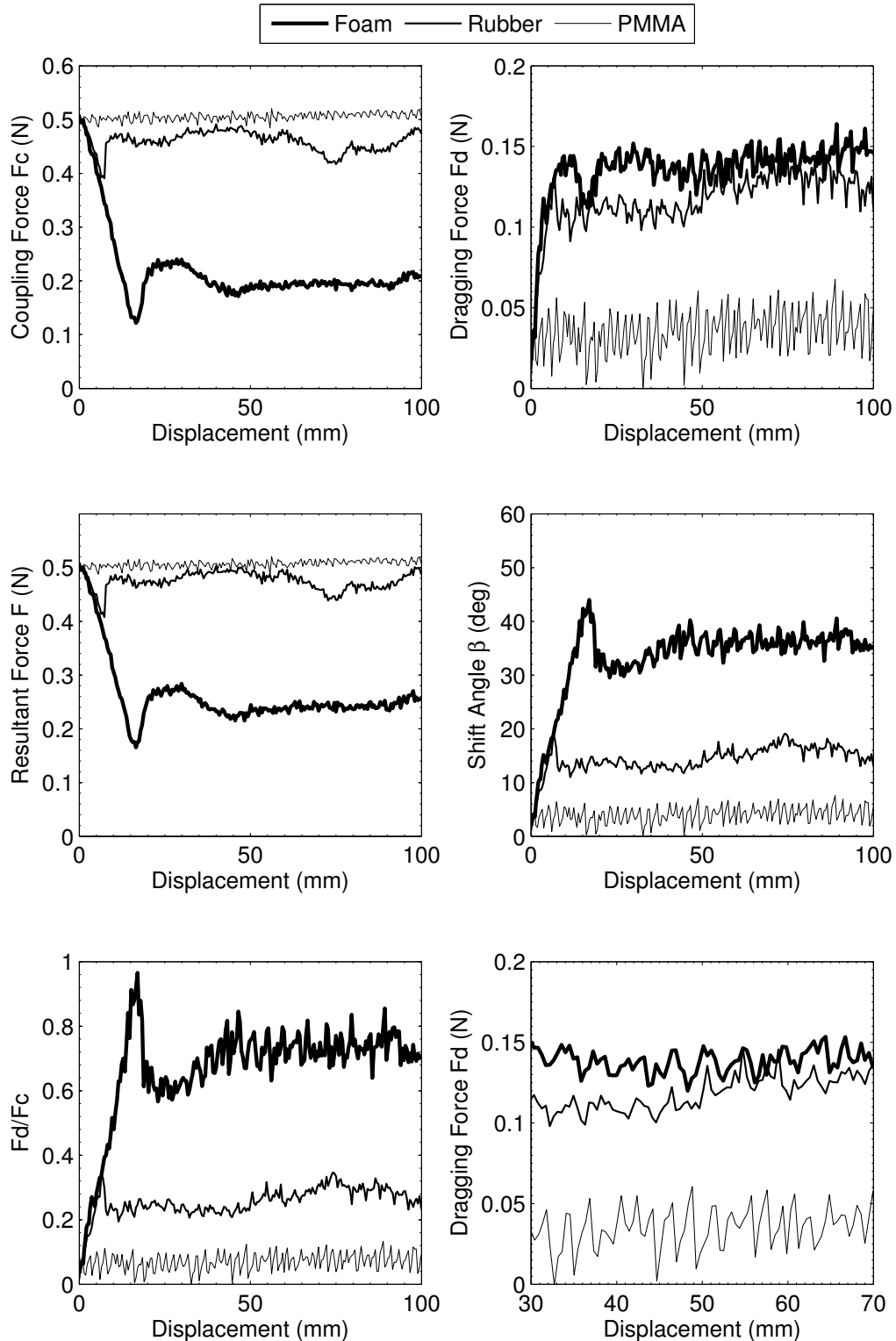


Figure 5.7: Measurements of the magnetic interactions occurring during the displacement of the MAGS controlled in a passive mode on three types of material: foam, rubber and PMMA. One can easily remark that the softer is the material, the wider is the shift angle, the friction coefficient or the decrease in the coupling force. A close look at the dragging force for the PMMA shows repetitive oscillations of larger amplitude, which correspond to regular stick-slips during the displacement.

5. Guidance Analysis

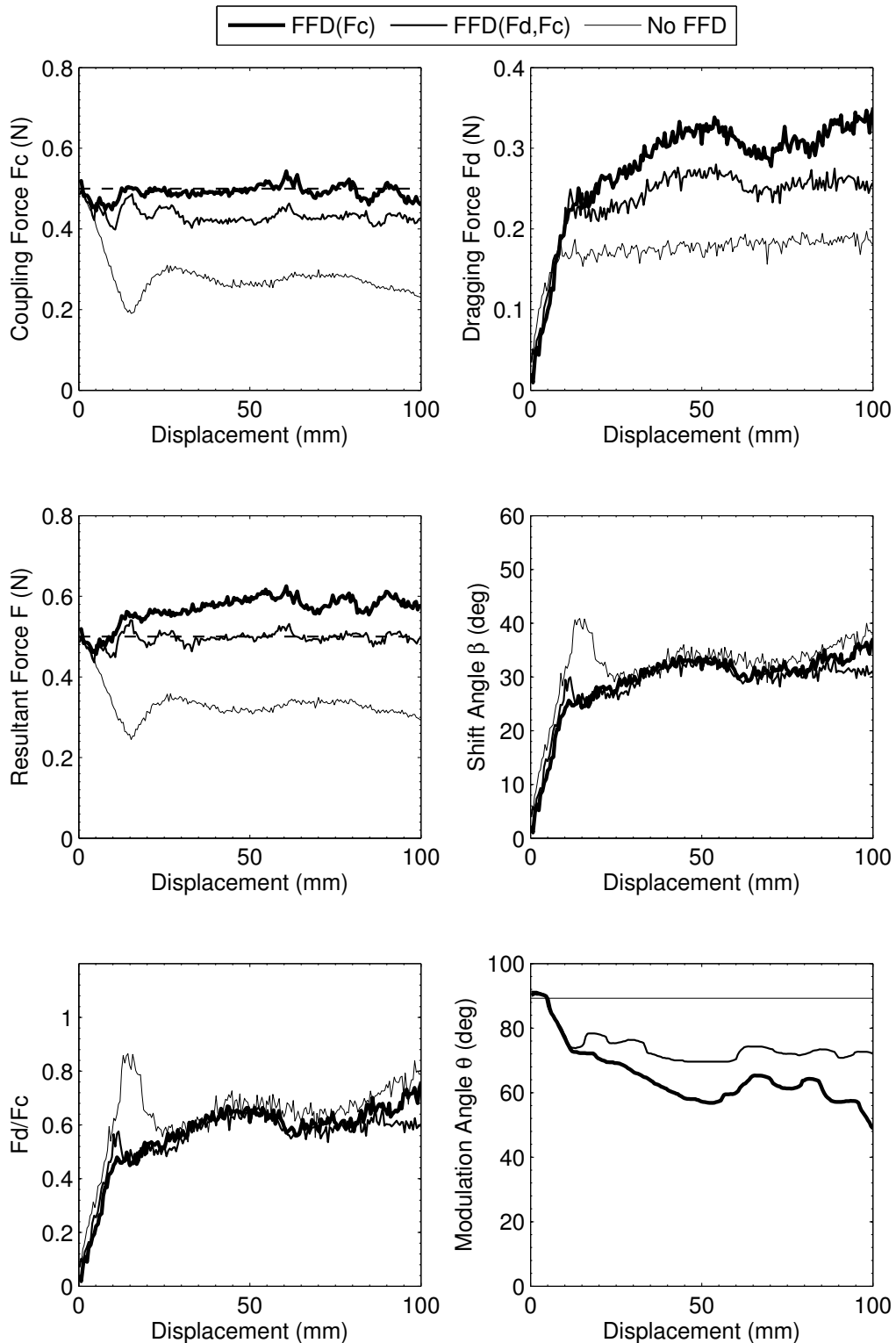


Figure 5.8: Comparison between active mode with force feedback and passive guidance mode. MAGS is initially coupled at 0.5 N on foam material. The process variable is the coupling force for the $FFD(F_c)$ case, and is the resultant coupling force for the $FFD(F_d, F_c)$. In the sliding phase, the shift angle and friction coefficient are not affected by the type of guidance mode.

Effect of the Coupling Force

Figure 5.9 shows that the coupling force may produce small differences of shift angle or friction force during the guidance. As mentioned previously, the difference in the static phase may be explained by the smooth start of movement of the passive magnet, which is achieved through the deformation of the foam material in the horizontal direction until the passive magnet starts to slide. This deformation and the smooth phase transition are related with the amplitude of the coupling force.

Regarding the sliding phase the difference may also come from the additional force required to deform the material at the front of the magnet during the sliding. The measured friction force is a combination of interfacial interactions and material deformation. The ratio between these two sources of friction is related to the coupling force. When the coupling force is high, the interfacial friction force is larger than the deformation force. The interfacial friction is the dominant source of friction and therefore the measured friction coefficient seems to be lower. On the other hand, when the friction coefficient is determined with low coupling force, the deformation force contributes further to the friction force, namely the dragging force, which leads to a larger contribution in the friction coefficient.

The decrease in the friction force coefficient when the coupling force is increased, occurs also for the two other materials as illustrated in the bar chart of figure 5.10. However, the explanation of this effect on the PMMA material can hardly be explained with the material deformation during the guidance, but rather by numerous stick and slips occurring during the sliding on this material. This jerky motion of the passive magnet creates sudden variations in the magnetic attractions forces within the MAGS. The offset noise caused by sudden jumps of the passive magnet generates mechanical oscillations of the modulator stage, which is most likely added to the measurements of the dragging force. The variance of the PMMA data is therefore bigger at low coupling force than at high coupling force, which may reinforce this explanation. This is to say that the kinetic friction coefficient is theoretically independent of the coupling force on hard material. The measured friction coefficient can be influenced by interfacial adhesion, asperities deformation and viscous film shearing action as these frictional contributions are correlated with the normal load on the surface. However, their contribution is too small to explain such differences. The mechanical oscillation due to sudden jumps of the passive magnet is the most probable explanation.

The friction phenomenon on soft material is very complex. More details are given in chapter 7.

Effect of the Feed-Forward Controller

The described feed-forward controllers of figure 5.1 were tested on three materials. The surfaces are too regular to detect any differences in the guidance behavior. Moreover, the PI controller is the part controlling the error in the system. The feed-forward part helps in predicting the modulation angle that corresponds to the desired coupling force, but the main controlling task is achieved by the PI controller.

5. Guidance Analysis

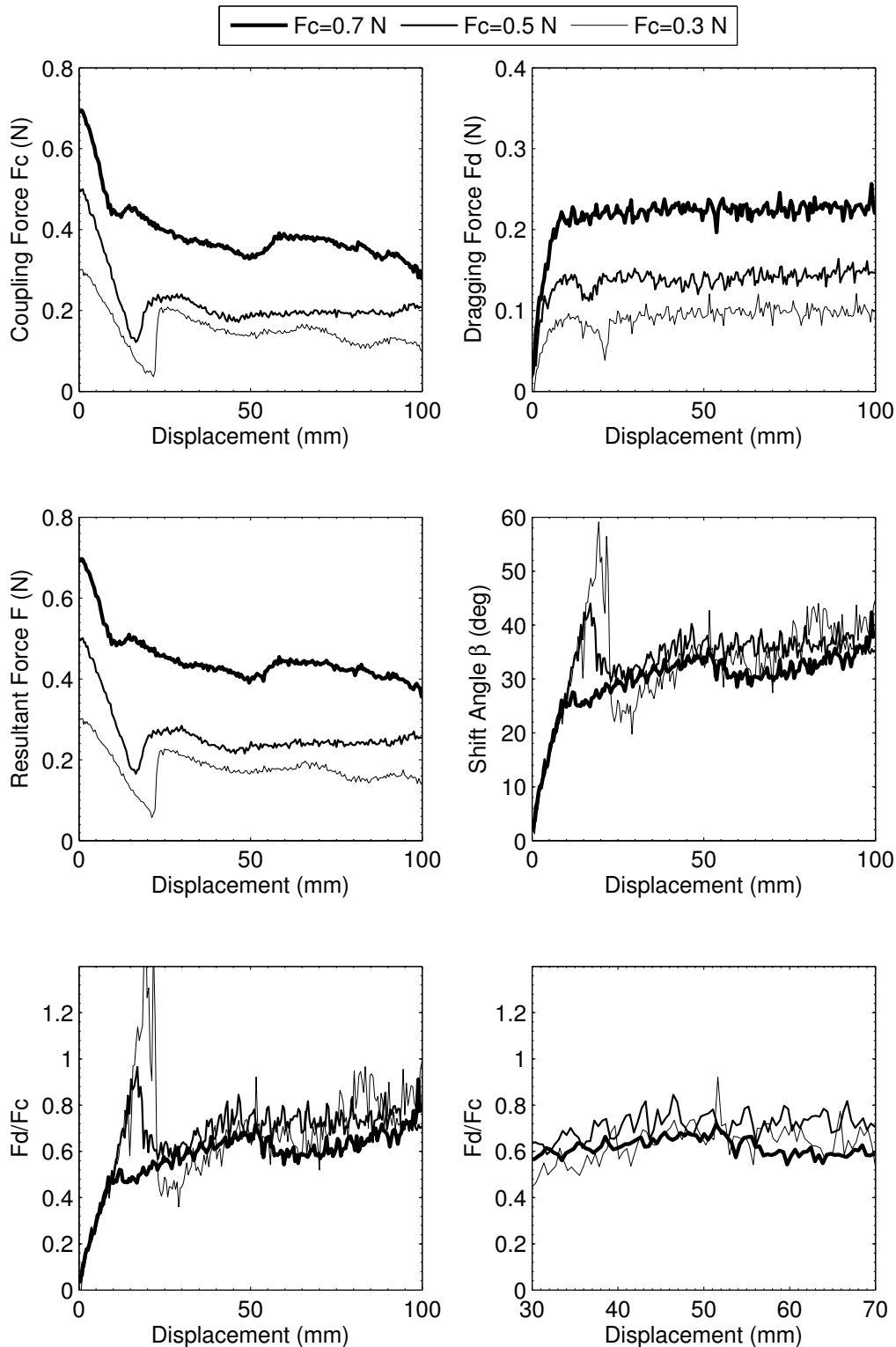


Figure 5.9: Effect of the coupling force on the magnetic guidance behavior. The MAGS is initially coupled at three different levels of force and displaced in a passive mode on foam material. The friction force coefficient is modified with the coupling force.

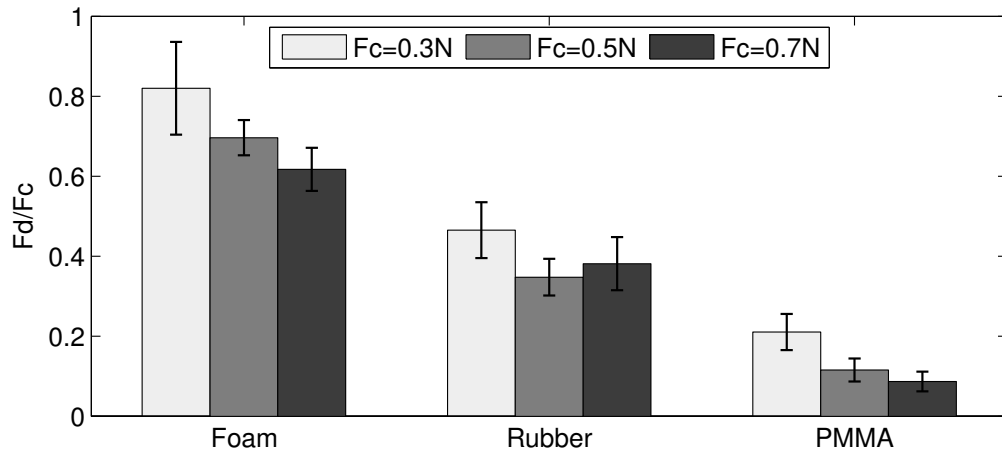


Figure 5.10: Effect of the coupling force on the kinetic friction coefficient measurement for three different hardness of material. The measured kinetic friction force is sensible to the coupling force within the MAGS. The measured friction force is a combination of interfacial interactions and material deformation (on foam and rubber). The ratio between these two sources of friction is related to the coupling force. When the coupling force is high, the interfacial friction force is larger than the deformation force. The interfacial friction is the dominant source of friction and therefore the measured friction coefficient seems to be lower. On the other hand, when the friction coefficient is determined with low coupling force, the deformation force contributes more in the friction force, namely the dragging force, which leads to a larger contribution in the friction coefficient. For the hard PMMA material, the difference may be explained by numerous stick and slips occurring during the sliding on this material. This jerky motion of the passive magnet creates sudden variations in the magnetic attractions forces within the MAGS. The offset noise caused by sudden jumps of the passive magnet generates mechanical oscillations of the modulator stage, which is most likely added to the measurements of the dragging force.

5. Guidance Analysis

5.3.3 Implementation Modes

While the active mode offers more robustness in the magnetic guidance than the passive mode, its implementation requires the need of a magnetic force modulator and a force feedback given either by an integrated force sensor or less accurately under a visual fluoroscopic vision. The ability to adapt the coupling force during the guidance is essential, especially on soft and irregular surfaces such as anatomical cardiac tissue.

In the passive control mode, as the guiding part is operated at a static magnetic field, the modulator could be replaced in reality by a single permanent magnet. Therefore, this mode requires no electronic and expensive components such as force sensors and control automation. The passive mode is particularly useful for magnetic guidance over tissue which is rather constant in thickness in order to keep the control of the MAGS adequate for the physician.

The active control mode requires force feedback information to guide the controller. In case of an integrated force sensor, adding such a component in the active part of the MAGS is very challenging, especially for catheterization applications where the size is limited. However, a concept of optical micro force sensor is currently under development. Its integration in the MAGS is planned for a near future.

5.4 Conclusion

Passive and active guidance modes have been introduced. The active mode architecture comprises three elements: a proportional-integral (PI) controller completed with a feed-forward (FFD) controller, and force feedback (FFB) loop. The passive and active control guidance modes have been compared under several different conditions. Typically, the active control mode shows smoother guidance and superior robustness in comparison with the passive guidance mode. The critical point in the magnetic guidance is the setting in motion of the passive MAGS member. The transition from the static phase to the sliding phase may lead to the failure of the MAGS guidance especially for the passive mode of guidance on soft material. In the static phase, the dragging offset of the passive magnet with the modulator, initiated by the movement of the modulator, affects quickly the coupling force within the MAGS. If no magnetic adjustment is done to compensate this drop of forces, the dragging offset may become too large until the dragging magnetic force becomes superior to the static friction force, which could potentially lead to the magnetic decoupling of the MAGS. *In vitro* tests on anatomical tissue are required to demonstrate the benefit of force modulation over static magnetic field. Indeed, anatomical tissue variations and resulting frictional interactions represents a more realistic environment to reinforce this demonstration.

6 Magnetic Guidance on Cardiac Tissue

The goal of this chapter is to demonstrate through *in vitro* experiments, the increase of robustness in the magnetic guidance provided by the ability of modulating the coupling force during the guidance. In the previous chapter, it was demonstrated on flat material that active control provides smoother guidance and robustness in comparison with the passive guidance mode. The delicate phase of the magnetic guidance is the setting in motion of the passive MAGS member. The transition from the static phase to the sliding phase may lead to the failure of the guidance. This is particularly true for the passive guidance in soft material. In the static phase, the growing misalignment of the MAGS, initiated by the movement of the modulator, decreases rapidly the coupling force within the MAGS. If no magnetic force adjustment is done, the misalignment may become too large until the axial magnetic dragging force becomes superior to the static friction force. This situation could potentially lead to the decoupling of the MAGS and therefore to the failure of the guidance.

Once the passive magnets is in motion and follows magnetically the guiding part, any variations in the separation distance of the MAGS due to tissue irregularities, may become critical. An increase of the tissue thickness reduces rapidly the magnetic coupling force; approximately with the square of the distance. A lack of force could therefore leads to the end of the guidance. On the other hand a decrease of tissue thickness increases the coupling force and at the same time the friction force. Indeed, frictional interactions will be increased by the sink of the guiding part in the tissue. If no magnetic force adjustments are done, an excessive coupling force may also damage or perforate the tissue.

6.1 Experiments

In vitro experiments were conducted on the custom made setup described in section 5.2. Fresh bovine cardiac tissue, sliced in variable and irregular thickness, were attached on the setup as illustrated in figure 6.1. For demonstration purposes, a slice of tissue was prepared with a variable thickness from 5 to 25 mm. The epicardial side of the heart (outer surface) has been chosen as the contact side with the sliding magnetic element.

6. Magnetic Guidance on Cardiac Tissue

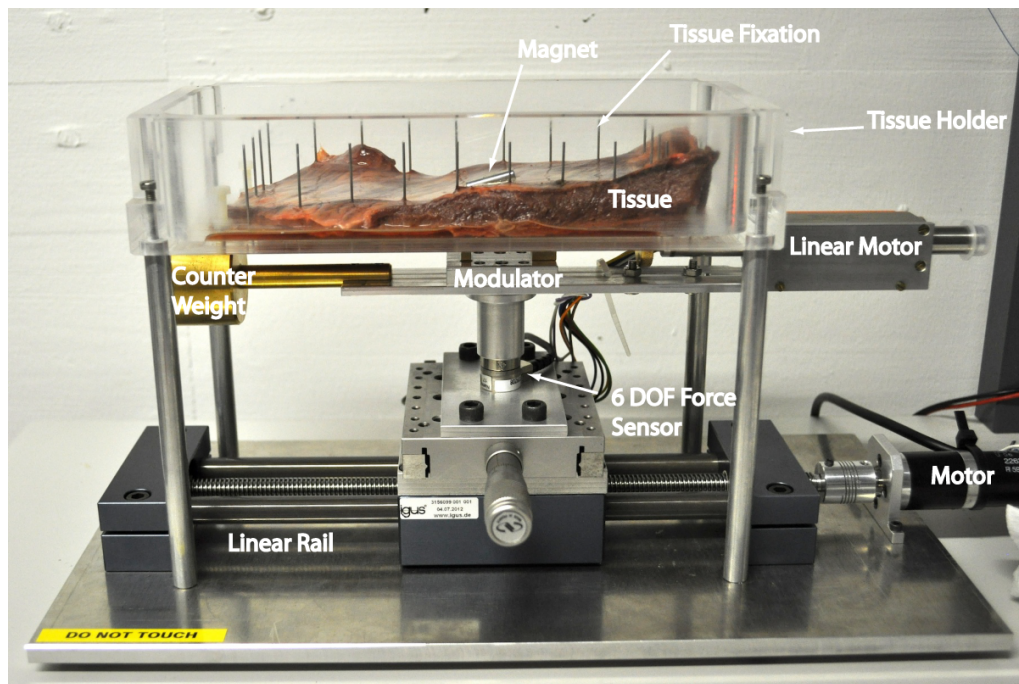


Figure 6.1: Custom made setup for analyzing the magnetic guidance on soft and irregular anatomical tissue.

Three kinds of obstacles, typically met in real cardiac applications, were reproduced *in vitro*:

- Increase of tissue thickness
- Presence of protuberances in the tissue
- Presence of cavities in the tissue

Regarding the control of the MAGS, passive and active control modes are tested and compared. A force feedback based only on the radial coupling force has been chosen to represent the active mode. The starting coupling force is set to 0.4 N for both modes as this value has been empirically proven to be sufficient to ensure guidance in our case.

6.2 Results

The magnetic guidance behavior on cardiac tissue is summarized in figures 6.2 and 6.3. These figures show the magnetic measurements collected by the force sensor. The passive magnet is magnetically guided over a slice of tissue that vary between 10 and 20 mm in average thickness. On a thinner part, a depression of few millimeter and a bump of similar dimension was reproduced. The passive magnets were guided on this tissue in two different directions. The guidance of the passive magnet starting from the thinner part to the thicker part are shown in figure 6.2. On the contrary, figure 6.3 shows the measurements for the MAGS starting on thick surface and going to a thinner portion of the tissue.

Looking at the measurement outputs give sufficient information to describe the different sequences occurring during the runs:

Guidance Storyboard for Figure 6.2

1. The first reduction of force is produced by setting in motion the modulator creating a misalignment with the passive magnet. The dragging force increases and the friction force decreases until the passive magnet starts moving, which suddenly bring the coupling force to a higher level.
2. The second decreasing peak is due to a cavity placed in this region. This little cavity increases the dragging offset (shift angle) which drops down the coupling force.
3. The magnet overcome the cavity as the force goes up and the shift angle goes down.
4. After 40 mm of guidance, the coupling and dragging forces decrease in amplitude together with an increase of the shift angle.
 - (a) For the passive mode, the coupling force continues to drop down leading to a decoupling of the MAGS after 60 mm of guidance. However, by looking at the data, this dangerous increase of shift angle or friction force coefficient could have been caused by a cavity or an increase of tissue thickness as well. In our case, the decoupling was due to the second scenario.
 - (b) For the active modulation mode, the controller compensates the decrease of coupling force due to the increase of thickness by increasing the magnetic field, which allows the magnet to overcome the bump to reach successfully a thicker section of the tissue. As a reminder, the magnetic field is maximum for a lower value of modulation angle θ .
5. The passive magnets reaches its final destination for the active control mode.

Guidance Storyboard for Figure 6.3

1. The first decrease of force appears by setting in motion the modulator creating a misalignment with the passive magnet. This drop is imperceptible on the modulation curve indicating that the setting in motion of the passive magnet is smooth.
2. At 40 mm of guidance a rapid increase of force indicates a nose dive of the magnet due to a decrease of tissue thickness or due to the presence of a cavity.
 - (a) For the mode without force modulation, the coupling force increases dangerously confirming the decrease of tissue thickness and not the presence of a cavity. The coupling force reaches a plateau at 1.2 N. The related pressure is high and tissue deformation is important.
 - (b) For the modulation mode, the modulator compensates the decrease of tissue thickness as shown by the variation of modulation angle.
3. The passive magnet in both modes reaches the thinner section of the tissue but at two different levels of coupling force.
4. The passive magnet is dragged over the tissue until facing a cavity represented by a double peak. The first decreasing peak appears when the passive magnet nose dive. As a reminder the coupling forces are sensitive to angular misalignment of the MAGS. This decrease is followed by an increase of coupling force indicating that the magnet is in the cavity and oriented parallel to the modulator. The second peak appears when the magnet is misaligned and tilted back to exit the cavity.
5. Both magnets reach their final destination but at two very different levels of coupling force.

6. Magnetic Guidance on Cardiac Tissue

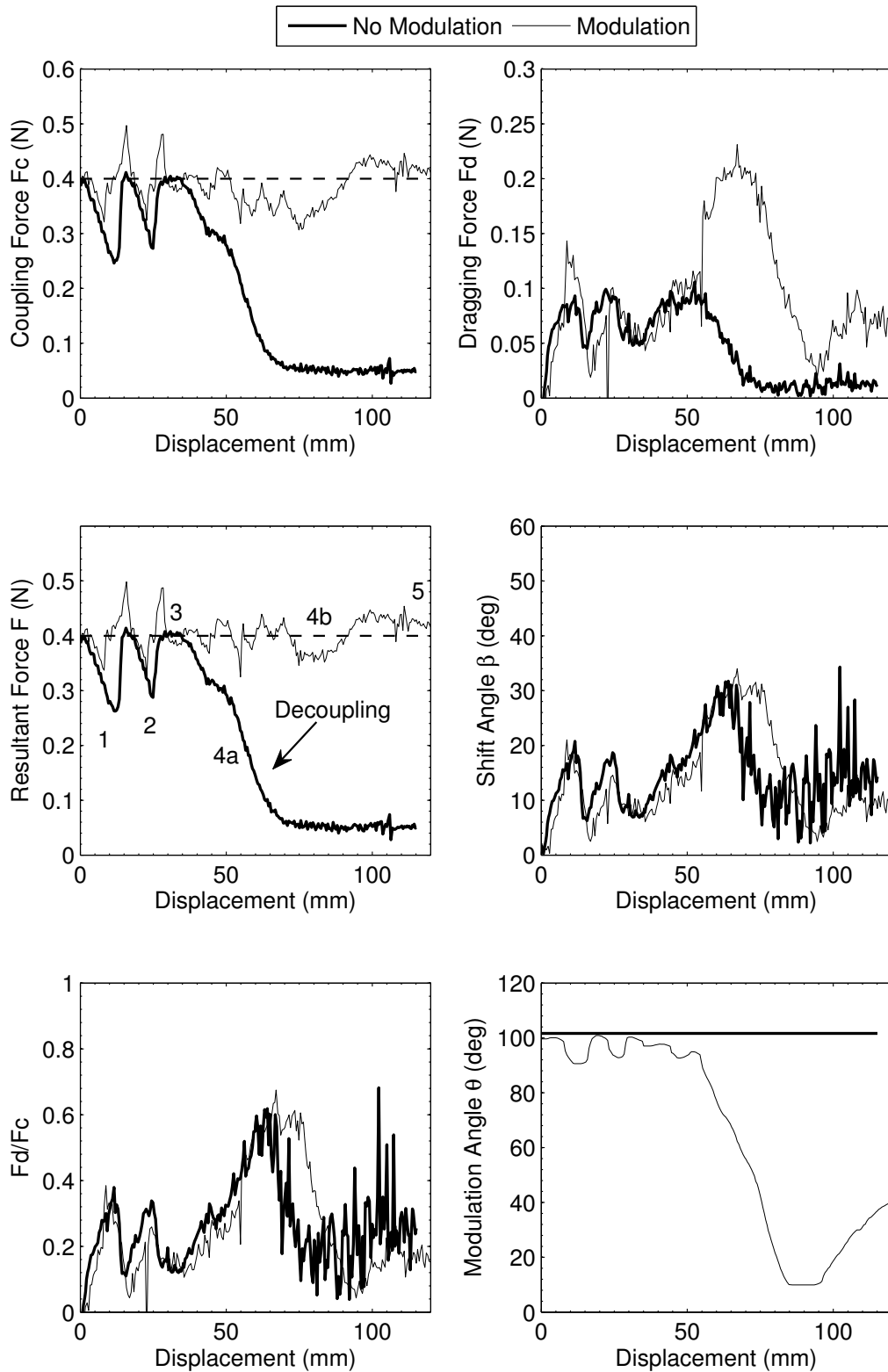


Figure 6.2: Comparison between the active and passive guidance mode on the same tissue conditions. The active modes allow an adjustment of the coupling force based on a force feedback loop. The MAGS is decoupled for the passive mode due to an increase of tissue thickness.

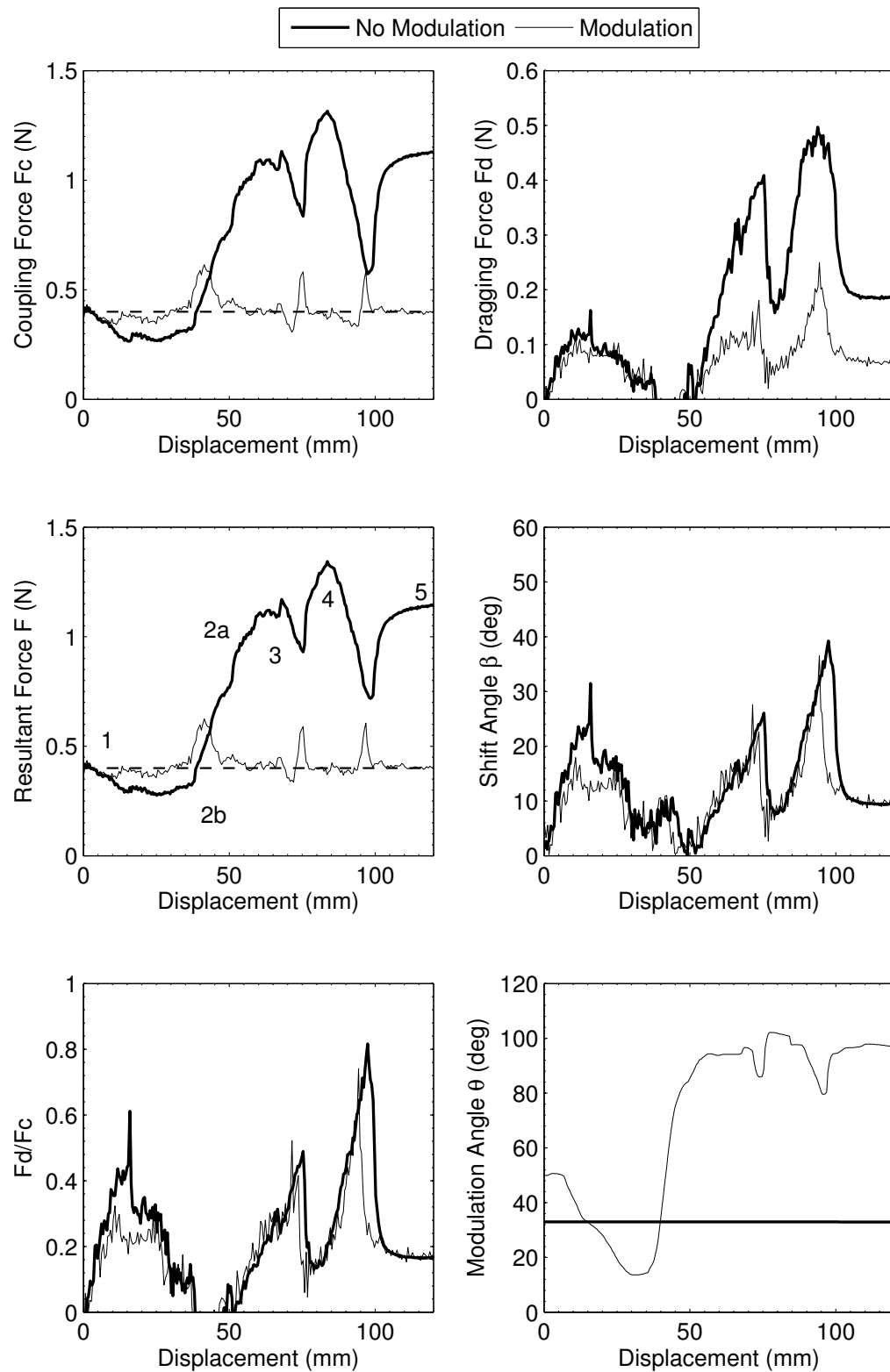


Figure 6.3: Comparison between the active and passive guidance mode on the same tissue conditions. The MAGS is sliding over an irregular cardiac tissue that decrease in thickness. The MAGS are started on the same coupling conditions, but arrive at their final destination with very different levels of coupling force. The level of coupling force for the passive mode is dangerously high and may potentially cause damage or a perforation in the tissue.

6. Magnetic Guidance on Cardiac Tissue

6.2.1 Guidance in Vibrating Mode

Due to the design of the modulator allowing a symmetric modulation of the magnetic field (figure 4.1), a vibrating mode could have been implemented on a trial basis. Modulating at a constant frequency the magnetic attraction within the MAGS can produce a vibrating state of the passive magnet. To create this mode, the required force variation is rather important, $\pm 50\%$. It is preferable to vary the magnetic field based on the coupling force feedback rather than the modulation angle as the magnetic forces are dependent on tissue thickness (separation distance). Therefore, a square signal of ± 0.2 N around the desired coupling force was implemented at a frequency of 2 Hz. The dynamics of the implemented MAGS is limited to a frequency of few Hz due to the bandwidth of the actuator under this load and the damping of the cardiac tissue. The measurements outputs are shown in figure 6.4. One can notice that the sensor output for the dragging force is varying as if the force was changing direction. This is due to mechanical oscillation resulting from back and forth movements of the actuator. These oscillations are another limitation for increasing the frequency of magnetic vibrations.

Even tough, this vibrational excitation is technically feasible through the modulation of the magnetic field, the low bandwidth of the system is the main source of limitation. As the damping of the tissue is considerable, large variations in force are required to produce any noticeable vibrations. In addition the required range of coupling force limits the use of this mode to a small variation of tissue thickness.

Therefore, vibrating the passive magnets using this design, and with sufficient amplitude, is difficult to realize. If a vibrational state of the guided part is desired, direct mechanical vibrations are more easily implemented. The mechanical vibrations may be either directly generated from the guided tip or initiated at the handle and propagated along the device up to its extremity. Another approach could consist of generating magnetic pulses by using an electromagnet made of a permanent magnet core. Although the range of force modulation is very limited when a continuous force is required, magnetic pulses of short period could be generated with this system.

6.2.2 Working Conditions

Experimentation on anatomical tissue with the realized MAGS has led to the following conclusions:

- The minimum coupling force to insure magnetic guidance on flat and regular cardiac tissue is 0.2 N.
- The maximum reasonable coupling force should be situated below 1.5 N. At this level of force, the passive magnet is sandwiching the tissue hardly, which can potentially cause damage or perforation of the tissue.
- The magnetic guidance behavior is more jerky and responsive for high level of coupling force. On the other hand, the guidance is much smoother for low level of coupling force.
- The risk of decoupling of the MAGS is highest on both extremities of the range of coupling force:
 - For high levels of force, even though the magnetic dragging force is largely superior to the friction force due to interfacial interactions, the energy required to deform the lip formed at the front of the magnet is the main source of

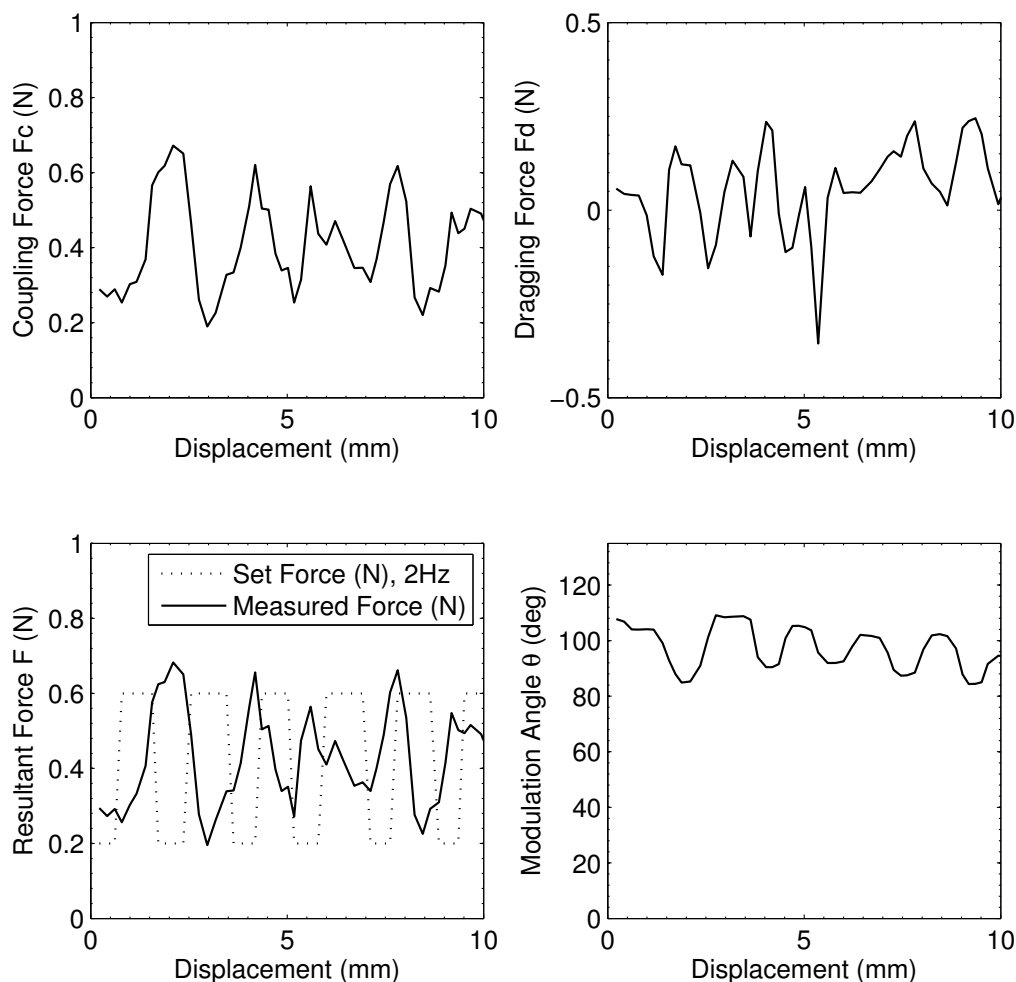


Figure 6.4: Magnetic guidance executed in a vibrational mode. The magnetic field is modulated with a square signal input. It is preferable to vary magnetic field based on the coupling force rather than the modulation angle as the magnetic forces depend on tissue thickness (separation distance). Unfortunately the bandwidth of the implemented MAGS associated with the damping of the tissue is limited to the excitation of few Hz.

potential decoupling. This is particularly true for MAGS passive element of small dimensions, where the tissue creep (deformation over time) could be of the same order of magnitude as the sliding element itself.

- For low levels of force, even though the friction force is low and limited to interfacial interactions, the dragging force might be insufficient to overcome any irregularities of the tissue.

6.2.3 Force Modulation Advantages

Experimentation on anatomical tissue with the realized MAGS operating with force modulation has led to the following conclusions:

- Offer a constant coupling force independent of tissue thickness variations or irregularities.

6. Magnetic Guidance on Cardiac Tissue

- Provide different levels of magnetic attractions that facilitate the coupling or decoupling of the MAGS.
- Reduce significantly the risk of decoupling during the setting in motion of the following part.
- Decrease the risk of perforation or tissue damage.
- Limit the magnitude of tissue creeping when the MAGS is left coupled in standby.

6.3 Conclusion

This chapter compares two modes of magnetic guidance through experiments on anatomical cardiac tissue. While the passive guidance mode uses static magnetic field, the active guidance mode allows the variation of the magnetic field during the guidance. Through the ability of adjusting the coupling force of the MAGS, the guidance is more robust, smoother and potentially safer.

A vibrational mode has been also tested. The coupling force is modulated with a square input signal around the desired nominal force. Unfortunately, the bandwidth of the implemented MAGS, the rigidity of the force sensor as well as the damping of the tissue limit the modulation to few Hz. Moreover, large variations of force are required to produce any noticeable vibrations, which limit the use of this mode to small variation of tissue thickness. Therefore, vibrating the passive magnets by this means is not an optimal solution. Mechanical vibration directly generated in the passive MAGS members seems to be more adequate. Improvement in the guidance by means of magnetic vibrations could not be demonstrated with the implemented MAGS and setup. However, applying vibrations on the following member of the MAGS, might bring some benefits as it will be brought to a dynamic state where the friction force coefficient is lower.

A coupling force of 0.2 N was identified as to be the minimum coupling force to ensure magnetic guidance of the passive magnet over regular cardiac tissue.

Sensing the coupling force is not only used to keep the coupling force constant in the active guidance mode, but it can also be helpful to understand the behavior of the MAGS during the guidance when direct visualization is difficult. A safety system preventing the decoupling of the MAGS could be easily implemented. One can imagine a sound beeping at variable amplitude and intervals. The amplitude of that sound could be given by the coupling force and the frequency of the sound could be provided by a function based on the coupling force and MAGS misalignment (shift angle or friction force coefficient).

7 Friction in Intracorporeal Guidance

The control of frictional interactions between the irregular cardiac tissue and a magnetically sliding guided part is a key point to the success of our proposed type of intracorporeal guidance. In this chapter, we propose to screen the factors affecting friction during magnetottractive guidance. However, the findings can be used to better control medical devices interacting with soft tissue such as catheters, capsules, and micro-robots.

7.0.1 Mechanical Friction Phenomenon

We define friction as the force that opposes or resists the lateral motion between an element and the tissue. This includes, not only surface force interactions such as interfacial adhesion, asperities deformation and viscous film shearing action but also morphological reaction forces due to surface viscoelastic deformation under the front of the slider. Knowledge of the frictional forces acting on the tips of medical devices are important to facilitate the guiding and manipulation of such devices. Furthermore, frictional forces applied on the internal wall of hollow organs or blood vessel walls can induce damage and injury with end-organ ischemia and infarction [Takashima et al., 2007]. Frictional forces are also important for realistic surgical simulations, procedure training, and autonomous and robot-assisted medical procedures. Accurate friction measurements are needed to model tissue response [O’Leary et al., 2003, Okamura et al., 2004].

Studies of friction generally focus on characterizing the interactions between two surfaces under specific conditions. Tribological literature abounds with several models of friction [Olsson et al., 1998]. However, friction on soft tissue is a more complex system still under investigation [Prokopovich and Perni, 2010, Prokopovich et al., 2009]. These models are mechanistic and aim to characterize physically the complex laws of friction by means of parameters, which are very often intrinsic to the material. In addition, these models generally do not consider the deformation of the tissue as well as parameters such as contact speed, material, device geometry, lubrication and tissue state [Takashima et al., 2007]. The limitations of such mechanistic models are in the fact that they are difficult to be used in medical applications where friction force needs to be predicted and controlled as the parameters characterizing the frictional interactions are rarely tunable [Blau, 2001]. We believe that these models cannot be directly applied in the biological domain where anatomical sites and operating conditions might be more important than classical mechanical factors [Adams et al., 2007].

Our approach is to investigate friction based on the application needs, where the continuous control of such interactions is crucial. Hence, the chosen parameters must be tunable. We could define our contribution in the field of tribology as application-oriented friction

7. Friction in Intracorporeal Guidance

characterization. Therefore, our aim is to approach the friction theory on soft tissue, from a different point of view, with a series of parameters, which can be easily determined and controlled.

The goal of this study is to empirically investigate the frictional interactions between a cylinder and cardiac tissue. The shape of the cylinder has been chosen as it easily represents a catheter tip, an endoscopic capsule or others sliding medical devices operating inside the human body. Therefore, the following factors have been selected:

- Normal force applied on the cylinder
- Diameter
- Length
- The distal rounded end of the cylinder¹
- Material
- Pitch angle
- The surrounding environment
- The cardiac tissue type
- Tissue thickness
- Tissue physiological state
- Sliding speed
- Creep time before sliding

The choice of cardiac tissue is selected based on the authors' research focus on medical instrumentations and particularly percutaneous catheter ablation.

7.1 Methodology

In this study, we utilize Design of Experiments (DOE), a statistical approach to explore the dominant factors affecting frictional forces between a tissue and a cylinder. This approach is used to optimize a complex system and reduce the number of experiments compared with conventional trial-and-error methods, which consists in varying one factor at a time (OFAT) [Fisher, 1971]. DOE allows for simultaneously investigating the factors affecting friction and their interactions; and shows how interconnected factors respond over a wide range of values, without requiring the testing of all possible values directly [Antony, 2003]. Factorial designs (FD) are used to reduce the number of experiments without reducing the information that could be extracted.

The experimentation protocol is to measure the friction force using a dedicated apparatus illustrated in figure 7.1(A). Compared with traditional methods, the DOE method has the following advantages:

- Larger region of factor space leads to less variation in response estimation
- Less resources required (time, material, experiments etc.)
- Less variability since the estimate of the effect for each factor is more precise
- Systematic estimation of the interaction between factors

¹R corresponds to the radius of the tip

7.1.1 Experimental Setup

An apparatus was developed to reproduce the sliding contact between a cylindrical element and the cardiac tissue. This apparatus consists of: a cylinder holder, a vertical loading mechanism, a tissue holder and a horizontal motorized linear stage. The cylinder holder is used to hold a horizontal cylinder. The cylinder holder contains a miniature goniometer (07 GON 508, CVI Melles Griot) to adjust the pitch angle of the cylinder and a traction/compression force sensor (KD45 5N, Transmetra) to measure the friction between the tissue and the cylinder. The accuracy of the friction measurement is determined to be ± 0.02 N. The cylinder holder is attached to a vertical loading mechanism via a vertical linear guide (UMR8-51A, Newport) and a loading stage. The loading stage contains calibrated weights used to exert a constant vertical force on the cylinder. The loading mechanism is a passive way of applying constant force independently of the tissue thickness and irregularities. The vertical linear guide has an inner friction measured around 0.25 N. Therefore the accuracy of the applied force is considered to be ± 0.25 N. In order to compensate for the weight of the sliding system, a mass-equivalent counterweight is linked to the vertical linear guide via low friction pulleys.

Cardiac specimens were fixed on the tissue holder as shown in figure 7.1(B). The tissue holder has an inferior and a superior part. The inferior part has a shape of a recipient to contain the specimen and a liquid environment such as porcine blood or saline. The tissue holder is made of PMMA and can be considered as in the same order of stiffness as the metallic master and slave components of the authors' application. The superior part is similar to a comb shape as it contains several pins on its perimeter to penetrate and hold the tissue. The base of the recipient contains in its center a higher plateau, which is used to slightly stretch biaxially the tissue when clamped with the superior part. This configuration allows for a robust fixation of the tissue.

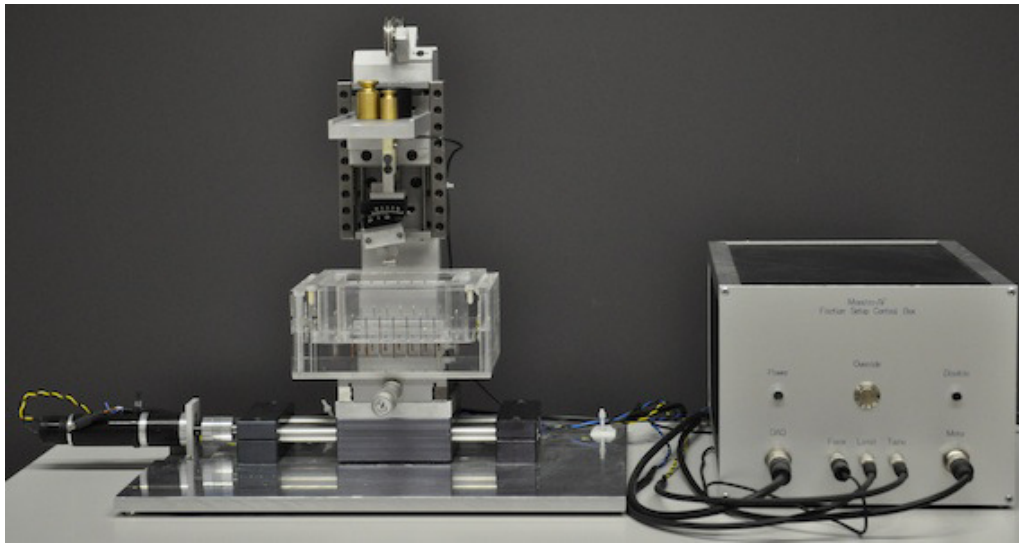
The tissue holder is mounted on the horizontal motorized linear stage. This stage contains a spindle linear system (SHT12-AWM, Igus) and a manual linear stage (UMR8-25, Newport). The spindle linear system is mounted along the x axis direction, which corresponds to the axis of the horizontal cylinder. The spindle is driven at constant speeds by a DC motor equipped with a gearbox and a tachometer (RE25+GP26+DCT22, Maxon Motor). The manual linear stage is oriented along the y axis direction and allows to position the cylinder on different areas of the tissue (Test area: 30x70 mm). The acquisition of the friction measurement and the control of the motor were done via a multifunction data acquisition card (NI USB-6221, 16-Bits, 250 kS/s, National Instrument) and a dedicated Labview interface.

7.1.2 Cylinder Material

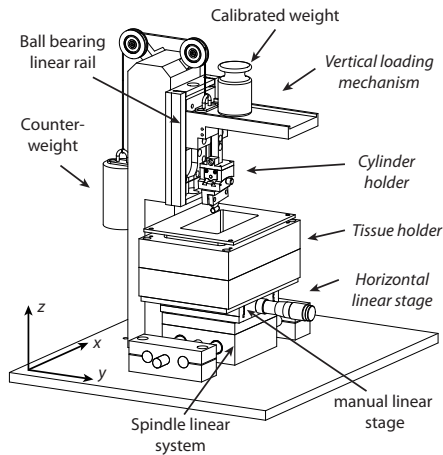
Three types of material have been chosen to represent the *cylinder material*, namely *Stainless Steel 316L*, *PTFE* and *AEP 60CM*². Cylinders of different sizes were manufactured from each of the materials. The use of hydrophilic or hydrophobic coating has been avoided as they are sensitive to wear and implementation quality. However, small size of cylinders could only be realized in stainless steel.

²AEP 60CM is an hydrophilic material from Polymeric Sciences Andrews Wright Ltd.

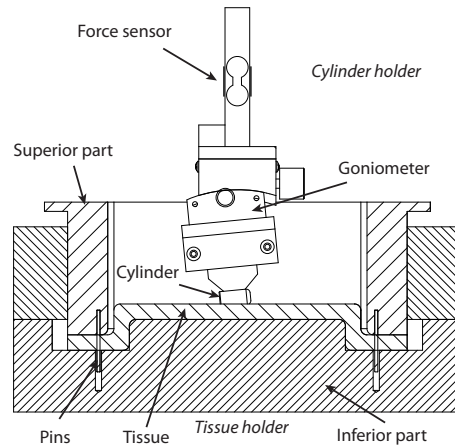
7. Friction in Intracorporeal Guidance



(A) A dedicated apparatus used to measure friction



(B) Components of the apparatus



(C) Close view of the cylinder holder and of the tissue holder

Figure 7.1: (A) Picture illustrating the dedicated apparatus to measure friction and its control and data acquisition box. (B) The apparatus contains the following groups such as a cylinder holder, a vertical loading mechanism, a tissue holder and a horizontal motorized linear stage. (The motor is not represented here). (C) The cylinder is mounted on a goniometer which allows its adjustment around the pitch axis. These two parts are attached to a force sensor used to measure the friction when the cylinder slides over the tissue.

7.1.3 Tissue and Blood Preparation

Fresh bovine hearts and porcine blood were purchased at a local slaughterhouse on the day of each experiments set. 4 and 8 mm slices of endocardial(inner layer) and epicardial (outer layer) tissue were prepared with a meat cutter and a scalpel. Heparin was added to the blood to avoid coagulation. Friction experiments with cardiac tissue, blood and saline water were performed at a temperature of 20° Celsius.

7.1.4 Factors Selection for a Screening on Friction

A list of 12 factors have been selected to represent the main parameters that could potentially affect friction (figure 7.2). These factors are of nature physical, geometrical, physiological and temporal. They can be divided into 3 groups: the continuous factors (*normal force*, *cylinder pitch*, *tissue thickness*, *sliding speed* and *creep time*), the 2-level discrete factors (*cylinder diameter*, *cylinder length*, *bath type*, *tissue physiological state*, *tissue type* and *cylinder round*), and the 3-level discrete factors (*cylinder material*). For exploring an experimental space of a factor, an inferior and a superior limit has been considered. Regarding the fractional FD prior knowledge helps in choosing the most appropriate experimental plan. The *normal force* is of course expected to be of significant effect (based on the well-known friction theory $F = \mu N$; it is also highly probable that two-way or three-way interactions (between 2 or 3 factors) could influence the friction force. Forces applied to the tissue during magnetotractive guidance and anchoring are in the order of a few Newtons, which in terms of pressure is similar to current catheter ablation contact pressure [Thiagalingam et al., 2010]. The range of pressure used in this study minimizes the contribution of the surface force interactions on the friction phenomenon. Therefore, morphological force interactions between the tissue and the cylinder are the main sources of friction. Table 7.1 summarizes the prior significance of these interactions. As for the three-way interactions, only the *normal force*, *cylinder diameter*, *cylinder length* interaction is expected to be important, as it represents a measure of pressure applied on the tissue. Tissue anisotropy was not considered as a parameter to be analyzed since this parameter is hard to be defined during an application on soft tissue. However, the orientation of the tissue during the experiments was random, which minimizes the effect of the tissue anisotropy on the friction measurements.

7.1.5 Designs of Experiments

Table 7.1: Expected significance of the two-way interactions; 1 = highly likely, 2 = likely, 3 = unlikely

	N. Force	Diameter	Length	Round	Material	Type	Ph. State	Thickness	Bath	Pitch
N. Force										
Diameter	1									
Length	1	3								
Round	2	2	2							
Material	3	3	3	3						
Type	2	2	2	2	1					
Ph. State	3	2	2	2	1	1				
Thickness	3	3	3	3	3	3	3			
Bath	3	3	3	3	2	2	2	3		
Pitch	1	3	2	2	3	2	2	3	3	

7. Friction in Intracorporeal Guidance

The proposed strategy consists of performing a screening of the factors and interactions affecting friction. This has been achieved with factorial designs. A linear model was chosen to perform the screening of these factors. This model is represented as the sum of the weighted contributions of several factors, or effects, as expressed by:

$$Y(x) = a_0 + \sum_{i=1}^N a_i x_i + \sum_{i \neq j}^N a_{ij} x_{ij} + \sum_{i \neq j \neq k}^N a_{ijk} x_{ijk} \quad (7.1)$$

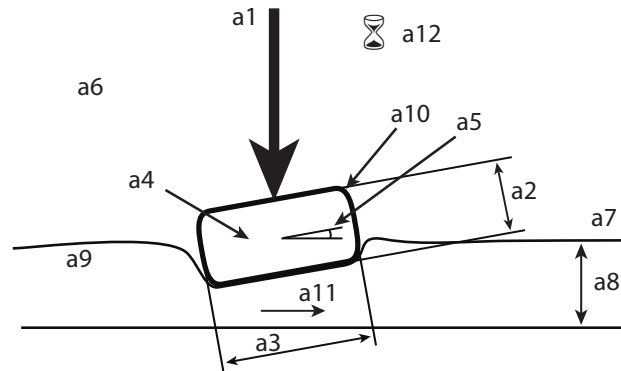
where Y is the friction force, x_i are the factors, x_{ij} their two-way interaction, a_0 is the constant effect (average of all the effects), a_i the main half effects and a_{ij} their two-way order interaction. In fact, a_i is the half effects because they corresponds to the variation between the center of the domain and the border. By misuse of language, the a_i are often referenced as the effects. (See Appendice A.1 for more details). Twelve factors have been considered for the screening. A full FD on 12 factors results in 2^{12} experiments which means a high experimental cost, not only because of the experiments time, but also because of the logistical needs for conditioning the cardiac tissue and blood. Therefore, in order to reduce the number of experiments, a fractional FD on 10 factors, followed by a full FD on 5 factors (3 factors are reconsidered here with different level) were performed [Box et al., 2005]. The resolution defines the depth of interactions and is an important concept in the fractional design as it represents the type of alias induced in the reduction of the full FD. A design of resolution III is not suitable for the fractional FD, as it aliases (confound) the main factors with two-way interactions. Therefore a IV-resolution fractional plan is chosen as it confounds only the two-way interactions coefficients between them but a shrewd choice of the factors order easily allows to bypass this issue. The selected design for the fractional FD is therefore of 2^{10-5} (resolution IV, 32 experiments).

As seen before, the *cylinder material* factor is a 3-level discrete factor, which means that a way must be found to correctly treat it in the factorial design. The first possibility is to consider only 2 materials instead of 3; however, having the prior knowledge of the experimental situation does not allow choosing which one could be neglected. Therefore, the strategy, which is chosen, is to perform 3 different factorial plans, each one taking into account 2 materials. Then, if the material appears to be a non-significant factor, it will mean that both materials have similar effect on friction response.

Temporal factors such as *sliding speed* and *creep time* are part of a full FD together with *normal force*, *cylinder diameter* and *cylinder length*. The levels of these 3 last factors are reduced to a smaller scale. Not only will the full FD provide additional information at a lower scale, but also an entire set of interactions between the factors. The number of experiments required for the proposed 4 FDs consist of 96 experiments for the fractional FD (3x32) and 32 experiments for the full FD. Figure 7.2 shows the choice of the factors levels as well as the design generators used to generate the aliases of the fractional FD. Thus, the number of experiments is reduced to 3x32=96. (Factors aliases are represented on Appendice A.2).

7.1.6 Experiments

A set of 128 experiments were performed based on the factorial designs described previously. For each experiment, up to 5 runs were measured. Preliminary experiments showed that friction measurement could vary after a few millimeters of sliding. Thus, loading the cylinder at a fixed position causes it to sink deeper in the tissue due to tissue creeping [Fung, 2010]. Therefore, each run corresponds to a relative displacement of



1st series

Fractional FD: Main factors

a1	Normal force [N]	2	5	
a2	Cylinder diameter [mm]	5	10	
a3	Cylinder length [mm]	10	20	
a4	Cylinder material	steel-teflon-AEP 60CM		
a5	Cylinder pitch[°]	0	10	Generators:
a6	Bath type	blood	saline	± 6 = 1234
a7	Tissue state	non abl.	abl.	± 7 = 1235
a8	Tissue thickness [mm]	4	8	± 8 = 1245
a9	Tissue type	endo.	epi.	± 9 = 1345
a10	Cylinder round [mm]	R/10	R/2	± 10 = 2345

2nd series

Full FD: Main factors

a1	Normal force [N]	1	2
a2	Cylinder diameter [mm]	2	5
a3	Cylinder length [mm]	5	10
a11	Sliding speed [mm/s]	0.2	0.5
a12	Creep time [s]	5	30

Figure 7.2: Main factors and their experimental workspace as well as the generators used for the 2^{10-5} fractional factorial design. The *cylinder round* has been defined in terms of the cylinder radius (R).

14 mm between the cylinder and the tissue. For each run, a unique region of the tissue has been chosen. Data analysis were performed on a spatial window of 10 mm where the friction profile has reached an equilibrium. The duration where the cylinder was placed in contact with the tissue in a static position before the motor starts was minimized and not exceeding 2 s. The experiments were performed in an order that facilitates the sequences of the experiments. For example, the replacement of the liquid environment or the tissue type is more complex than replacing the type of cylinder or its orientation. 8 specimens of tissue from different hearts were used for all the experiments. Once all the experiments were executed for a non-ablated specimen, the specimen was RF ablated and replaced on the tissue holder to continue the experiments. RF ablation of the specimens was performed using a standard ablation catheter at 50 W power during 10 min. One or two steam-pops were observed during the ablation procedure on each specimen.

7.2 Results

Figure 7.3 shows the profile of the friction force while the cylinder is sliding over the tissue. Friction force increases until a plateau is reached, corresponding to a dynamical equilibrium. This transitory phase can be explained by the fact that the cylinder is slowly stretching the tissue in the direction of the displacement until the dragging force becomes higher than the static friction force, which results in a relative displacement [Blau, 2009]. This transition of friction is also reinforced by the fact the cylinder is slowly, during the displacement, embedded within the tissue by deforming it until reaching equilibrium in depth. The variation of the friction value during the equilibrium phase is explained by the irregularities of the tissue. This irregularities are associated with the formation of temporary on-growing steps at the front of the cylinder due to tissue deformation during the sliding.

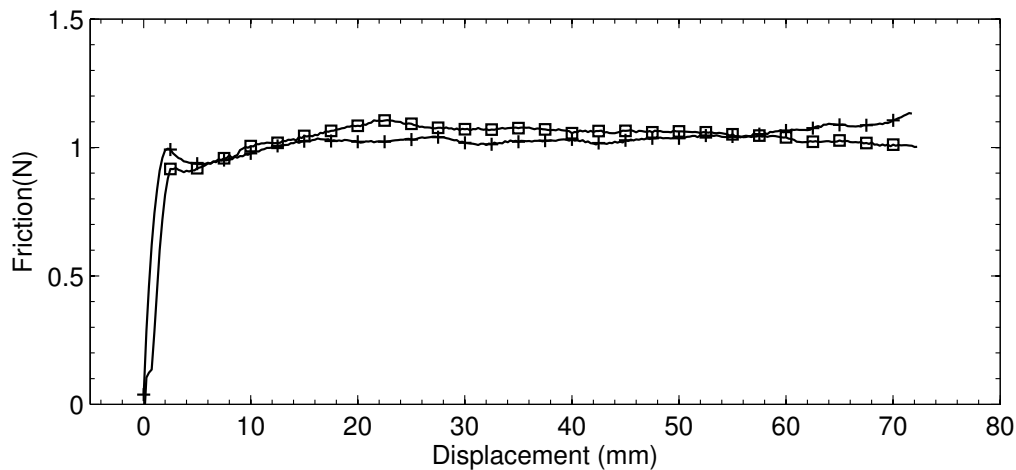
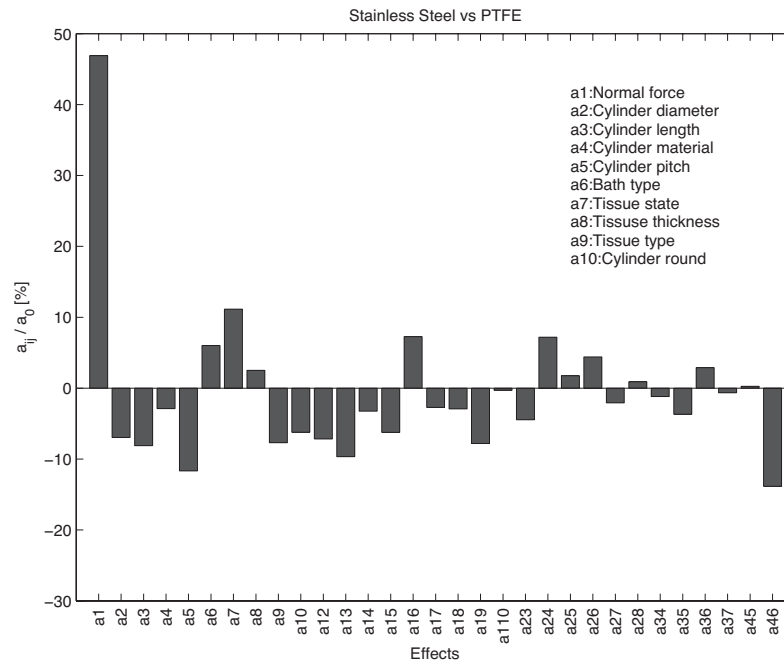


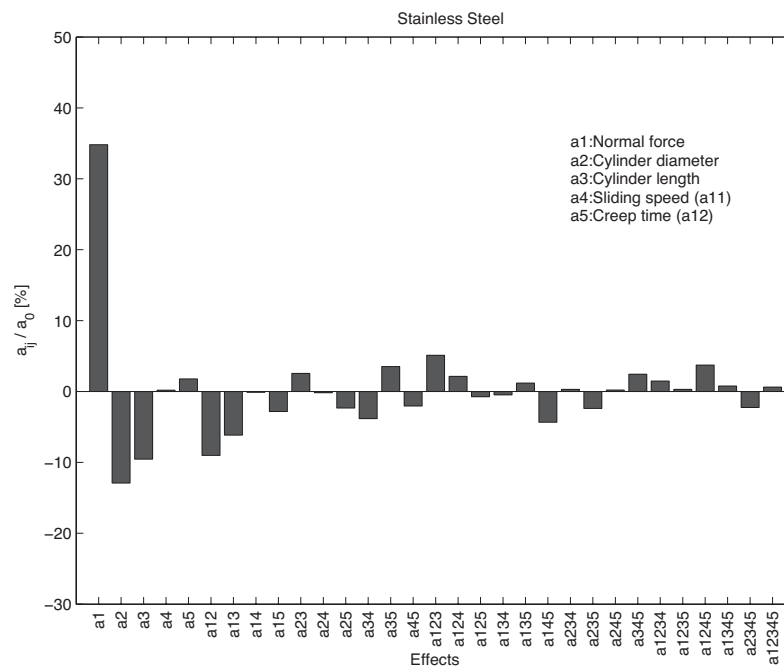
Figure 7.3: Typical measurements of friction force profiles acquired during experiments. The two plots are traces at different areas of the tissue. (Normal force = 2 N, Tip material = Steel, Tip dimension = 5x10 mm, Rounded end = R 2 mm, Pitch angle = 0°, Tissue type = Non-ablated Epicardium, Tissue thickness = 4mm, Bath type = Saline).

7.2.1 Factors Affecting Friction

As it relates to fractional FD, the effects of the 10 main factors and the 21 two-way interactions are computed, the aliased interactions thus represented only once. For simplification reasons, the details of only one of the three fractional FD are presented, as the other two are similar. Figure 7.4 shows the bar charts of the relative effects (effect divided by the average of the measurements, expressed in percentage) for the two FD. As expected, the *normal force* a_1 constitutes the main influence on the friction force. Three effects appear to be also important in all three factorial plans, namely *the pitch angle* (a_5), *the tissue physiological state* (a_7) and the two-way interaction a_{46} . As for a_{46} , prior knowledge of the experiments allows for interpreting it, not as the two-way interaction (*cylinder material, bath type*), but rather its third-order alias a_{123} (*normal force, cylinder diameter, cylinder length*), which is the expected effect representing the pressure applied on the cardiac tissue. (See Appendice A.2 for the list of factors aliases).



(A) Relative effects for the fractional FD.



7. Friction in Intracorporeal Guidance

This bar chart can be better understood according to equation 7.1, which shows in which way - increasing or decreasing - the factors are affecting the friction force. As, too many effects present a percentage near 10%, it is difficult to discriminate the significant factors and interactions using the bar charts. The next step consists of comparing the sum of squares of each effect with the total sum of squares of all the effects. The evaluation of this ratio provides an indication on how each factor is impacting the total variance of friction data, as illustrated on figure 7.5. These indications need to be confirmed by an analysis of variance (ANOVA). An ANOVA cannot be computed on all the effects, as the number of effects including the mean a_0 is equal to the number of experiments. Thus, there would not remain any degrees of freedom for the residuals. Consequently, we decided to consider the effects representing a cumulative sum of square up to 95%.

Tables 7.2 and 7.3 show the output of the ANOVA for the different FD. The effects for the fractional and the full FD are considered to be significant for a p-value below 1%. A p-value below 5% represents a tendency to be significant. Significant parameters are represented in boldface in the ANOVA tables. Therefore, the significant effects obtained for the fractional FD are listed below:

- a_1 : *normal force*
- a_{46} , (a_{123}): *normal force, cylinder diameter, cylinder length interaction*
- a_5 : *cylinder pitch angle*
- a_7 : *tissue physiological state*

The effect a_{12} and a_{13} corresponding to the *normal force - cylinder diameter* and *normal force - cylinder length* interactions show a tendency to be significant. At this scale, the *cylinder diameter, cylinder length, bath type, tissue type, cylinder round* and the *tissue thickness* seem to be non-significant. The significant effects obtained for the full FD are:

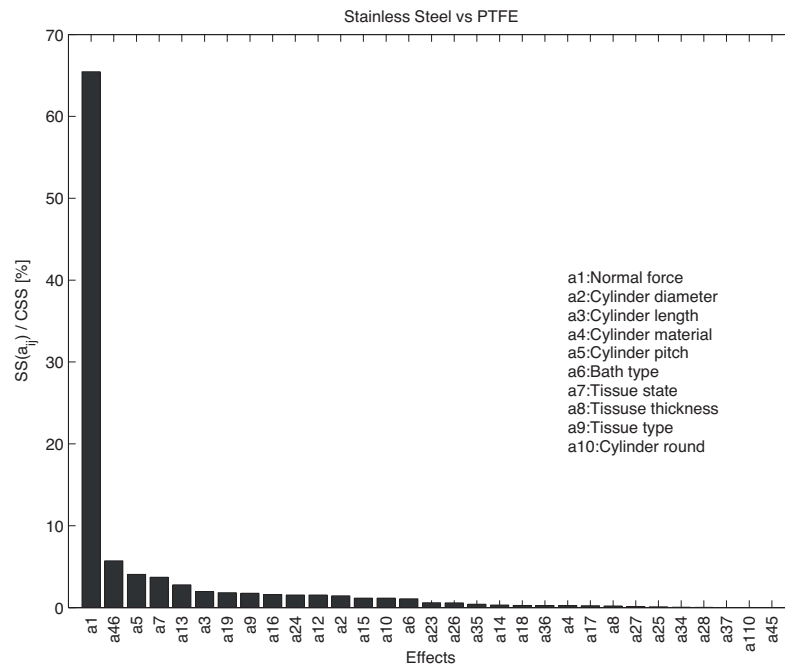
- a_1 : *normal force*
- a_2 : *cylinder diameter*
- a_3 : *cylinder length*
- a_{12} : *normal force, cylinder diameter interaction*
- a_{13} : *normal force, cylinder length interaction*

The effect a_{123} corresponding to the *normal force - cylinder diameter - cylinder length* interaction shows a clear tendency to be significant. The domain of experiments used for the full FD reveals that the *cylinder diameter, cylinder length* as well as the interaction of these two factors with the *normal force* appear to be significant at this scale. The *sliding speed* and *creep time* before dragging seem to be non-significant at these levels.

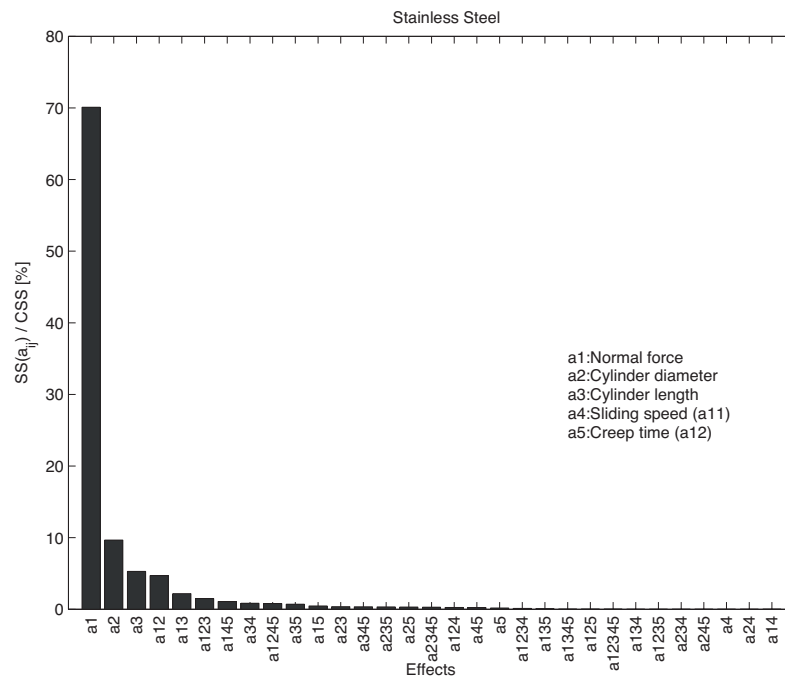
7.3 Discussion

The results from the different factorial designs show that the *normal force* applied to the cylinder against the tissue is by far the most significant factor affecting the friction. This also corresponds to the friction theories for rigid bodies where there is a linear relation between normal and friction force.

The geometric parameters of the cylinder such as the *cylinder diameter* and the *cylinder length*, are significant only for the full factorial design where the levels of these factors are reduced. These morphological interactions can be explained by the fact that the dimensions of the cylinder are in the same order of magnitude as the deformation capacity



(A) Sum of square of the effect for the fractional FD.



(B) Sum of square of the effect for the full FD.

Figure 7.5: Bar charts illustrating, in a descending order, the relative sum of square of effects over the total sum of square of all the effects. The fractional FD Stainless Steel vs Teflon is represented on the chart (A) and the full FD on chart (B).

7. Friction in Intracorporeal Guidance

Table 7.2: ANOVA based on a cumulative sum of square selection.

(a) Stainless Steel vs PTFE

Source	Sum Sq.	DoF	Mean Sq.	F	Prob>F
a_0	645046.41	1	6.5e+05	9.6e+02	0
a1	141952.41	1	1.4e+05	2.1e+02	2.1e-11
a_2	3115.44	1	3.1e+03	4.6	0.045
a_3	4240.64	1	4.2e+03	6.3	0.022
a5	8786.39	1	8.8e+03	13	0.002
a7	8017.76	1	8e+03	12	0.0028
a_9	3806.59	1	3.8e+03	5.7	0.028
a_{12}	3312.29	1	3.3e+03	4.9	0.039
a13	6011.40	1	6e+03	9	0.0078
a_{15}	2507.90	1	2.5e+03	3.7	0.069
a_{16}	3413.02	1	3.4e+03	5.1	0.037
a_{19}	3936.74	1	3.9e+03	5.9	0.026
a_{24}	3339.90	1	3.3e+03	5	0.039
a46	12360.31	1	1.2e+04	18	0.00044
Residual	12066.66	18	6.7e+02		
Total	861913.85	32			

(b) Stainless Steel vs AEP 60CM

Source	Sum Sq.	DoF	Mean Sq.	F	Prob>F
a_0	649534.55	1	6.5e+05	1.0e+03	0
a1	126471.57	1	1.3e+05	2.0e+02	3.7e-11
a2	11908.58	1	1.2e+04	19	0.00041
a5	7448.37	1	7.4e+03	12	0.0031
a_7	2761.64	1	2.8e+03	4.3	0.052
a_{10}	3712.33	1	3.7e+03	5.8	0.027
a_{12}	3001.47	1	3e+03	4.7	0.044
a_{13}	2946.05	1	2.9e+03	4.6	0.046
a_{110}	4171.63	1	4.2e+03	6.5	0.02
a_{23}	3917.44	1	3.9e+03	6.1	0.023
a_{26}	2358.50	1	2.4e+03	3.7	0.071
a_{28}	2489.13	1	2.5e+03	3.9	0.064
a_{36}	2839.74	1	2.8e+03	4.4	0.049
a46	9081.99	1	9.1e+03	14	0.0014
Residual	11494.62	18	6.4e+02		
Total	844137.59	32			

(c) AEP 60CM vs PTFE

Source	Sum Sq.	DoF	Mean Sq.	F	Prob>F
a_0	766771.93	1	7.7e+05	1.2e+03	2.2e-16
a1	115787.17	1	1.2e+05	1.8e+02	4.9e-10
a_4	5435.39	1	5.4e+03	8.2	0.011
a5	14063.35	1	1.4e+04	21	0.00029
a_6	4838.39	1	4.8e+03	7.3	0.016
a7	7982.30	1	8e+03	12	0.0031
a_9	1539.39	1	1.5e+03	2.3	0.15
a_{12}	2417.64	1	2.4e+03	3.7	0.074
a_{13}	4029.30	1	4e+03	6.1	0.025
a_{16}	3744.44	1	3.7e+03	5.7	0.03
a_{17}	1861.65	1	1.9e+03	2.8	0.11
a_{34}	2247.29	1	2.2e+03	3.4	0.084
a_{35}	4278.61	1	4.3e+03	6.5	0.022
a_{37}	4405.94	1	4.4e+03	6.7	0.02
a_{45}	1892.21	1	1.9e+03	2.9	0.11
a46	13511.86	1	1.4e+04	20	0.00035
Residual	10578.76	16	6.6e+02		
Total	965385.63	32			

Table 7.3: ANOVA based on a cumulative sum of square selection.

(a) Stainless Steel

Source	Sum Sq.	DoF	Mean Sq.	F	Prob>F
a_0	321706.07	1	3.2e+05	2.5e+03	0
a_1	38966.18	1	3.9e+04	3.1e+02	3.6e-15
a_2	5370.14	1	5.4e+03	42	1e-06
a_3	2936.75	1	2.9e+03	23	6.8e-05
a_{12}	2614.54	1	2.6e+03	21	0.00014
a_{13}	1216.19	1	1.2e+03	9.6	0.005
a_{123}	841.82	1	8.4e+02	6.6	0.017
a_{145}	603.91	1	6e+02	4.7	0.039
Residual	3052.50	24	1.3e+02		
Total	377308.10	32			

of the tissue. Indeed, creep tests, by means of a measuring probe (DIT 10.81, RSF Elektronik), were performed for three different *cylinder diameter* under a constant normal load of 2 N. Figure 7.6 illustrates deformation depths of the tissue surface versus time. A plateau is reached in less than 1 s which indicates that these results might be applicable for a sliding of a cylinder over the tissue in quasi-static conditions. For this range of load, we notice slight variations of amplitudes for the three configurations. These differences can be explained by the variation of tissue thickness and composition, but also by the complexity of define the contact point between the cylinder and the surface of tissue at the beginning of the tests. The ratios (*deformation depth/cylinder diameter*) indicate the portion of the *cylinder diameter* pressed down in the tissue as shown in table 7.4. These results could explain why the *cylinder diameter* is a significant factor at small scale, as the tissue lip in contact with the cylinder generates resistance to sliding in a nonlinear manner. The *normal force* coupled with the *cylinder diameter* and/or the *cylinder*

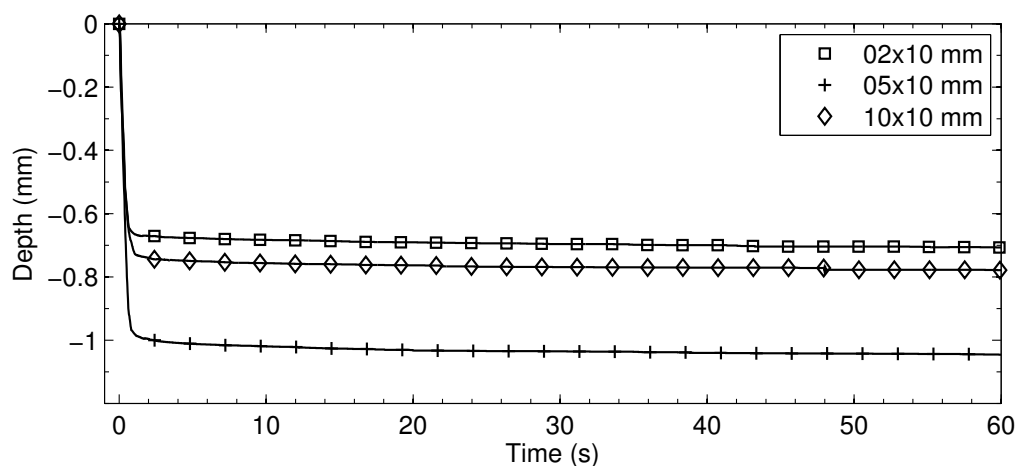


Figure 7.6: Deformation depth of a 4 mm thick bovine endocardial tissue surface under a constant normal load of 2 N for three dimensions of cylinders.

length contribute to the friction response. When a normal force is applied, the areas of contact between the cylinder and the tissue play an important role. The contact areas are represented by the front and side surfaces of the cylinder in direct contact with tissue. The interaction between the *normal force*, the *diameter* and/or the *length* of the cylinder

7. Friction in Intracorporeal Guidance

Table 7.4: Portion of the cylinder pressed down in the tissue

Cylinder dimensions	2x10 mm	5x10 mm	10x10 mm
Deformation depth	0.7 mm	1.0 mm	0.8 mm
Depth/diameter	34.8%	20.1%	7.7%

represents a dimension of pressure. Especially, the three-way interaction (*normal force* - *cylinder diameter* - *cylinder length*) represents the pressure applied on the tissue. A high pressure applied on the tissue will therefore result in an increase of friction in the considered range.

The front area represented by the *cylinder diameter* is interacting with the tissue when the cylinder is dragged under an applied *normal force*. This interaction comes from the fact that the tissue is deformed when a *normal force* is applied. Therefore, the front of the cylinder is in contact with the tissue resulting in a reaction force opposed to motion as illustrated on figure 7.7. This pressure not only varies with the normal force or the geometric parameters of the cylinder, but also varies with the pitch angle between the cylinder and the tissue. As the cylinder is tilted, it minimizes a direct contact with tissue at the front of the cylinder. The effect of the pitch angle on the friction response is higher when the *normal force* increases as the front contact with tissue become more important. The pitch angle of the cylinder is an attractive parameter for minimizing the friction response. However, a wide angle will result in a significant reduction in surface contact, which a consequence increases of friction. In other words, the topology of the tissue is a sensitive parameter affecting the friction. A small imperfection in the tissue will affect friction. The shape of the cylinder, represented by the *cylinder round*, should play an evident role as the shape could affect the repulsion force with tissue during dragging. A spindle-shaped cylinder should reduce the friction. However, the chosen levels and range of rounded edges did not lead to this conclusion as this parameter was not significant. The

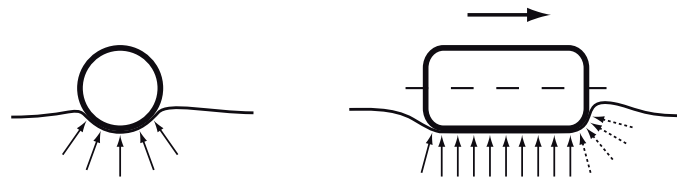


Figure 7.7: The contact areas consist of a side surface and a front surface of contact with tissue

ANOVA shows a significant main factor for the *tissue state*; ablated tissue leads to larger friction force. A radio-frequency ablation of tissue modifies the mechanical and tribological properties of the tissue. We experienced by touching an increase in stiffness and roughness of the tissue mainly due to water evaporation inside the tissue during RF ablation. In contrast, the *bath type*, *tissue thickness* and *tissue type* factors seem to have no influence on the friction response. The use of saline water to perform ex-vivo experiments instead of blood seems to have unnoticeable impact on the friction. This may signify that saline water could replace blood for applications with blood environment which could facilitate experimentation. Thus, epicardium layer compared to endocardium layer appears to have unnoticeable effect on friction.

As for the *cylinder material*, this factor is not significant in all FD for the tested materials, which means that the general behavior of the friction force is similar for all

three materials, but does not lead to the conclusion that this factor has no influence on the value of the force. Indeed, lubricious coatings have demonstrated their potential to reduce the friction with tissue [Nurdin et al., 1996]. However, the circumstance that these three materials did not show any difference on friction was not expected. We argue that the adhesion phenomenon for the tested materials is of minor effect considering our experimental data. The deformation component of the friction response seems to be the main contribution. It is known that the adhesion component at the interface of the materials is greatly reduced for very well-lubricated surfaces. The remaining frictional contribution is mainly due to surface deformation energy [Greenwood et al., 1961].

Regarding the temporal factors, namely the *dragging speed* and *creep time* before dragging, a variation of speed seems to have no effect for this range of motion. The *creep time* before dragging modified the transient part of the friction profile. The creep of the tissue over time results in a dip of the cylinder inside the tissue. A dragging of the cylinder in this condition, reaches steady state much quicker. However, no friction maxima has been recorded between the transient and the steady state. A larger temporal domain for this factor should be further analyzed to establish how the creep time could provide a resistance to dragging at the beginning of a sliding. Frictional interactions

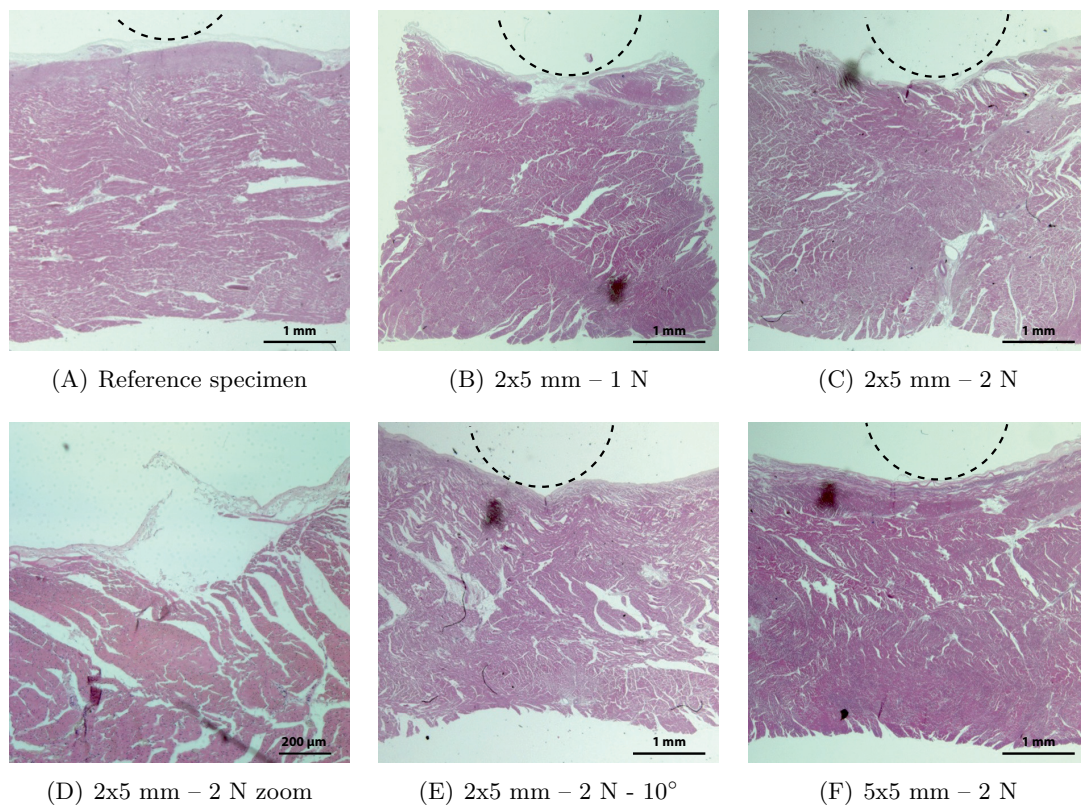


Figure 7.8: Histological cross-sections of a 4 mm thick bovine endocardial tissue resulting from different frictional conditions during sliding at 0.5 mm/s in saline environment: (A) reference specimen, (B) 1 N of normal force applied on a 2x5 mm cylinder, (C) 2 N of normal force on a 2x5 mm cylinder, (D) zoom on the break of the surface for 2 N of normal force on a 2x5 mm cylinder, (E) 2 N of normal force on a 2x5 mm cylinder tilted of 10°, (F) 2 N of normal force on a 5x5 mm cylinder

7. Friction in Intracorporeal Guidance

encountered during the experiments have been investigated by means of a histological study. Friction on endocardial tissue for different cylinder dimensions, normal forces and pitch angles has been realized. Following the experiment, tissues were fixed for 16 hours at room temperature in formalin, rinsed three times in PBS 1x and dehydrated for paraffin embedding. $4 \mu\text{m}$ sections were collected on SuperFrost Plus slides. Paraffin sections were dewaxed, rehydrated to water, and stained with hematoxylin and eosin (H&E) using a standard protocol on a Sakura Prisma automate. A selection of tissue cross-sections are shown in figure 7.8. An indentation, due to the path of the loaded cylinder on the tissue, is visible on every sample. The highest pressure applied to the tissue during sliding is shown in figures 7.8(C), 7.8(D) and 7.8(E). The formation of a lip at the front of the tissue has resulted in a break of the first layer of the endocardium. However, a slight tilt of the cylinder for the same pressure condition has left the surface intact.

7.4 Conclusion

The proposed analysis determines the parameters playing a significant role in the friction between a cylinder sliding over the cardiac tissue. By means of four factorial designs representing a set of 128 experiments, we could study the impact on friction of twelve parameters as well as the interactions between the parameters. Statistical analysis of the experimental data allows us to list five parameters, two two-way interactions and one three-way interaction that are most likely to influence the friction response. The results of our analysis, based on experimental data, show statistically how each parameter or interactions of parameters are contributing on their own to the generation of friction. Thereafter, the friction phenomenon can be represented with a minimum number of parameters and interactions that maximize the exactitude of the friction model. Moreover, the design of our intracorporeal magnetottractive guidance system can be optimized based on the outcome of this study. As an example, the normal force, the surface of contact and the pitch angle are important parameter to be considered. On the other hand, the material of the tip, tissue thickness, the cardiac tissue type, the surrounding environment and the sliding speed are parameters, which were expected to be important, turned out not to be relevant for our application. The methodology presented in the chapter can be easily applied to other soft tissues interacting with a cylindrical element sliding over it. However, the findings may vary for different tissues while still using the same methodology. The variation of mechanical, physiological and surface properties encountered in soft tissues may result in different frictional interactions, especially the contribution of the morphological interactions between the tissue and the cylindrical element. Nevertheless, we can suggest that cardiovascular tissue such as cardiac atria and blood vessels should result in very similar frictional behavior [Duck, 1990].

As a conclusion, we would like to emphasize the parameters, which could minimize the friction with a soft tissue such as cardiac tissue:

- The normal force applied to the element should be as small as possible
- The surface of the contact between the element and the tissue should be maximized
- The pitch angle of the element might be positive of few degrees

This study gives some guidelines to minimize friction interactions between a cylindrical element and tissue. Further experiments could be performed in the future in order to propose a model of friction including the main parameters involved in the complex friction

phenomenon. Such models predicting the friction interactions with tissue may represent a very useful tool in the design of intracorporeal guiding systems.

8 Applications for Intracorporeal Guiding Systems

On-site magnetic guidance is particularly achievable in the cardiovascular system. Thanks to the numerous vessels surrounding the heart, we believe that intracorporeal guiding systems has the potential to facilitate catheterization procedures to cardiac arrhythmias. Although on-site guidance is not limited to our field of research, we describe in this chapter how intracorporeal MAGS could be applicable for the treatment of cardiac arrhythmias such as atrial fibrillation, Wolff-Parkinson-White syndrome or ventricular tachycardia.

Cardiac arrhythmia is a condition in which the heart's normal rhythm is disrupted. The cardiac rhythm is set by a small region of cardiac muscle cells, called the sinoatrial (SA) node, which are located in the right atrium and that acts as a spontaneous pacemaker. The normal heart rhythm is called sinus rhythm. In this rhythm, the SA node produces electrical impulses that propagate throughout the four chambers of the heart in a coordinated fashion, figure 8.1. The electrical impulses start in the sinus node and travel to both atria, causing them to contract, and trigger the atrioventricular (AV) node which conducts electrical impulses from the atria to the ventricles.

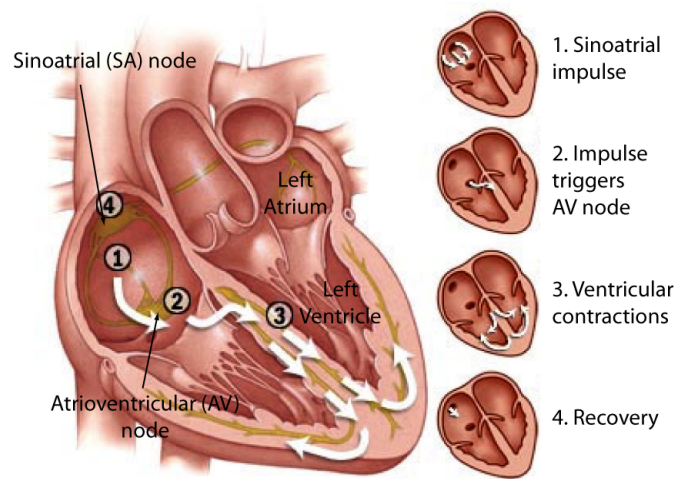


Figure 8.1: Sinus rhythm sequences: Electrical impulses are initiated by the sinoatrial (SA) node (1). The signal travels to both atria, causing them to contract, and triggers the atrioventricular (AV) node (2). From the AV node, the signal travels through the ventricles (3), causing them to contract and pump out blood. After a sort pause, the process starts over (4). Source: Mayo Clinic.

8.1 Atrial Fibrillation

Maestro-AF project was introduced in our laboratory by Dr. Vitali Verin in 2008. The acronym stands for **M**agnetic **A**blation **E**scorting for **T**reatment **O**f **A**trial **F**ibrillation. The idea behind this project is to treat Atrial Fibrillation (AF) with a pair of magnetic catheters, which may provide a simple, efficient, reproducible and controllable catheter ablation with higher safety.

8.1.0.1 Project Description

Atrial fibrillation is the most common cardiac rhythm disorder accounting for approximately one-third of hospitalizations, and is a major stroke risk factor [Prystowsky, 2008]. AF significantly affects the quality of life of at least 1% of western world population. Prevalence of AF increases with age: from 0.5% for those between 50 and 59 to about 10% for those between 80 and 89 [Fuster et al., 2006].

Radiofrequency (RF) Percutaneous Catheter Ablation (PCA) is widely used for more than 10 years to treat AF by inactivating abnormal electrical pathways in the left atrium of the heart. With existing catheters, it is difficult to control the position and the quality of lesions produced. The main component of PCA is the catheter. It has several functionalities such as therapy delivery, electrical sensing using four electrodes, irrigation of the tip, and temperature monitoring. Moreover, it needs to be very flexible in reaching points at various locations. Despite all the functionalities mentioned, the catheter is unable neither to glide on the inner surface of the atrium in a controllable way nor to measure the direct tissue temperature during the ablation.

The optimal method for catheter ablation of AF is still debated. The current techniques consist of creating structured-lesions, called ablation pattern, that may eliminate the mechanisms involved in the initiation and maintenance of AF, figure 8.2 [Dewire and Calkins, 2010]. Treating atrial fibrillation with these ablation patterns require 4 to 6 hours of procedure.

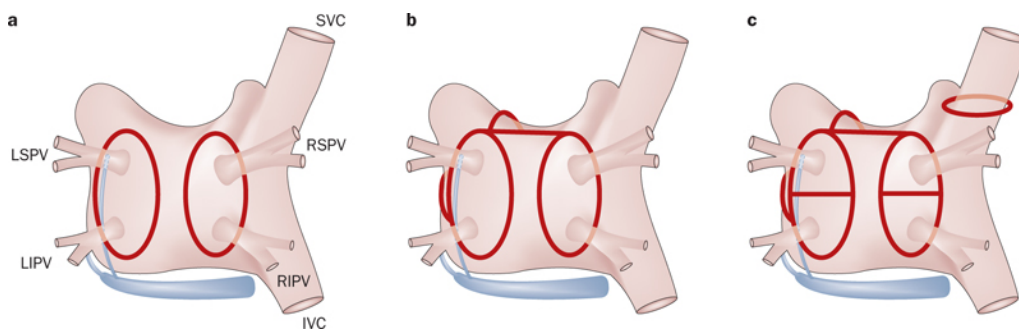


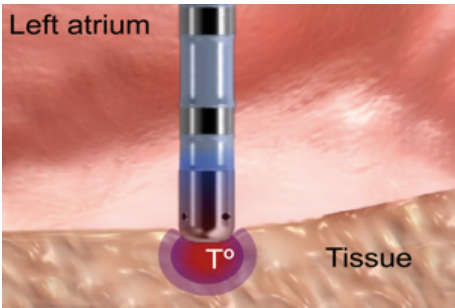
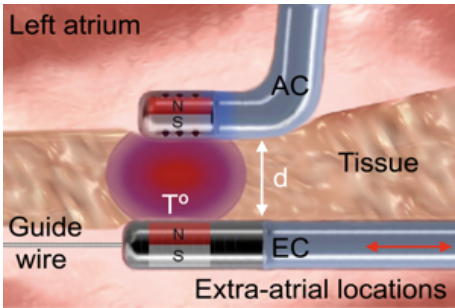
Figure 8.2: Posterior view of the current ablation patterns to treat atrial fibrillation. Realizing these patterns take up to 4 hours of procedure. a) Classical Pulmonary Vein Isolation (PVI) pattern. b) Addition of lines to the PVI pattern. c) Eight lesions PVI pattern. Abbreviations: IVC, inferior vena cava; LIPV, left inferior pulmonary vein; LSPV, left superior pulmonary vein; RIPV, right inferior pulmonary vein; RSPV, right superior pulmonary vein; SVC, superior vena cava.

The electrophysiologist has to move the catheter tip from one point to another in a jumping manner. With this technique ablation points are created rather than lines. The distance between those points is difficult to be controlled as well as the depth of

the ablation points. Insufficient energy delivery and gaps between the points lead to the relapse of the arrhythmia. Excessive amounts of energy may result in formation of vapour bubbles leading to perforation or thrombi formation which is a major safety concern. Temperature monitoring directly inside the tissue as well as good mechanical and electrical contact with tissue over time are necessary to deliver the right amount of energy. These conditions are not achievable with the currently available ablation catheters. Limitations of PCA result from the complexity of navigating a catheter inside the beating heart and controlling energy delivery to targeted locations. These shortcomings also lead to the relapse of the arrhythmia. Left untreated AF could cause sometimes severe life-threatening complications.

The key idea of Maestro-AF is to eliminate the two major limitations of catheter ablation with the help of a magnetically coupled second catheter, namely the Escorting Catheter (EC), placed in the vessels surrounding the left atrium. This second magnetic catheter provides a stable contact with tissue as well as a controlled dragging of the Ablation Catheter (AC) resulting in continuous ablation lines. Moreover, precise tissue temperature monitoring from the opposite side of the atrial wall ensures optimal and controlled thermal lesions. Table 8.1 gives a comparative overview between the current catheter ablation technology and the proposed technology. The escorting catheter is placed in three well-defined locations in the heart from where it will be displaced by the physician to drag magnetically the ablation catheter. This involves a new pattern of ablation. However, the resulting pattern is similar to the surgical pattern performed in open-heart surgery, which is the gold standard in terms of efficiency, figure 8.3. These concepts are unique to Maestro-AF and have been patented.

Table 8.1: Comparison overview between the current PCA and the Maestro-AF technology. AC: ablation catheter. EC: escorting catheter.

Current PCA	Maestro-AF
	
<ul style="list-style-type: none"> Dynamic tissue contact “Points by points” lines Variable lesions dimensions Indirect tissue measurement Depends on physician’s skills 	<ul style="list-style-type: none"> Stable tissue contact Continuous lines Transmural lesions Direct tissue measurement from EC Reproducibility of the procedure

8. Applications for Intracorporeal Guiding Systems

8.1.0.2 Scientific, Technical and Business Objectives

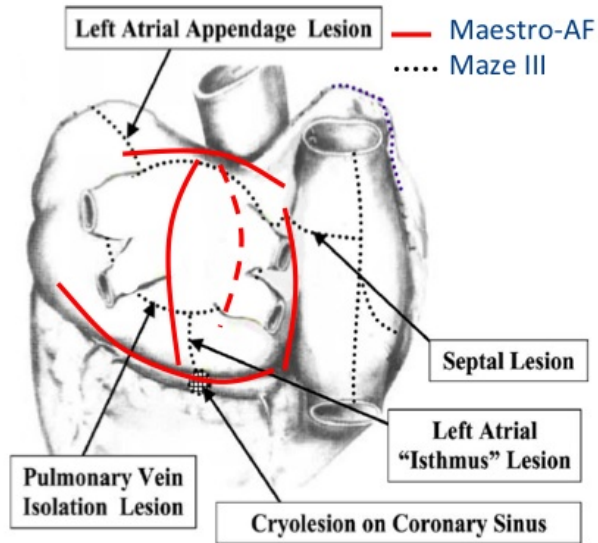
Maestro-AF technology will provide a new simple, efficient, reproducible and controllable PCA approach to treat AF with higher safety. Thus, the system will significantly reduce duration of the PCA procedure and shorten the learning curve of the operator. The concept of magnetic coupling of two catheters provides multiple advantages such as:

- A stable position of the AC against the atrium wall. It provides optimal conditions to deliver energy inside the tissue.
- A smooth displacement of AC by means of an EC placed within vessels surrounding the heart. The displacements are continuous and not affected by the beats of the heart.
- A unique opportunity to measure the tissue temperature from the back side of the atrial wall during ablation. Temperature monitoring guides the propagation of energy depending on the tissue thickness and ensures that the ablation has been done in the entire thickness of the tissue.
- A reproducible ablation pattern anatomically based on the cardiovascular anatomy.

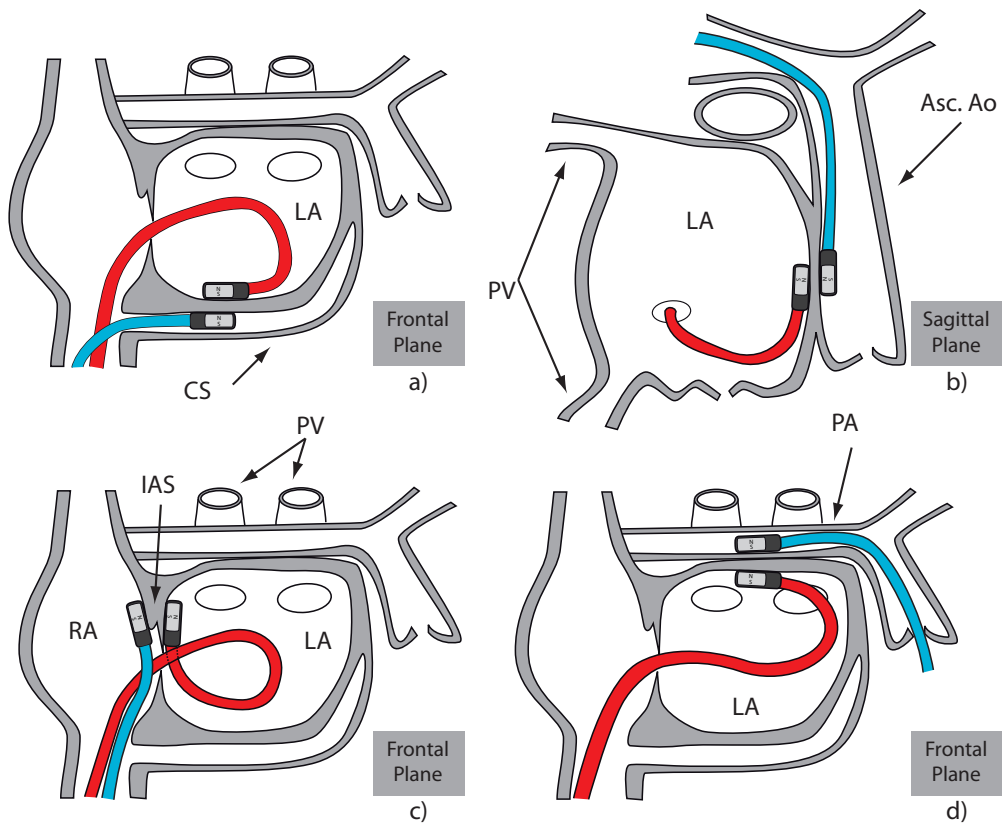
Maestro-AF approach will drive the growth of the catheter ablation for the AF market (only 6.7% today) and increase the number of patients treated [St Jude Medical Inc., 2010]. The current market for AF PCA therapy is CHF 380 million. It grows with 15% - 20% annually resulting in a CHF 1 billion market by 2015. From about 6 Million AF patients, 1.5 Million patients are indicated for catheter ablation procedure. Only 100'000 catheter ablations are performed annually, showing the urgent need of efficient and simple to use ablation devices.

8.1.0.3 Implementation Stage and Perspectives

In vitro and *in vivo* experiments have shown that catheters with single permanent magnets are not sufficient to provide a robust guidance for our application. The Maestro-AF anatomical ablation pattern to treat atrial fibrillation varies in tissue thickness. We understood that more complex magnetic tip of catheters allowing an adjustment of the coupling strength should be developed. Design and analysis of different magnetic force modulation principles have been presented in this dissertation. These mechanisms are able to vary the field intensity and/or direction between two magnetic components. This will allow for better magnetic guidance between the ablation and escorting catheters, as it will provide adequate coupling forces independently of the tissue thickness. A magnetic force modulator have been manufactured and successfully tested *in vitro*. The next step is to scale down and implement the modulator in a catheter in order to be tested *in vivo*. Guidance and ablation with this last generation of active catheters will confirm or not the technical and anatomical feasibility of this approach for the treatment of atrial fibrillation.



(A) Comparison of Maestro-AF with Maze III surgical pattern



Coronary sinus line (b) Septum line (c) Pulmonary artery line (d) Ascending aorta line
 LA: left atrium, RA: right atrium, PA: Pulmonary artery, PV: Pulmonary vein,
 CS: coronary sinus, IAS: inter-atrial septum

(B) Maestro-AF ablation pattern

Figure 8.3: Maestro-AF system comprises two magnetic catheters. The ablation catheter is displaced with the help of a second catheter placed in the vicinity of the left atrium. This technology requires a new pattern of ablation similar to the very efficient surgical pattern (Maze III).

8.2 Wolff-Parkinson-White Syndrome

Intracorporeal magnetic guidance is technically applicable to another type of heart disorder, Wolff–Parkinson–White syndrome (WPW). Wolff–Parkinson–White syndrome affects 0.1% to 0.3% of the general population [Cohen et al., 2012] and is characterized by abnormal electrical pathways causing a disruption of the heart’s sinus rhythm. A specialized group of cells called the atrioventricular (AV) node is responsible for conducting electrical impulses from the atria to the ventricles.

People with Wolff–Parkinson–White syndrome are born with an extra connection in the heart. This extra connection, called accessory pathway, allows electrical signals to bypass the AV node and move from the atria to the ventricles faster than usual, figure 8.4.

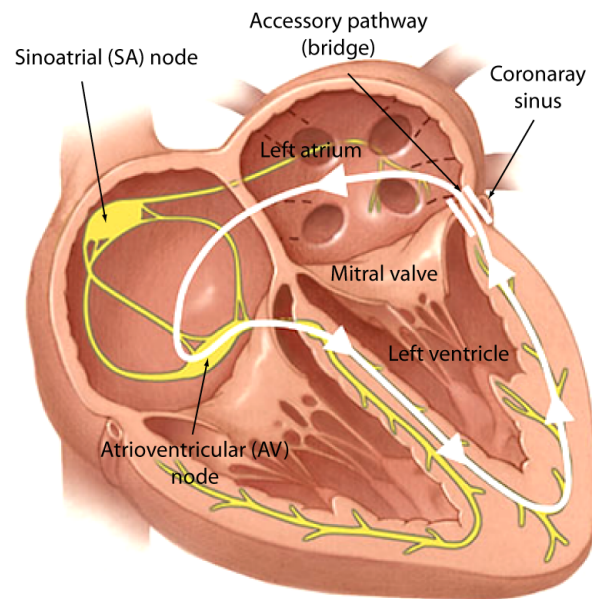


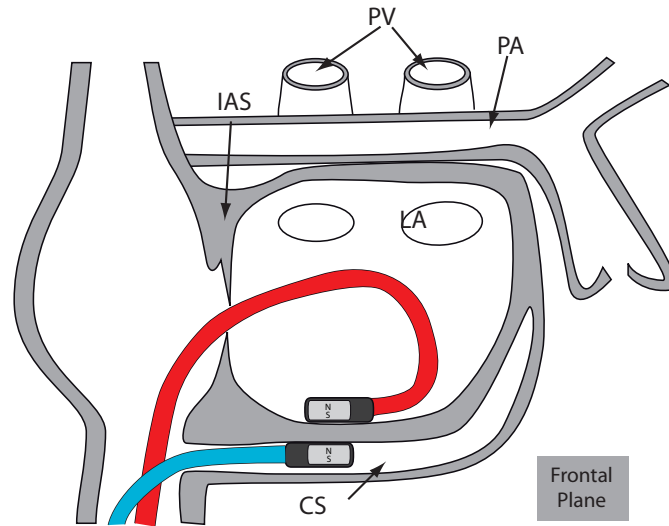
Figure 8.4: Wolff–Parkinson–White syndrome is cardiac arrhythmia caused by an extra electrical pathway between the atria and the ventricles. Source: Mayo Clinic.

This extra connection can disrupt the coordinated propagation of electrical signals through the heart, leading to an abnormally fast heartbeat rate (tachycardia) and other arrhythmias. Dizziness, palpitations, shortness of breath or fainting are the resulting symptoms. In rare cases, arrhythmias associated with WPW syndrome can lead to cardiac arrest and sudden death.

The most common procedure to treat WPW is catheter ablation. The region of treatment is located in a highly dynamic region of the heart close to the mitral valve, which makes the procedure difficult and very dependant of the physician’s skills. The electrical bridge to disconnect is situated near the coronary sinus. The coronary sinus is a vessel running transversely on the posterior surface of the heart between the left atrium and left ventricle. By introducing a magnetic guiding catheter in the coronary sinus, the magnetic ablation catheter could be coupled and dragged in a controlled manner over the area of treatment as shown in figure 8.5. Therefore, we believe that intracorporeal magnetic guidance can provide a stable contact for the ablation catheter tip which can improve the detection of reentrant circuit path as well as the delivery of efficient RF lesions. The feasibility of this approach has already been demonstrated *in vivo* on a

8.2 Wolff-Parkinson-White Syndrome

porcine beating heart. As the separation distance between the walls of the left atrium and the coronary sinus is regular and constant in thickness, catheters equipped with single permanent magnets is sufficient to drag the ablation catheter and ablate the the region of interest.



LA: left atrium, RA: right atrium, PA: Pulmonary artery,
PV: Pulmonary vein, CS: coronary sinus, IAS: inter-atrial septum

Figure 8.5: Treatment of Wolff-Parkinson-White Syndrome by intracorporeal magnetic catheter ablation. The ablation catheter located in the left atrium is displaced magnetically with the help of a second catheter placed in the coronary sinus.

8.3 Ventricular Tachycardia

Ventricular tachycardia (VT) is a fast but regular rhythm that initiates in the ventricles, figure 8.6. If left untreated, some forms of VT may lead to ventricular fibrillation, which can be life-threatening as the heart beats are so fast and irregular that the heart stops pumping blood. Ventricular fibrillation is a leading cause of sudden cardiac death.

Catheter ablation is now an important option to control recurrent ventricular tachycardias. Depending on the arrhythmic substrate, VT circuits can be close to the endocardium (inner layer of heart tissue) or can be deeper within the myocardium (intermediate layer of heart tissue) [Zipes et al., 2006]. Traditional RF delivery ablation may not create deep enough lesions and fail to interrupt some deep reentry circuits [Soejima et al., 2001]. Inability to create a sufficiently deep lesion in the ventricle is an important cause of ablation failure particularly for some forms of VTs where the reentry circuits are intramural or epicardial (outer layer of heart tissue) [Aliot et al., 2009].

Intracorporeal magnetic guidance may be address for VTs that are extremely deep within the myocardium or located epicardially. The idea is to sandwich the wall of the ventricle with both magnetic catheters. It will involve a transthoracic pericardial access for the guiding catheter. The second catheter is inserted like any conventional catheter in the ventricle. Sandwiching the myocardium with magnetic catheters will allow to create deep lesions by applying RF energy from both side of the tissue.

Manual navigation with a magnetic catheter into the pericardial space (space in which the heart is located) has not been tested yet. However, recent techniques performing mapping of the epicardium from the pericardial space have already shown the feasibility of this access [Sosa et al., 1996, Della Bella and MacCubelli, 2011].

Therefore, we believe that intracorporeal magnetic catheters can deliver RF energy from both sides of the thick tissue which may result in transmural and optimal lesions.

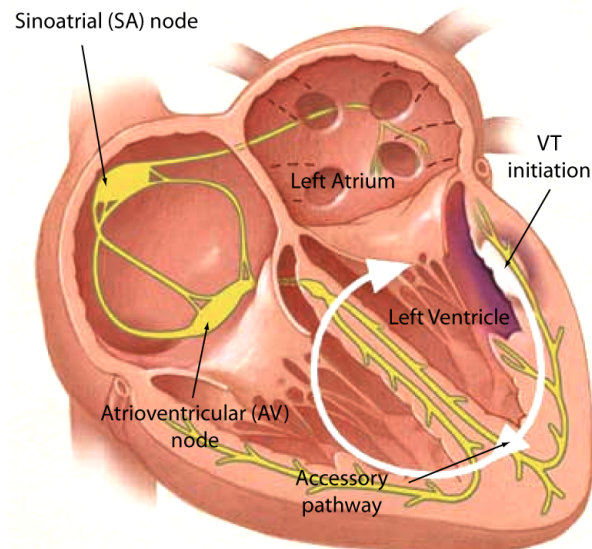


Figure 8.6: Treatment of ventricular tachycardias by magnetic anchoring of ablation catheters. The ablation catheter in the ventricle is displaced magnetically with the help of a second catheter placed the pericardial space. Sandwiching the myocardium with magnetic catheters allow to create deep lesions. Source: Mayo Clinic.

9 Synthesis and Conclusion

This thesis work deals with different challenges, scientific and technical, that have been studied in depth. Our main goal has been to propose an original, efficient and simple magnetic anchoring and guidance system for medical applications. The endeavours, outcomes, analysis of the accomplished work and future expectations are described in the following sections.

Intracorporeal Magnetic Guidance

Magnetic Anchoring and Guidance Systems (MAGS) are applied in many fields of modern medicine. Therapeutic and diagnostic capabilities offered by such technology are growing with the clinical need to make procedures less invasive and traumatic for the patient. Technically, magnetic manipulation requires variable, reshapable or steerable magnetic fields and therefore are generally associated with large magnetic arrangement of coils or permanent magnets surrounding the patients; while temporary anchoring functions are insured by external permanent magnets of adequate size placed or dragged manually on the surface of the body.

In this dissertation, we introduced a novel type of magnetic guidance. Instead of having the guiding part external to the body, we proposed to perform the guidance locally, on-site, by having the guiding part within the body in close vicinity of the element to be guided. The ultimate goal of this thesis was to evaluate the technical feasibility of such magnetic guidance.

Force Modulation with Permanent Magnets

Intracorporeal magnetic guidance consists in providing a “magnetottractive” force to a guided element sandwiching the tissue. Our prior *in vitro* and *in vivo* investigations showed that intracorporeal guidance of catheters equipped with single permanent magnets is feasible in constant and regular tissue thickness, but hardly achievable on tissue varying in thickness as well as in dynamic anatomical conditions. These limitations are most likely attributed to inadequate coupling forces. On one hand, the magnetic catheters should be powerful enough to be automatically attracted and coupled when brought in close vicinity. On the other hand, once they are coupled and sandwiching the tissue, their magnetic attraction as well as the resulting friction with tissue may be too strong to allow a proper guidance. Consequently, the assumption of this thesis was that the magnetic fields within the MAGS should be adjustable in order to provide a constant guiding force independent of tissue irregularities and thickness variation. We have demonstrated by

9. Synthesis and Conclusion

FEM modelling that such a system providing a modulation of the magnetic field cannot be achieved, at this size, by electromagnets. Rare-earth magnets produce strong magnetic fields but the resulting attractive forces are strongly dependent on the distance, which can lead to large frictional interactions with tissue and potential risks of perforation.

The goal of this thesis was to find solutions to overcome these technical hurdles. We have demonstrated through several examples that the magnetic forces applied to the guided element can be modulated by combining permanent magnets together or with other ferromagnetic materials. Our investigations have led to the development of a modulator composed of two steerable magnets and a fixed magnet. The steerable magnets modulate the intensity of the field while the fixed magnet boosts the coupling strength.

In comparison to a MAGS equipped with a single static permanent magnet, our solution offers a large modulation range and a good coupling strength from zero to nearly 80% of the maximal force given by static permanent magnets. However, this reasonable decrease of coupling force can be compensated by slightly increasing the length of the magnetic system.

Actuation Mechanism

As permanent magnets produce a constant magnetic field, a combination of several steerable permanent magnets is necessary to modulate the overall magnetic field perceived between the MAGS elements. However, actuating movable magnets is a challenge due to the high internal forces and torques acting on the components of the modulator. To solve this issue, we have demonstrated that a mechanical actuation of the steerable magnets could be achieved by means of an inverted “lip-stick” mechanism that converts an axial movement of a cable into a synchronous rotation of the permanent magnets. The measured actuation force is below 10 N which is reasonable. As an example, the force required to actuate a cable driven system for deflecting the tip of ablation catheters can be up to 15 N. We developed a model that could predict the actuation force based on the dimensions of the modulator. For example, we could predict that a force below 5 N is sufficient to actuate a modulator integrated in catheter tip of 5 mm in diameter.

Benefit of Force Modulation

Our goal was also to analyze and understand better the guidance behavior of the proposed magnetottractive guiding system. By measuring the magnetic attraction force occurring during the guidance, we analyzed the system behavior in two operating modes, namely the passive and the active mode. While the passive guidance mode uses static magnetic fields, the active guidance mode allows the variation of the magnetic field during the guidance. Guidance with static magnetic field implies that the coupling force within the MAGS is depending on the tissue thickness and irregularities. As the coupling force varied approximately with the square of the distance, level of coupling force could change rapidly over an irregular substrate such as anatomical tissue. Therefore having the capability to adjust the coupling force is potentially advantageous.

Our analysis has shown that the transition from the static phase to the sliding phase is a delicate phase in magnetottractive guidance. This is particularly true for the passive guidance in soft materials. In the static phase, the growing misalignment of the MAGS, initiated by the movement of the guiding element, decreases rapidly the coupling force within the MAGS. If no magnetic force adjustment is done, the misalignment may become too large until the magnetic dragging force becomes superior to the static friction force.

In addition, once the passive magnets is in motion and follows magnetically the guiding part, any tissue irregularities may become critical. These situations could potentially lead to the decoupling of the MAGS and therefore to the failure of the guidance. Operating in the passive mode with bigger magnets on irregular tissue is not the answer. Increasing the magnetic attractions of the MAGS increases at the same time the friction force. Frictional interactions will become even larger with the sink of the guided part in the tissue. This is particularly true for guided elements of small dimensions, where the tissue creep could be of the same order of magnitude as the guided element itself.

Consequently, we have demonstrated *in vitro* that active control provides smoother guidance and superior robustness in comparison with the passive guidance mode.

Empirical Friction Analysis

Our analysis would not have been complete without investigating the friction phenomenon occurring under magnetottractive guidance. From a list of twelve parameters of physical, geometrical, physiological and temporal nature we identified by means of factorial design methods five parameters, and three combination of parameters that are most likely to influence the friction response during the guidance on soft anatomical tissues. The normal force, the surface of contact and the pitch angle are important parameters to be considered to reduce friction. On the other hand, the material of the tip, tissue thickness, the cardiac tissue type, the surrounding environment and the sliding speed are parameters, which were expected to be important, and turned out not to be not so relevant for our application. Therefore, this study not only gives some guidelines to minimize friction interactions during guidance, but also it allows the representation of the friction phenomenon with a minimum number of parameters and interactions that maximize the exactitude of the friction model.

Applications

Although magnetic materials and permanent magnets characteristics have improved considerably with rare-earth magnets, the proposed type of guidance is limited to a centimetric working volume. On-site magnetic guidance is particularly achievable in the cardiovascular system due to the presence of numerous vessels surrounding the heart. We believe that intracorporeal guiding systems have the potential to facilitate catheterization procedures for the treatment of cardiac arrhythmias such as atrial fibrillation, Wolff-Parkinson-White syndrome or ventricular tachycardia. Moreover, intracorporeal MAGS not only provides local guidance of a guided object, but by the fact that both magnetic parts sandwich the tissue, it has the advantage to be used for collecting or monitoring tissue information (temperature, echography, etc...). during diagnostic or therapeutic procedures.

Outlook

In this thesis work, we have demonstrated that modulating the magnetic field provides smoother guidance and more robustness as the modulator can provide a constant force over variable and dynamic anatomical conditions. It is important to keep in mind that these findings were obtained for an untethered guided tip and in an automated active guidance mode, which requires force feedback information to control the coupling force within the MAGS. Depending on the applications, the force feedback could be of different types. Integrating a force sensor in the guiding part is very challenging, especially for

9. Synthesis and Conclusion

catheterization applications where the size is limited. However, a concept of optical micro-force sensor is currently under development and evaluation in our laboratory. Off-the-shelf magnetic sensors could represent a force feedback alternative and may facilitate integration in the system. However, the complexity of the magnetic field shape, the large variation of magnetic field intensity and the freedom in the orientation of the guided part during the guidance make this solution difficult to calibrate and probably less accurate than the use of an optical force sensor. Another approach could consist of monitoring the guidance behavior under visual feedback by means of live fluoroscopic images and adjusting manually the coupling force according to tissue variations.

The next logical step is to design and fabricate a second prototype force modulator implemented in a complete catheter of 5 mm in diameter that could be inserted in the cardiovascular system in order to be tested on a animal beating heart. Expected magnetic performances of this version evaluated by FEM modelling are encouraging. Its complete fabrication is planned for the next few months and will require the expertise of a company in the field of catheterization.

One technical limitation of our system concerns the single configuration in which the coupling of MAGS is achievable. The physician should control the guiding part carefully to avoid any rotation of modulator during the guidance. As the guidance is achieved locally, the dragging distance is limited to few centimeters which should help in realizing this task.

Based on the findings from our tribological analysis, the design of the guided but also of the guiding part can be optimized. For example, few degrees of pitch angle on the guided part reduces the frictional interactions with tissue during the guidance, as bit like a skier in powder snow. Having the guided part slightly back-tilted can be achieved magnetically or by a meticulous design of the guided part. In this sense, further experiments could be performed in order to propose a model of friction including the main parameters involved in the complex friction phenomenon. Having such a model predicting the frictional interactions as a function of geometric and magnetic parameters could be very helpful in the design of magnetic guidance systems.

Even though, we provide technical solutions that improve the guidance of our magnetottractive device, the road leading to clinical acceptance is still long and is strewn with obstacles. *In vivo* experimentation will evaluate the anatomical and medical feasibility of intracorporeal magnetic guidance to facilitate for example the treatment of cardiac arrhythmias.

A Appendices

A.1 Factorial Design Matrices

A linear model has been chosen to perform the screening of these factors. This model is represented as the sum of the weighted contributions of several factors, or effects, as expressed by:

$$Y(x) = a_0 + \sum_{i=1}^N a_i x_i + \sum_{i \neq j}^N a_{ij} x_{ij} + \sum_{i \neq j \neq k}^N a_{ijk} x_{ijk} \quad (\text{A.1})$$

where Y is the friction force, x_i are the factors, x_{ij} their two-way interaction, a_0 is the constant effect (average of all the effects), a_i the main (half) effects and a_{ij} their two-way order interaction. The corresponding system of equation is:

$$Y = \begin{bmatrix} y_1 \\ \vdots \\ y_N \end{bmatrix} = X \begin{bmatrix} a_0 \\ a_1 \\ \vdots \\ \vdots \\ a_{123\dots K} \end{bmatrix} + \begin{bmatrix} \varepsilon_1 \\ \vdots \\ \varepsilon_N \end{bmatrix} \quad (\text{A.2})$$

$$Y = X\alpha + \varepsilon \quad (\text{A.3})$$

$$X = \begin{bmatrix} 1 & x_{11} & x_{12} & \cdots & x_{11}x_{12} & x_{11}x_{13} & \cdots \\ 1 & x_{21} & x_{22} & \cdots & x_{21}x_{22} & x_{21}x_{23} & \cdots \\ 1 & x_{31} & x_{32} & \cdots & x_{31}x_{32} & x_{31}x_{33} & \cdots \\ \vdots & \vdots & \vdots & & \vdots & \vdots & \\ 1 & x_{N1} & x_{N2} & \cdots & x_{N1}x_{N2} & x_{N1}x_{N3} & \cdots \end{bmatrix} \quad (\text{A.4})$$

Where: Y : column vector $N \times 1$ with N experimental response X : matrix vector with the (unknown) coefficient of the model ε : column vector of the experimental errors

Therefore, if the response of the system is organized in a vector R :

$$R = \begin{bmatrix} R_1 & R_2 & \cdots & R_N \end{bmatrix}^T \quad (\text{A.5})$$

A. Appendices

and the coefficient of the model in a vector A :

$$R = \left[a_0 \ a_1 \ a_2 \ \cdots \ a_{12\dots N} \right]^T \quad (\text{A.6})$$

Then the system of equation is written and solved the following manner:

$$XA = R \Rightarrow A = (X^T X)^{-1} X^T R \quad (\text{A.7})$$

The matrices of a FD are Hadamard matrices and then have the following properties:

$$X^T X = NI_N \quad (\text{A.8})$$

The vector of coefficient becomes:

$$A = \frac{1}{N} I_N X^T R \quad (\text{A.9})$$

A.2 List of Factors Aliases

5 generators have been used to generate the aliases for the 2^{10-5} fractional factorial designs [Box et al., 2005]:

$$a_6 = a_{1234} \quad a_7 = a_{1235} \quad a_8 = a_{1245} \quad a_9 = a_{1345} \quad a_{10} = a_{2345}$$

Therefore, the generated aliases can be listed:

$$\begin{aligned} a_{16} &= a_{234} = a_{510} \\ a_{26} &= a_{134} = a_{59} \\ a_{36} &= a_{124} = a_{58} \\ a_{46} &= a_{123} = a_{57} \\ a_{56} &= a_{12345} = a_{38} = a_{47} = a_{29} = a_{110} \\ \\ a_{17} &= a_{235} = a_{410} \\ a_{27} &= a_{135} = a_{49} \\ a_{37} &= a_{125} \\ a_{47} &= a_{12345} = a_{56} = a_{38} = a_{29} = a_{110} \\ a_{57} &= a_{123} = a_{46} \\ a_{67} &= a_{45} \\ \\ a_{18} &= a_{245} = a_{310} \\ a_{28} &= a_{145} \\ a_{38} &= a_{12345} = a_{47} = a_{56} = a_{29} = a_{110} \\ a_{48} &= a_{125} = a_{37} \\ a_{58} &= a_{124} = a_{36} \\ a_{68} &= a_{35} \\ a_{78} &= a_{34} \end{aligned}$$

$$a_{19} = a_{345} = a_{210}$$

$$a_{29} = a_{12345} = a_{56} = a_{47} = a_{38} = a_{110}$$

$$a_{39} = a_{145} = a_{28}$$

$$a_{49} = a_{135} = a_{27}$$

$$a_{59} = a_{134} = a_{26}$$

$$a_{69} = a_{25}$$

$$a_{79} = a_{24}$$

$$a_{89} = a_{23}$$

$$a_{110} = a_{12345} = a_{56} = a_{47} = a_{38} = a_{29}$$

$$a_{210} = a_{345} = a_{19}$$

$$a_{310} = a_{245} = a_{18}$$

$$a_{410} = a_{235} = a_{17}$$

$$a_{510} = a_{234} = a_{16}$$

$$a_{610} = a_{15}$$

$$a_{710} = a_{14}$$

$$a_{810} = a_{13}$$

$$a_{910} = a_{12}$$

Bibliography

- [Abbott et al., 2007] Abbott, J. J., Ergeneman, O., and Kummer, M. P. (2007). Modeling Magnetic Torque and Force for Controlled Manipulation of Soft-Magnetic Bodies. *Robotics*.
- [Adams et al., 2007] Adams, M. J., Briscoe, B. J., and Johnson, S. A. (2007). Friction and lubrication of human skin. *Tribology Letters*.
- [Aliot et al., 2009] Aliot, E. M., Stevenson, W. G., Almendral-Garrote, J. M., Bogun, F., Calkins, H., Delacretaz, E., Bella, P. D., HINDRICKS, G., Jais, P., Josephson, M. E., Kautzner, J., Kay, G. N., Kuck, K. H., Lerman, B. B., Marchlinski, F. E., Reddy, V. Y., Schalij, M.-J., Schilling, R., Soejima, K., Wilber, D., European Heart Rhythm Association, European Society of Cardiology, and Heart Rhythm Society (2009). EHRA/HRS Expert Consensus on Catheter Ablation of Ventricular Arrhythmias: developed in a partnership with the European Heart Rhythm Association (EHRA), a Registered Branch of the European Society of Cardiology (ESC), and the Heart Rhythm Society (HRS); in collaboration with the American College of Cardiology (ACC) and the American Heart Association (AHA). In *Europace*, pages 771–817. CHU de Nancy, Hôpital de Brabois, Vandoeuvre-les-Nancy, France.
- [Andrä and Nowak, 2007] Andrä, W. and Nowak, H. (2007). *Magnetism in Medicine: A Handbook*. Wiley, 2nd edition.
- [Angeloglou, 1970] Angeloglou, M. (1970). *A History of Make-Up*. Macmillan.
- [Antony, 2003] Antony, J. (2003). *Design of Experiments for Engineers and Scientists*. Butterworth-Heinemann.
- [Arain et al., 2011] Arain, N. A., Cadeddu, J. A., Best, S. L., Roshek, T., Chang, V., Hogg, D. C., Bergs, R. A., Fernandez, R., Webb, E. M., and Scott, D. J. (2011). A randomized comparison of laparoscopic, magnetically anchored, and flexible endoscopic cameras in performance and workload between laparoscopic and single-incision surgery. *Surg Endosc*, 26(4):1170–1180.
- [Best et al., 2010] Best, S. L., Bergs, R. A., Gedeon, M., Paramo, J., Fernandez, R., Cadeddu, J. A., and Scott, D. J. (2010). Maximizing coupling strength of magnetically anchored surgical instruments: how thick can we go? *Surg Endosc*, 25(1):153–159.
- [Best and Cadeddu, 2010] Best, S. L. and Cadeddu, J. A. (2010). Use of Magnetic Anchoring and Guidance Systems to Facilitate Single Trocar Laparoscopy. *Curr Urol Rep*, 11(1):29–32.

Bibliography

- [Blau, 2001] Blau, P. J. (2001). The significance and use of the friction coefficient. *Tribology International*, 34(9):585–591.
- [Blau, 2009] Blau, P. J. (2009). *Friction Science and Technology*. From Concepts to Applications. CRC Press I Llc.
- [Box et al., 2005] Box, G. E. P., Hunter, J. S., and Hunter, W. G. (2005). *Statistics for experimenters*. design, innovation, and discovery. Wiley-Blackwell.
- [Brewer et al., 2008] Brewer, R. D., Loewke, K. E., Duval, E. F., and Salisbury, J. K. (2008). Force control of a permanent magnet for minimally-invasive procedures. In *Proceedings of the 2nd Biennial IEEE/RAS-EMBS International Conference on Biomedical Robotics and Biomechatronics, BioRob 2008*, pages 580–586.
- [Cadeddu et al., 2009] Cadeddu, J. A., Fernandez, R., Desai, M., Bergs, R. A., Tracy, C., Tang, S.-j., Rao, P., Desai, M., and Scott, D. J. (2009). Novel magnetically guided intra-abdominal camera to facilitate laparoendoscopic single-site surgery: initial human experience. *Surg Endosc*, 23(8):1894–1899.
- [Carpi and Pappone, 2009] Carpi, F. and Pappone, C. (2009). Magnetic maneuvering of endoscopic capsules by means of a robotic navigation system. *IEEE Trans. Biomed. Eng.*, 56(5):1482–1490.
- [Chiba et al., 2005] Chiba, A., Sendoh, M., Ishiyama, K., and Arai, K. I. (2005). Moving of a Magnetic Actuator for a Capsule Endoscope in the Intestine of a Pig. *J. Magn. Soc. Jpn*, 29:343–346.
- [Ciuti et al., 2009] Ciuti, G., Donlin, R., Valdastrì, P., Arezzo, A., Menciassi, A., Morino, M., and Dario, P. (2009). Robotic versus manual control in magnetic steering of an endoscopic capsule. *Endoscopy*, 42(02):148–152.
- [Cohen et al., 2012] Cohen, M. I., Triedman, J. K., Cannon, B. C., Davis, A. M., Drago, F., Janousek, J., Klein, G. J., Law, I. H., Morady, F. J., Paul, T., Perry, J. C., Sanatani, S., and Tanel, R. E. (2012). PACES/HRS Expert Consensus Statement on the Management of the Asymptomatic Young Patient with a Wolff-Parkinson-White (WPW, Ventricular Preexcitation) Electrocardiographic Pattern. *Heart Rhythm*, 9(6):1006–1024.
- [Della Bella and MacCabelli, 2011] Della Bella, P. and MacCabelli, G. (2011). Towards a safer approach to epicardial ablation. *Journal of Cardiovascular Electrophysiology*, 22(11):1281–1283.
- [Devine and Devine, 1953] Devine, J. W. and Devine, J. W. J. (1953). Duodenal intubation. *Surgery*, 33(4):513–515.
- [Dewire and Calkins, 2010] Dewire, J. and Calkins, H. (2010). State-of-the-art and emerging technologies for atrial fibrillation ablation. *Nat Rev Cardiol*, 7(3):129–138.
- [Dominguez et al., 2009] Dominguez, G., Durand, L., Rosa, J., Danguise, E., Arozamena, C., and Ferraina, P. A. (2009). Retraction and triangulation with neodymium magnetic forceps for single-port laparoscopic cholecystectomy. *Surg Endosc*, 23(7):1660–1666.

- [Driller et al., 1969] Driller, J., Hilal, S. K., Michelsen, W. J., Sollish, B., Katz, B., and Konig, Jr, W. (1969). Development and use of the POD catheter in the cerebral vascular system. *Medical research engineering*, 8(4):11–16.
- [Duck, 1990] Duck, F. A. (1990). *Physical properties of tissue*. a comprehensive reference book. Academic Pr.
- [Equen et al., 1957] Equen, M., Roach, G., Brown, R., and Bennett, T. (1957). Magnetic removal of foreign bodies from the esophagus, stomach and duodenum. *AMA Arch Otolaryngol*, 66(6):698–706.
- [Faddis et al., 2002] Faddis, M. N., Blume, W., Finney, J., Hall, A., Rauch, J., Sell, J., Bae, K. T., Talcott, M., and Lindsay, B. (2002). Novel, magnetically guided catheter for endocardial mapping and radiofrequency catheter ablation. *Circulation*, 106(23):2980–2985.
- [Faddis et al., 2003] Faddis, M. N., Chen, J., Osborn, J., Talcott, M., Cain, M. E., and Lindsay, B. D. (2003). Magnetic guidance system for cardiac electrophysiology: a prospective trial of safety and efficacy in humans. *Journal of the American College of Cardiology*, 42(11):1952.
- [Fakhry et al., 2008] Fakhry, M., Gallagher, B., Bello, F., and Hanna, G. B. (2008). Visual exposure using single-handed magnet-driven intra-abdominal wireless camera in minimal access surgery. *Surg Endosc*, 23(3):539–543.
- [Fisher, 1971] Fisher, S. R. A. (1971). The design of experiments.
- [Frei, 1967] Frei, E. H. (1967). Magnetic Propulsion of Diagnostic or Therapeutic Elements through the Body Ducts of Animal or Human Patients.
- [Fuimaono et al., 2003] Fuimaono, K. B., Rangel, M. G., and Dipen, S. (2003). Basket Catheter with Multiple Location Sensors. (US20010017029):A61B 5/ 0408 A I; A61B 5/ 042 A I; A61B 5/ 0478 A I; A61B 5/ 0492 A I; A61B 5/ 06 A I; A61M 25/ 00 A I; A61B 17/ 00 A N; A61B 19/ 00 A N.
- [Fung, 2010] Fung, Y. C. (2010). *Biomechanics*. Mechanical Properties of Living Tissues. Springer.
- [Fuster et al., 2006] Fuster, V., Rydén, L. E., Cannom, D. S., Crijns, H. J. G., Curtis, A. B., Ellenbogen, K. A., Halperin, J. L., Le Heuzey, J.-Y., Kay, G. N., Lowe, J. E., Olsson, S. B., Prystowsky, E. N., Tamargo, J. L., and Wann, S. (2006). ACC/AHA/ESC 2006 Guidelines for the Management of Patients With Atrial Fibrillation. *Journal of the American College of Cardiology*, 48(4):e149–e246.
- [Gang et al., 2011] Gang, E. S., Nguyen, B. L., Shachar, Y., Farkas, L., Farkas, L., Marx, B., Johnson, D., Fishbein, M. C., Gaudio, C., and Kim, S. J. (2011). Dynamically shaped magnetic fields: Initial animal validation of a new remote electrophysiology catheter guidance and control system. *Circulation: Arrhythmia and Electrophysiology*, 4(5):770–777.
- [Gillies et al., 1994] Gillies, G. T., Ritter, R. C., Broaddus, W. C., Grady, M. S., Howard, M. A., and McNeil, R. G. (1994). Magnetic manipulation instrumentation for medical physics research. *Review of Scientific Instruments*, 65(3):533–562.

Bibliography

- [Greenwood et al., 1961] Greenwood, J. A., Minshall, H., and Tabor, D. (1961). Hysteresis Losses in Rolling and Sliding Friction. *Proceedings of the Royal Society A: Mathematical, Physical and Engineering Sciences*, 259(1299):480–507.
- [Hilal et al., 1974] Hilal, S. K., Michelsen, W. J., Driller, J., and Leonard, E. (1974). Magnetically guided devices for vascular exploration and treatment. *Radiology*, 113(3):529–540.
- [Iddan et al., 2000] Iddan, G., Meron, G., Glukhovsky, A., and Swain, P. (2000). Wireless capsule endoscopy. *Nature*, 405(6785):417–418.
- [Keller et al., 2012] Keller, H., Juloski, A., Kawano, H., Bechtold, M., Kimura, A., Takizawa, H., and Kuth, R. (2012). Method for navigation and control of a magnetically guided capsule endoscope in the human stomach. In *Biomedical Robotics and Biomechatronics (BioRob), 2012 4th IEEE RAS & EMBS International Conference on*.
- [Kendall, 1924] Kendall, W. G. (1924). Lip-Stick Holder. (US19220579242):A45D 40/ 06 A I.
- [Kósa et al., 2008] Kósa, G., Jakab, P., Jólesz, F., and Hata, N. (2008). Swimming capsule endoscope using static and RF magnetic field of MRI for propulsion. In *Proceedings - IEEE International Conference on Robotics and Automation*, pages 2922–2927.
- [Kósa et al., 2012] Kósa, G., Jakab, P., Székely, G., and Hata, N. (2012). MRI driven magnetic microswimmers. *Biomedical Microdevices*, 14(1):165–178.
- [Krings et al., 2006] Krings, T., Finney, J., Niggemann, P., Reinacher, P., Lück, N., Drexler, A., Lovell, J., Meyer, A., Sehra, R., Schauerte, P., Reinges, M., Hans, F. J., and Thron, A. (2006). Magnetic versus manual guidewire manipulation in neuroradiology: in vitro results. *Neuroradiology*, 48(6):394–401.
- [Kume et al., 2008] Kume, M., Miyazawa, H., Iwasaki, W., Abe, F., Uchinami, H., and Yamamoto, Y. (2008). The use of magnetic anchors in the bowel lumen for laparoscopic anterior resection of rectosigmoid colon in pigs: with video. *World J Surg*, 32(11):2425–2428.
- [Kummer et al., 2010] Kummer, M. P., Abbott, J. J., Kratochvil, B. E., Borer, R., Sengul, A., and Nelson, B. J. (2010). Octomag: An electromagnetic system for 5-DOF wireless micromanipulation. *Ieee T Robot*, 26(6):1006–1017.
- [Lehman et al., 2008] Lehman, A. C., Dumpert, J., Wood, N. A., Redden, L., Visty, A. Q., Farritor, S. M., Varnell, B., and Oleynikov, D. (2008). Natural orifice cholecystectomy using a miniature robot. *Surg Endosc*, 23(2):260–266.
- [Martinez-Ferro, 2012] Martinez-Ferro, M. (2012). International innovations in pediatric minimally invasive surgery: the Argentine experience. *Journal of Pediatric Surgery*, 47(5):825–835.
- [Maslanka, 1987] Maslanka, H. (1987). Biopsy Forceps. (US19850735313):A61B 10/ 00 A I; A61B 10/ 02 A I; A61B 17/ 28 A I; A61B 19/ 00 A N; A61M 3/ 02 A N.
- [Mason, 1923] Mason, J. B. J. (1923). Toilet Article. (US19220575479):A45D 40/ 04 A I.

- [McCarthy, 1962] McCarthy, H. F. (1962). Method of Performing Intestinal Intubation.
- [McNeil et al., 1995a] McNeil, R. G., Ritter, R. C., Wang, B., Lawson, M. A., Gillies, G. T., Wika, K. G., Quate, E. G., Howard, M. A., and Grady, M. S. (1995a). Characteristics of an improved magnetic-implant guidance system. *IEEE Trans. Biomed. Eng.*, 42(8):802–808.
- [McNeil et al., 1995b] McNeil, R. G., Ritter, R. C., Wang, B., Lawson, M. A., Gillies, G. T., Wika, K. G., Quate, E. G., Howard, M. A., and Grady, M. S. (1995b). Functional design features and initial performance characteristics of a magnetic-implant guidance system for stereotactic neurosurgery. *IEEE Trans. Biomed. Eng.*, 42(8):793–801.
- [Modny, 1958] Modny, M. T. (1958). Vein Stripper and a Method of Stripping Veins.
- [Molcho et al., 1970] Molcho, J., Karny, H. Z., Frei, E. H., and Askenas, H. M. (1970). Selective Cerebral Catheterization. *IEEE Trans. Biomed. Eng.*, BME-17(2):134–140.
- [Montgomery et al., 1969] Montgomery, D. B., Weggel, R. J., Leupold, M. J., Yodh, S. B., and Wright, R. L. (1969). Superconducting magnet system for intravascular navigation. *Journal of Applied Physics*, 40(5):2129–2132.
- [Morita et al., 2010] Morita, E., Ohtsuka, N., Shindo, Y., Nouda, S., Kuramoto, T., Inoue, T., Murano, M., Umegaki, E., and Higuchi, K. (2010). In vivo trial of a driving system for a self-propelling capsule endoscope using a magnetic field (with video). *Gastrointestinal Endoscopy*, 72(4):836–840.
- [Morley and Wallace, 2003] Morley, T. A. and Wallace, D. T. (2003). Roll-Pitch-Roll Surgical Tool. (US20030340129):A61B 19/ 00 A I; A61B 17/ 04 A N; A61B 17/ 068 A N.
- [Nurdin et al., 1996] Nurdin, N., Weilandt, E., Textor, M., Taborelli, M., Spencer, N. D., and Descouts, P. (1996). Reduced frictional resistance of polyurethane catheter by means of a surface coating procedure. *Journal of Applied Polymer Science*, 61(11):1939–1948.
- [Okamura et al., 2004] Okamura, A. M., Simone, C., and O’Leary, M. D. (2004). Force Modeling for Needle Insertion Into Soft Tissue. *IEEE Trans. Biomed. Eng.*, 51(10):1707–1716.
- [O’Leary et al., 2003] O’Leary, M. D., Simone, C., Washio, T., Yoshinaka, K., and Okamura, A. M. (2003). Robotic needle insertion: Effects of friction and needle geometry. *Robotics and Automation, 2003. Proceedings. ICRA’03. IEEE International Conference on*, 2:1774–1780 vol. 2.
- [Olsson et al., 1998] Olsson, H., Åström, K. J., Canudas De Wit, C., Gäfvert, M., and Lischinsky, P. (1998). Friction Models and Friction Compensation. *European Journal of Control*, 4(3):176–195.
- [Padilla et al., 2011] Padilla, B. E., Dominguez, G., Millan, C., and Martinez-Ferro, M. (2011). The use of magnets with single-site umbilical laparoscopic surgery. *YSPSU*, 20(4):224–231.

Bibliography

- [Park et al., 2007] Park, S., Bergs, R. A., Eberhart, R., Baker, L., Fernandez, R., and Cadeddu, J. A. (2007). Trocar-less Instrumentation for Laparoscopy. *Annals of Surgery*, 245(3):379–384.
- [Patterson et al., 2006] Patterson, M. S., Schotten, J., van MIEGHEM, C., Kiemeneij, F., and Serruys, P. W. (2006). Magnetic navigation in percutaneous coronary intervention. *Journal of interventional cardiology*, 19(6):558–565.
- [Prokopovich and Perni, 2010] Prokopovich, P. and Perni, S. (2010). Prediction of the frictional behavior of mammalian tissues against biomaterials. *Acta Biomaterialia*, 6(10):4052–4059.
- [Prokopovich et al., 2009] Prokopovich, P., Perni, S., Piccirillo, C., Pratten, J., Parkin, I. P., and Wilson, M. (2009). Frictional properties of light-activated antimicrobial polymers in blood vessels. *J Mater Sci: Mater Med*, 21(2):815–821.
- [Prystowsky, 2008] Prystowsky, E. N. (2008). The History of Atrial Fibrillation: The Last 100 Years. *Journal of Cardiovascular Electrophysiology*, 19(6):575–582.
- [Ram and Meyer, 1991] Ram, W. and Meyer, H. (1991). Heart catheterization in a neonate by interacting magnetic fields: A new and simple method of catheter guidance. *Catheterization and Cardiovascular Diagnosis*, 22(4):317–319.
- [Raman et al., 2009] Raman, J. D., Scott, D. J., and Cadeddu, J. A. (2009). Role of Magnetic Anchors During Laparoendoscopic Single Site Surgery and NOTES. *J Endourol*, 23(5):781–786.
- [Rohrbach, 2002] Rohrbach, J. M. (2002). *Ophthalmologische Traumatologie.: Textbuch und Atlas*. Schattauer.
- [Scaglione et al., 2011] Scaglione, M., Biasco, L., Caponi, D., Anselmino, M., Negro, A., Di Donna, P., Corleto, A., Montefusco, A., and Gaita, F. (2011). Visualization of multiple catheters with electroanatomical mapping reduces X-ray exposure during atrial fibrillation ablation. *Europace*, 13(7):955–962.
- [Simi et al., 2010] Simi, M., Valdastrì, P., Quaglia, C., Menciasì, A., and Dario, P. (2010). Design, fabrication, and testing of a capsule with hybrid locomotion for gastrointestinal tract exploration. *IEEE/ASME Transactions on Mechatronics*, 15(2):170–180.
- [Soejima et al., 2001] Soejima, K., Delacretaz, E., Suzuki, M., Brunckhorst, C. B., Maisel, W. H., Friedman, P. L., and Stevenson, W. G. (2001). Saline-cooled versus standard radiofrequency catheter ablation for infarct-related ventricular tachycardias. *Circulation*, 103(14):1858–1862.
- [Sosa et al., 1996] Sosa, E., Scanavacca, M., D’Avila, A., and Pilleggi, F. (1996). A new technique to perform epicardial mapping in the electrophysiology laboratory. *Journal of Cardiovascular Electrophysiology*, 7(6):531–536.
- [Spivey and Washburn, 2010] Spivey, J. T. and Washburn, T. T. (2010). Surgical Scissors. (US20090364172):A61B 17/ 3201 A I; B21D 11/ 20 A I; B23P 11/ 00 A I.
- [Springer, 1970] Springer, S. (1970). Beitrag zur Frage der Magnetoperation am Auge unter besonderer Berücksichtigung des methodischen Vorgehens.

- [St Jude Medical Inc., 2010] St Jude Medical Inc. (2010). Investor Presentation. In *St. Jude Medical Inc.*
- [Stereotaxis, 2012] Stereotaxis (2012). Investor Presentation. In *Stereotaxis Inc.*
- [Stevens-Wright et al., 2000] Stevens-Wright, D., Cuscuna, D. F., Russo, M., Nielsen, P., and Bertram, P. (2000). Actuator for Use with a Catheter with Independent Proximal and Distal Control. (EP20000114145):A61B 18/ 14 A I; A61M 25/ 01 A I.
- [Takashima et al., 2007] Takashima, K., Shimomura, R., Kitou, T., Terada, H., Yoshinaka, K., and Ikeuchi, K. (2007). Contact and friction between catheter and blood vessel. *Tribology International*, 40(2):319–328.
- [Thiagalingam et al., 2010] Thiagalingam, A., D’Avila, A., Foley, L., Guerrero, J. L., Lambert, H., Leo, G., Ruskin, J. N., and Reddy, V. Y. (2010). Importance of catheter contact force during irrigated radiofrequency ablation: Evaluation in a porcine ex vivo model using a force-sensing catheter. *Journal of Cardiovascular Electrophysiology*, 21(7):806–811.
- [Tillander, 1951] Tillander, H. (1951). Magnetic guidance of a catheter with articulated steel tip. *Acta radiologica*.
- [Tillander, 1970] Tillander, H. (1970). Selective Angiography with a Catheter Guided by a Magnet. *IEEE Trans. Magn.*, MAG-6(2):355–358.
- [Towbin et al., 1990] Towbin, R. B., Dunbar, J. S., and Rice, S. (1990). Magnetic catheter for removal of magnetic foreign bodies. *AJR Am J Roentgenol*, 154(1):149–150.
- [Tunay, 2004] Tunay, I. (2004). Modeling magnetic catheters in external fields. *Engineering in Medicine and Biology Society*.
- [Valdastri et al., 2011] Valdastri, P., Ciuti, G., Verbeni, A., Menciassi, A., Dario, P., Arezzo, A., and Morino, M. (2011). Magnetic air capsule robotic system: proof of concept of a novel approach for painless colonoscopy. *Surg Endosc*, 26(5):1238–1246.
- [Valdastri et al., 2010] Valdastri, P., Quaglia, C., Buselli, E., Arezzo, A., Di Lorenzo, N., Morino, M., Menciassi, A., and Dario, P. (2010). A magnetic internal mechanism for precise orientation of the camera in wireless endoluminal applications. *Endoscopy*, 42(6):481–486.
- [Vantassel et al., 2000] Vantassel, R. A., Schwartz, R. S., and Holmes, D. R. (2000). Steerable Catheter with External Guidewire as Catheter Tip Deflector. (US19990329386):A61M 25/ 01 A I; A61M 25/ 09 A I.
- [Verin and Flaction, 2011] Verin, V. and Flaction, L. (2011). Medical Device for Tissue Ablation. (EP20090786640):A61B 18/ 14 A I.
- [Verin and Sandtner, 2008] Verin, V. and Sandtner, J. (2008). Medical Device for Tissue Ablation. *WO Patent WO/2008/010,039*.
- [Vokoun et al., 2009] Vokoun, D., Beleggia, M., Heller, L., and Šittner, P. (2009). Magnetostatic interactions and forces between cylindrical permanent magnets. *Journal of Magnetism and Magnetic Materials*, 321(22):3758–3763.

Bibliography

- [Zipes et al., 2006] Zipes, D. P., Camm, A. J., and Borggrefe, M. (2006). ACC/AHA/ESC 2006 Guidelines for Management of Patients With Ventricular Arrhythmias and the Prevention of Sudden Cardiac Death. *Journal of the American College of Cardiology*, 48(5).

List of Figures

2.1	First case of magnetic extraction of intraocular foreign bodies with the help of an electromagnet developed by Hirshberg in 1885.	6
2.2	A “giant magnet” developed at ETHZ and used by Haab to remove intraocular foreign bodies in 1892.	6
2.3	Octomag, an electromagnetic system for 5-DoF wireless micromanipulation.	7
2.4	Intravascular magnetic guidance developed by Tillander in the early 1950s.	8
2.5	Percussion-type electromagnetic probe of Sobiepanek in 1969.	9
2.6	Ram and Meyer reports the first clinical case of heart catheterization in a neonate with complex congenital heart disease, using a strong external permanent magnet to control the magnetic tip of a catheter in the body.	10
2.7	Method developed by Modny and Bambara for stripping varicose veins by using a “plumb line” magnetically guided with an external hand-held magnet, 1957.	11
2.8	Magnetic propulsion of a POD catheter tip attached to a stiffer polymer tube.	12
2.9	Magnetic navigation systems from Stererotaxis, Inc..	12
2.10	The CGCI magnetic system from Magnetecs Corp..	13
2.11	Magnetic propulsion of capsule endoscopy developed at Tohoku University, 2003.	14
2.12	Magnetic propulsion for capsule endoscopy.	14
2.13	Capsule endoscopy with a large external magnet controlled manually or robotically, Scuola Superiore Sant’Anna.	15
2.14	Method for guiding a medical instrument with magnetic force control, Brewer <i>et al.</i>	16
2.15	Magnetic Anchoring and Guidance System (MAGS) for deployable instrumentations, Cadeddu <i>et al.</i>	17
2.16	Magnetic Stereotaxis Systems.	19
2.17	Forces and torques applied to a element of magnetic moment m under a external magnetic field.	20
2.18	MAGS: Magnetic Anchoring and Guidance System.	22
3.1	Coupling force modulation by varying the separation distance between the permanent magnets.	31
3.2	3-dimensional FEM results of the coupling force as a function of the axial displacement of the magnet and its length.	32
3.3	Coupling force modulation by varying the separation distance between the permanent magnets.	33

List of Figures

3.4	3-dimensional FEM results of the coupling force in function of the radial displacement of the magnet and of its diameter.	35
3.5	Electromagnet principle.	35
3.6	3-dimensional FEM results of the coupling force as a function of the magnetomotive force.	36
3.7	Arrangement of parallel permanent magnets to modulate the magnetic field.	37
3.8	Modulator with 2 steerable magnets: the magnetic field representation for different steering angles θ of the magnet	39
3.9	Modulator with 2 steerable magnets and 1 fixed magnet: the magnetic field representation for different steering angles θ of the magnet.	40
3.10	3-dimensional FEM results of the coupling force in function of magnets angle for the two concepts using steerable parallel magnets.	41
3.11	Arrangement of three coaxial diametrically magnetized permanent magnets to modulate the magnetic field.	42
3.12	Coaxial modulator: the magnetic field is represented for different steering angles θ of the middle magnet.	43
3.13	3-dimensional FEM results of the coupling force in function of the steering magnet angle for the modulator composed of three coaxial magnets.	44
3.14	A pair of tubular ferromagnetic sections is used to shield and modulate the magnetic attraction between the permanent magnets.	45
3.15	Shielding modulator: the magnetic field is represented for different steering angles θ of the shield.	46
3.16	3-dimensional FEM results of the coupling and lateral force as a function of steerable shield angle and different shield section angles.	47
3.17	3-dimensional FEM results of the coupling and lateral force as a function of steerable shield angle and different shield thickness.	48
3.18	3-dimensional FEM results of the coupling and lateral force in function of steerable shield angle and different permeabilities.	49
3.19	Cable actuation in medical devices.	52
3.20	Force comparison of the modulators.	53
4.1	Concept of magnetic force modulator based on two steerable permanent magnets.	58
4.2	View of the magnetic force modulator integrated into the tip of an ablation catheter of 5 mm in diameter.	59
4.3	Patent drawings of lipstick tube mechanisms.	60
4.4	Selective views of the actuation mechanism used to steer the magnets of the magnetic force modulator integrated in a catheter tip.	61
4.5	View of the scaled-up magnetic force modulator for <i>in vitro</i> validation.	62
4.6	Free-body diagrams of modulator subsystems used in the different systems of equations and to calculate the resulting actuations forces.	63
4.7	Modulator: 3D-FEM results of the lateral and vertical magnetic forces as well as the magnetic torque acting on the steerable magnets.	64
4.8	Theoretical actuation force for pull-push cycle based on model I.	66
4.9	Theoretical normal force acting on the helical slot using model I.	66
4.10	Theoretical actuation force for pull-push cycle based on model II.	68
4.11	Measurement of the actuation force F_a required to rotate the steerable magnets as well as the magnet forces and torques within the MAGS.	69

4.12	Measurement of the force required to actuate the <i>in vitro</i> modulator in a full pull-push cycle.	70
4.13	Theoretical calculation and experimental measurements of the actuation force.	70
4.14	Theoretical calculation of the actuation force in function of the modulation range.	71
4.15	Theoretical FEM and experimental coupling force at different separation distances Δ_z	72
4.16	Experimental measurements of the magnetic forces and torque as a function of an dragging shift of the passive magnet for two separation distances Δ_z	73
4.17	Experimental measurements of the magnetic forces and torques within the MAGS as a function of an dragging shift Δ_x as well as a lateral misalignment Δ_y of the passive magnet.	74
4.18	Expected magnetic and mechanical performances of a catheteric modulator.	75
5.1	Control architectures composed of a PI controller, a force feedback (FFB) loop and three different feed-forward (FFD) parts.	83
5.2	Magnetic forces within the MAGS during the guidance.	84
5.3	FEM results representing the coupling force within the MAGS as a function of the modulator angle and the separation distance.	84
5.4	Schematic representation of the setup for characterizing the magnetic guidance under different control modes as well as various sliding conditions.	85
5.5	Views of the custom made setup for analyzing the magnetic guidance behavior of the <i>in vitro</i> modulator.	86
5.6	Measurements of the magnetic interactions occurring during the displacement of the MAGS on a foam material.	89
5.7	Measurements of the magnetic interactions occurring during the displacement of the MAGS controlled in a passive mode on three types of material: foam, rubber and PMMA.	91
5.8	Comparison between active mode with force feedback and passive guidance mode.	92
5.9	Effect of the coupling force on the magnetic guidance behavior.	94
5.10	Effect of the coupling force on the kinetic friction coefficient measurement for three different hardness of material.	95
6.1	Custom made setup for analyzing the magnetic guidance on soft and irregular anatomical tissue.	98
6.2	Comparison between the active and passive guidance mode on the same tissue conditions, example A	100
6.3	Comparison between the active and passive guidance mode on the same tissue conditions, example B	101
6.4	Magnetic guidance executed in a vibrational mode.	103
7.1	apparatus to measure friction.	108
7.2	Main factors and their experimental workspace as well as the generators used for the 2^{10-5} fractional factorial design.	111
7.3	Typical measurements of friction force profiles acquired during experiments.	112
7.4	Bar charts illustrating the relative effects of friction.	113

List of Figures

7.5	Friction: bar charts illustrating the relative sum of square of effects over the total sum of square of all the effects.	115
7.6	Deformation depth of a 4 mm thick bovine endocardial tissue surface under a constant normal load of 2 N for three dimensions of cylinders.	117
7.7	The contact areas consist of a side surface and a front surface of contact with tissue	118
7.8	Histological cross-sections of a 4 mm thick bovine endocardial tissue resulting from different frictional conditions during sliding at 0.5 mm/s in saline environment.	119
8.1	Sinus rhythm sequences.	123
8.2	Current ablation patterns to treat atrial fibrillation.	124
8.3	Maestro-AF system of two magnetic catheters.	127
8.4	Wolff-Parkinson-White syndrome.	128
8.5	Treatment of Wolff-Parkinson-White Syndrome by intracorporeal magnetic catheter ablation.	129
8.6	Treatment of ventricular tachycardias by magnetic anchoring of ablation catheters.	130

List of Tables

2.1	Characteristics of the types of permanent magnets.	21
3.1	Comparison between electromagnets and permanent magnets.	29
3.2	Overview of the force modulators.	55
7.1	Factorial design: expected significance of the two-way interactions.	109
7.2	ANOVA based on a cumulative sum of square selection.	116
7.3	ANOVA based on a cumulative sum of square selection.	117
7.4	Portion of the cylinder pressed down in the tissue	118
8.1	Comparison overview between the current PCA and the Maestro-AF technology.	125

Curriculum Vitae

Last name: Flaction
First name: Lionel
Date of birth: 2 May 1980
Nationality: Swiss

Education

2009 – 2013.3 PhD Research at Laboratoire de Systèmes Robotiques, Ecole Polytechnique Fédérale de Lausanne (EPFL)
– Development of a new system of magnetic catheters to treat atrial fibrillation – Focus on internal magnetic guidance
2007 - 2009 Research Assistant at Laboratoire de Systèmes Robotiques, EPFL
2005 - 2007 MSc in Microengineering at EPFL,
– Specialization: Techniques de production
2002 - 2005 BSc in Microengineering at EPFL
2000 - 2002 Faculté de Biologie at Université de Lausanne (UNIL), 4 semesters
1995 - 2000 Maturité fédérale, scientific section at Ecole du Valentin in Lausanne

Publications

L. Flaction, B. M. Hakim, J. Sandtner, V. Verin and H. Bleuler. Mechanical Force Modulation with Permanent Magnets at Small Scale. The 23rd International Congress of Theoretical and Applied Mechanics (ICTAM), Beijing, China, 2012.

L. Flaction, B. M. Hakim, G. Rognini, V. Verin and H. Bleuler. Screening of the factors influencing frictional interactions between a cylindrical tip and the cardiac wall using factorial analysis, in Tribology International, 2011.

E. Samur, **L. Flaction** and H. Bleuler. Design and Evaluation of a Novel Haptic Interface for Endoscopic Simulation, in IEEE Transactions on Haptics, 2011.

E. Samur, **L. Flaction** and H. Bleuler. Experimental Evaluation of a Haptic Interface for Endoscopic Simulation . 2011 IEEE World Haptics Conference (WHC), Istanbul, Turkey, 2011.

P. Maillard, **L. Flaction**, E. Samur, D. Hellier and J. Passenger et al. Instrumentation of a Clinical Colonoscope for Surgical Simulation. 30th Annual International IEEE EMBS Conference, Vancouver, British Columbia, Canada, 2008.

List of Tables

E. Samur, **L. Flaction**, U. Spaelter, H. Bleuler and D. Hellier et al. A Haptic Interface with Motor/Brake System for Colonoscopy Simulation. Haptics Symposium, Reno, NV, USA, 2008.

E. Samur, U. Spaelter, **L. Flaction**, P. Maillard and R. Wuthrich et al. Control of a Haptic Interface and a Micromachining Setup with an Open Source Real-Time System. The 3rd ASME/IEEE International Conference on Mechatronic and Embedded Systems and Applications, Las Vegas, Nevada, USA, 2007.

Patents

Medical Device for Tissue Ablation and Method, PCT/IB2009/053123.

Haptic Interface for Simulator, such as a Colonoscopy Simulator, PCT/IB2010/053997.